Synthesis, Structural Characterization and Redox Properties of Porphyrinoids with Thiophene and Thienothiophenes

विद्या वाचस्पति की
उपाधि की अपेक्षाओं की आंशिक पूर्ति में प्रस्तुत शोध प्रबंध
A Thesis Submitted in Partial Fulfilment of the Requirements for the

Degree of **Doctor of Philosophy**

द्वारा / By

रामेश नागेश हिरेमठ / Ramesh Nagesh Hiremath

20193635

शोध प्रबंध पर्यवेक्षक / Thesis Supervisor: **Prof. V. G. Anand**

भारतीय विज्ञान शिक्षा एवं अनुसंधान संस्थान पुणे
Indian Institute of Science Education and Research (IISER), Pune

2024

Dedicated to,

My Grandparents

Smt. (late) Vijayabai and Shri. Virupakshayya Shankad

&

My parents

Smt. Mahadevi and Shri. (late) Nagesh S. Hiremath

CERTIFICATE

Certified that the work incorporated in the thesis entitled ***Synthesis, structural characterization and redox properties of porphyrinoids with thiophene and thinothiophenes*** Submitted by *Mr. Ramesh Nagesh Hiremath* was carried out by the candidate, under my supervision. The work presented here or any part of it has not been included in any other thesis submitted previously for the award of any degree or diploma from any other University or institution.

Date: 31/07/2024

V. G. Anand

Declaration

Name of Student: **Ramesh Nagesh Hiremath**

Reg. No.: **20193635**

Thesis Supervisor: **Prof. V. G. Anand**

Department: **Chemistry**

Date of joining Program: **01st May 2019**

Date of Pre-Synopsis Seminar: **07th July 2023**

Title of Thesis: **Synthesis, structural characterization and redox properties of porphyrinoids with thiophene and thinothiophenes.**

I declare that this written submission represents my ideas in my own words and where others' ideas have been included; I have adequately cited and referenced the original sources. I also declare that I have adhered to all principles of academic honesty and integrity and have not misrepresented or fabricated or falsified any idea/data/fact/source in my submission. I understand that violation of the above will be cause for disciplinary action by the Institute and can also evoke penal action from the sources which have thus not been properly cited or from whom proper permission has not been taken when needed.

The work reported in this thesis is the original work done by me under the guidance of Prof. V. G. Anand.

Date: 31/07/2024

Ramesh N. Hiremath

Roll No. 20193635

Acknowledgement

I would like to express my sincere gratitude towards my mentor, my thesis advisor Prof. V.G. Anand for his guidance, patience, support throughout my research work. I thank him for believing in abilities and gave freedom to work during my Ph.D. work.

I would like to express my deepest gratitude to you for your unwavering support, guidance, and mentorship throughout this challenging yet rewarding experience. your expertise, patience, and encouragement have been invaluable, shaping not only my research but also my growth as a researcher and an individual.

I am grateful to the Research Advisory Committee members Prof. Nirmalya Ballav (Chair Dept. of Chemistry, IISER Pune) and Dr. Benudhar Punji (NCL Pune) for their suggestions and advices.

My journey will not be complete without the support of my friends, lab mates and family. To my lab mates, thank you for the collaborative spirit, shared insights, and the sense of community we built together. The exchange of ideas and the collective effort in overcoming obstacles have contributed immensely to the quality of my research. Also, I would like to thank Dr. Sujit P. Chavan, Dr. Sunita Gadakh, Dr. Madan Ambhore, Dr. Ashokkumar B., Dr. Prachi Gupta, Dr. Udaya, Markose Joshy, Dr. Pragati Shukla, Vishnu Mishra, and Rakesh kumar. I thanks to all my friends from NCL, Siddheshwar Ankade, Balaji Ghodake, Anil.

I would like thank to all staff members of IISER Pune and chemistry department especially Mayuresh, Tushar, Nitin, Mahesh, Sandeep, Yatish, Ravindra, and Sandeep for their support during my PhD work.

Special thanks to my batchmates Akash, Abhijeet, Rishu, Umashish, Deepak, Nahid, Sandeep, Bharat, Ravi, Akash Jamdade, Vijay, Bhawakshi, Ruksana, Cavya, Sarika, for their support on time to time.

I would like to extend special thanks to my lab mate Dr. Udaya for his support in crucial time is really mean to me and also thanks to Rishu Pandey for his assistance in crystal solving.

Also, thanks to principal of Maharashtra Mahavidyalaya, Nilanga Dr. M. N. Kolpuke and president of MSS, Mr. Vijay S. Patil sir for giving me space to do my research work.

There are no words to convey my sincere gratitude towards all my family members and their love, unconditional support that have made me today who I am. Also, I am deeply grateful to my grandfather, Virupakshyya Virayya Shankad whose support has been instrumental in helping me reach this point. To my mother, Mahadevi Nagesh Hiremath, the backbone of my life and my constant source of inspiration- my heartfelt thanks to you avva. I am also deeply thankful to both my uncles and aunts, Mr. Sidharam and Uma Shankad, as well as Dr. Mallikarjun and Suvarna Shankad. My uncles played a crucial role in ensuring I completed my education successfully, and I feel that no words or actions could ever repay their kindness and support. I am equally grateful to my mavshi/second mother, Avi Mavshi, for her unwavering kindness, care, and support as well as to Bidar Baba for his steadfast support. Thank you from the bottom of my heart. Also thankful to uncles and aunts Prakash & Ganga, Vijay & Parvati, Dayanand & Nanda.

Special thanks to my brothers & sister, Viresh-Pooja, Mahesh, Shubham, Channvir, Naresh, Shakti, Vivek, Lingesh, Anand, Vidhya, Anant, shubhada, ujjawla, yogita for having in my life and their support in my overall journey.

I would like to express my heartfelt gratitude to everyone who, directly or indirectly, has supported and helped me reach this point in my journey.

At last, I am thankful to UGC for fellowship and IISER Pune for all the facilities.

Contents

Synopsis 1

Publication 4

I. Introduction

I.1 Annulene to Porphyrin 6
I.2 Isophlorin 9
I.3 Porphyrins and its structural variants 10
I.4 Confused Porphyrins 11
I.5 Core-modified Porphyrins 14
I.6 π-Expanded Porphyrinoids 16
I.7 Redox Chemistry 21
I.8 Aim of the thesis 25

II. Synthesis and characterization of thiophene based [8] and [16] annulene

II.1 Introduction 27
II.2 Synthesis of [8] and [16] thiophene fused isophlorin using strategy I 29
II.3.1 Isolation and Characterisation of symmteric [8] dithia isophlorin 30
II.3.2 ^{1}H NMR study of symmteric [8] cyclooctatetraene 30
II.4 Synthesis of [8] and [16] thiophene fused isophlorin using strategy II 32
II.4.1 Isolation and Characterization of Asymmetric [8] dithiafused cyclooctatetraene 32
II.4.2 Molecular structure of [8] dithiafused cyclcooctatetraene 33
II.4.3 Electronic absorption and cyclic voltammogram studies 34
II.5.1 Isolation and characterization of [16] tetrathia isophlorin 35
II.5.2 ^{1}H NMR study of [16] tetrathia isophlorin 36
II.5.3 Molecular staructure of [16] tetrathia isophlorin 38
II.5.4 Electronic absorption and Cyclic Voltammogram studies 39
II.6 Quantum mechanical calculations 40
II.7 Conclusions 45
II.8 General Experimental Methods 46
II.9 Experimental section 47

III. Aromaticity in Thieno[3,2-b]thiophene Incorporated Expanded Porphyrinoids

III.1 Introduction 52
III.2 Synthesis of Thieno[3,2-b]thieno incorporated [34] Hexaphyrin 54
III.3.1 Isolation and Characterisation of [34] Hexaphyrin (III.3) 55

III.3.2 ^{1}H NMR study of [34] Hexaphyrin (III.3) 55
III.3.3 Electronic absorption and Cyclic Voltammogram studies 57
III.3.4 Molecular structure of [34] Hexaphyrin (III.3)……..... 58
III.4 Synthesis of Thieno[3,2-b]thieno incorporated [34] Hexaphyrin (III.6) 59
III.5.1 Isolation and Characterisation of [34] Hexaphyrin (III.6) 59
III.5.2 ^{1}H NMR study of [34] Hexaphyrin (III.6) 60
III.5.3 Molecular structure of [34] Hexaphyrin (III.6) 62
III.5.4 Electronic absorption and Cyclic Voltammogram studies 63
III.6 Quantum mechanical calculations 64
III.7 Conclusions 68
III.8 Experimental section 69

IV. Synthesis and Characterisation of 24π core-modified sapphyrin and its higher analogues

IV.1 Introduction 74
IV.2 Synthesis of [24] Sapphyrins and higher analogues (IV.11) 77
IV.3.1 Isolation and Characterisation of [24]Sapphyrin (IV.11) 78
IV.3.2 ^{1}H NMR study of [24]Sapphyrin (IV.11) 79
IV.3.3 Molecular structure of [24]sapphyrin (IV.11) 81
IV.3.4 Electronic absorption and Cyclic Voltammogram studies 81
IV.4.1 Isolation and Characterisation of [48]decaphyrin (IV.12) 84
IV.4.2 ^{1}H NMR study of [48]decaphyrin (IV.12) 84
IV.4.3 Molecular structure of [48]decaphyrin (IV.12) 86
IV.4.4 Electronic absorption and Cyclic Voltammogram studies 87
IV.5.1 Isolation and Characterisation of [72]pentadecaphyrin (IV.13) 89
IV.5.2 ^{1}H NMR study of [72]pentadecaphyrin (IV.13) 89
IV.5.3 Molecular structure of [72] pentadecaphyrin (IV.13) 91
IV.5.4 Electronic absorption studies 92
IV.6 Quantum mechanical calculations 94
IV.7 Synthesis of [24] Sapphyrins and higher analogues (IV.19) 95
IV.8.1 Isolation and Characterisation of [24]Sapphyrin (IV.19) 96
IV.8.2 ^{1}H NMR study of [24]Sapphyrin (IV.19) 97
IV.8.3 Molecular structure of [24]sapphyrin (IV.19) 98
IV.8.4 Electronic absorption and Cyclic Voltammogram studies 99
IV.8.5 Sythesis and characterization of [22] Sapphyrins dication (IV.22) 101
IV.8.6 Molecular structure of [22]sapphyrin dication (IV.22) 103
IV.9.1 Isolation and Characterisation of [48]decaphyrin (IV.20) 103
IV.9.2 ^{1}H NMR study of [48]decaphyrin (IV.20) 104
IV.9.3 Molecular structure of [48]decaphyrin (IV.20) 106

IV.9.4 Electronic absorption and Cyclic Voltammogram studies..... 107
IV.10.1 Isolation and Characterisation of [72]pentadecaphyrin (IV.21) 109
IV.10.2 ^{1}H NMR study of [72]pentdecaphyrin (IV.21) 110
IV.10.3 Electronic absorption studies 111
IV.11 Quantum mechanical calculations 112
IV.12 Conclusions..... 114
IV.13 Experimental section 115

V. **Summary of the Thesis** 122

VI . **References** 124

Synopsis

This thesis entitled as "**Synthesis, Structural Characterization and Redox Properties of Porphyrinoids with Thiophenes and Thieno[3,2-b]thiophene**" describe the synthetic chemistry of core modified contracted and expanded isophlorinoids and exploration the chemistry of aromatic and antiaromatic systems. This was achieved by utilizing different precursors and varying the concentration of the reaction mixture. Usually, antiaromatic systems are recognized for their tendency to disrupt the π-electron delocalization compared to aromatic systems. The tetrapyrrolic 20π isophlorin was hypothesized to be an intermediate stage in porphyrin production. Because of its inherent instability, it experiences a rapid two-electron oxidation process, which is then followed by deprotonation, resulting in the aromatic porphyrin. Vogel and his coworkers made significant endeavours to synthesize stable 20π macrocycles from several heterocycles, including thiophene, furan, and selenophene. Several additional groups also made effective attempts to synthesize 20π isophlorin.

Many other groups synthesised expanded core modified isophlorin with 4nπ electrons. A stable isophlorin and its extended derivatives provide an opportunity to investigate antiaromatic systems in this particular context. Delving into the study of these systems from the perspective of annulene chemistry is really interesting. The exploration of aromaticity, molecular geometry and its topological studies in expanded isophlorinoids is quite limited. Hence, this thesis aims to address this gap by synthesizing expanded non-pyrrolic porphyrinoids. The main objective is to explore their (non)-aromaticity/antiaromaticity through the redox chemistry. The macrocycles were thoroughly characterized using several spectroscopic techniques, such as UV-Vis absorption spectroscopy, NMR spectroscopy, and single-crystal X-ray diffraction analysis, which provided evidence of their solid-state geometries and conformational dynamics. The redox characteristics of these macrocycles were determined using electrochemical techniques, including Cyclic Voltammetry (CV) and Spectro-electrochemical studies. Moreover, the electronic and redox properties of the macrocycles supported by suitable and appropriate of quantum mechanical calculations such as NICS and AICD values to prove the aromatic properties as inferred from experimental results.

This thesis consists of four chapters. The initial chapter provided an overview of porphyrin and its structural variants with detailed insights on the exploration of aromaticity/antiaromaticity in porphyrin and its extended derivatives. It also explains the porphyrin with an annulene

backbone and its possible modifications by inserting the appropriate heterocyclic groups. The porphyrin macrocycle can be subjected to various modification to yield different porphyrinoids. One of them is expanded porphyrins which displays distinct structural and electronic properties. As the ring size increases, the topological properties exclusively alter by adopting non-planar geometry and as a result it affects its reactivity and redox properties.

The second chapter discusses the process of synthesis and characterization of contracted [8] and [16] isophlorin utilizing two distinct precursors/strategies. Instead of using conventional condensation methods, a coupling reaction was employed i.e. McMurry reaction which gives moderate yields. In the first strategy a stepwise coupling reaction resulted in the symmetric [8] dithia-cyclooctatetraene, whereas in the second strategy, the one step coupling reaction yields the structural isomers of asymmetric cyclooctatetraene and besides this a higher analogue is also obtained i.e. [16] tetrathia isophlorin.

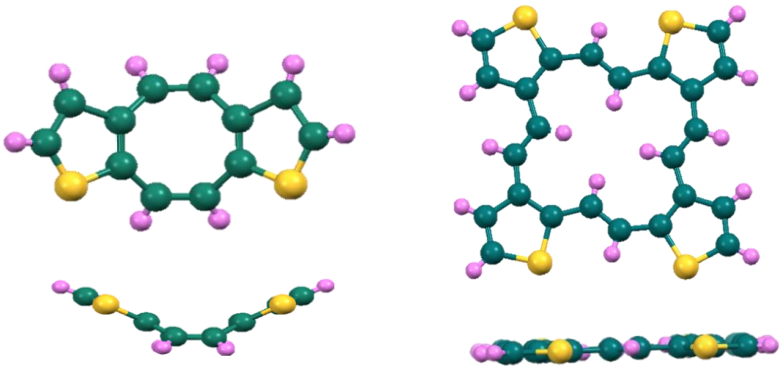

As these macrocycles account for 4nπ antiaromatic macrocycles, it is expected to show paratropic ring current. However, their ^{1}H NMR analysis revealed the absence of ring current in both the macrocycles, attributed to the absence of global conjugation and fluxional nature of ethylene protons in solution state. Further, its fluxional character could not be restricted and even at lower temperatures. The single crystal X-ray diffraction studies verified that [16] isophlorin has a planar structure, while [8] isophlorin had the expected tub shape. The electrochemical study indicated that these macrocycles are harder to oxidize compared to the typical isophlorin despite its 4nπ antiaromatic systems.

The third chapter discusses the synthesis and characterization of [34] hexaphyrin which adheres to Huckel's aromatic macrocycles. The replacement of two thiophene from the typical [30] hexaphyrin and incorporation of two thieno-thiophene unit as fused thiophene leads to the formation of [34] hexaphyrin macrocycles and maintains the aromaticity. This was achieved by utilizing the McDonald type condensation between thieno-thiophene diol and

furan/selenophene based dipyrromethene to give two distinct [34] hexaphyrin. Being an aromatic state, the biselenophene based hexaphyrin showed the substantial diatropic ring current effect whereas in bifuran based hexaphyrin exhibits the absence of diatropic ring current.

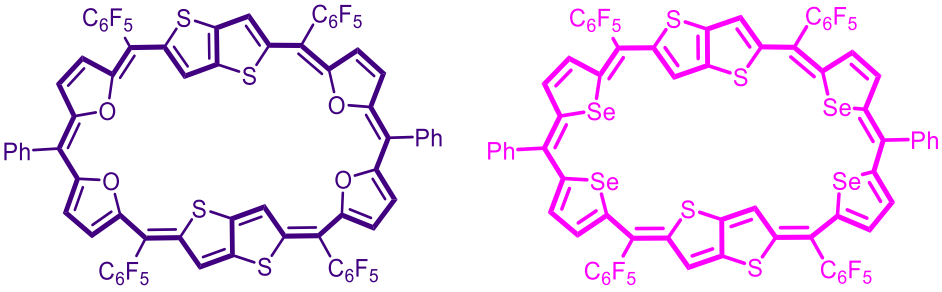

Single crystal X-ray studies revealed the molecular structure of biselenophene hexaphyrin as a nearly planar structure, indicating aromatic character of the macrocycle while the bifuran hexaphyrin exhibits the loss of planarity and adopted the twisted structure in both solution and solid states. Both the macrocycles displayed reversible ring oxidation upon the addition of oxidizing agent. All the studies suggest that the insertion of Thieno-thiophene ring significantly change the results in terms of molecular structure and redox property.

The last chapter describes the first attempts to synthesis completely core modified [24] sapphyrin along with its higher analogues and characterized in both solution and solid form. The [3+2] type condensation of an equimolar concentration of Thieno-thiophene with furan or selenophene based tripyrromethane diol.

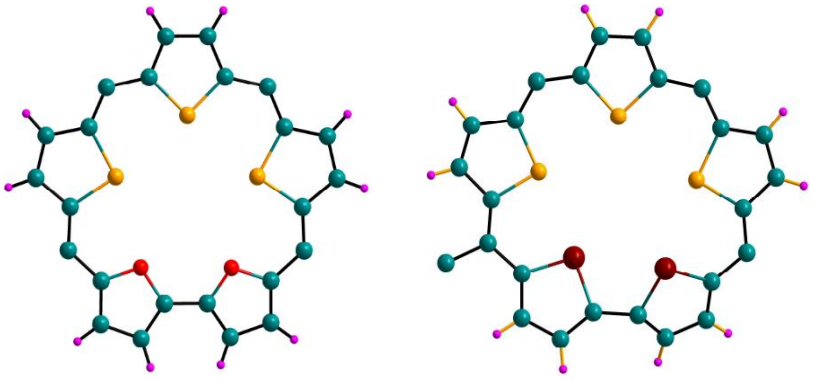

The ^{1}H NMR spectrum of both sapphyrin showed diverse ring current effect and single crystal X-ray study also supported to these results. Furan based sapphyrin exhibited the strong paratropic ring current effect whereas in the selenophene based sapphyrin showed the absence

of ring current effect. These results are attributed to the effect of size of oxygen and selenophene atoms, which force to adopt different topology. Because of its antiaromatic nature, it experiences a two-electron ring oxidation process to form the [22] aromatic dicationic species. This has been confirmed by using ^{1}H NMR spectroscopy and verified via computational investigations. The next analogue of both furan/selenophene based [48] decaphyrin was isolated in good yields. The X-ray diffraction study revealed that these macrocycles lost their planarity and acquired a twisted figure-of-eight shape in both solution and solid states. Due to this non-planar geometry, they are devoid of any significant ring current in the macrocycle and hence it becomes non-antiaromatic in nature. Similar to the [24] congeners, both the decaphyrin molecules likewise showed a reversible two-electron oxidation process, resulting in the formation of their respective dicationic species. This has been validated using electronic absorption and electrochemical experiments.

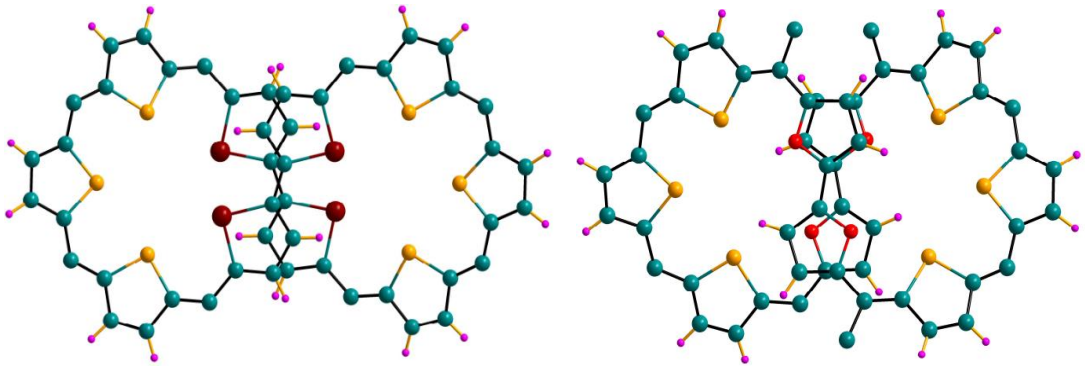

The highest analogue in the series, [72] pentadecaphyrin was obtained in very poor yields. The molecular structure of selenophene based macrocycle revealed a symmetric three pentaphyrin pockets as three folded structure and each pocket possessing the C_2-axis of symmetry It didn't display any ring current, confirming the macrocycle is non-antiaromatic. The electronic absorption analysis revealed a reversible process of two-electron ring oxidation of [72] macrocycles, forming the corresponding [70] dication species. This was observed as a red-shifted absorption in the near-infrared (NIR) region.

Publications

- Ramesh N. Hiremath, Hosahalli S. Udaya and Venkataramanarao G. Anand, Ring Contracted 16π Tetrathia Core-Modified Isophlorin, *ChemRxiv*, 2024, DOI: 10.26434/chemrxiv-2024-w1s7f.

Chapter 1

Introduction

I.1 Introduction

I.1.1 Annulene to Porphyrin

Annulenes are fully conjugated monocyclic hydrocarbons composed of alternate single and double bonds. The number within the square brackets represents the number of π-electrons present in the conjugated route. One of the simple and best example is benzene which is considered as a [6]annulene.[11,2] The [8]annulene, known as the cyclooctatetraene, displayed full cyclic conjugation in the carbon ring; however, its characteristics were notably different from those of benzene. Hückel's rule aids in understanding the characteristics of cyclic conjugated molecules. Conjugated systems with a total of (4n+2)π electrons display aromatic properties, as seen in the case of benzene. On the other hand, molecules that have 4nπ electrons and hence do not adhere to Huckel's (4n+2)π rule for aromaticity were previously referred to as "pseudoaromatic."

Nevertheless, both theoretical and experimental studies suggest that, in some instances within the cyclic systems of the 4nπ series, the delocalization of the π-electrons significantly reduces the molecule's stability. This is in contrast to the stability typically associated with aromaticity. Due to this observation, R. Breslow[3] coined the term “antiaromaticity” in 1965 to characterize such systems. Significant progress in the study of annulenes did not occur until the late 1950s and 1960s, when Sondheimer and his colleagues synthesised a range of larger-ring annulenes such as 12, 14, 16, 18, 20, 24 and 30 carbon atoms. Several types of annulenes from both the 4nπ and (4n+2)π system were successfully synthesized and thoroughly characterized using NMR spectroscopy.[1] (figure – I.1)

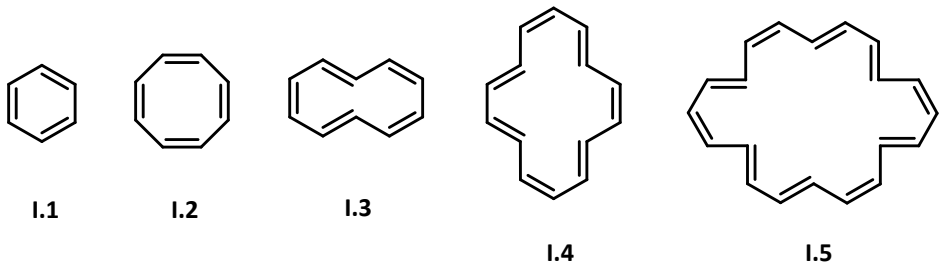

Figure I.1: Annulenes possessing 4nπ or (4n+2)π electrons.

An understanding of interplay between annulenes and aromaticity is crucial in organic chemistry for predicting the stability and behaviour of these cyclic, conjugated systems. The chemical properties such as stability, reactivity and the delocalization of π-electrons, spectroscopy particularly NMR and magnetic anisotropies are of significant interest. The

examination of these properties has played a pivotal role throughout the history of annulene chemistry.

The phenomenon of π-electron delocalisation allows for the formation of either a diamagnetic ring current or a paramagnetic ring current in the presence of a magnetic field. Proton NMR spectroscopy analysis detects the presence of diamagnetic or paramagnetic ring currents. In case of aromatic annulenes, it shows diatropic ring current effects, wherein the inside protons experience shielding, while the outside protoos undergo deshielding. In contrast, annulenes with 4nπ electrons shows opposite results and expected to sustain a paramagnetic ring current. As the number of sp^2 carbon atoms increases, ring size will increase therefore it undergoe conformational flexibility, and as a result, the molecule gains structural flexibility, allowing it to adopt many stable conformers. When subjected to elevated temperatures, the ^{1}H NMR spectra of all examined annulenes, which are relatively stable, consistently exhibit a singlet. In order to limit this conformational flexibility and explore the ring current effects on its protons, the observations were specifically conducted at low temperatures.[4]

The ^{1}H NMR spectra of aromatic annulene systems such as [14]annulene, [18]annulene, and [22]annulene recorded at lower temperatures exhibited characteristics typical of diatropic ring current. These include outer proton signal resonated at low a field δ 10.61, 12.99 and 10.4-11.2 ppm, respectively and inside protons signals at up filed δ 2.12, 0.72, and 0.35-1.4 ppm, respectively.[5] However, the low-temperature spectra of the antiaromatic annulene systems [16]annulene and [24]annulene display a paratropic ring current. This is primarily observed in the peripheral proton signals at high field, with chemical shifts of -0.56 and -2.9 to -1.2 ppm, respectively. Additionally, inside proton signals are observed at down field with chemical shifts of 4.67 and 5.27 ppm, respectively.[6,7] An increase in the ring size leads to inherent conformational flexibility, disrupts the conjugation pathway and causes a gradual weakening of ring current in the systems. Subsequently the higher annulenes with 28π electrons or more were synthesised; however, recording their the ^{1}H NMR spectra was challenging to obtain since the compound had extremely low solubility in commonly used organic solvents.

The synthesis of annulenes has been on the rise as researchers dig into the concept of aromaticity. One of the effective strategies for imparting rigidity to annulenes is by bridging the rings through alkyl groups to promote π-electron delocalization. Smaller annulenes exhibit non-planar structures as a result of steric interactions between protons located within the molecule while larger annulenes grapple with conformational flexibility to maintain sufficient

planarity, essential for the occurrence of π-electron delocalization.[1,2,8] Internal 1,6-two hydrogen atoms of [10]annulene **I.3**, undergo steric interactions to avoid it, possibly by replacing both the hydrogen atoms and connected by methine group to become 1,6-methano[10]annulene **I.7** (figure – I.2).[8] Hence, [10]annulene becomes a planar and rigid structure to follow the Huckel's aromatic state.

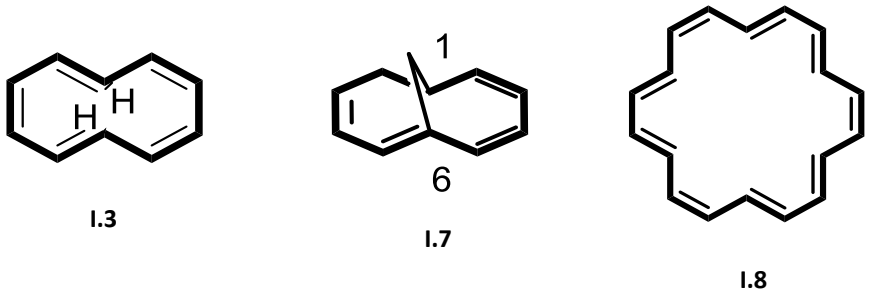

I.3 **I.7** **I.8**

Figure I.2: Structures of [10], 1,6-methano[10]annulene and [18] annulene

[18]annulene **I.8** and 1,6-methano[10]annulene are classical instances of Huckel's (4n+2) annulenes (figure – I.2). Both of these instances meet the requirements for aromaticity in terms of their spectral and structural characteristics. However, the rigidly bridged [10]annulene shows benzenoid properties and [18]annulene, due to its conformational flexibility becomes highly reactive. Hence it undergoe polymerization rather than electrophilic substitution reactions.[9] There are several bridged [18]annulenes reported as stable aromatic compounds that have already been amenable to synthesis. Numerous bridged [18]annulene have been reported as stable aromatic compounds and have been successfully synthesised.

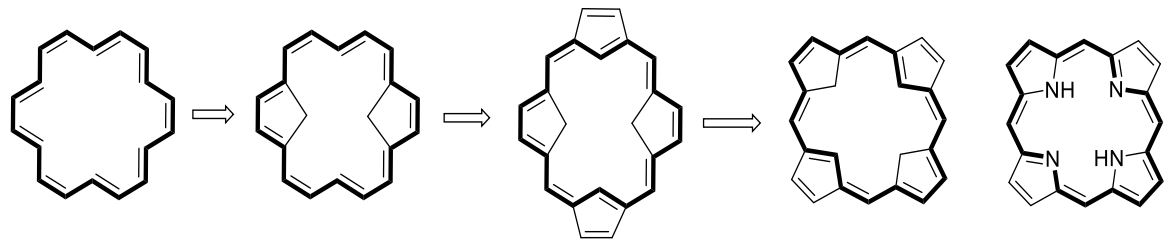

I.8 **I.9** **I.10**

Scheme I.1: Conversion of [18] annulene to Porphyrin

One of the effective methods of maintaining planarity while introducing rigidity involves the sequential incorporating of two inside CH_2 bridges and two outside CH=CH bridges in **I.8**. This process results in the formation of bridging [18]annulene or tetracyclopentadienic hydrocarbon **I.9**, which can be considered as the parental structure of porphyrin, **I.10**, (scheme – I.1). Especially in medium-sized annulenes, such as [10] and [14]annulenes, the introduction

of bridge atoms aids in resolving the congestion created by inside hydrogen atoms, resulting in planarity and aromaticity. Vogel and his colleagues have effectively demonstrated the effectiveness of this notion by synthesizing and characterizing 1,6-imino[10]annulene and syn-1,6-diimino[14]annulenes.[10]

I.2 Isophlorin

Isophlorin is a 20π macrocycle comprising of four pyrrole units. In 1960, R. B. Woodward hypothesised the concept of isophlorin. It was identified as an unstable intermediary in the synthesis of chlorophyll.

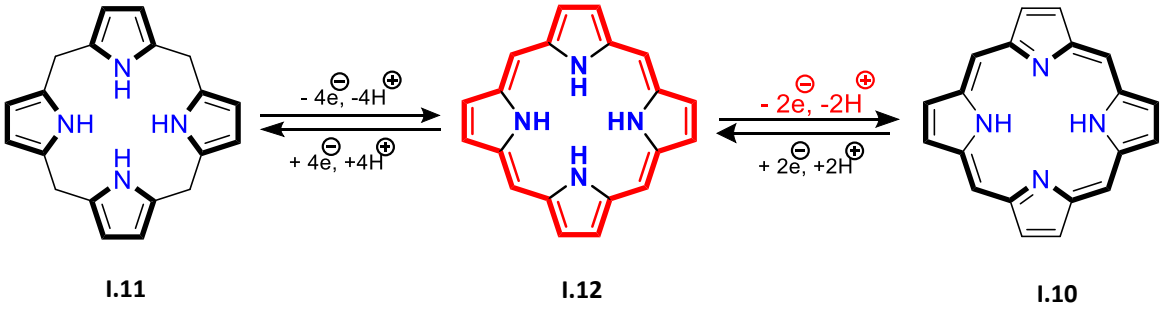

Scheme I.2: Synthesis of 18π porphyrin (**I.10**) from porphyrinogen (**I.11**) through transient 20π Isophlorin (**I.12**).

The acid catalysed condensation of aldehyde with four pyrrole units, results in the formation of an unconjugated tetrapyrrole porphyrinogen **I.11**. Initially, porphyrinogen undertakes a four-electron oxidation to generate the intermediate isophlorin, **I.12**. Afterwards, isophlorin experiences a two-electron oxidation, resulting in the formation of aromatic 18π porphyrin, **I.10**. The conversion of porphyrinogen **I.11**, to porphyrin undergoe through an intermediate 20π isophlorin **I.12**. Isophlorin shares structural similarities with porphyrin but differs in its conjugation pathway, where all electrons flow through only carbon skeleton while in porphyrin, sp^2 hybridized nitrogen of the pyrrole also participate in the conjugation. This change in conjugation pathway makes remarkable difference in its electronic and magnetic properties. There has been no experimental confirmation of a planar tetrapyrrolic isophlorin since it is inherently unstable under ambient conditions (scheme – I.2).[11–13]

The 20π isophlorin falls in the category of Huckel's 4nπ systems, while the 18π porphyrin follows Huckel's (4n+2)π systems. The unstable nature of isophlorin is partially attributed to steric interactions caused by the internal four hydrogens within the core of the macrocycle, leading to a non-planar geometry.[14] Consequently, it undergoe a quick two electron oxidation to achieve a stable and planar 18π aromatic porphyyrin under ambient conditions. This

insatbility of antiaromatic systems poses challenges in the isolation and stabilization of such species. Multiple attempts have been made to synthesize a stable isophlorin through different modifications to study the intriguing properties of stable antiaromatic systems.

I.3 Porphyrins and its structural variants

Isophlorin's unstable nature is of synthetic interest to researchers to obtain a stable antiaromatic isophlorin. Numerous structural variants of porphyrin macrocycles emerge through modifications either from the core of the porphyrin or periphery, yielding a range of conjugated macrocycles (figure – I.3). The porphyrin ring can be subjected to various modification to yield different porphyrinoids: a) by removing one of the meso-carbon atoms to generate a corrole skeleton **I.14**, having a direct pyrrole-pyrrole link;[15] b) inverting one pyrrole ring, resulting macrocycle termed as "N-confused porphyrin" **I.15,**[16] c) by replacing the one or more nitrogen atom of pyrrole with chalcogen based hetero atom like O, S, Se, Te, P and Si etc., forming "core-modified porphyrins" **I.13**,[17] d) to increase the π-electron conjugation, one can either add more heterocyclic rings or introduce additional meso-carbon atoms into the porphyrin skeleton. This can be done while maintain the same number of heterocyclic rings in the parent porphyrinoid. The result is a new category of macrocycles known as "expanded porphyrins" **I.11**.[15–18]

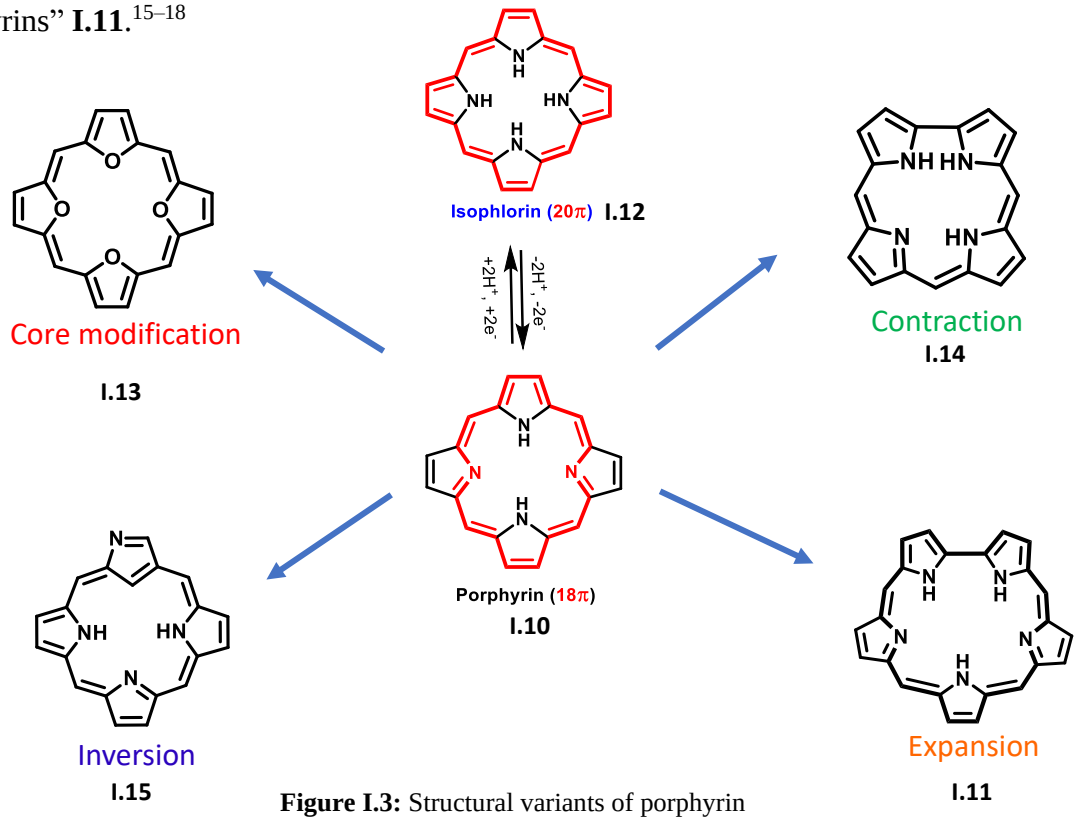

Figure I.3: Structural variants of porphyrin

Expanded porphyrins have diverse applications in multiple domains, including as sensitizers for photodynamic therapy (PDT), contrasting agents in magnetic resonance imaging (MRI), and models for studying aromaticity. This has appealed to many researchers to study the synthesis, characterization, structure, as well as spectroscopic and electrochemical properties of diverse expanded porphyrins. Expanded porphyrins, with their large ring size and a more significant number of donor atoms, offer a favourable coordination environment for forming a wide range of coordination complexes.

I.4 Confused Porphyrins

A confused porphyrin is a structural isomer of porphyrin in which one or more hetero atoms are situated outer side of the porphyrin ring. In simple words, it involves modifying the connectivity between pyrrole and meso-carbon atoms from the usual -2,5- to -2,4- carbons of the heterocyclic ring. More specifically, there has been increased research focus on N-confused porphyrins. It has attracted significant interest in synthetic chemistry due to their unique structural and versatile coordination chemistry with various metal ions.

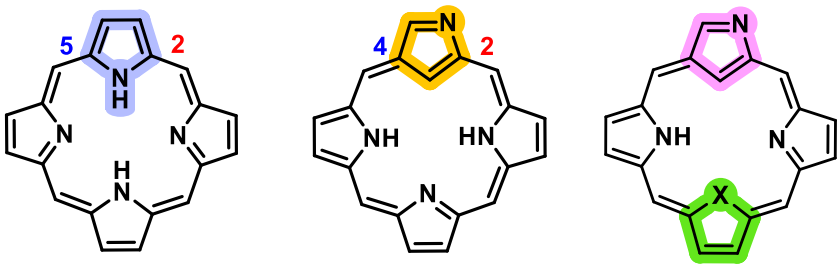

Figure I.4: Structural illustartions of porhyrin, N-confused porphyrin, **I.15**, and core modified NCP, **I.16**.

In 1994, Latos-Grazynksi et al. and Furuta et al. separately discovered the emergence of N-confused porphyrin 5,10,15,20-tetraaryl-2-aza-21-carbaporphyrin (figure - I.4).[19,20] The alpha-beta linkage of an inverted pyrrole forms this porphyrin. It has a CH atom on the inside and a nitrogen atom on the outside. The peripheral nitrogen atoms in N-confused porphyrinoids function as binding sites for various cations, anions, and neutral substances, forming the supramolecular building blocks. The chemistry of NCP has received significant attention from studies since its beginning, leading to the discovery of various novel confused porphyrinoids with unique metal coordination characteristics. Substituting the pyrrole with different heteroatoms like thiophene, selenophene, and furan has also been documented by the

alteration of the macrocyclic core **I.16** (figure - I.4). An example of a core-modified NCP was initially documented by three separate research teams, and these complexes exhibit atypical metal bonding.[21–23]

In addition to NCP, exploration has extended to employ other heterocycles such as selenophene, furan, and thiophene. This class of macrocycles termed as heteroatom-confused heterophyrins.[21] Chandrashekar and coworkers reported a series of N-confused porphyrins having a thiophene, selenophene and furan with 20-32% yields.[23]

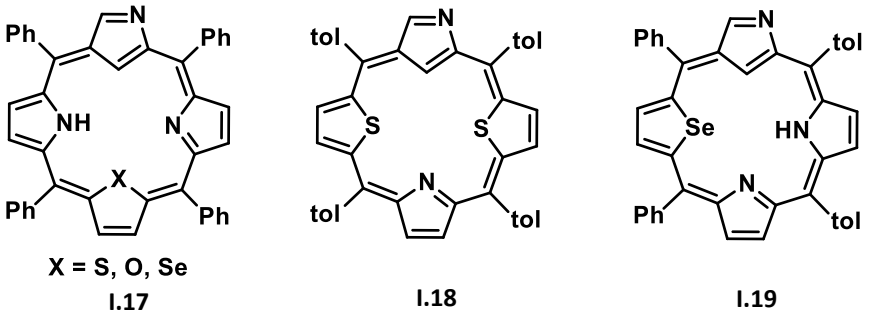

Figure I.5: Structural illustrations of core modified N-confused porphyrin **I.17**, **I.18**, and **I.19**.

The same group extended their work and synthesised 5,10,15,20-tetraaryl-2-aza-21-carba-22-selenaporphyrin **I.19**, constructed by the exchange of a nitrogen atom and a methine carbon atom of the cis-pyrrole ring (figure - I.5).[22] This was achieved by condensation of 2,5-bis(phenylhydroxymethyl)selenophene and 5,10-bis(p-tolyl)tripyrrane, catalysed by $BF_3.OEt_2$ and followed by addition of *p*-chloranil as oxidizing agent to obtain the macrocycle in 1% yields. In the subsequent year, the same group reported the first diheteroporphyrin with inverted pyrrole ring known as dithiaporphyrin **I.18**, this was synthesised through acid catalysed condensation between pyrrole and 2,5-bis(p-tolylhydroxymethyl)thiophene subsequently oxidation with *p*-chloranil.[24]

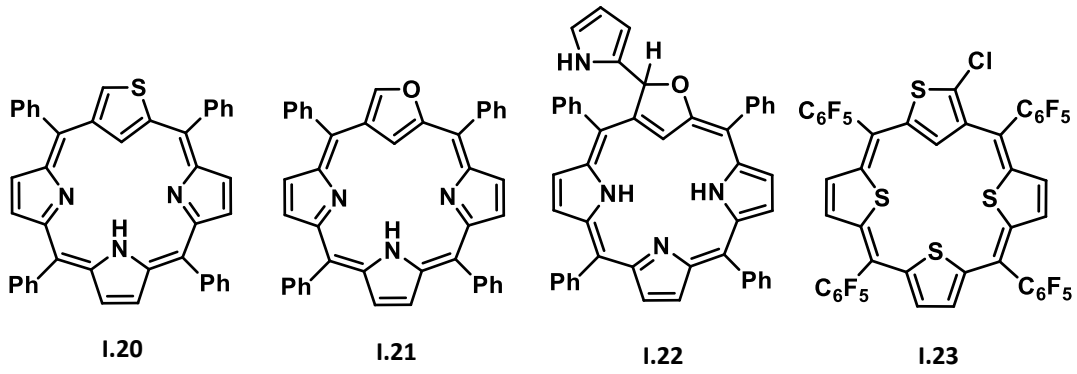

Figure I.6: Heteroatom-confused heterophyrins **I.20**, **I.21** and **I.22** and core modified S-confused porphyrin.

In 1999, Latos-Grazynski and coworkers reported the synthesis of the first heteroatom confused heterophyrin, specifically S-confused porphyrin, known as 5,10,15,20-tetraphenyl-2-thia-21-carbaporphyrin I.20. This compound was synthesised through either a one-pot, two-step condensation reaction of 2,4-bis-(phenylhydroxymethyl)thiophene with benzaldehyde and pyrrole, or through the condensation of 2,4-bis-(phenylhydroxymethyl)thiophene with 5,10-diphenyltripyrrane subsequently oxidation with DDQ or *p*-chloranil.[25,26] Pawlicki and Latos-Grazynski reported another isomer of heteroatom confused porphyrin for example O-confused porphyrin **I.21**, and utilized the same reaction conditions previously employed for the synthesis of S-confused porphyrin. However, they were not able to isolate the anticipated product and instead found that an additional pyrrole was added which leads to the formation of **I.22,** with yields of approximately 10%.[27]

In a tetrathia isophlorin one of the thiophene can be inverted and connected through α,β-linkages. Hence it alters the conjugated pathway to 20π network rather than 18π systems. In 2017, Anand and group reported a completely core modified confused porphyrinoids where they replaced all four pyrrole rings of NCP with thiophene leading to A novel class of inverted isophlorin, referred to as S-confused Isophlorin, has been developed **I.23**, (figure - I.6).[28] This resembles Lash and coworkers reported the first example of novel carbaporphyrinoid system where a pyrrole nitrogen itself is connected to a meso-carbon atom and its termed as Neo-confused porphyrin. This system can be formally called as 1-aza-21-carba-1H,23H-porphyrin **I.26,** and still retain its aromatic character. The [2+2] MacDonald type condensation of **I.24,** with dipyrrylmethane **I.25,** was performed in presence of *p*-TSA in Methanol/DCM followed by oxidation with DDQ (scheme -I.3).[29]

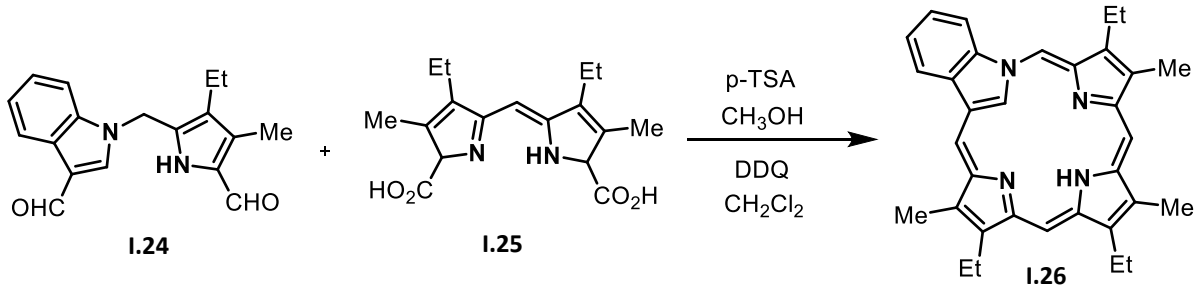

Scheme I.3: Synthesis of Neo-confused porphyrin **I.26**.

Porphycene was the first synthesized constitutional isomer of porphyrin. It is structurally related to porphyrin and it consists of two pyrrole rings connected by methine bridges and rest two pyrrole rings through ethylene bridges resulting in a squarely arranged compact porphyrin. In 1986, Vogel and coworkers prepared the first porphycene **I.27**, consisting of two bipyrrole

subunits linked by two double bonds. The resultant macrocycle is planar and aromatic, formally known as [18]porphyrin-(2.0.2.0.) (figure - I.7).[30] obtained by the intermolecular reductive coupling reaction of bipyrrole dialdehyde. The absorption spectrum of porphycene gives rise to characteristic strong absorbance band, the B-band (Soret) and Q-bands in the red shifted portion of the visible spectrum. Same group used identical strategy with either bifuran or bithiophene dialdehydes to synthesis core modified tetra-oxa and tetrathia porphycenes.

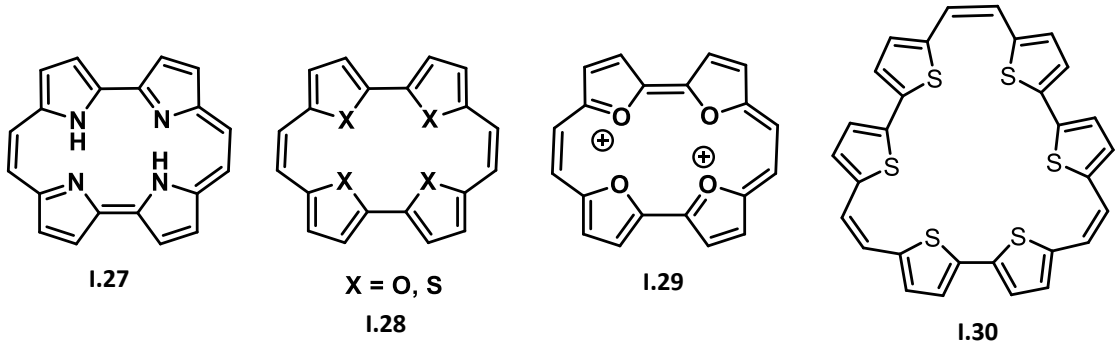

Figure I.7: Structural illustrations of porphycene **I.27**, tetrathia/oxa porphycene **I.28**, their dication **I.29**, and hexapthiaporphycene **I.30.**

In contrast to the parent 18π porphycene, the tetraoxa and tetrathia porphycenes **I.28**, accounts for 20π electrons and are prone to two electron redox reactions to give the 18π dication species **I.29**, and the 22π dianionic species respectively.[31,32] Cava and coworkers utilized the similar synthetic methodology with the bithiophene dialdehyde and terthiophene dialdehyde to yield hexathiophene expanded porphycenes **I.30**, (figure - I.7).[33]

I.5 Core-Modified Porphyrin

Core-modified porphyrins refer to a class of porphyrin derivatives where alterations have been made in the central macrocyclic core structure. These alterations consist modified pyrrole rings or introduction of different hetero atoms, resulting in variations form the traditional porphyrin structure. In the continuous quest for synthesizing a stable pyrrole derivative antiaromatic isophlorin is through a systematic core alteration of a porphyrin. This involves replacing individual pyrrole rings with different chalcogen based heterocycles, such as thiophene or furan, sequentially.[34] Until replacement of two pyrrole, it doesn't change in the 18π electronic framework in a porphyrin. However, when three or all four pyrroles are replaced by thiophene or furan, the conjugated path shifts from an 18π to a 20π network with a slight alteration in ring size. These replacements avoid the steric interference in the centre of cavity. The 20π isophlorin **I.31**, represents the electrons flow through the peripheral carbons even in presence of pyrrole.[35]

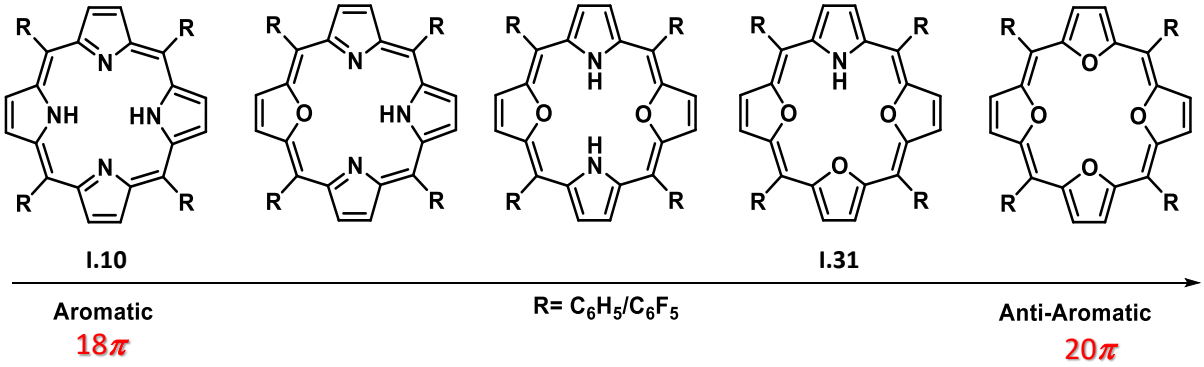

Figure I.8: successive replacement of pyrrole transforms 18π Porphyrin to 20π Isophlorin.

At low temperatures, its ^{1}H NMR spectrum showed high field chemical shift values in the region of δ 3-1.8 ppm for the β-protons of the heterocyclic rings, whereas the pyrrolic NH resonance was observed significantly downfield at δ 29.2 ppm and these values clearly reflects the strong antiaromatic nature of the macrocycle. Anand and coworkers synthesised a completely core modified 20π tetraoxisophlorin with meso-pentafluorophenyl substituents **I.32**, (figure – I.8).[36] An acid-catalysed intermolecular condensation was carried out on a pentafluorophenyl furfural compound, followed by oxidation. The macrocycle was purified using column chromatography, and no indication of instability was observed under ordinary conditions. Its proton NMR spectrum showed, a singlet at δ 2.49 ppm for the β-proton of the furan rings, indicating the highly symmetrical structure. The large upfield chemical shift value indicated the paratropic ring current effects inherent to a 4nπ cyclic system. The X-ray diffraction analysis of **I.32,** revealed a planar macrocycle, with all the furans positioned in the same plane as the macrocycle's average plane.

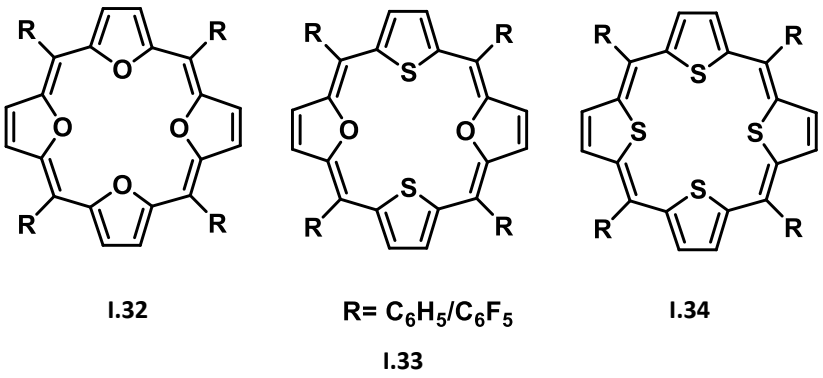

Figure I.9: Chemical structures of Core-modified 20π Isophlorin

Same group modified the reaction protocol to synthesize dithia-dioxa-isophlorin **I.33**. It was achieved by condensing furan with thiophene diol in dichloromethane, followed by the addition

of $FeCl_3$ and the resulting macrocycle accounts for 20π electronic network. Similar to **I.32**, it also exhibited β-protons resonance in the upfield region at δ 3.37 and 3.33 ppm. The X-ray diffraction studies showed a planar conformation with slight geometrical variation in the macrocyclic core due to unequal or increase in the distance between the diagonally opposite oxygen atoms. Hence, it forces the macrocycle to transform the geometry form a typical square shape of **I.32**, to rectangular **I.33**, (figure – I.9).

Unlike the planar and antiaromatic characteristics of **I.32** and **I.33**, the tetrathia isophlorin, **I.34**, was discovered to be non-planar and non-antiaromatic. The ^1H NMR spectrum displayed a singlet at δ 6.19 ppm, is significantly shifted towards the downfield. X-ray diffraction study revealed a non-planar structure, which can be attributed to steric effects caused by the large sulphur atoms. These effects cause a diagonally opposite thiophene molecule to deviate from the average plane of the macrocycle. As a result, it reduces the π-conjugation and causes a loss of antiaromaticity due to the structural changes.[37]

I.6 π-Expanded Porphyrinoids

Over the last three decades, there has been an intense exploration in the chemistry of expanded porphyrins which are higher homologues of parent porphyrin. The simple definition of an expanded porphyrin is a "porphyrinoid larger than a porphyrin".[38,39]

These expanded systems display distinct structures, coordination chemistry, electronic properties, and reactivities compared to conventional porphyrins. Sessler and Seidel in their 2003 review, proposed a definition of expanded porphyrin as "macrocycles that contain pyrrole, furan, thiophene, or other heterocyclic subunits linked together either directly or through one or more spacer atoms in such a manner that the internal ring pathway contains a minimum of 17 atoms".[39] Unlike the porphyrins, the chemistry of expanded porphyrins remained undiscovered and started only after the serendipitous discovery of sapphyrin by R. B. Woodward in 1966. However, the full report on this discovery was not published until 1983.[40,41] In early stages of 1966-1990, Johnson and coworkers identified sapphyrin **I.11,** as a [22]pentaphyrin(1.1.1.1.0) as a dark blue coloured solid and penatpyrrolic macrocycle having four bridging methine groups and a bipyrrole group which obeys Huckel's rule of aromaticity (figure – I.10).[42]

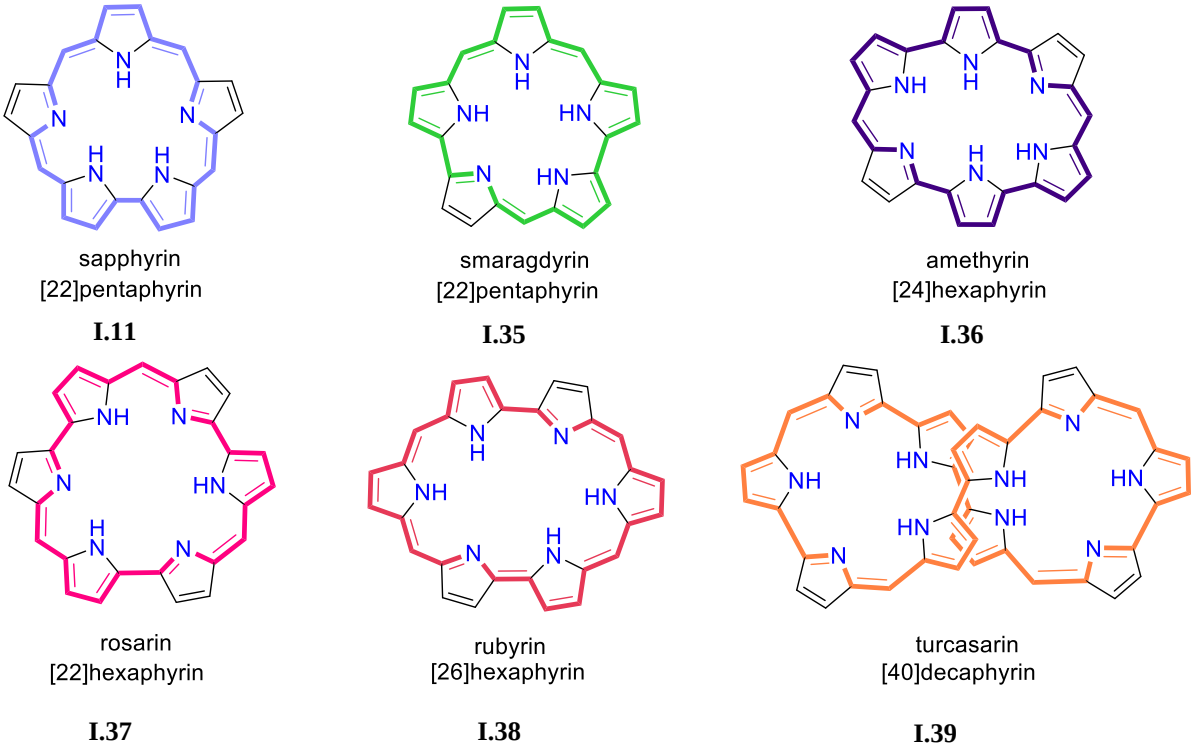

Figure I.10: Structures of expanded porphyrins.

In 1995, Sessler and coworkers reported a [22]pentaphyrin macrocycle having five pyrrolic or heterocycles containing two direct heterocycle links and three meso-carbon centres known as smaragdyrins **I.35**. Due to synthetic challenges and their inherent instability, smaragdyrin has not been much explored.[43] Expanded porphyrins containing one or more bipyrrole unit present were identified such as [24]- hexaphyrin(1.0.0.1.0.0) (amethyrin) **I.36,** [22]-hexaphyrin(1.0.1.0.1.0) (rosarin) **I.37,** [26]hexaphyrin(1.1.0.1.1.0) (rubyrin) **I.38,** and [40]dodecaphyrin(1.0.1.0.0.1.0.1.0.0) (turcasarin) **I.39,** have been the subject of research in the past twenty years (figure – I.10).[44–48]

In an expanded isophlorin the π-delocalized macrocycle synthesised by connecting the heterocyclic unit with bridging meso-carbon atoms the electronic π-circuit flows only through the peripheral carbon atoms. The absence of pyrrole units can prevent the rapid interconversion of amine to imine. Osuka and coworkers synthesised a series of meso aryl substituted expanded porphyrins that were synthesised by utilizing Rothemund-Lindsey conditions.[49,50] One pot sythesis of commercially available pyrrole and pentafluorobenzaldehyde in acidic conditions yielded a series of macrocycles such as prophyrin, N-fused pentaphyrin, hexaphyrin, heptaphyrin, octaphyrin, nonphyrin, decaphyrin and higher analogues.

Anand and coworkers employed similar reaction conditions and reported the one pot synthesis of macrocyclic oligothiophenes having a series of expanded isophlorinoids from four membered to sixteen membered macrocycles and these macrocycles exist between 4nπ and (4n+2)π electrons. (figure – I.11).[51] The same group synthesised expanded 30π macrocycles with different heteroatoms by using the identical strategy. Thiophene, furan, and selenophene were condensed with the thiophene diol to give the respective 30π expanded hexaphyrins (figure – I.12).[52]

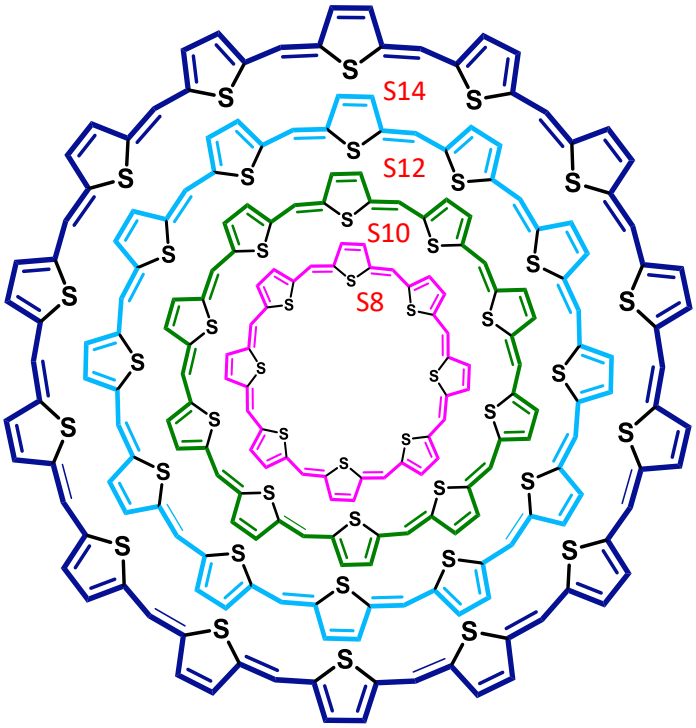

Figure I.11: Structures of aromatic and antiaromatic expanded isophlorins.

In the 30π hexaphyrins **I.40**, and **I.41**, macrocycles arranged in a rectangular shape. In these macrocycles, the thiophene and selenophene rings located diagonally opposite one other are reversed, resulting in a decreased geometry of the macrocycle. By substituting three thiophenes by three furans in **I.40**, it influenced to alternate ring inversions and the proton NMR spectrum of **I.42**, displayed the two singlets at δ7.99 and 1.87 ppm corresponding to β-protons of the heterocyclic ring and similar observation of **I.43**, showed two singlets at δ 7.85 and 2.5 ppm.[53] Again, the same group found an alternate way to synthesize similar 30π expanded isophlorins carried out by acid catalysed condensation of 2,2'-(pentafluorophenylmethylene)dithiophene/difuran with either thiophene diol or selenophene diol. The resulting hexaphyrin **I.44** and **I.45** macrocycle having four furan rings and two of them which are positioned diagonally opposite direction were inverted.

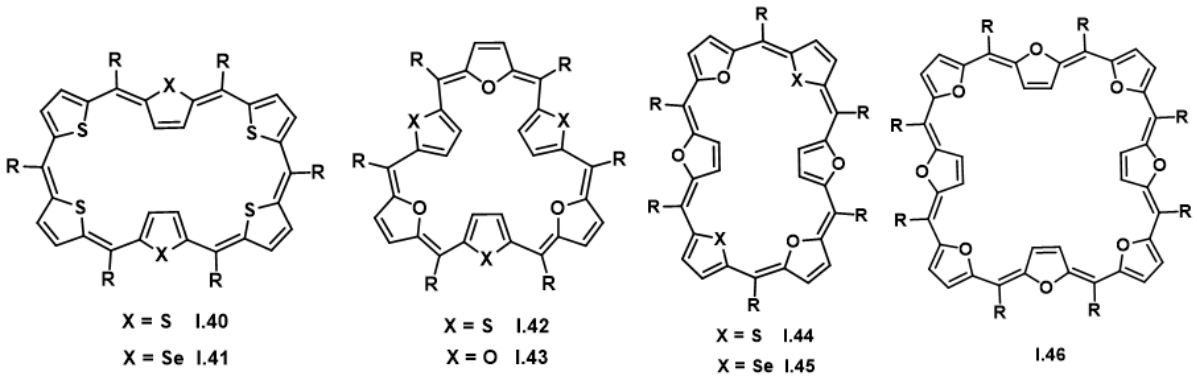

Figure I.12: Structures of 30π hexaphyrin **I.40 - I.45**, and 40π octaphyrin **I.46**.

The proton NMR spectrum of all these hexaphyrin macrocycles showed diatropic ring current effects consistent with (4n+2)π aromatic character.[53] This resulted in upfield and downfield shifts for the inside and outside protons of the macrocycle respectively. A one pot synthesis of furan and pentaflurobenzaldehye in acidic conditions yielded a 30π hexaphyrin and higher analogue 40π octaphyrin. Both showed contrasting ring current effects and attributed to aromatic and antiaromatic character of respective macrocycle. The X-ray diffraction study of **I.46**, revealed that it is an extended version of **I.43**, accommodating alternate furan ring positioned in the macrocycle.[53]

When aromatic benzene was introduced into a porphyrin framework, its aromaticity typically hampered the global conjugation of the macrocycle. In 2001, Latos-Grazynski reported the tetraphenylbenziporphyrin **I.47**, where a benzene in tripyrrole-like precursor was connected through 1,3-positions. As a result, the global conjugation could not be attained and hence loses aromaticity to become non-aromatic system. When the connectivity of benzene was modified from 1,3 to 1,4-position, an aromatic benzi-porphyrin was achieved and its protons NMR spectrum revealed the existence of a diatropic ring current.[54]

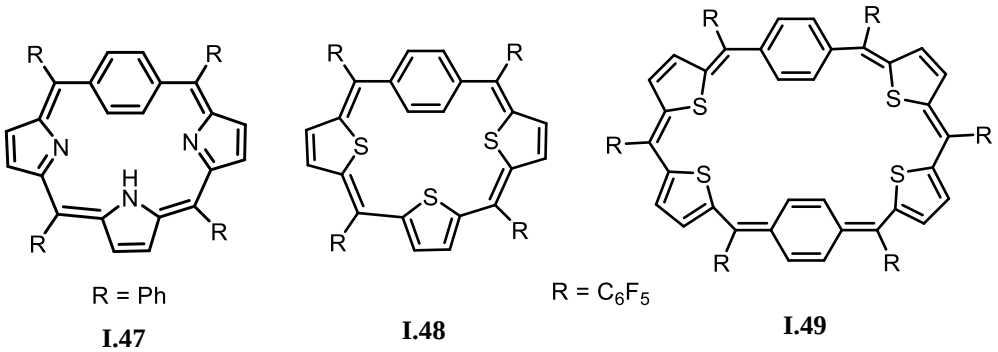

Figure I.13: Structures of benzene incorporated 18π, 20π, and 30π isophlorinoids

For more exploration and understanding the effect on the stability of non-pyrrolic expanded isophlorin, Anand and coworkers synthesised benzene incorporated isophlorin, by replacing the two thiophene rings in **I.40,** with benzene units. The synthesis of this macrocycle can be achieved using two methods: the condensation of thiophene with a 1,4-benzene diol or the condensation of 2,2'-(pentaflouorophenylmethylene)-thiophene with a 1,4-benzene diol. Both methods result in the formation of a mixture of macrocycles **I.48** and **I.49**.[55]

In case of dibenzo 30π isophlorin, two types of the benzene rings are plausible and one of them adopted a quinone-like structure while the second one exists in benzenoid from to sustain the 30π aromatic character. On the other hand, **I.48**, did not show neither diatropic nor paratropic ring current effects and therefore appears to be benzenoid in nature (figure – I.13).[55] In addition, the incorporation of additional heterocyclic rings serves to extend the π-conjugated network of isophlorin, addition of an extra meso-carbon bridge can alter π electron framework and ring current effect.

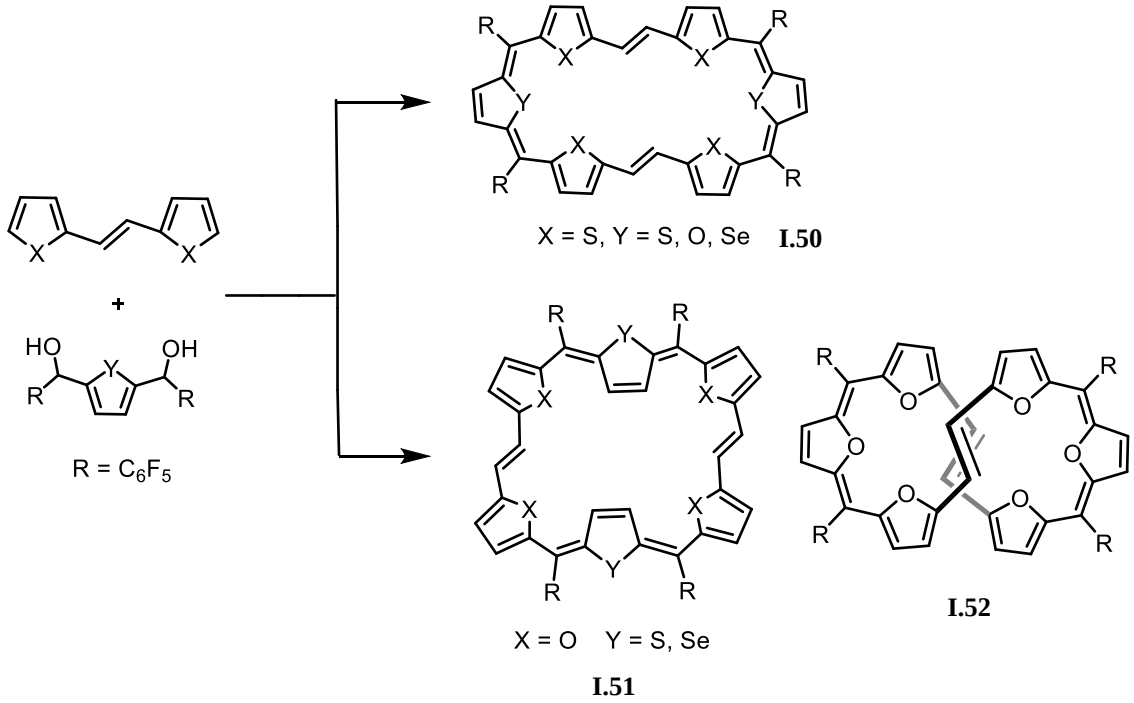

Scheme I.4: Synthesis of ethylene bridged 32π Expanded Isophlorinoids

There are only very few examples that have been reported and offers a wide scope to explore this chemistry. With this regard, Anand and coworkers synthesised a different derivative of ethylene bridged 32π expanded isophlorin. The 30π expanded hexathia isophlorin **I.40**, can be modified by adding two meso-bridges. This can be done using the acid-catalyzed condensation of bis-thiophene ethylene or bis-furan ethylene with appropriate diols of

thiophene/furan/selenophene, followed by in situ oxidation (scheme – I.4).[56,57] As expected, adding two more meso-carbons changed the aromatic 30π macrocycle into the antiaromatic 32π expanded isophlorin. The proton NMR spectra for **I.50** and **I.51**, revealed the expected paratropic ring current effect. However, **I.52**, exhibited absence of ring current effects. Further supported by X-ray diffraction analysis, the rectangular geometry and squarish framework were identified for **I.50**, and **I.51**, respectively. An unexpected twisted conformation was observed for **I.52**, and therefore didn't show ring current effect.

I.7 Redox Chemistry

Porphyrin and its derivatives are very well known for its redox active nature. Most of the chemical reactions proceed through redox reactions. Proton Coupled Electron Transfer (PCET) and Electron Transfer (ET), are the most predominant reactions. In porphyrin macrocycles, the redox reaction is carried out by PCET, facilitated by the amine-imine interconversion and the easy protonation of imine nitrogen. According to Huckel's aromatic (4n+2)π or antiaromatic (4n)π characteristics they can be expected to undergo reversible redox transformation through two electrons and protons. The best example to understand this phenomenon is the [18] porphyrin and [20] isophlorin reversible redox reaction switch via PCET.[58]

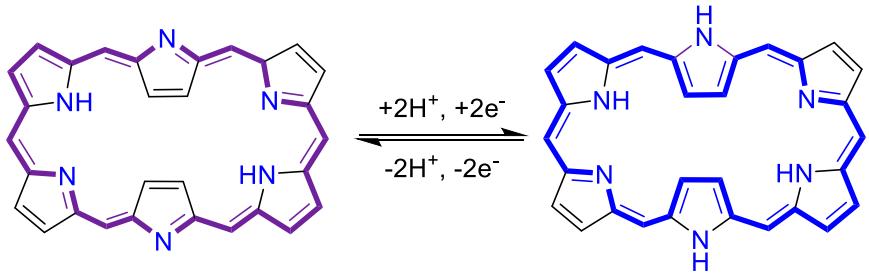

[26]hexaphyrin(1.1.1.1.1.1) **I.53** [28]hexaphyrin(1.1.1.1.1.1) **I.54**

Scheme I.5: redox study of [26] **I.53** to [28] hexaphyrin **I.54** through PCET.

Pyrrole-based macrocycles prefer to undergo PCET whereas the non-pyrrolic macrocycle favours ring oxidation reactions. In 1999, Cavaleiro and coworkers synthesised meso-substituted [26] hexaphyrin **I.53**, accounts to (4n+2)π aromatic character where the diagonally opposite pyrrole units were inverted (scheme – I.5).[59] They obtained two compounds through the column chromatography and surprisingly both compounds show same molecular ion peaks was an unexpected and novel observation. It is noteworthy, that their interconversion is through hydrogenation-dehydrogenation processes. Upon the reaction of [28] hexaphyrin **I.54**,

macrocycle with DDQ in $CHCl_3$ it turns to violet coloured compound i.e. [26] hexaphyrin **I.53**, through oxidation and it reduced back to the [28] hexaphyrin in presence of $TsNHNH_2$. The entire reaction involves interconversion from imine to amine and showcasing a PCET reaction. Core-modified expanded octaphyrin has been synthesised by Latos and coworkers containing alternate pyrrole and furan with eight meso-carbon centres. Hence, there are two distinct octaphyrin molecules that have been changed at their core. These molecules have a unique figure-eight shape and contain 36π and 38π electrons, respectively. (scheme – I.6).[60] These two octaphyrin exhibited interconvertibility through PCET redox reactions.

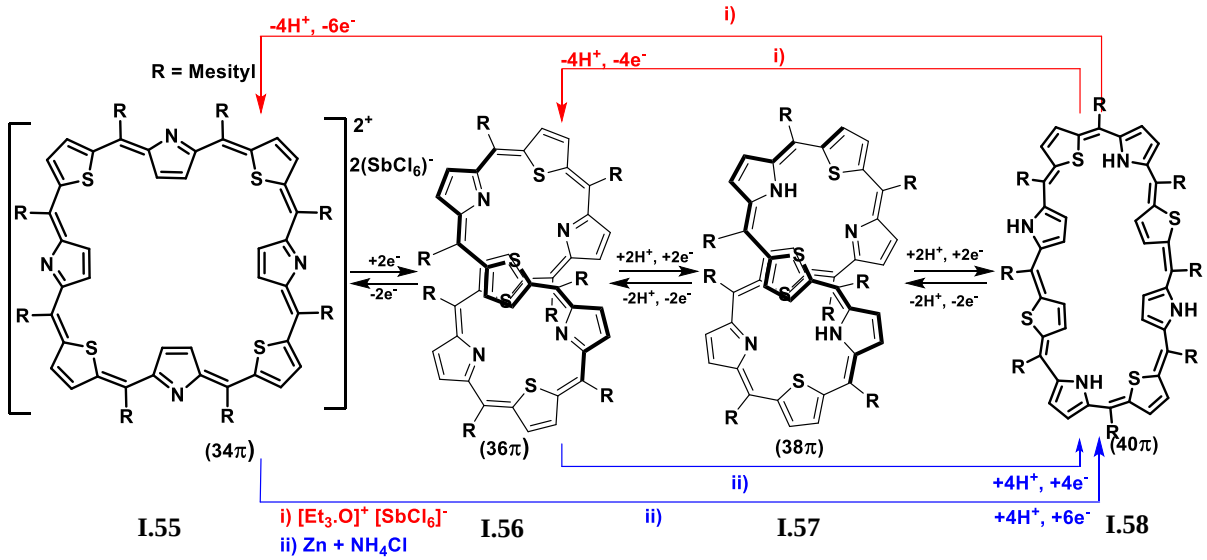

Scheme I.6: Four reversible redox states of core-modified octaphyrin.

The 36π octaphyrin **I.56**, could be reduced to the 38π octaphyrin **I.57**, using $NaBH_4$ and upon the addition of *p*-chloranil it oxidised to 36π system through quantitative dehydrogenation. Anand and coworkers extended the work and reported two more redox states for octaphyrin, highest oxidation state 34π octaphyrin **I.55**, and highest reduced state 40π system **I.58**. In the presence of Meerwein salt, 36π octaphyrin was oxidised quantitatively to 34π dicationic macrocycle **I.55**, displayed the expected diatropic ring current effects in its proton NMR spectrum. This oxidized species reduced with Zinc dust and aq. ammonium chloride resulted to highly reduced 40π octaphyrin **I.58**. This reduction alters molecular structure from squarish to rectangular geometry for octaphyrin. Moreover, beyond the reversible six-electrons redox, four electron reversible redox process between **I.56** and **I.58**, was demonstrated using MnO_2/($Zn+NH_4Cl$) couple. (scheme - I.6).[61] Octaphyrin showed a range of four distinct species with 34π, 36π, 38π, and 40π electrons was observed. All variations were achieved through redox inter-conversion, employing a combination of both PCET and ET processes.

Anand and coworkers synthesised non-pyrrolic core-modified ethylene bridged 32π hexaphyrin which shows remarkable structural diversity and susceptible to ring oxidation to form stable aromatic dicationic species. Its proton NMR spectrum suggested the highly symmetrical structure for **I.59**, lacking significant paratropic ring current effects and attributed to its figure of eight conformation. After the addition of trifluoroacetic acid (TFA) to **I.59**, the colour of solution drastically changed from the brownish-red to a deep-blue colour (scheme – I.7). The proton NMR spectrum displayed strong diatropic ring current effect.

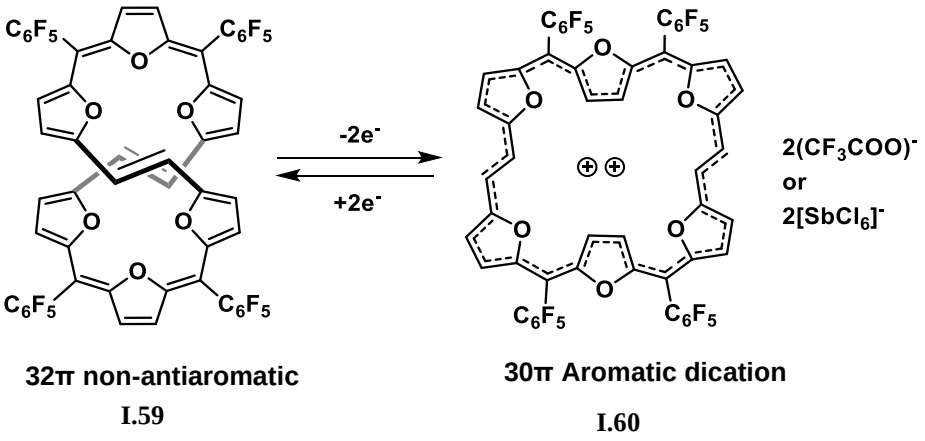

Scheme I.7: Redox reaction of ethylene bridged 32π hexaphyrin.

The chemical shift of the inner and outer ethylene protons exhibited a significant disparity, clearly indicating the presence of a pronounced ring current effect in the macrocycle. The interconversion of [32] non-antiaromatic **I.59**, to [30] aromatic dicationic species **I.60**, carried through ring oxidation is an example of ring oxidation reaction.[57] Same group reported the first stable mono-pyrrolic 20π antiaromatic isophlorin upon partial core-modification in the porphyrin can be used as suitable synthetic strategy to obtain the various isomer of this isophlorin.[35] The aromatic systems are known to be oxidized to yield the radical cation and antiaromatic macrocycles incline to undergo two electrons oxidation to the corresponding dicationic species.[59]

As previously observed, the pyrrole NH is susceptible to oxidize in order to accommodate the nitrogen atom of pyrrole in the conjugation but in the case of **I.61**, macrocycle undergoes two electron ring oxidations to yield the 18π aromatic dicationic species **I.62**, rather than 19π radical (scheme – I.8).

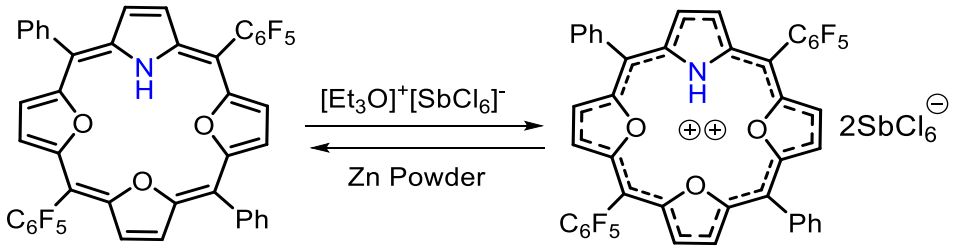

20π Antiaromatic **18π Aromatic dication**

I.61 **I.62**

Scheme I.8: Redox reaction of ethylene bridged 32π hexaphyrin

Surprising part is that, the proton NMR spectra revealed the pyrrole NH signal resonated in the high filed region at δ 29.2 ppm which clearly signifies the antiaromatic character of the macrocycle. Even in the presence of the pyrrole NH proton, it prefers to undergo ring oxidation rather than PCET reaction.[35]

I.8 Aim of the thesis

The available examples in literature have been reviewed clearly and indicates that synthesis and isolation of stable 20π isophlorin are quite challenging and there has been many such reports tried to stabilize it. An excellent method involves substituting all the pyrroles in a porphyrin molecule with different heterocyclic units like thiophene, furan, and selenophene. This results in the formation of a stable 20π isophlorin. The nature of heteroatoms and substituents on the meso-carbons is crucial for providing stability to the isophlorin. Porphyrin as [18]annulene can be tuned to form a new class of macrocycles such as contracted porphyrin, expanded porphyrin, core-modification and confused porphyrin. Specially, the expanded macrocycles can be synthesised by introducing the meso-carbons, incorporating heterocyclic rings which leads to formation of higher membered macrocycle. The structural diversity of these expanded macrocycles, which are antiaromatic, is characterized by planar, figure-of-eight, and ruffled conformations. This demonstrates the importance of planarity even in antiaromatic systems. These non-planar structures exhibit the lack of paratropic ring current effects caused by their structure. A trademark of these antiaromatic systems, particularly isophlorin lies in the reversible two-electron oxidation leading to their corresponding aromatic dicationic species. The undiscovered characteristics of antiaromatic isophlorin can be uncovered simultaneously by exploration of porphyrinoids. This thesis aims to describe the synthesis, structural characterization and electronic properties of expanded as well as contracted isophlorinoids. Particularly, the focus on the utilization of simple precursors and methodology to synthesis the series of expanded macrocycles. The macrocyclic conjugation has been modified through synthetic alterations aimed to obtain either increased or decreased π-electron count in various porphyrinoids. Additionally fused heterocyclic units can be employed to extend the π-electronic conjugation without altering the aromaticity of the system. All these macrocycles have been characterized using analytical techniques such as single crystal X-ray analysis. Their redox studies were done through electronic absorption spectroscopy and cyclic voltammetry studies. Moreover, the redox study is supported by spectro-electrochemical studies. Computational analysis such as NICS and AICD values provides additional evidence for the aromatic properties as inferred from the experimental studies.

Chapter 2

Synthesis and characterization of thiophene based [8] and [16] annulene

II.1 Introduction

Huckel's Aromaticity (4n+2)π and antiaromaticity 4nπ can be considered as a two-electron reversible redox process. 18π Porphyrin, **1** and 20π isophlorin, **3,** represents a classic example for such reversible redox interconversion, even though not achieved till date. Porphyrin is the skeleton of a 18π aza-annulene similar to isophlorin for 20π annulene. Stabilization of a 18π aza-annulene is relatively easier than the 20π annulene π-conjugated system due to the accompanying aromatic stabilization. With the aim of achieving stability for the 20π isophlorin, Vogel and co-workers replaced the nitrogen atom with different chalcogens such as O, S, and Se in the 20π isophlorin network.[62] Interestingly, these core-modified isophlorins underwent rapid two-electron ring oxidation, resulting in the formation of the 18π dicationic species. In their later endeavours, the same group synthesised a thiaporphyrinogen by cyclocondensation of 3, 4-diethyl-2-hydroxymethylthiophene in the presence of p-TsOH, and subsequent oxidation using DDQ and $HClO_4$ yielded a18π porphyrin dication instead of the expected 20π isophlorin.[63] In 2012, Teruo Shinmyozu and co-workers introduced a phenyl group at the meso-carbon of thiaporphyrinogen followed by oxidation with DDQ/$HClO_4$, which yielded only a dicationic species **2** (figure – II.1).[64]

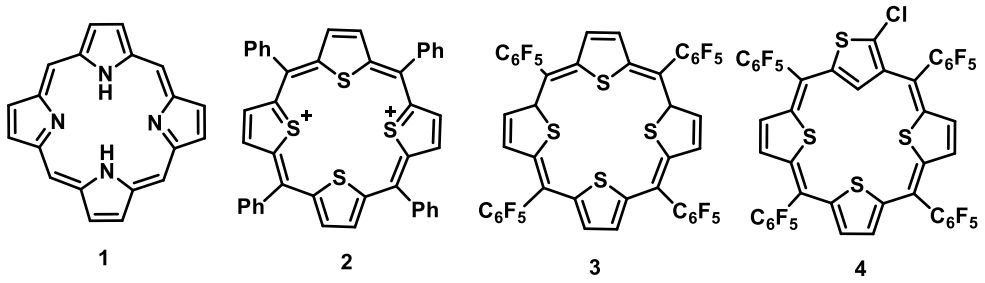

Figure II.1: Structural illustration for 18π porphyrin and core modified 18π and 20π isophlorins.

In contrast, the introduction of strong electron withdrawing group such as pentafluorophenyl, at the meso-position of the macrocyclic system followed by the oxidation with anhydrous $FeCl_3$ result in the formation of stable 20π isophlorin **3.** In the molecular structure, the macrocycles **2** and **3** exhibited a non-planar conformation because of the steric hurdle caused by the large sulphur atom in the core of the macrocycle.[64]

Anand and co-workers synthesised its structural isomer that is S-confused 20π isophlorin **4** (figure – II.1), where one of the thiophene is connected through 2,4-connectivity instead of common 2,5-connection.[65] Due to the acidic nature of the α-hydrogen of S-confused thiophene, it undergoe quick halogenation upon the addition of anhydrous $FeCl_3$, used as oxidising agent.

Addition of Meerwein's salt to this macrocycle resulted in two-electron of the ring oxidation, yielding an uncommon 18π monocationic species. It was confirmed by the presence of only one counter anion instead of usual two counter anions corresponding to two-electron oxidation. This was attributed to the chlorine at α-position which was replaced by an oxygen to form keto group.

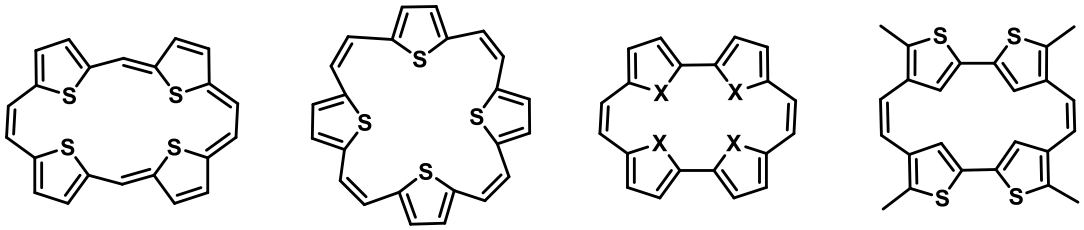

Figure II.2: Structural isomers of tetrathia isophlorin.

Cava and co-workers synthesised a series of sulphur bridged annulenes/ethylene bridged thia-isophlorins **6**, by McMurry coupling in presence of $TiCl_4$/Zn and pyridine in THF under reflux conditions. These reactions were started with the mono/bi/terthia dialdehydes to yield the corresponding mono/bi/terthiophene derived annulenes. Interestingly, for the first time the neutral 22π aromatic tetrathia[22]annulene[2,1,2,1] **5**, was synthesised in relatively good yields and its aromaticity was confirmed by ^{1}H NMR studies. It was observed that all the thiophene β-protons resonated in the downfield region, and the macrocycle displayed diatropic ring current, reminiscent of Vogel's 18π aromatic porphycene **7a**. Here also, all the β-protons of the pyrrole resonate at the downfield and inner –NH protons resonate in the upfield confirming the aromatic nature of the macrocycle.[3331] With suitable synthetic modifications, incorporation of both ethylene and S-confused systems, Anand and co-workers designed a new synthetic strategy with completely thia-confused porphycene through 2,4 connectivity having series of confused 20π **8**, 28π, and 30π porphycenes (figure – II.2).[28]

This chapter describes modifying this novel strategy to yield a new class of isophlorin through 2,3-connectivity between heterocyclic units and ethylene bridges. Due to 2,3-connectivity, the system is much reduced to 16π electronic state, distinct from the 18π and 20π systems as discussed so far. Hence, the macrocycle synthesised through McMurry coupling, should ideally yield a macrocycle in which where all the thiophene units are symmetrically arranged in the same orientation along with ethylene bridge. Interestingly, under these reaction conditions, its lower member 8π COT was also obtained along with thiophene in the same 2,3-connectivity but the thiophene are arranged in the same or opposite orientation.

II.2 Synthesis of [8] and [16] thiophene fused isophlorin using strategy I

To synthesize the contracted 8π and 16π isophlorin two different strategies were attempted and accordingly observed two different results. In the first strategy (scheme - II.2), (E)-3,3'-(ethene-1,2-diyl)bis(thiophene-2-carbaldehyde) **II.9**, was employed for the well-known McMurry coupling reaction. A slow addition of $TiCl_4$ in the THF at 0 ^oC, was followed by the portion wise addition of Zn dust to the reaction mixture and the reaction mixture was stirred for the one hour. To this mixture was added the dialdehyde solution **II.9**, and was warmed to room temperature followed by refluxing it overnight. MALDI-TOF/TOF mass spectrum of the reaction mixture revealed a series of *m/z* confirming the success of expected coupling reaction (figure - II.3).

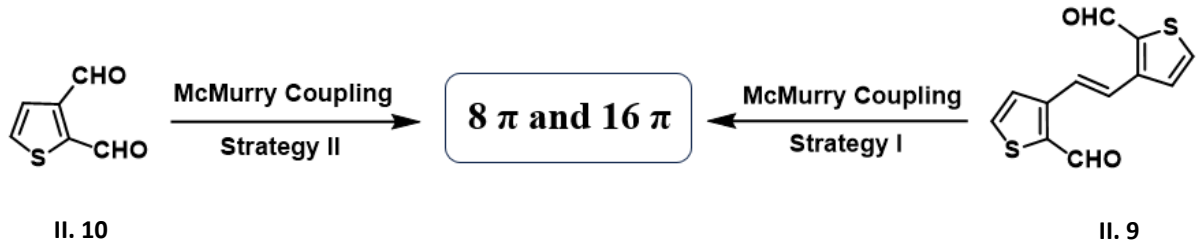

Scheme II.1: synthesis of 8π and 16π macrocycle using two different synthetic strategy.

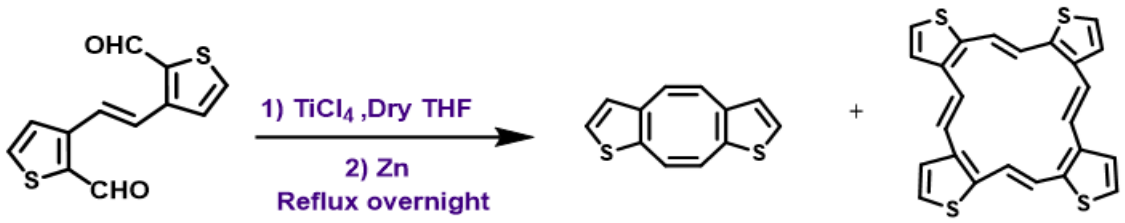

Scheme II.2: Synthesis of dithiafused cyclooctatetraene 8π **II.11a** and higher analogues.

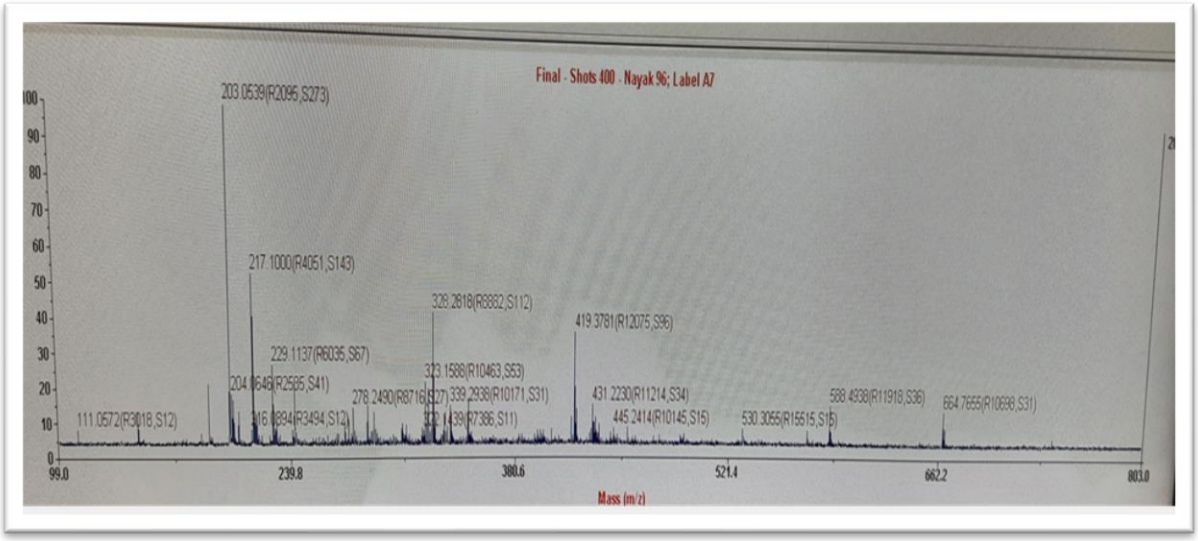

Figure II.3: MALDI-TOF/TOF mass spectrum of reaction mixture (scheme **II.2**)

II.3.1 Isolation and Characterisation of symmetric [8] dithia isophlorin

The reaction mixture was concentrated under reduced pressure and its TLC analysis revealed two major spots which had small difference of retention factor. As observed in the MALDI-TOF/TOF mass spectrum, it showed the expected mass 8π along with 16π system. The purification/isolation of macrocycle was performed through silica-gel column chromatography using hexane as solvent. The first faint yellowish colour band isolated corresponded to the cyclooctatetraene **II.11a**, 8π system. An *m/z* value of 217.0417 obtained from the HR-ESI-MS confirmed the composition of this macrocycle (figure - II.4).

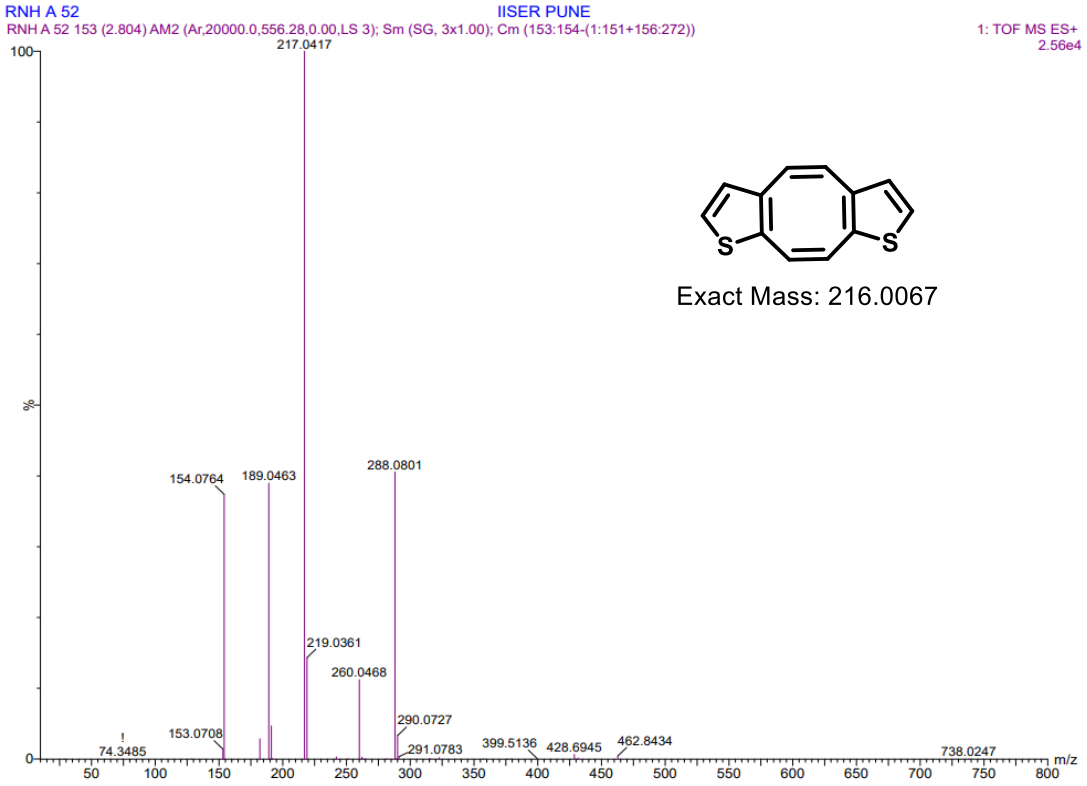

Figure II.4: HR-ESI-TOF mass spectrum of **II.11a**

II.3.2 ^{1}H NMR study of Symmetric [8] cyclooctatetraene (II.11a)

Intramolecular coupled macrocycle, **II.11a**, encompasses 8π electrons, and according to Huckel's theory, should exhibit antiaromatic nature. The ^{1}H NMR spectrum of **II.11a** recorded in chloroform-d revealed four distinct signals, corresponding to the four non-equivalent protons, in the range between δ 6.3 to 7.3 ppm (figure - II.5). This observation implies a highly symmetrical structure in solution state showcasing the presence of C_2 axis of symmetry within the macrocycle. Notably, the cyclooctatetraene moiety in **II.11a**, should have adopted a boat conformation, as evidenced by the absence of ring current effect in the observed spectrum. The hydrogen atoms in the ethylene bridges exhibited resonance as two singlets at δ 6.36 and 6.51

ppm, whereas the hydrogen atoms in the thiophene rings were seen as two doublets at δ 6.59 and 7.30 ppm. Furthermore, the ^{1}H-^{1}H COSY spectrum, recorded at 298 K, exhibited a correlation suggestive of the protons associated with the thiophene rings (figure - II.6).

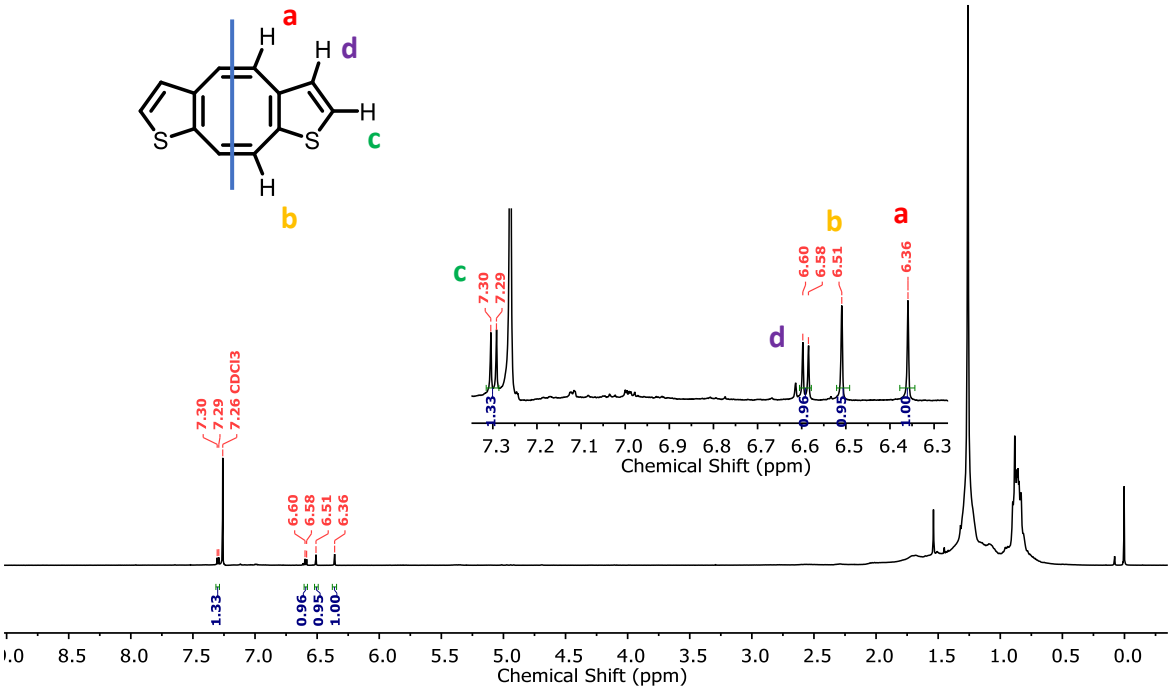

Figure II.5: ^{1}H NMR spectrum of **II.11a** in Chloroform-d at 298 K.

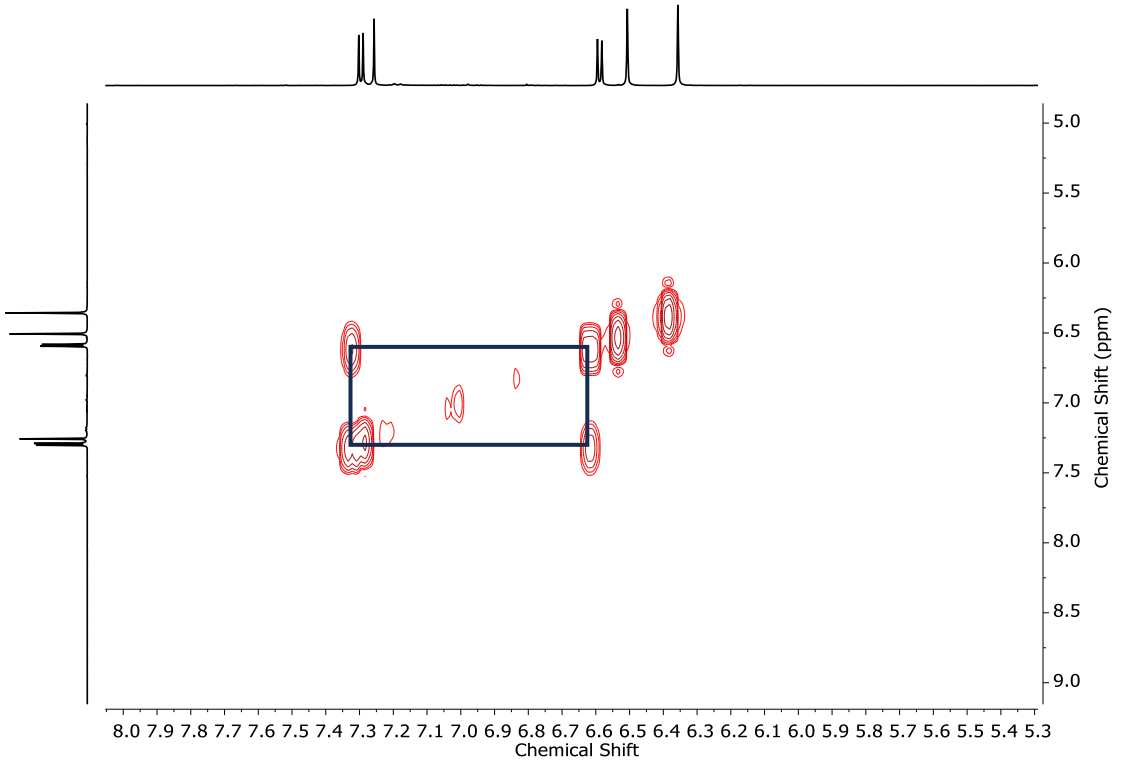

Figure II.6: ^{1}H-^{1}H COSY spectrum of **II.11a** in Chloroform-d

II.4 Synthesis of [8] and [16] thiophene fused isophlorin using strategy II

In an alternative strategy, the thiophene-2,3-dicarbaldehyde **II.10**, (scheme – II.3) was employed under identical reaction protocol as followed above with few changes. The mass spectrum of the resulting mixture exhibited observations similar to those observed in the previous strategy.

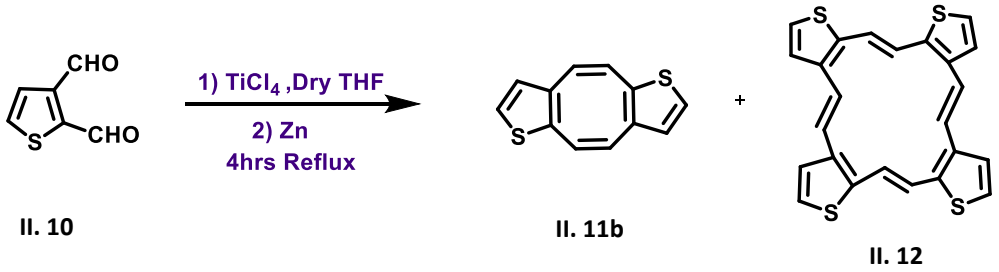

Scheme II.3: Synthesis of asymmetric dithiafused cyclooctatetraene [8] **II.11b** and higher analogues.

II.4.1 Isolation and Characterisation of Asymmetric [8] dithiafused cyclooctatetraene

The isolation/purification of the anticipated macrocycle **II.11b**, was accomplished by silica-gel column chromatography employing hexane as the eluent. A faint yellow coloured band was isolated and the composition of the product was confirmed by HR-ESI-MS mass spectrum. Unlike the **11a**, the ^{1}H NMR spectrum of **11b** (figure – II.7), exhibited a greater number of signals than expected. In the spectrum it showed total of eight signals as against the expected four similar to **II.11a**. It suggested that the possible flexible nature of the starting material might have led to the formation of two different structural isomers.

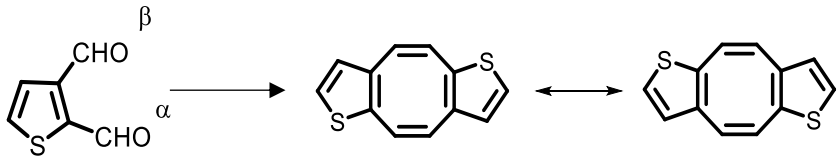

In **II.11a**, both thiophene units were oriented on the same face, which can be classified as a symmetric 8π dithiafused cyclooctatetraene. Therefore its ^{1}H NMR was very symmetric. However, in the second case **II.11b**, both the thiophene units were positioned in opposite directions, leading to as the exclusive formation of an asymmetric 8π system. The spectrum showed three multiplets resonating at δ 7.29, 6.59 and 6.44 ppm along with two singlets corresponding to ethylene bridges resonating at δ 6.51 and 6.36 ppm. The signals of ethylene bridges confirmed the admixture of structural isomers in solution. All the signals reflect absence of paratropic ring current effect which can be attributed to its non-planar structure.

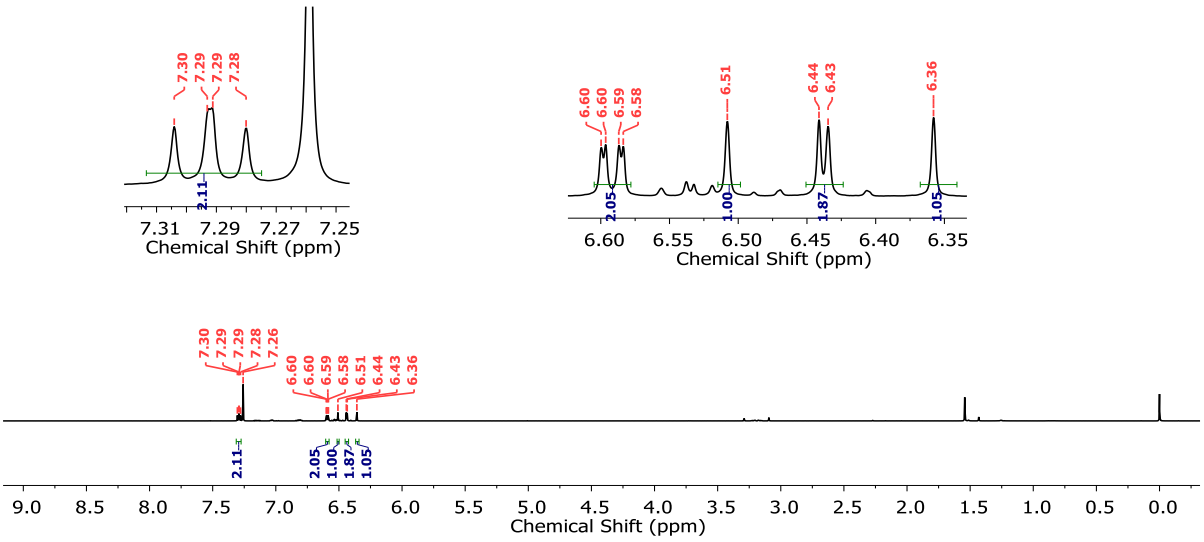

Figure II.7: ^{1}H NMR spectrum of **II.11b** in Chloroform-d.

The proton NMR spectra of compound **11b**, displayed a signal count that was twice as high as anticipated. It displayed a total of eight signals,which exceeded the expected four resonance as observed in **11a**. The thiophenes in isolated 8π cyclooctatetraene lacked regioselective cyclization leading to formation of inseparable structural isomers, **11a** and **11b**.

II.4.2. Molecular structure of [8] dithiafused cyclooctatetraene

Since ^{1}H NMR spectrum for both the macrocycles were different, so it's important to obtain the absolute structure for these possible structural isomers. Therefore, efforts were made to develop high-quality single crystals by introducing n-hexane vapor into a solution of **II.11**, in DCM using vapor diffusion.

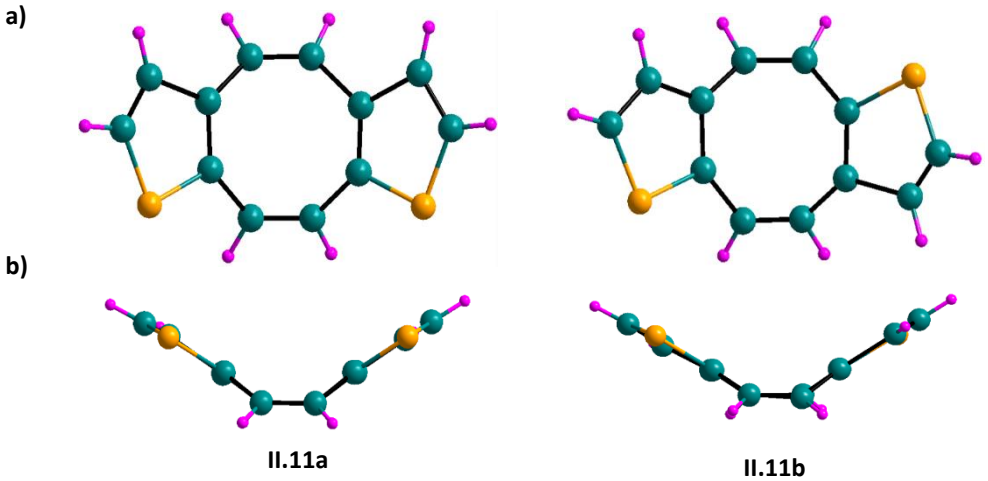

Figure II.8: Molecular structure of [16] tetrathia isophlorin (**II.11a)** and **(II.11b)** as determined from single crystal X-ray diffraction. (a) (top view) and (b) (side view)

The molecular structure of dithiafused cyclooctatetraene was elucidated by single crystal X-ray diffraction analysis (figure – II.8). Few yellow colour needle shaped crystals were achieved through recrystallization. The crystal structure of **II.11a,** obtained from the first precursor observed that both the sulphur atoms occupied the symmetrical position, resulting in the same puckered/boat shaped structure where both ethylene bridges adopted the *Z* conformation. Like the **II.11a**, the molecular structure of **II.11b**, revealed a puckered structure consistent with the established topology of cyclooctatetraene. However, X-ray data analysis of **II.11b**, provided only 50% occupancy either for S or C for the positions to cyclooctatetraene ring. This can be envisaged due to the poor regioselectivity for the cyclization during the McMurry coupling and perhaps resulting from an admixture of the isomers in the crystallization process.

II.4.3 Electronic absorption and Cyclic Voltammogram studies

This macrocycle accounts for 8π electron in conjugation, corresponding to antiaromatic 4nπ system. Being a non-planar, antiaromatic system it is expected undergo two-electron ring oxidation to yield the dicationic species.

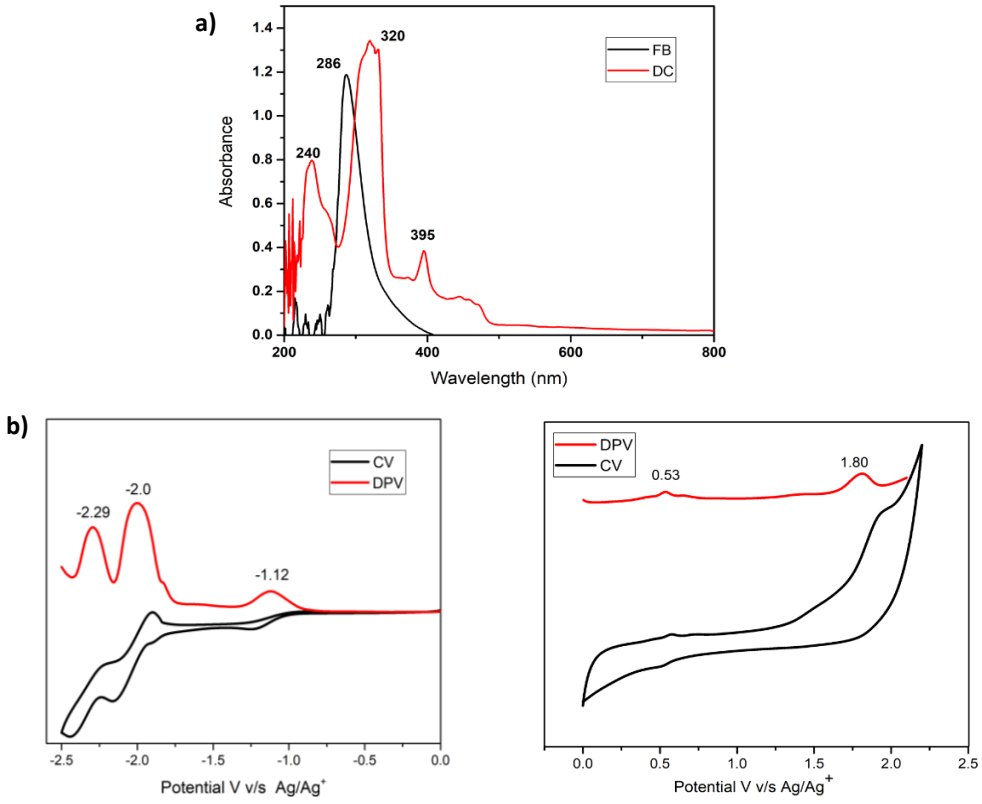

Figure II.9: a) Electronic absorption spectrum of 10^{-5} M solution of **II.11** (black) (FB: Free Base) and its oxidised species [**II.13**]$^{2+}$ (red) (DC: Dication) recorded in CH_2Cl_2. b) Cyclic voltammogram (CV, black) and differential pulse voltammogram (DPV, red) of **II.11** in CH_2Cl_2 (with 0.1 M **$(Bu)_4NPF_6$** as the supporting electrolyte).

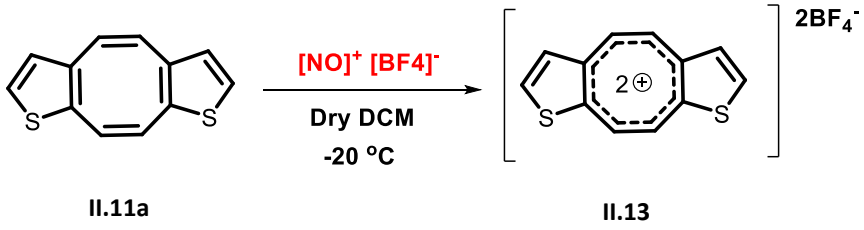

II.11a II.13

Scheme II.4: Two-electron oxidation of **II.11a** by $NOBF_4$ to its dication [**II.13**]$^{2+}$

In UV-Vis spectrum, it displayed an intense absorption band at 286 nm (26000) in dichloromethane. Upon the addition of the oxidizing agent such as $NOBF_4$ to the solution of **II.11a**, in DCM (scheme – II.4) it exhibited a small red shift at 320 nm along with high energy band at 240 nm (Figure – II.9a). The redox property of the macrocycle was studied through cyclic voltammetry (CV) and differential pulse voltammetry (DPV) in dichloromethane. In the oxidation window, it displayed two potentials at + 0.53 V and + 1.80 V while in reduction window it showed three potentials at -1.12, -2.0 and -2.29 V respectively (figure - II.9b).

II.5.1 Isolation and Characterisation of [16] tetrathi isophlorin

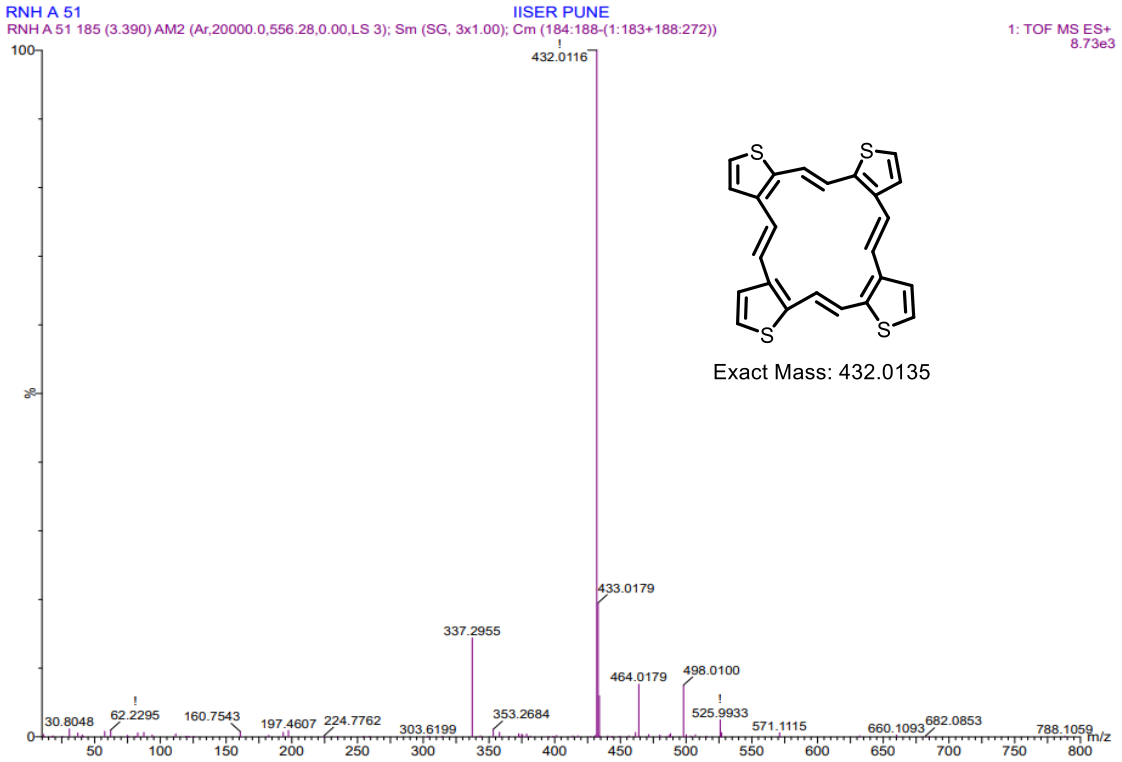

Figure II.10: HR-ESI-TOF mass spectrum of **II.12**.

Next higher membered macrocycle in the series was isolated after the **II.11**. A red-orange coloured band was purified through silica-gel column chromatography**.** The composition of the macrocycle was confirmed through HR-ESI-MS mass spectrum in which showed an *m/z* value of 432.0116 (expected an *m/z* 432.0135 corresponds to $C_{24}H_{16}S_4$) (figure - II.10).

II.5.2 ^{1}H NMR study of [16] tetrathia isophlorin

This novel tetrathia macrocycle **II.12**, consists of 16π electrons in global conjugation and accounts for Huckel's antiaromatic system. The ^{1}H NMR spectrum of **II.12**, displayed a symmetrical pattern and the signals resonated in the region between δ 7.5 to 6.2 ppm at room temperature (figure – II.11). Therefore, the macrocycle is expected to be non-antiaromatic in solution state. A minimal difference in chemical shift values, less than 0.50 ppm, between the most shielded and deshielded signals indicated a weak paratropic ring current effect. The presence of a two different ethylene bridges in **II.12**, is attributed to the α-α and β-β connectivity between the four thiophene rings. The macrocycle possesses the plane of symmetry (σ) or C_2 symmetry and suppose to show eight signals in its ^{1}H NMR spectrum but at room temperature it exhibited few signals than expected. Suspecting a fluxional character, its ^{1}H NMR spectrum was recorded at lower temperatures (figure – II.12). To restrict the supposed fluxionality ^{1}H NMR spectra was recorded up to 177 K. However, it was observed that the signals only broadened and disappear at low temperatures. This observation could potentially be attributed to the aggregation of the compound at such low temperatures.

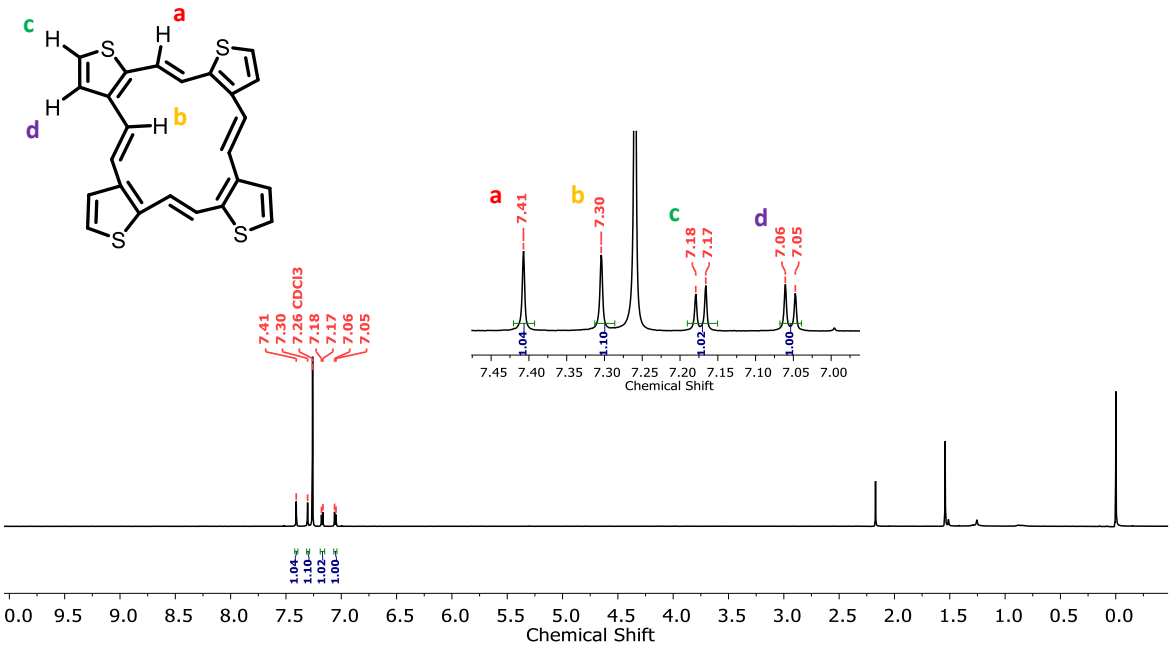

Figure II.11: ^{1}H NMR spectrum of **II.12** in Chloroform-d

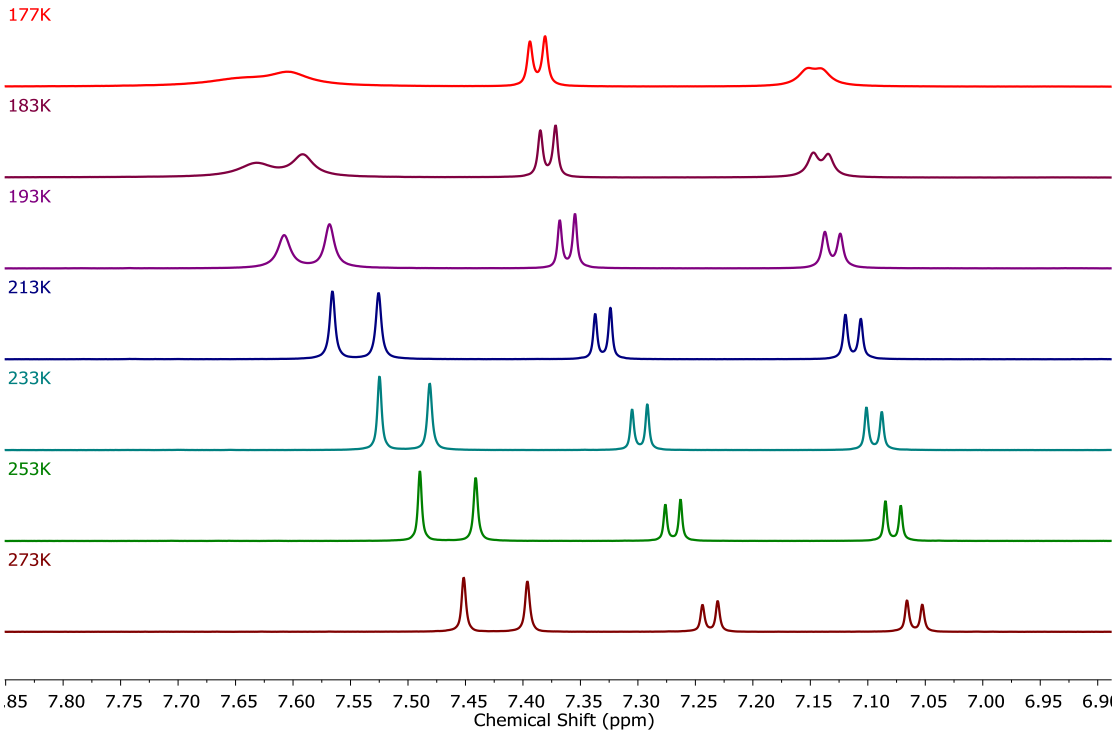

Figure II.12: Variable temperature ^{1}H NMR spectra of **II.12** in THF-d_8

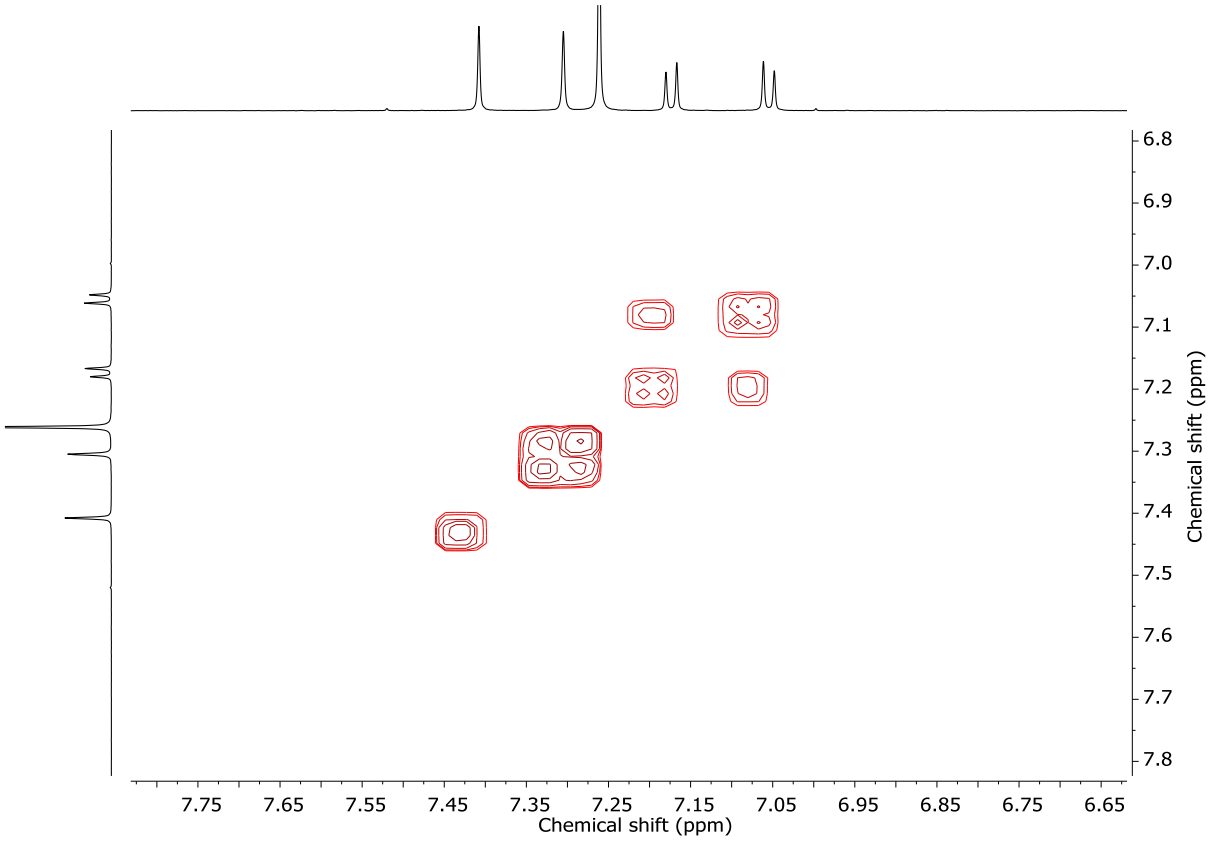

Figure II.13: ^{1}H-^{1}H COSY spectrum of **II.12** in Chloroform-d

Notably, no new signals emerged indicating that the given macrocycle exhibits a highly fluxional nature even at such reduced temperature. Therefore, only four signals were observed. Two doublets at δ 7.16 and 7.05 ppm correspond to the thiophene protons and two singlets at δ 7.41 and 7.30 ppm to the ethylene protons. Results were additionally supported by the 1H-1H COSY spectra of **II.12**, which was obtained in chloroform-d and exhibited only two sets of correlations. One correlation between doublets at δ 7.17 and 7.06 ppm and another one for singlet at δ 7.41 and 7.30 ppm (figure – II.13).

II.5.3 Molecular structure of [16] tetrathia isophlorin

A high-quality single crystal was successfully grown by methanol vapour diffusion into a solution of **II.12,** in DCM. The molecular structure of **II.12**, was determined via single-crystal X-ray diffraction investigation (figure – II.14a, b) which revealed a highly planar structure wherein all the four ethylene bridges adopted *E* conformation with each hydrogen positioned towards and away from the macrocyclic cavity, respectively. The planar geometry of **II.12**, contains 16π electrons, contrasting with 18π and 20π electrons found in porphyrin or tetrathia cation, **2**, and porphycene, **7b**, respectively. Additionally, the ethylene bridges and the four thiophene rings were coplanar, contributing to the flat geometry of the macrocycle. An inter planar distance of 3.479 Å confirmed significant π stacking in the solid state (figure – II.14c).

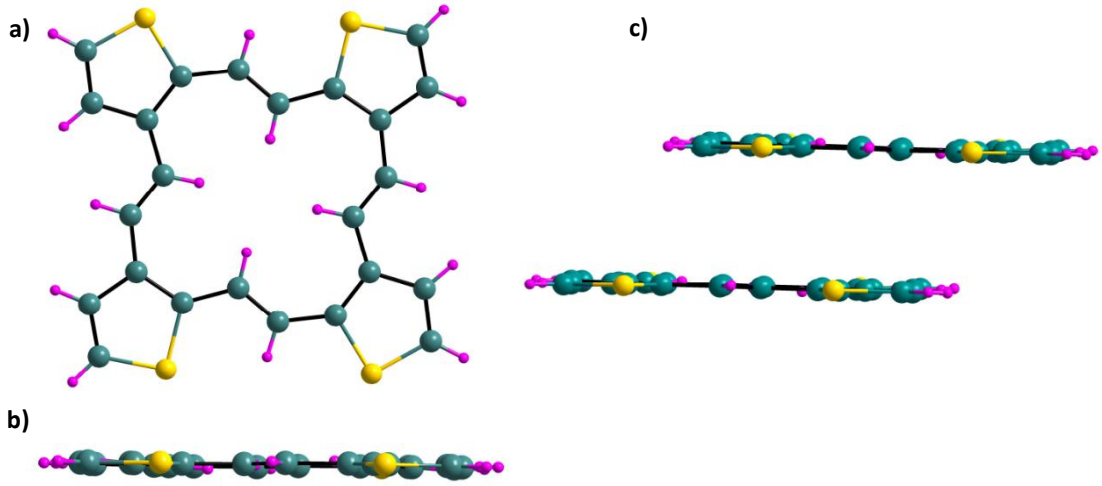

Figure II.14: Molecular structure of [16] tetrathia isophlorin (**II.12)** as determined from single crystal X-ray diffraction. (a) (top view), (b) (side view) and (c) π-π interaction with 3.479 Å interplanar distance.

II.5.4 Electronic absorption and Cyclic Voltammogram studies

A 16π electron count of macrocycle belongs to antiaromatic system and hence it is expected facial two-electron to undergo ring oxidation. To understand the redox property of **II.12**, its electronic absorption spectrum was recorded in dichloromethane. A reduced number of π-electrons with only the 16π electrons network led to a considerably blue shifted absorption peak at 318 nm (30400). Electronic absorption spectrum suggested that the molecule exhibited only a modest macrocyclic conjugation despite its planar nature and there were no significant changes observed in the ^{1}H NMR spectrum and absorption spectrum. These findings suggest that thiophene and ethylene bridge units in the molecule behave as independent entities, lacking any substantial conjugation between them. Upon the addition of oxidizing agent such as Meerwein's salt, (scheme - II.5) the oxidized species displayed the λ_{max} at 292 nm (30400) along with low energy band at 470 nm (figure - II.15a).[63,66]

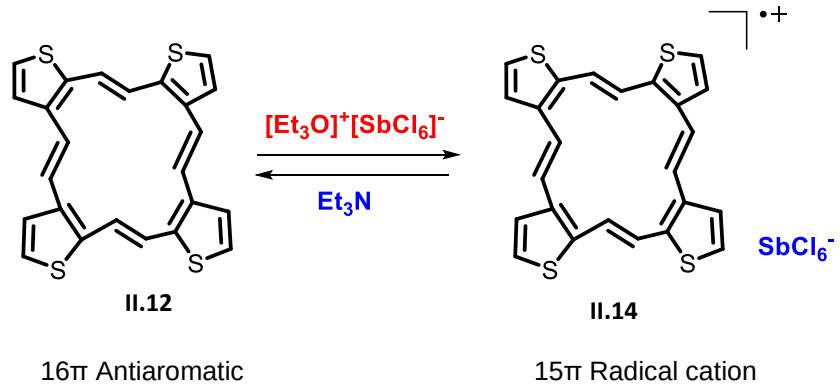

Scheme II.5: Two-electron oxidation of **II.12** by Meerwein salt to its radicalcation [**II.14**]$^{\cdot+}$

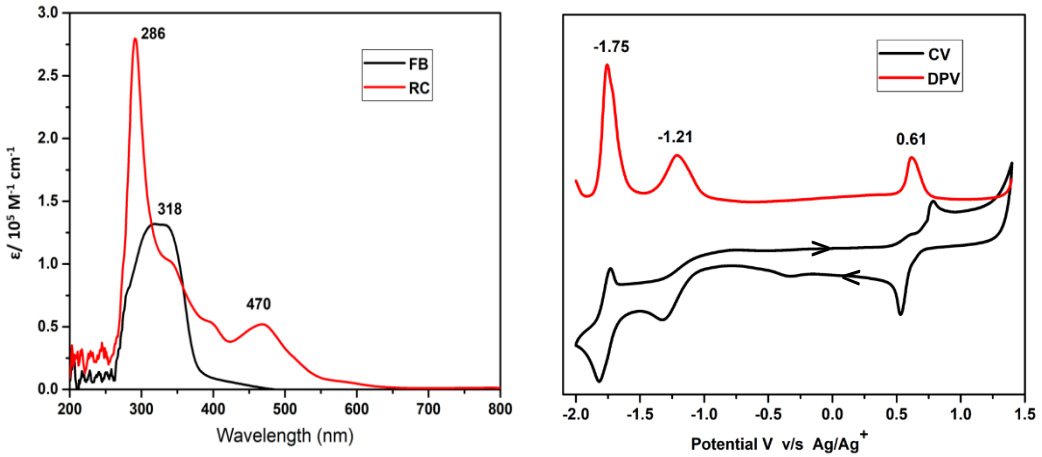

Figure II.15: a) UV/vis/NIR absorption spectrum of 10^{-5} M solution of **II.12** (Black) (FB: Free Base) and its oxidised species [**II.12**]$^{\cdot+}$ (red) (RC: Radicalcation) recorded in CH_2Cl_2. b) Cyclic voltammogram (CV, black) and differential pulse voltammogram (DPV, red) of **II.12** in CH_2Cl_2 (with 0.1 M $(Bu)_4NClO_4$ as the supporting electrolyte).

Its optoelectronic and chemical redox property were further studied through electrochemical analysis, such as cyclic voltammetry and differential pulse voltammetry. The cyclic voltammogram revealed an irreversible oxidation at + 0.61 V and it also displayed harsher and irreversible reduction at – 1.21 and – 1.75 V. The conformation of these potentials was further substantiated through differential pulse voltammetry (figure – II.15b).

II.6 Quantum mechanical calculations

The Gaussian09 rev D program suite was utilized to perform quantum mechanical calculations, allowing for a more thorough understanding of the molecular orbitals and evaluation of antiaromaticity. The calculations used Density Functional Theory (DFT) with Becke's three-parameter hybrid exchange functional and Lee-Yang-Parr correlation functional (B3LYP). The calculations used a 6-31G(d,p) basis set for all atoms. The geometry-optimized structures were obtained using molecular structures derived from single crystal analysis.

The aromaticity of π-conjugated macrocycles is assessed based on the strength of the magnetic field, resulting in either paratropic or diatropic ring current effects. In the exploration of various methods for quantifying the aromaticity of conjugated systems, Nucleus Independent Chemical Shift (NICS) emerged as a successful index. Introduced by Schleyer, NICS serves as a magnetic criterion for measuring aromaticity, antiaromaticity, or non-aromaticity.[67,68] It is designed as "Absolute magnetic shielding, computed at the ring centre (non-weighted mean of the heavy atom coordinates) or at another point of interest in the molecule. When the NICS value is negative at the interior positions of the rings, it indicates a magnetically shielded environment induced by a diatropic ring current, termed as 'aromatic'. Conversely, if NICS value is positive shows opposite ring current effect and indicate an 'antiaromatic' feature of the macrocycle. Basically, the computed values are inverted in order to conform to the conventional NMR chemical shift convention. Basically, there is no fixed range for NICS value and don't require any reference standards. Firstly, optimization of the molecular structure and secondly fix the position of the Bq (Banquo, a ghost atom representing the smallest ionic metal, typically Li^+) (as dummy) atom. Then used the GIAO (Gauge Independent Atomic Orbital) method are employed in these calculations.

The Anisotropy of the Induced Current Density (AICD) is a comprehensive method used to quantify and visualize the density and direction of delocalized electrons.[69] This is achieved by applying the Continuous Set of Gauge Transformation (CSGT) method to estimate the current

density. The results are then a plotted using POVRAY 3.7 for windows. In this method, standard iso-surface value of 0.05 is typically used for calculations. The interpretations of the AICD results are based on the direction of the delocalization of π-electrons cloud current density. If the current density exhibits a clockwise direction, it indicates that the molecule is aromatic. On the other hand, if the current density is anti-clockwise, it suggests that the molecule is antiaromatic. This provides valuable insights into the electronic structure and aromaticity characteristics of the studied molecule.

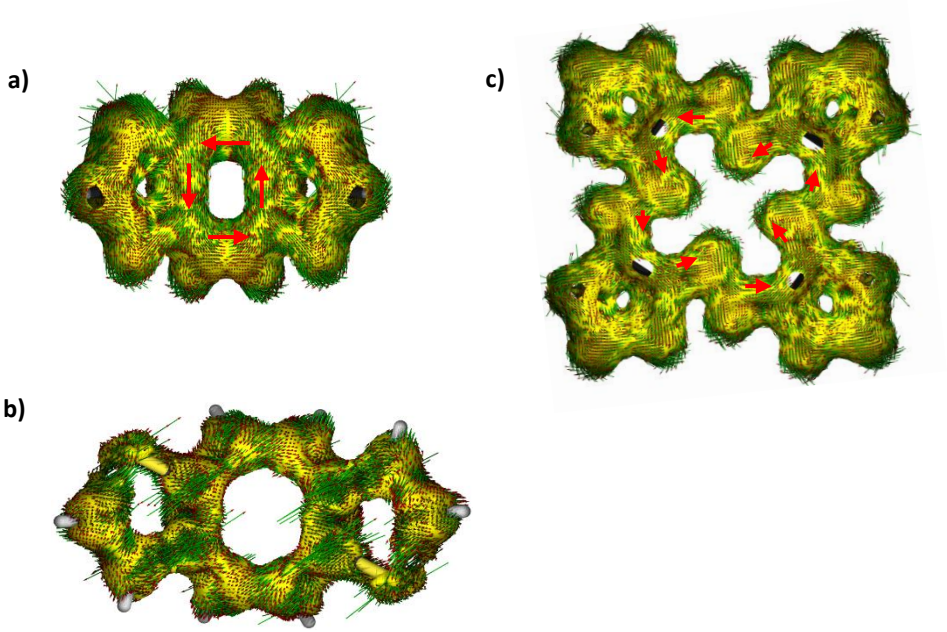

Figure II.16: AICD plot of a) **II.11a,** b) **II.11b** and c) **II.12** at an iso surface value 0.05 the external magnetic field is applied orthogonal to the macrocyclic plane.

The estimated nucleus independent chemical shift (NICS) value for **II.12**, was found to be δ +7.5 ppm (table – II.1). The moderate result indicates that the π-electrons in the structure are partially delocalized and have a feeble antiaromatic character of **II.12**. AICD plot displayed anti-clockwise ring current (figure – II.16), recommends the paratropic ring current in the macrocycle. The HOMO and LUMO energy gap for both macrocycles **II.11a**, and **II.12** are 3.79 and 2.17 respectively. (figure - II.17 and figure - II.18).

Macrocycle	NICS (0) ppm	ACID
II.11a	**+4.19**	**Anti-clockwise**
II.11b	**+5.98**	**Anti-clockwise**
II.12	**+7.5**	**Anti-clockwise**

Table II.1: Experimental and computational parameters to classify ring current effects on **II.11a, II.11b** and **II.12**. NICS values for macrocycles determined from quantum chemical calculations. ACID plot gives the direction of ring current.

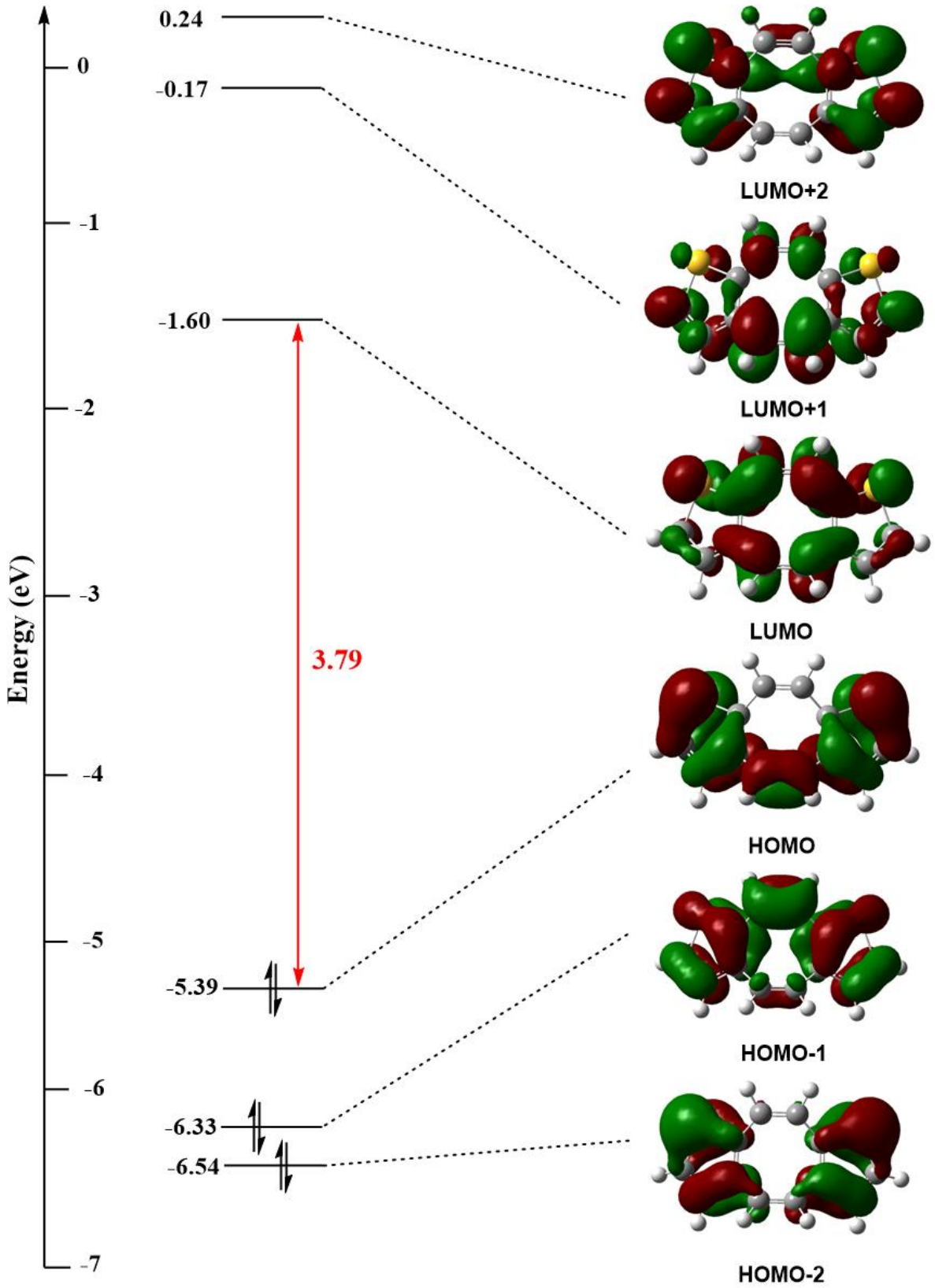

Figure II.17: Selected frontier MOs of **II.11a,** calculated at the B3LYP/6-31G(d,p) level.

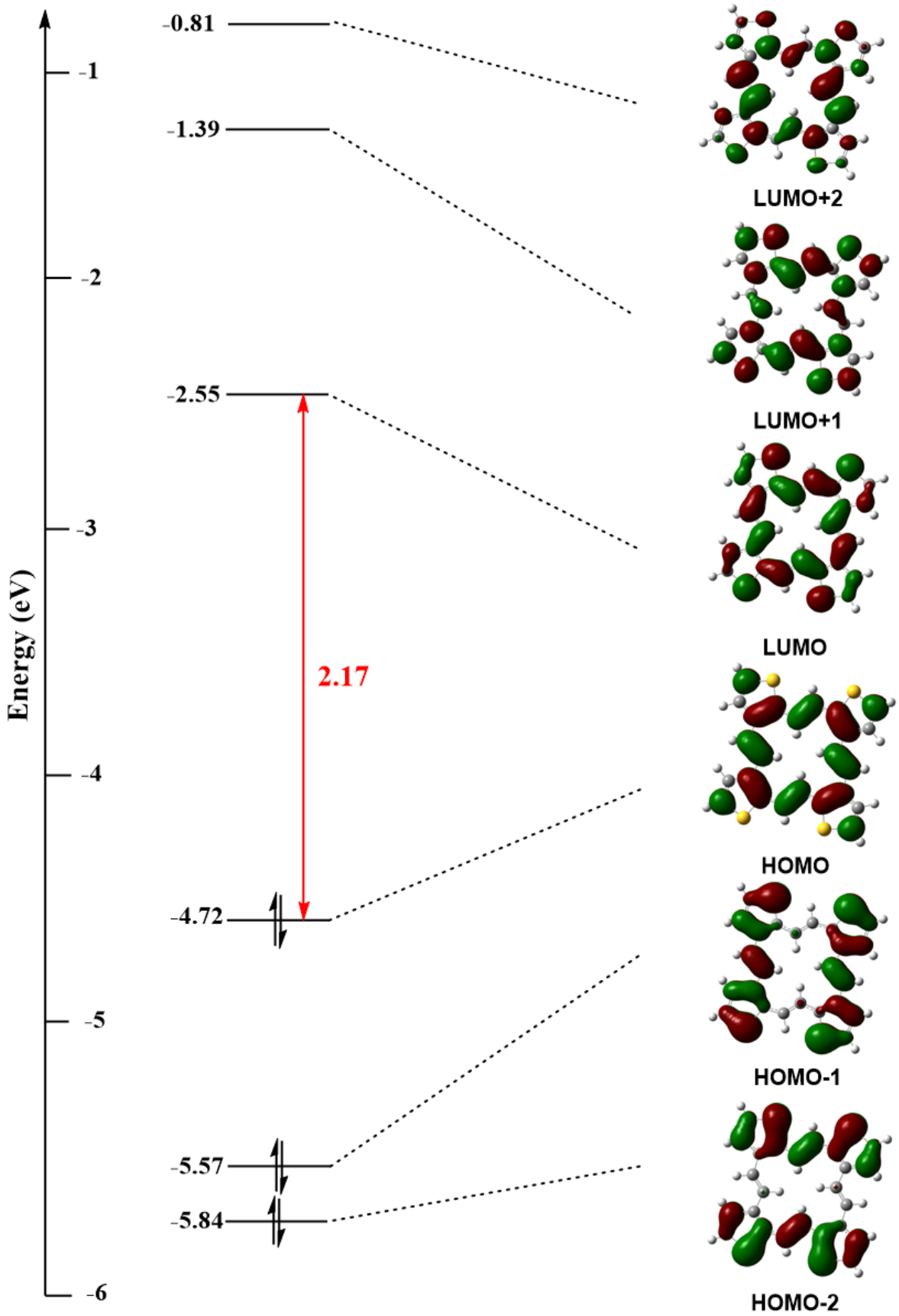

Figure II.18: Selected frontier MOs of **II.12,** calculated at the B3LYP/6-31G(d,p) level.

II.7 Conclusions

This chapter illustrates the synthesis of contracted 16π and 8π systems, which exhibit varied structural features depending on the nature and number of heteroatoms present in the core of the macrocycle. The 16π tetrathia and 8π dithia isophlorin has been successfully synthesised using simple precursors. Instead of the conventional acid catalysed cyclization reaction, a simple coupling reaction was explored to achieve the synthesis and to avoid the formation of undesired polymeric products which reduces the yield of desired product.

In a one pot McMurry coupling reaction of dialdehyde **II.9**, a structural isomer product, **II.11b**, was obtained. Subsequently, an alternate synthetic approach was employed which involved step-by-step coupling reactions to obtain the symmetrical isomer **II.11a**. Along with that a 16π tetrathia isophlorin **II.12**, was also obtained which showed the highly planar and rigid geometry in solid state. Low temperature ^{1}H NMR analysis reveal a fluxional character in solution state, and hence, result exhibited only few signals even at low temperatures. Analytical techniques employed in this study confirmed that the both contracted isophlorin have lost their aromaticity significantly due to the absence of global conjugation within the macrocycle. Furthermore, the electrochemical analysis indicated a harder oxidation compared to the typical isophlorin despite their association with the 4nπ antiaromatic system.

II.8 General experiment methods

All the reagents and solvents utilized in the experiment were of commercial reagent grade and were employed without additional purification, except when specified. Dry CH_2Cl_2 was prepared by refluxing and distilling it over P_2O_5.

Column chromatography was carried out using basic alumina, silica gel, and gel permeation chromatography with Bio-Beads S-X100 (BIO-RAD). The 1H-NMR spectra were obtained using a JEOL 400 MHz, Bruker 400 MHz, or Bruker 600 MHz spectrometer. Chemical shifts (δ) are expressed in units of parts per million (ppm). The Electronic spectra were recorded using a Perkin-Elmer λ-35 ultraviolet−visible (UV−vis) spectro-photometer and a Shimadzu UV-3600 spectrophotometer. A quartz cuvette with a path length of 1 cm was used, and the measurements were taken in the wavelength range of 300-2000 nmThe WATERS G2 Synapt Mass Spectrometer was used to acquire high-resolution mass spectra. The single-crystal X-ray diffraction examination results were obtained at a temperature of 100K using a BRUKER KAPPA APEX II CCD Duo diffractometer. The diffractometer was operated at a power of 1500 W, with a voltage of 50 kV and a current of 30 mA. Graphite-monochromated Mo Kα radiation with a wavelength of 0.71073 Å was used. The scattering contributions caused by the disordered solvent molecules in the crystal were eliminated using the SQUEEZE feature in the PLATON software suite. The BAS electrochemical system was used to perform cyclic voltammetry (CV) and differential pulse voltammetry (DPV) measurements. A typical three-electrode cell was employed, and the experiments were conducted in a dry CH_2Cl_2 solution with 0.1 M tetrabutylammonium perchlorate (TBAP) as the supporting electrolyte. The measurements were conducted in Argon gas atmosphere. The experimental setup included a glassy carbon as the working electrode, a platinum wire as the counter electrode, and either calomel or Ag/Ag+ as the reference electrode. The ultimate outcomes were adjusted using the ferrocene/ferrocenium pair.

Density Functional Theory (DFT) Calculations

The Gaussian09 (rev-D) program suite was employed to conduct quantum mechanical calculations, employing the High-Performance Computing Cluster facility of IISER PUNE. The calculations were performed using Density Functional Theory (DFT) with Becke's three-parameter hybrid exchange functional, and the Lee-Yang-Parr correlation functional (B3LYP) 6-31G(d,p) basis set was used for all atoms in the computations.

The molecular structures derived from single crystal analysis were utilized to obtain the geometry-optimized structures. The determination of molecular orbital contributions was performed using GaussSum 2.2. Program package. The NICS (0) values' global ring centers were designated at the non-weighted mean centres of the macrocycles. The NICS (0) value was determined using the gauge-independent atomic orbital (GIAO) approach, which relied on the optimized geometries. We computed the Anisotropy of the current-induced density (ACID) in order to visually represent the dispersion of delocalized π electrons. The AICD plots provide a direct visualization of both the magnitude and direction of the induced ring current when an external magnetic field is applied perpendicular to the plane of the macrocycle. The current density plots were generated using the continuous set of gauge transformations (CSGT) approach to compute the current densities. The resulting plots were created using POVRAY 3.7 for Windows. The visualization of the molecular orbitals was performed using Gauss View 4.1.

II.9 Experiment section

Synthetic Procedure and Characterisation

Synthetic Strategy I:

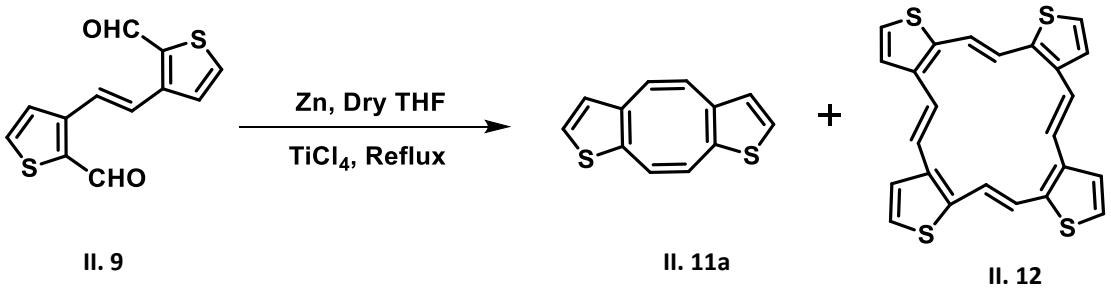

II. 9 II. 11a II. 12

Synthesis of (*E*)-3,3'-(ethene-1,2-diyl)-bis(thiophene-2-carbaldehyde) (II.9)

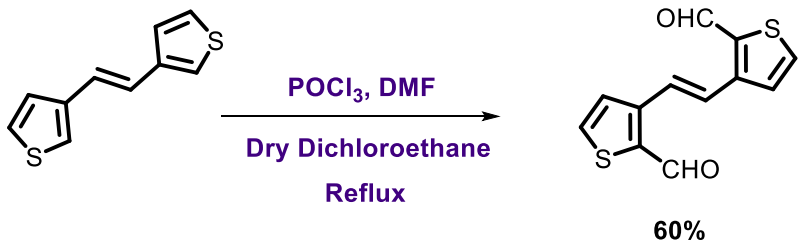

60%

(*E*)-1,2-Di(thiophen-3-yl)-ethene (0.192 g, 1 mmol) was dissolved in 1,2 dichloroethane (10 mL) and DMF (0.311 mL, 4 mmol). The solution was cooled to 5° C and $POCl_3$ (0.327 mL, 3.5 mmol) was added dropwise. The mixture was then heated to reflux overnight. After cooling, 50 mL of saturated solution of $NaCO_2CH_3$ were added and the mixture was stirred for an

additional one hour. The mixture was then extracted with ethyl acetate, washed with a saturated solution of $NaHCO_3$, water and dried over magnesium sulphate. The solvent was removed under vacuum and the product was purified by silica column chromatography (eluent: Pet ether/ EtOAc 8:2) to give (60%) of the desired product as yellow solid.

^{1}H NMR (400 MHz, $CDCl_3$) (**II.9**): δ 10.18 (d, *J* = 0.8 Hz, 1H), 7.83 (s, 1H), 7.72 (dd, *J* = 5.2, 0.9 Hz, 1H), 7.53 (d, *J* = 5.1 Hz, 1H); ^{13}C NMR (101 MHz, $CDCl_3$) δ 182.03, 145.24, 138.61, 134.74, 127.03, 125.20.

Synthesis of Symmetric Thiophene fused COT (II.11a) and Tetrathiaporphycene (II.12)

To a two-necked round-bottom flask, anhydrous THF (100 mL) was introduced. $TiCl_4$ (2.19 ml, 20 mmol) was slowly added and the mixture was maintained at 0° C for 35 min. Zinc powder (2.6 gm, 40 mmol) was then added portion-wise, and the reaction mixture was refluxed for additional 1 h. After cooling to 0° C, (*E*)-3,3(ethene-1,2-dial)-bis(thiophene-2-carbaldehyde), **II.9** (0.248 g, 1 mmol) was added followed by refluxing for 4 hrs. Then, the reaction mixture was quenched with ice water (50 mL), and extracted with ethyl acetate (100 mL) three times. The combined organic layers were dried over $MgSO_4$, and the solvent was removed under vacuum. The residue was purified by column chromatography on a silica gel column using hexane as eluent which gives **II.11a** as the first running band and the second band for **II.12**.

^{1}H NMR (400 MHz, $CDCl_3$) of (**II.11a)** (COT)): δ 7.30 (d, *J* = 5.1 Hz, 1H), 6.59 (d, *J* = 5.1 Hz, 1H), 6.51 (s, 1H), 6.36 (s, 1H). (Yellow needle) (5%);^{13}C NMR (101 MHz, $CDCl_3$) δ 138.43, 137.65, 130.07, 130.01, 128.52, 128.16; UV-vis λ_{max} (nm)(ε) $Lmol^{-1}cm^{-1}$ (in CH_2Cl_2) 286(26000); **MALDI TOF/TOF** mass spectra calculated for $C_{12}H_8S_2$ is 216.3160, found 216.1750. **HR-MS** (ESI-TOF): m/z=216.3160 (found $[M]^+$), 216.0067 (calcd. for $C_{12}H_8S_2$).

Selected Crystal data of II.11a: $C_{12}H_8S_2$, (M_r = 216.30), orthorhombic, space group *P bca*, *a* = 6.4392(10), *b* = 14.769(2), *c* = 21.618(4) Å, $\alpha = 90^0$, $\beta = 90^0$, $\gamma = 90^0$; *V* = 2055.9(6) $Å^3$, *Z* = 8, *T* = 100 K, D_{calcd} = 1.398 gcm^{-3}, R_1 = 0.0420 (I > 2sigma (I)), R_w (all data) = 0.0996, GOF = 1.077;

^{1}H NMR (400 MHz, $CDCl_3$) of (**II.12)**: δ 7.41 (s, 1H), 7.30 (s, 1H), 7.17 (d, *J* = 5.3 Hz, 1H), 7.05 (d, *J* = 5.3 Hz, 1H). (Orange needle) (20%);^{13}C NMR (101 MHz, $CDCl_3$) δ 138.08, 137.16,

127.70, 126.27, 124.85, 124.49; UV-vis λ_{max} (nm)(ε) $Lmol^{-1}cm^{-1}$ (in CH_2C1_2) 318 (30400);. **MALDI TOF/TOF** mass spectra calculated for $C_{24}H_{16}S_4$ is 432.0135, found 432.0940. **HR-MS** (ESI-TOF): m/z=432.0116 (found $[M]^+$), 432.0135 (calculated for $C_{24}H_{16}S_4$).

Selected Crystal data of II.12: $C_{24}H_{16}S_4$, (M_r = 432.61), monoclinic, space group *C 2/c*, *a* = 23.47(3), *b* = 4.846(6), *c* = 17.57(2) Å, $\alpha = 90^0$, $\beta = 94.67^0$ (3), $\gamma = 90^0$; *V* = 1992 $Å^3$, *Z* = 4, *T* = 150 K, D_{calcd} = 1.443 gcm^{-3}, R_1 = 0.0498 (I > 2sigma (I)), R_w (all data) =0.1791, GOF = 0.864;

Synthetic strategy II:

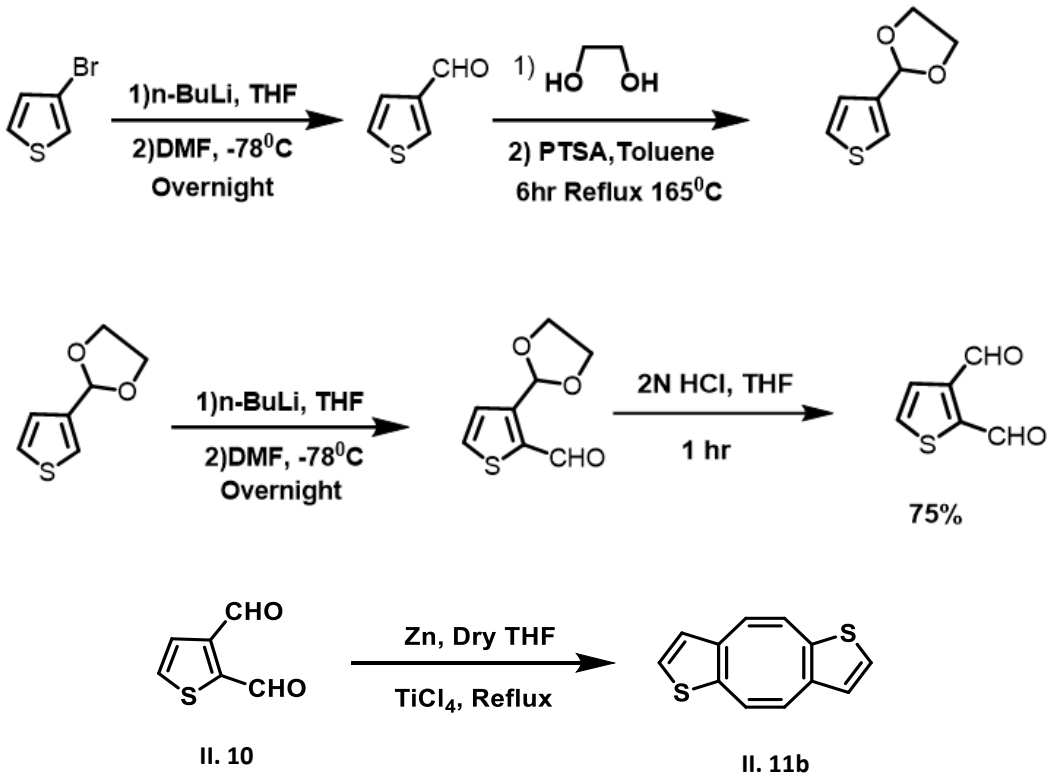

II. 10 **II. 11b**

Synthesis of Asymmetric Bithiophene fused COT (II.11b):

To a stirred solution of thiophene-2,3-dicarbaldehyde[70] **II.10** (0.140 g, 1 mmol) in dry THF (100 ml),titanium(IV)chloride (2.19 mL, 20 mmol) was added over a period of 0.4 h, zinc powder (2.6 gm, 40 mmol) was added in portion wise over period of 1 h. the resulting mixture was stirred at -18 ^{0}C for 1 h, warmed to room temperature, and refluxed for 4 hrs. then, the reaction mixture was quenched with ice cold water (50ml), and extracted with ethyl acetate 9100ml) thrice. The combined organic layers were dried over MgSO4, and the filtrate was removed under vacuum. The residue was purified by column chromatography on a silica gel column using hexane as eluent which gives **II.11b** in 10% yield.

^{1}H NMR (400 MHz, Chloroform-*d*) of **15b** (COT)): δ 7.29 (dd, *J* = 5.2, 4.4 Hz, 2H), 6.59 (dd, *J* = 5.1, 1.3 Hz, 2H), 6.51 (s, 1H), 6.44 (d, *J* = 2.7 Hz, 2H), 6.36 (s, 1H). (Yellow needle) (10%); (Yellow needle) (10%); UV-vis λ_{max} (nm)(ε) $Lmol^{-1}cm^{-1}$ (in CH_2Cl_2) 286(26000); **MALDI TOF/TOF** mass spectra calculated for $C_{12}H_8S_2$ is 216.3160, found 216.1750. **HR-MS** (ESI-TOF): m/z=216.3160 (found $[M]^+$).

Selected Crystal data of II.11b: $C_{12}H_8S_2$, (M_r = 216.30), monoclinic, space group *C 1*, *a* = 18.877(3), *b* = 6.4130(12), *c* = 8.5193(16) Å, $\alpha = 90^0$, $\beta = 99.211^0$, $\gamma = 90^0$; *V* = 1018.0(3) $Å^3$, *Z* = 4, *T* = 100 K, D_{calcd} = 1.411 gcm^{-3}, R_1 = 0.0302 (I > 2sigma (I)), R_w (all data) = 0.0766, GOF = 1.087;

Chapter 3

Aromaticity in Thieno[3,2-*b*]thiophene Incorporated Expanded Porphyrinoids

III.1 Introduction

Porphyrin is recognized for its pivotal roles in biological systems, and long been esteemed for distinctive aromatic and conjugate structures. The conjugated π-systems of porphyrins impart unique electronic properties, rendering them central to various biological processes. The structural expansion enhances the π-conjugation, leading to unconventional manifestations of aromaticity and antiaromaticity. The expanded macrocycle alters its electronic, structural properties and redox study. The resulting expanded porphyrins exhibit remarkable conformational flexibility, contributing to their multifunctional nature.

There are multiple ways to increase the length of a π-conjugated network by incorporating more heterocyclic units **1**, or additional meso-carbon atoms and such type of macrocycles comes under class of expanded macrocycles.[52,56] Replacing the meso-carbon atoms with ethylene linkages to get the higher homologues of isophlorin **3**.[33] The expanded porphyrins display absorbance bands are red-shifted relative to those of porphyrin (figure – III.1).

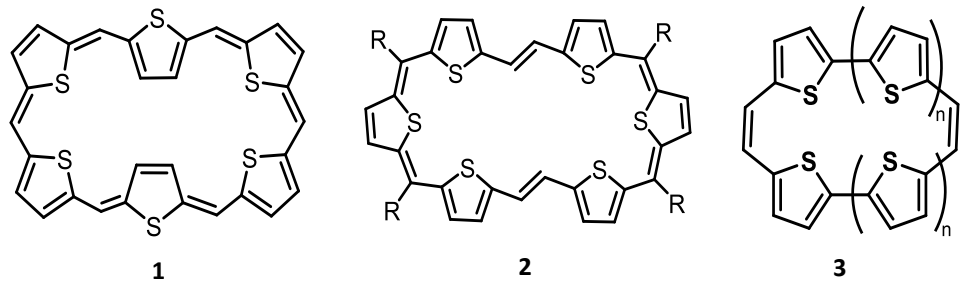

Figure III.1: Structural illustration of expanded and ethylene bridged isophlorins.

Rath and co-workers synthesised the first [22] aromatic core-modified expanded porphyrin **4,** by replacing the two pyrroles with fused thieno-thiophene heterocycles.[71] This strategic alteration resulted in the extended π-conjugation, leads to exhibit absorption in the NIR region. X-ray study revealed that thieno-thiophene moiety adopted an orthogonal orientation to the macrocyclic plane due to the steric hindrance induced by phenanthrene moiety. Later, the same group reported the synthesis of [30] Thieno-thiophene fused macrocycle **5,** with four meso-carbons.[72] The large difference in chemical shift of inner and outer protons of thieno-thiophene and planar structure of the macrocycle gave strong evidence of aromatic nature (figure – III.2).

By continuing this methodology, Rath and co-workers reported the [32] heteroannulene **6,** where they replaced the bipyrrole unit with dipyrromethene and synthesised the aromatic Thieno-thiophene incorporated 32π core modified hexaphyrin.[73] Molecular structure showed the twisted conformation both in solution and solid state. The ^{1}H NMR spectrum of free base and protonated species supported its conformational flexibility.

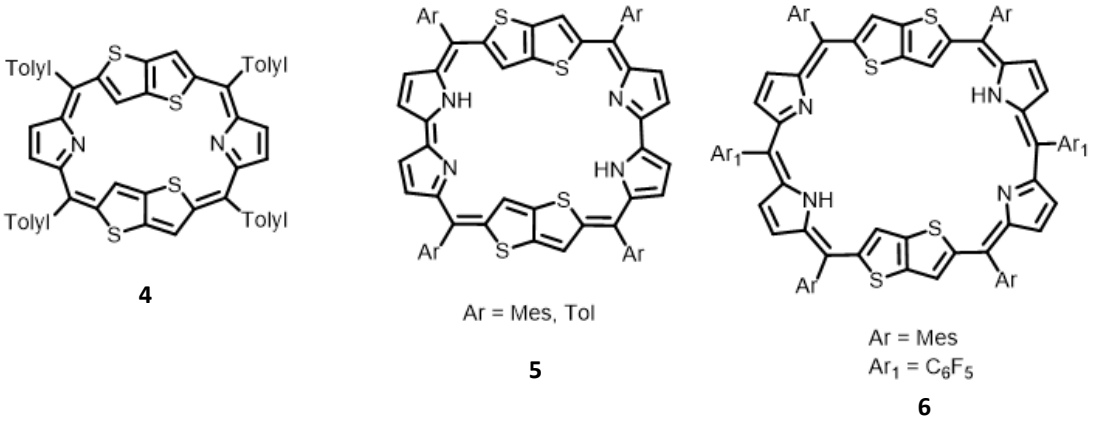

Figure III.2: Thieno[3,2-*b*]thiophene incorporated [22], [30] and [32] macrocycles.

Similarly, Osuka and co-workers reported the Thieno-thiophene bridged [46] decaphyrin and molecular structure exhibited the doubly twisted annulene variant but the contribution of the local circuits is small because of the orthogonal orientation of the bridged thieno-thiophene.[74] The absorption of all these Thieno-thiophene-containing heteroporphyrins well extend into the NIR region.

Exploring the intriguing properties of heterocycle fused expanded porphyrin has become a compelling avenue for further investigation. Since Thieno-thiophene incorporated macrocycles have not been studied much, therefore an attempt was made to explore its effect upon replacing it with thiophene. Herein, the synthesis was attempted towards the 34π hexaphyrin by maintaining the aromaticity of 30π isophlorin's extended the π-conjugation and [34] hexaphyrin having furan and selenophene units to study the effect of electronic and optical properties on the macrocycle.[52]

III.2 Synthesis of Thieno[3,2-*b*]thiophene incorporated [34] Hexaphyrin (III.3)

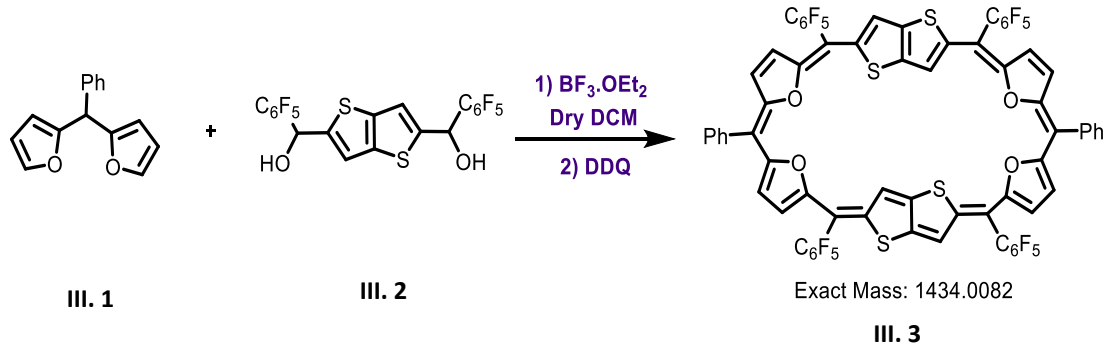

Scheme III.1: Synthesis of Thieno[3,2-*b*]thiophene incorporated 34π isophlorin **III.3**.

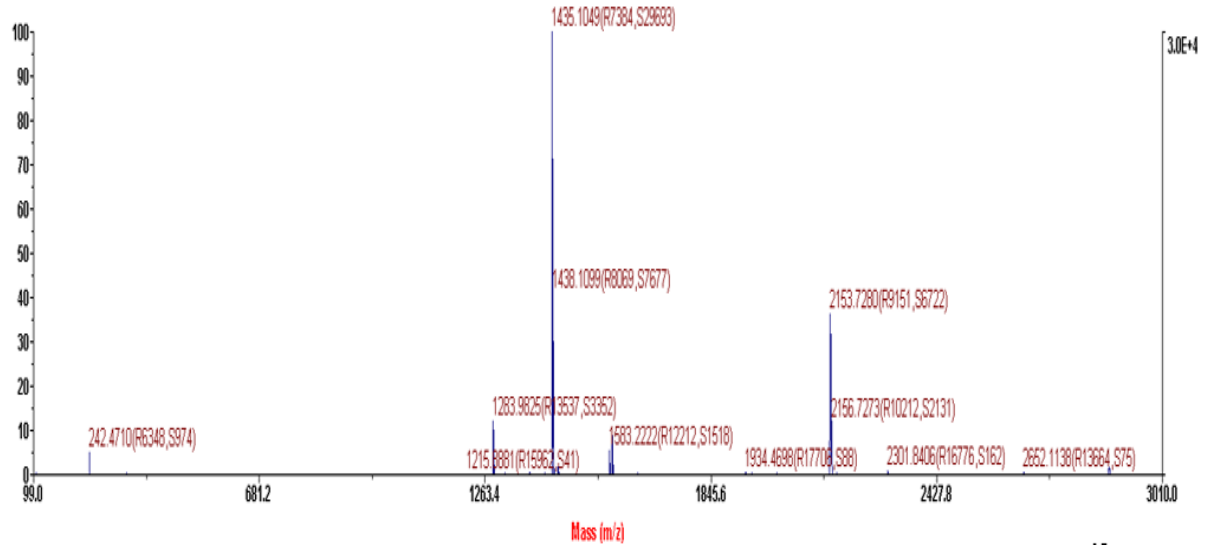

Figure III.3: MALDI-TOF/TOF spectrum of reaction mixture (scheme **III.1**)

The Thieno[3,2-*b*]thiophene incorporated isophlorin was synthesised by the condensation of Thieno thiophene diol **III.2**, with furan-dipyrromethane **III.1**, in presence of $BF_3.OEt_2$ under dark and inert conditions and stirred at room temperature for two hours (scheme - III.1). Later, DDQ was added as the oxidising agent and stirred for another two hours in open atmosphere. Subsequently, the reaction mixture was filtered through a small amount of basic alumina, and the resulting mixture was then concentrated under reduced pressure. The reaction combination was confirmed using MALDI-TOF/TOF mass spectrometry, which detected the desired mass as well as higher analogues (figure – III.3).

III.3.1 Isolation and Characterisation of [34] Hexaphyrin (III.3)

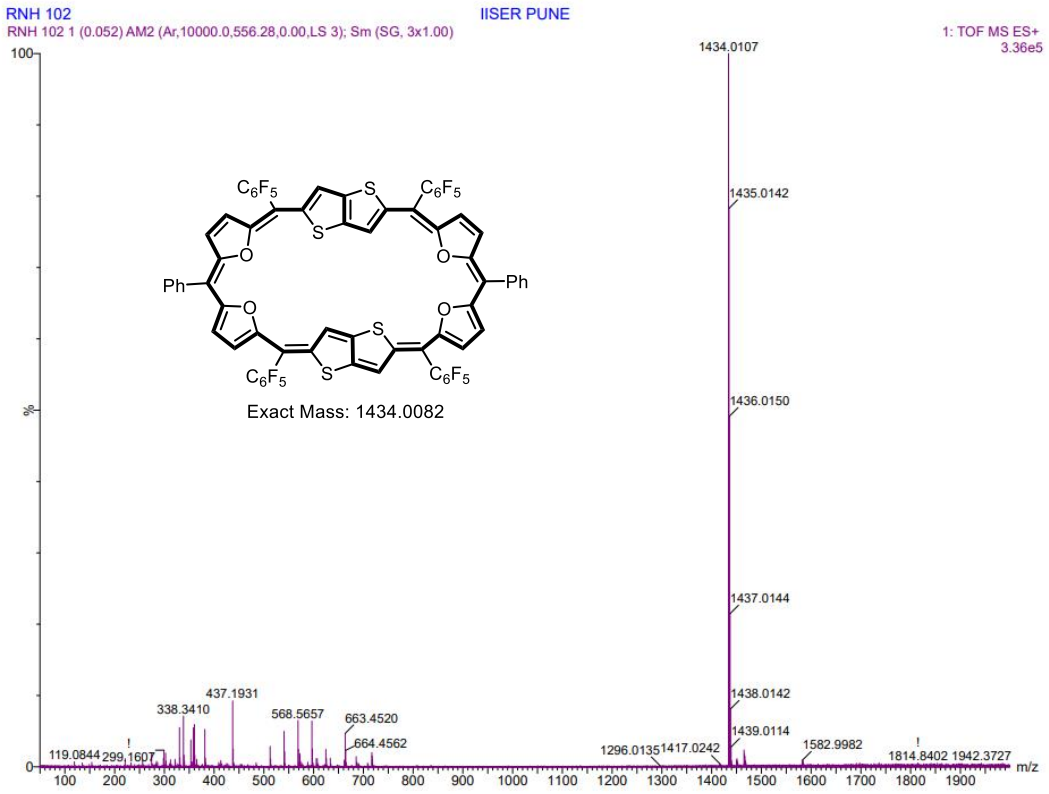

Figure III.4: HR-ESI-TOF mass spectrum of **III.3**

The desired macrocycle was purified using basic alumina column chromatography. A violet-coloured band was isolated and the composition of the isolated macrocycle **III.3,** was confirmed by High Resolution Mass spectrometry (HR-MS), which displayed an *m/z* value of 1434.0107 (Calculated mass 1434.0082) (figure – III.4).

III.3.2 ^{1}H NMR study of [34] Hexaphyrin (III.3)

Hexaphyrin, with 34π electrons in a conjugated pathway, was expected to show diatropic ring current effect. ^{1}H NMR spectrum of the macrocycle **III.3,** in $CDCl_3$ at room temperature (figure – III.5) displayed well resolved signals. The presence of distinct eight signals indicated the symmetrical structure of macrocycle **III.3**, confirming its possession of a C_2 axis of symmetry. Specifically, four different signals corresponding to an equal number of protons were observed in the region between δ 7 to 5 ppm. The four doublets are resonated at δ 6.8, 6.53, 6.22 and 6.0 ppm corresponding to the β-protons of the Thieno[3,2-*b*]thiophene and furan units. Additionally, two singlets were observed for the Thieno-thiophene unit, one proton resonating at the downfield δ 6.7 ppm and another proton resonate at upfield δ 5.3 ppm.

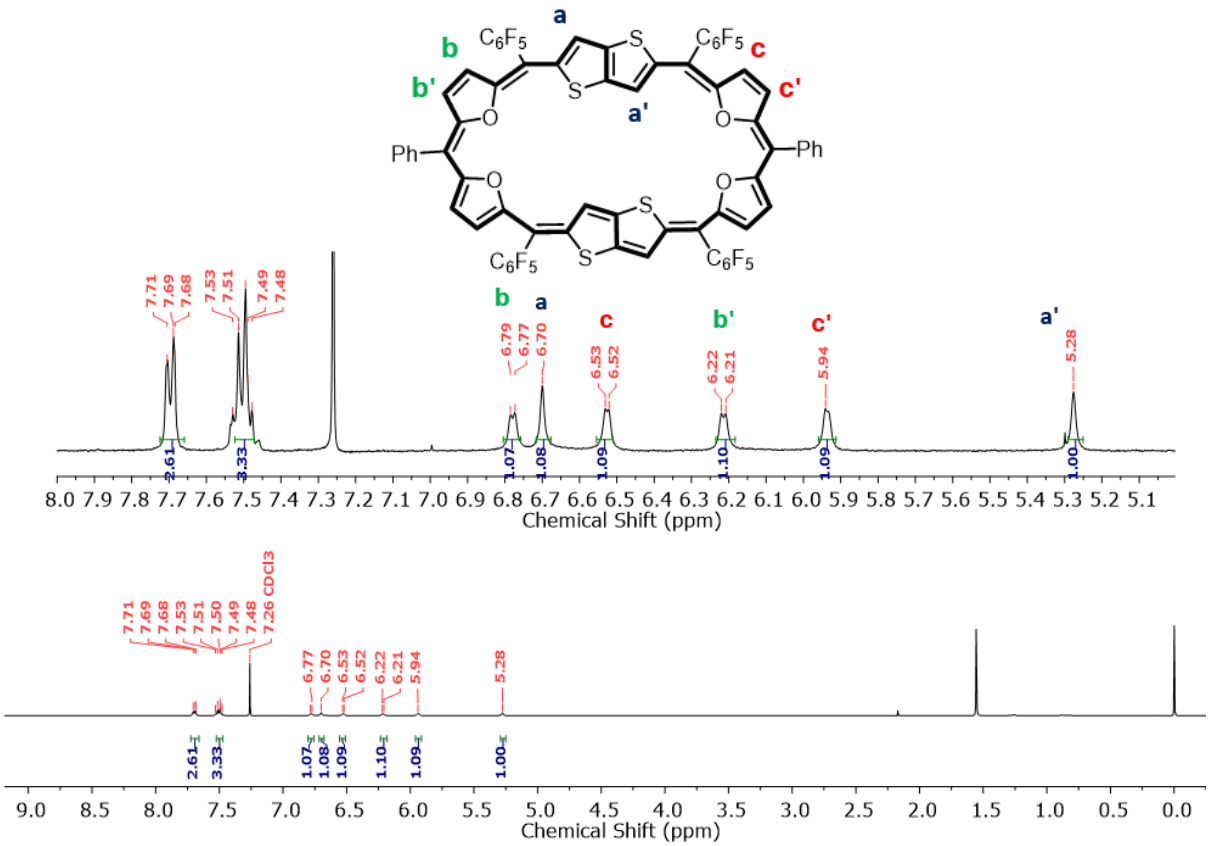

Figure III.5: ^{1}H NMR spectrum of **III.3** in Chloroform-*d*.

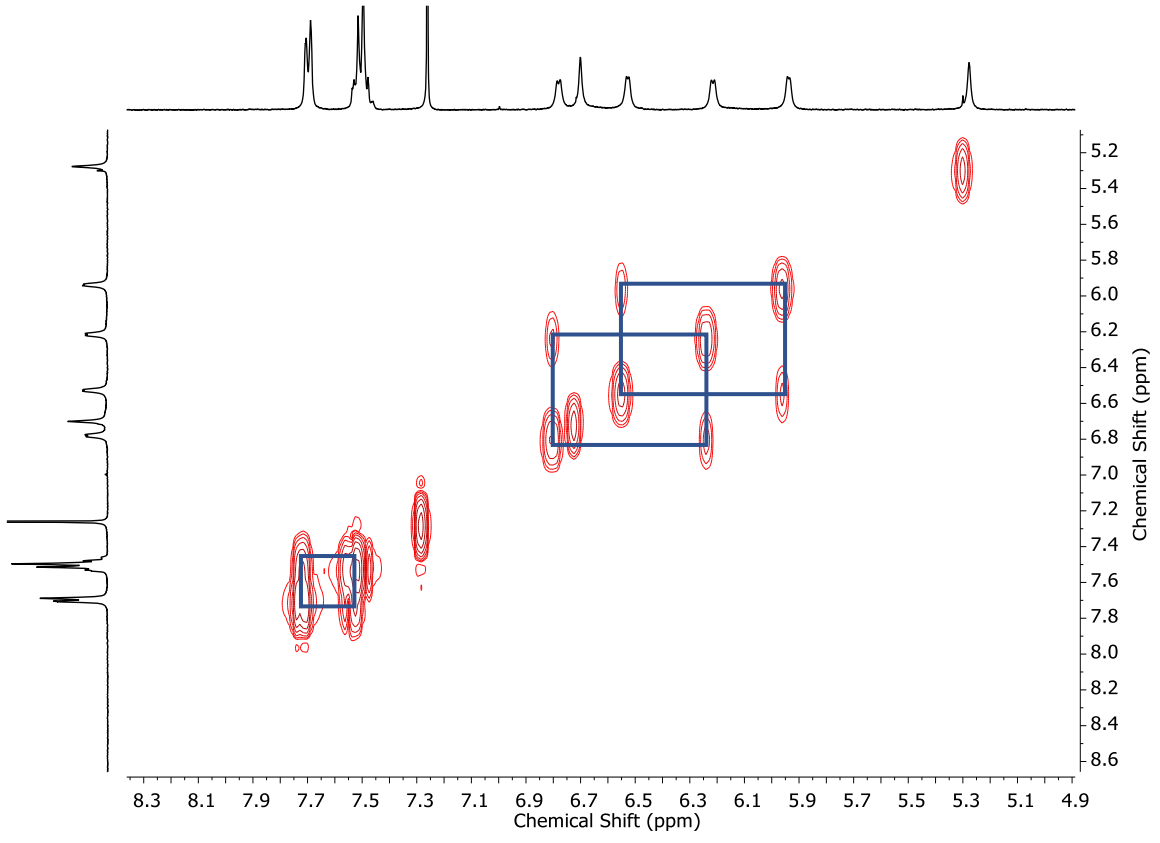

Figure III.6: ^{1}H-^{1}H COSY spectrum of **III.3** in Chloroform-*d*.

The Δδ 1.5 ppm difference between these two singlets indicated a weak diatropic ring current effect experienced by Thieno-thiophene protons. The overall observations suggested that the macrocycle did not exhibit a significant diatropic ring current effect.

Further correlation of these protons was obtained from ^{1}H-^{1}H COSY spectrum (figure – III.6), which showed two sets of correlations accounting for the four protons from two furan rings and another two sets of correlations for phenyl protons.

III.3.3 Electronic Absorption and Cyclic Voltammogram studies

Due to extended π-conjugation of 34π hexaphyrin, shows absorption in the visible region of electromagnetic spectrum and found to be multiple absorption at 575 nm (94300) with high extinction co-efficient along with a less intense band at 342 nm (54200) (figure – III.7a).

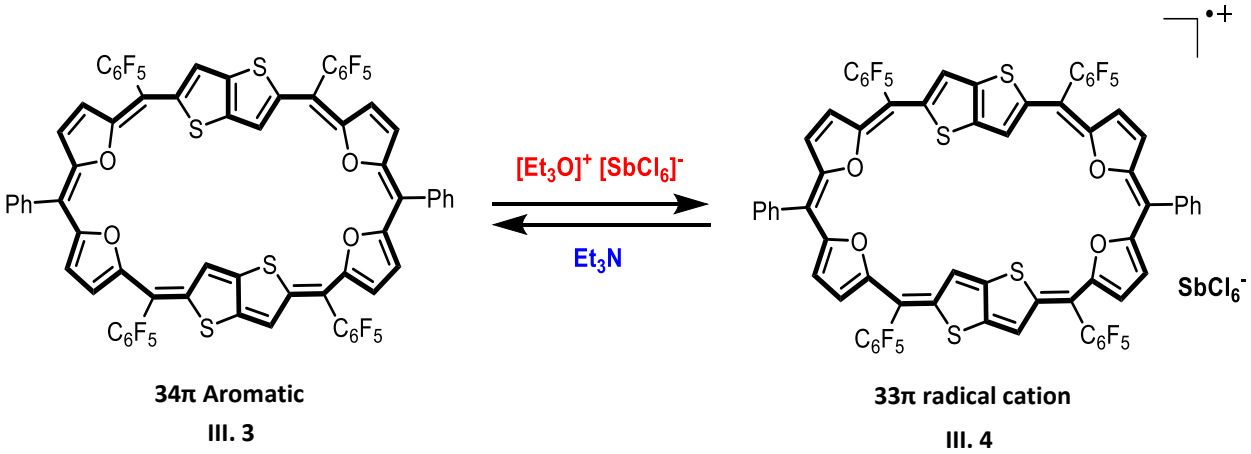

Scheme-III.2: oxidation of 34π (**III.3**) to 32π radicalcation (**III.4**) upon addition of Meerwein's salt

Meerwein's salt $[Et_3O]^+$ $[SbCl_6]^-$ acts as an effective one-electron oxidizing agent for a π-conjugated system.[66] Aromatic systems are frequently found to undergo single-electron oxidation, resulting in the formation of a radical cation. On the other hand, antiaromatic macrocycles typically experience two-electron oxidation, leading to the formation of the corresponding dicationic species. In a recent study, it was observed that (4n+2)π non-aromatic/aromatic [50]decaphyrin macrocycle undergoe reversible two-electron ring oxidation to yield the corresponding anti-aromatic dication[12,57] Upon the addition of Meerwein's salt to a solution of **III.3**, it showed a subtle colour change from violet to pink suggesting the one electron ring oxidation and formation of radical cation (scheme - III.2). The radical cationic species **[III.4]**$^{+\cdot}$, showed a significant red shift to 600 nm along with shoulder band at 740 nm. The oxidised species reverted back to its free base upon the addition of reducing agent such Zn dust or Et_3N. To support the redox study of **III.3**, cyclic voltammetry and differential pulse

voltammetry experiments were conducted. The 34π hexaphyrin showed three oxidation waves at + 0.58, + 0.81 and + 1.2 V and two reduction waves at - 0.70, - 0.95 V (figure – III.7b) respectively.

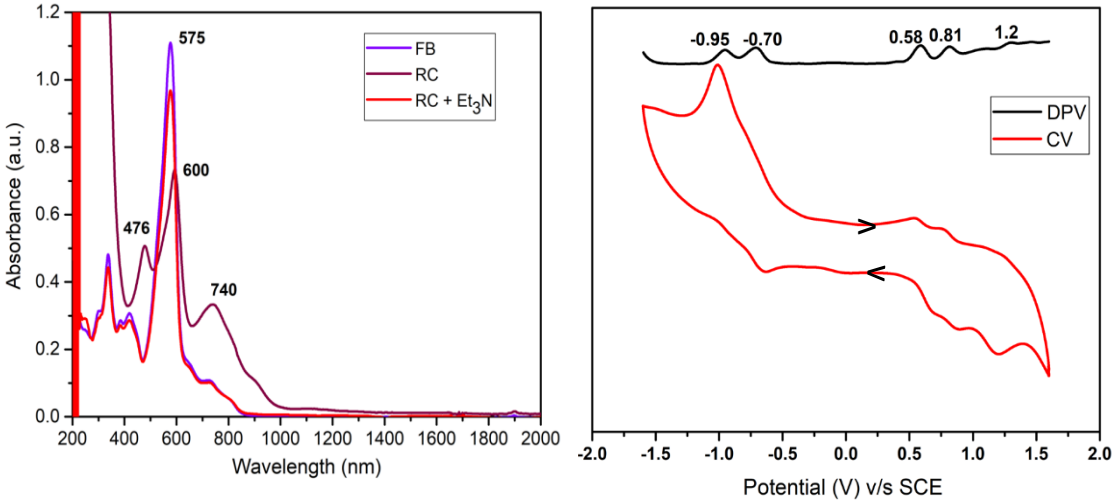

Figure III.7: a) UV/vis/NIR absorption spectrum of 10^{-5} M solution of **III.3** (34π) (Violet) (FB: Free Base) and its oxidised species [**III.4**]$^{\cdot+}$ (32π) (Brown) (RC: Radical cation) recorded in CH_2Cl_2. b) Cyclic voltammogram (CV, red) and differential pulse voltamomgram (DPV, black) of **III.3** in CH_2Cl_2 (with 0.1 M $(Bu)_4NPF_6$ as the supporting electrolyte).

III.3.4 Molecular structure of [34]hexaphyrin (III.3)

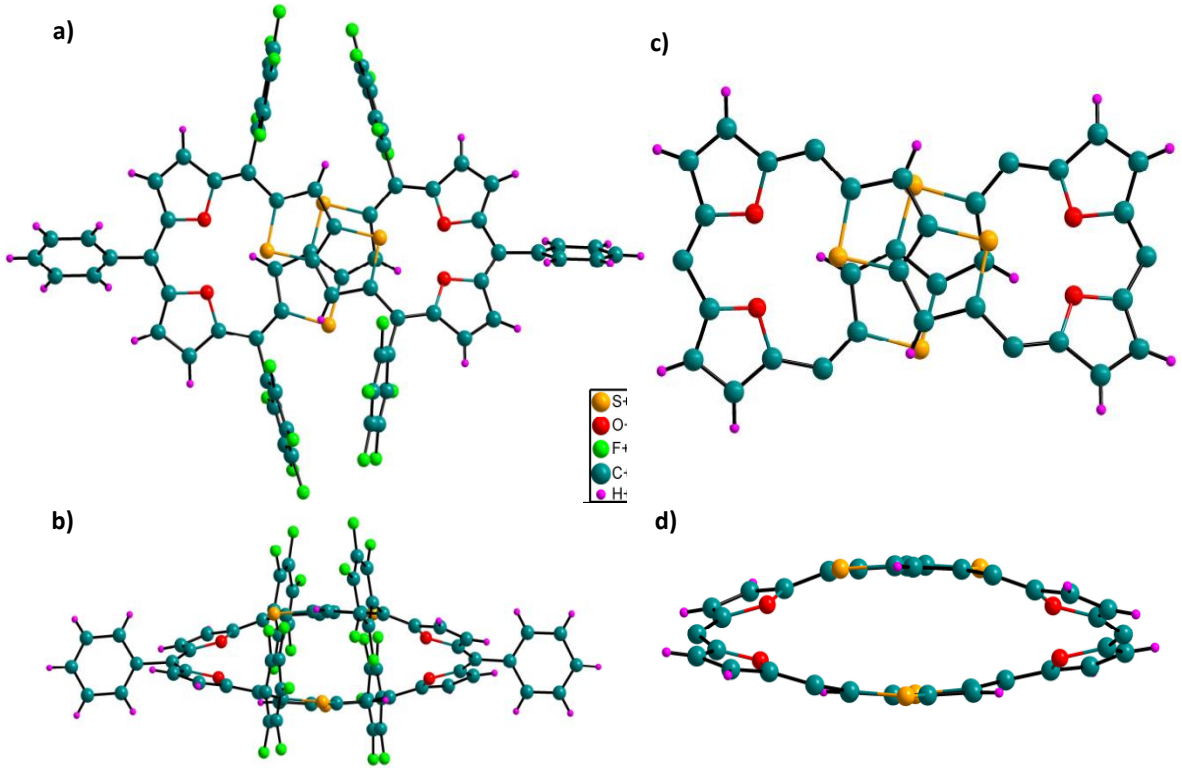

Figure III.8: Molecular structure of 34π hexaphyrin (**III.3)** as determined from single crystal X-ray diffraction a) (top view) b) side view and pentafluorophenyl and phenyl rings are omitted of clarity in the c) (top view) and d) (side view).

After several attempts, good quality crystals were obtained by vapours of n-hexane diffused into a solution of the macrocycle in dichloromethane. The single crystal X-ray diffraction analysis unveiled the absolute molecular structure, indicating a twisted figure of eight conformation (figure - III.8). The Thieno-thiophene unit was situated at the centre of the macrocycle, dividing the molecule into equal parts with three-membered rings. The same non-planar and twisted conformation is in support of its observed ^{1}H NMR spectrum.

III.4 Synthesis of Thieno[3,2-*b*]thiophene incorporated 34π Hexaphyrin

The structural diversity and impact of aromaticity in the hexaphyrin macrocycle was studied by substituting furan unit with isoelectronic species selenophene in **III.3**. The objective of this exploration was to investigate how these changes could influence the electronic, structural characteristics and aromaticity of the macrocycle. An equimolar concentration of 2,2'-(phenylmethylene)bis(selenophene) **III.5,** and Thieno-thiophene diol **III.2**, was dissolved in 100 ml of dry dichloromethane and degassed with argon for ten minutes. A catalytic amount of $BF_3.OEt_2$ was introduced into the reaction mixture in the dark condition and agitated for two hours. Following that, 2.5 equivalents of DDQ were introduced and stirred for a further two hours under ambient conditions (scheme - III.3). In addition to the expected result, the MADLI/TOF-TOF mass spectrum of the reaction mixture also showed modest yields of larger macrocycles.

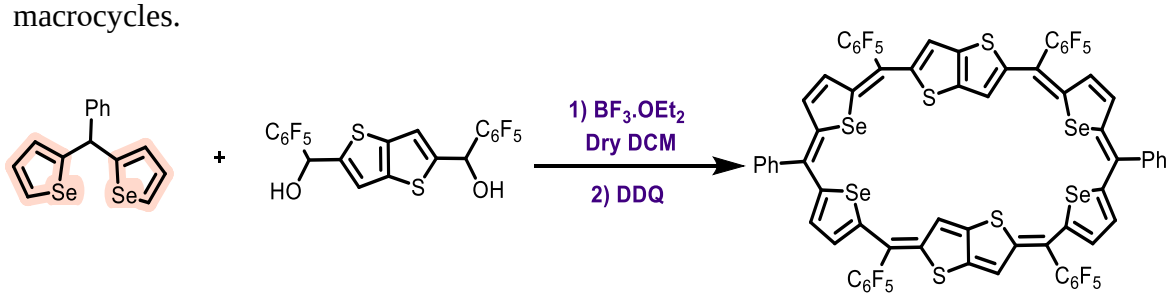

III. 5 III. 2 Exact Mass: 1689.6946 III. 6

Scheme III.3: Synthesis of Thienothiophene incorporated 34π isophlorin **III.6**.

III.5.1 Isolation and Characterisation of 34π Hexaphyrin (III.6)

After confirming the formation of the desired product by MALDI-TOF/TOF mass spectrometry, the reaction mixture was passed through a short bed of basic alumina and then concentrated the resultant mixture under vacuum. The isolation of desired macrocycle was

performed by basic alumina column chromatography using CH_2Cl_2/Hexane as eluent. As observed in the mass spectrum, two different macrocycles were isolated one by one through repeated basic alumina column chromatography. The first violet coloured band was isolated and it corresponded to the desired macrocycle **III.6**. Subsequently, the HR-ESI-TOF mass spectrum of **III.6,** was recorded, confirming the formation of the desired product with an *m/z* value of 1689.7057 (calculated mass 1689.6946) (figure – III.9).

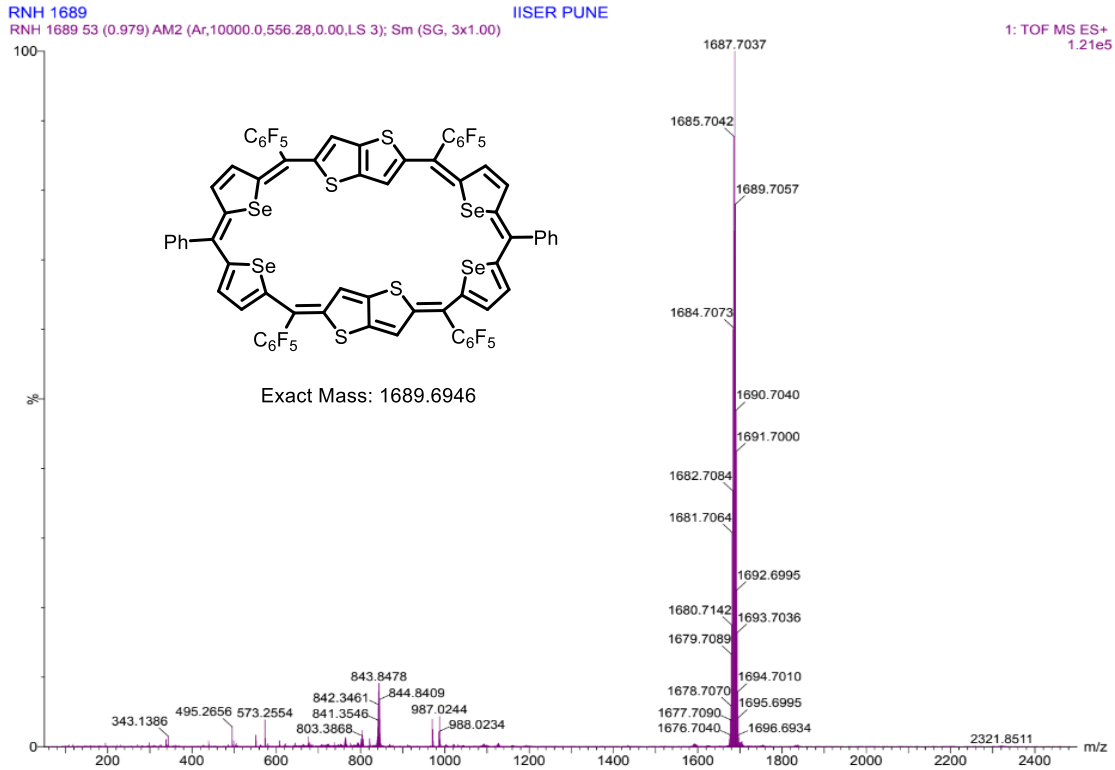

Figure III.9: HR-ESI-TOF mass spectrum of **III.6**.

III.5.2 ^{1}H NMR study of [34] Hexaphyrin (III.6)

The macrocycle **III.6**, accounts for 34π electrons along its conjugated path and hence expected to be an aromatic macrocycle. The ^{1}H NMR spectrum of **III.6,** recorded in $CDCl_3$ solvent at 298 K, displayed ten signals that resonated in the region between δ 4 to10 ppm (figure – III.10). suggesting its near planar conformation having C_2 axis of symmetry. Two doublets corresponding to two protons were observed at δ 9.96 and 9.82 ppm are attributed to the β-protons of selenophene ring. A broad singlet resonated at δ 4.0 ppm in the upfield region, for the β-protons of Thieno-thiophene owing to the rapid fluxionality between the inner and outer protons. Unlike the **III.3**, the chemical shift difference $\Delta\delta$ of approximately 6 ppm between Thieno-thiophene and selenophene protons clearly signifies that **III.6**, exhibits a strong diatropic ring current effect. Additionally, the phenyl protons were found to resonate in the

region between δ 8.0 and 8.5 ppm. A comprehensive analysis revealed that **III.6,** showed strong diatropic ring current compared to the **III.3,** supporting the aromatic nature of the macrocycle.

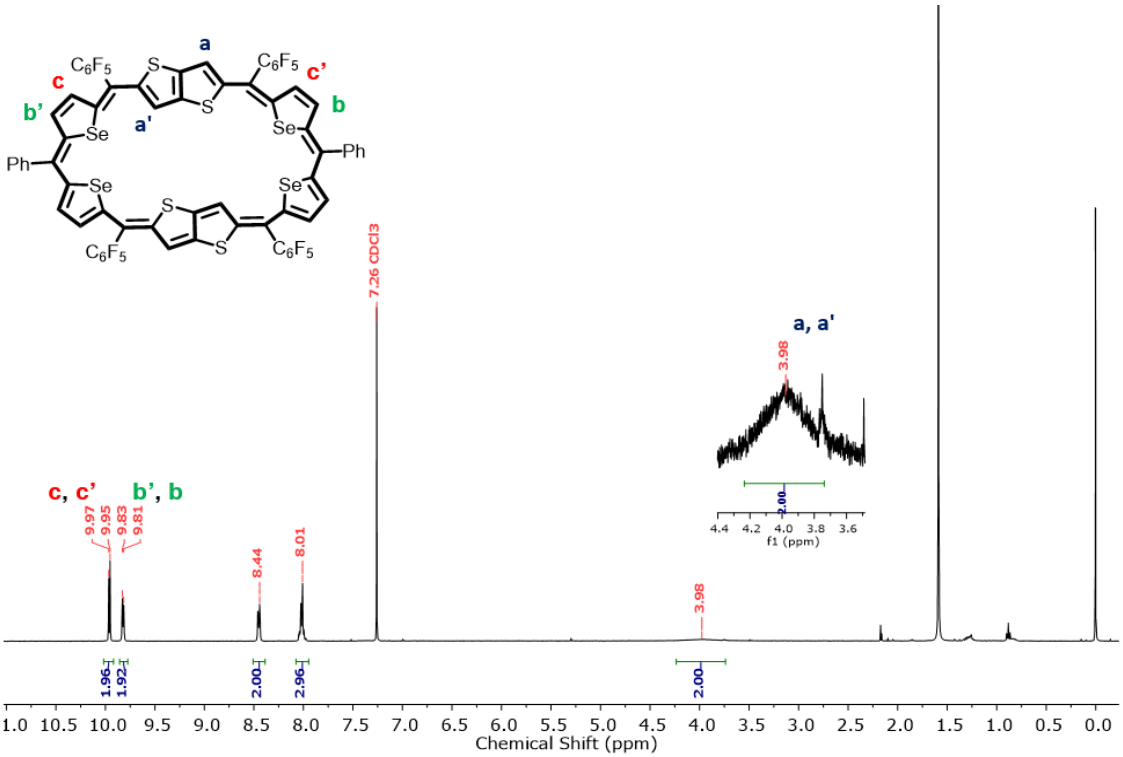

Figure III.10: ^{1}H NMR spectrum of **[III.6]** in $CDCl_3$

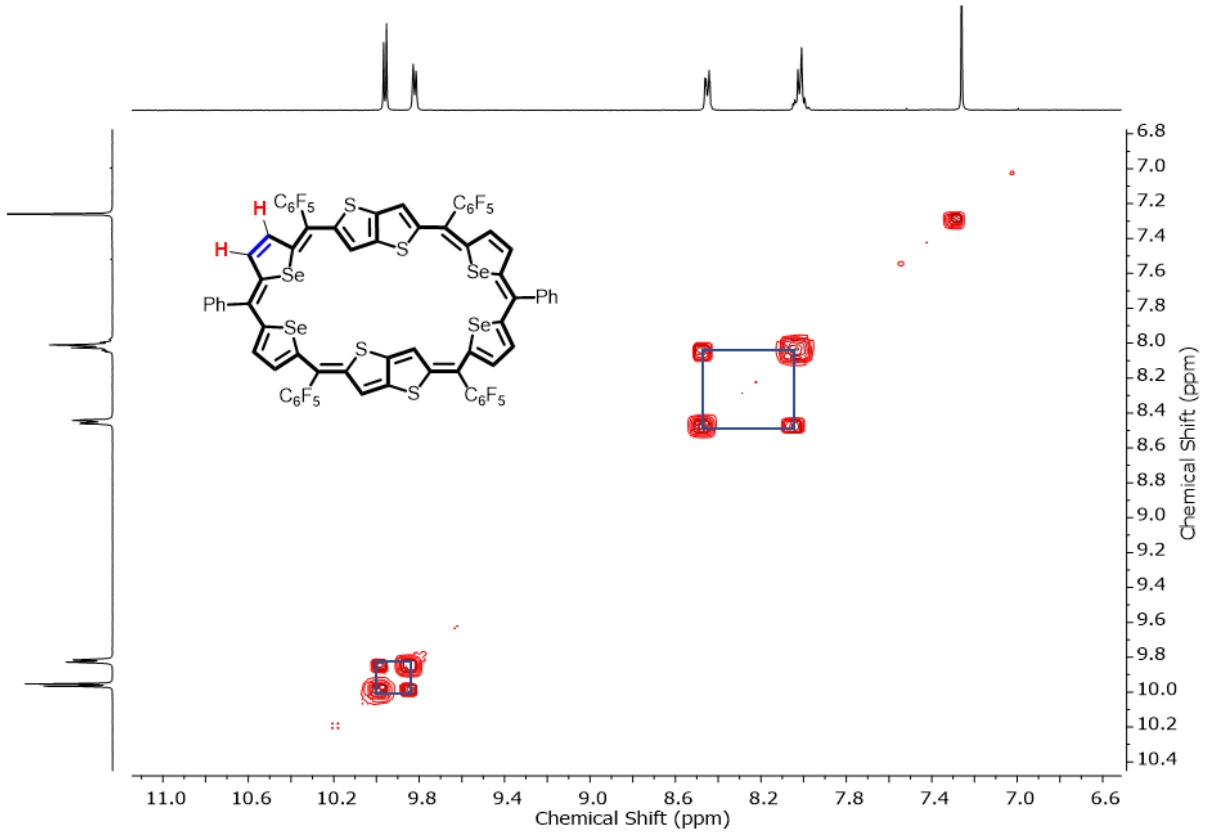

Figure III.11: ^{1}H-^{1}H COSY NMR spectrum of **III.6** in Chloroform-d

The ^{1}H-^{1}H COSY spectrum displayed the distinct correlation for the phenyl and selenophene protons (figure - III.11). The correlations at δ 9.96 and 9.82 ppm were identified for the β-protons of selenophene. These findings were consistent with the results observed in the ^{1}H NMR spectrum.

III.5.3 Molecular structure of [34]hexaphyrin (III.6)

High-quality single crystals were grown by diffusing hexane vapours into a dichloromethane solution of the macrocycle. Unlike **III.3**, The investigation of X-ray diffraction on a single crystal revealed a nearly planar structure, where all selenium atoms of the selenophene are orientated towards the core of the macrocycle. (figure – III.12) Due to bulkiness of the selenium, the macrocycle slightly deviated from an absolute planar structure. Both ^{1}H NMR and molecular studies confirmed the near planar conformation for the macrocycle.

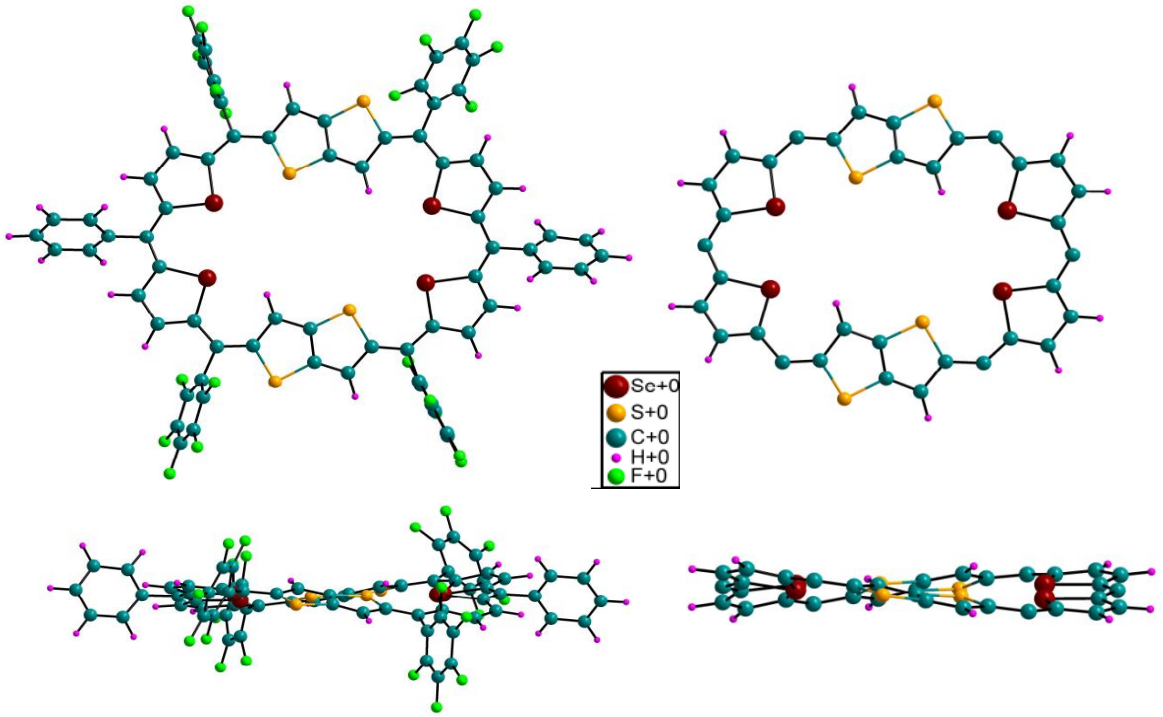

Figure III.12: Molecular structure of 34π hexaphyrin (**III.6)** as determined from single crystal X-ray diffraction a) (top view) b) side view and Pentafluorophenyl and phenyl rings are omitted of clarity in the c) (top view) and d) (side view).

The Thieno-thiophene was positioned planar to the macrocycle ring and due to their high fluxionality at room temperature exhibited the average signals for the both protons and showed broad signal.

III.5.4 Electronic absorption and Spectro-Electrochemical studies

The UV/Vis/NIR absorption spectrum of 34π hexaphyrin, **III.6**, was recorded in dry dichloromethane, which displayed a Soret-like band at 578 nm along with a shoulder peak at 595 nm (123900) and the low energy bands at 792 nm (55400) (figure – III.13a). Unlike **III.3**, Addition of Meerwein's salt to the solution of **III.6**, results in the strong red shift at 730 nm and a less intense band at 605 nm suggesting the formation of dicationic species.[66] The oxidised species could be reduced back to its free base by the addition of Zn dust or Et_3N (scheme - III.4).

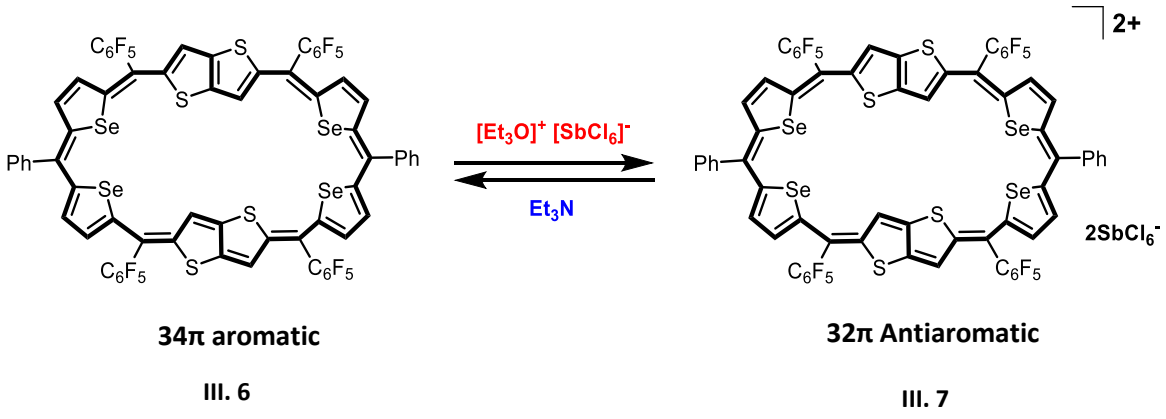

Scheme-III.4: oxidation of 34π (**III.6**) to 32π dication (**III. 7**)$^{+2}$ upon addition of Meerwein salt

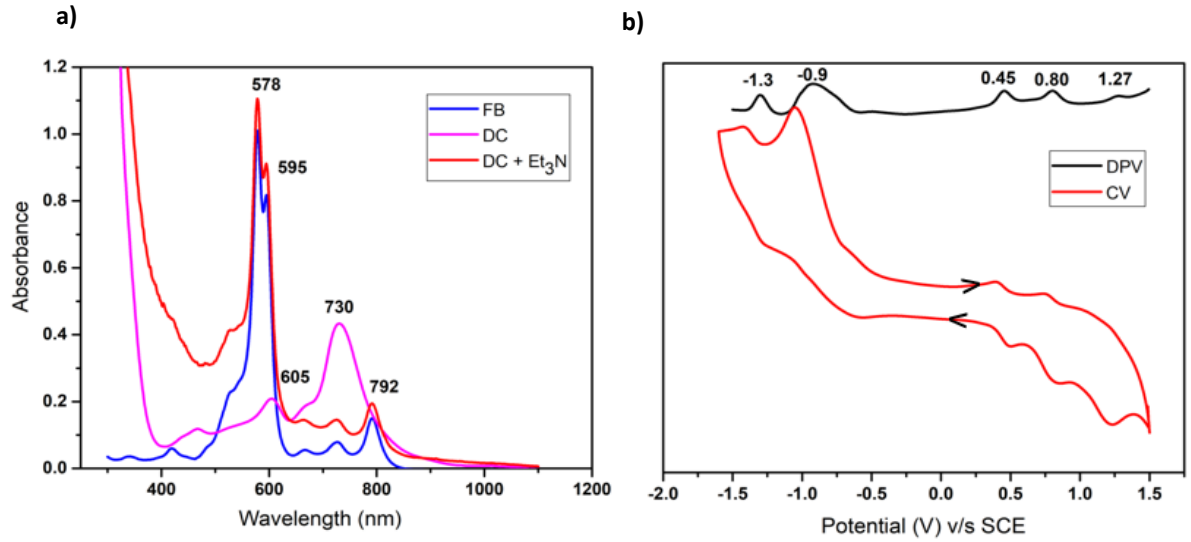

Figure III.13: a) UV/vis/NIR absorption spectrum of 10^{-5} M solution of **III.6** (34π) (Blue) (FB: Free Base) and its oxidised species [**III.7**]$^{2+}$ (32π) (pink) (DC: Dication) recorded in CH_2Cl_2. b) Cyclic voltammogram (CV, red) and differential pulse voltammogram (DPV, black) of **III.6** in CH_2Cl_2 (with 0.1 M $(Bu)_4NClO_4$ as the supporting electrolyte).

For better understanding, the redox chemistry of macrocycle was studied by cyclic voltammetry and differential pulse voltammetry in dichloromethane where it showed the three

oxidations peak at + 0.45, + 0.80, + 1.27 V and two reduction potential at - 0.9 and - 1.3 V (figure – III.13b) respectively.

III.6 Quantum mechanical calculations

The confirmation of the aromaticity and antiaromaticity of the macrocycles was determined using DFT calculations, namely the nucleus independent chemical shift (NICS) and the anisotropy of the induced current density (AICD), for the 34π hexaphyrin. The calculated NICS value of **III.6**, was found to be δ = -14.07 ppm (table – II.1), such large negative value of NICS value showed its strong [4n+2] π electron aromatic character and further supported by the clockwise ring currents suggest the aromatic nature of macrocycle. Whereas in case of **III.3**, showed the NICS value of δ = -2.76 ppm suggest the weak antiaromatic character and also supported by the AICD plot (figure – III.14).

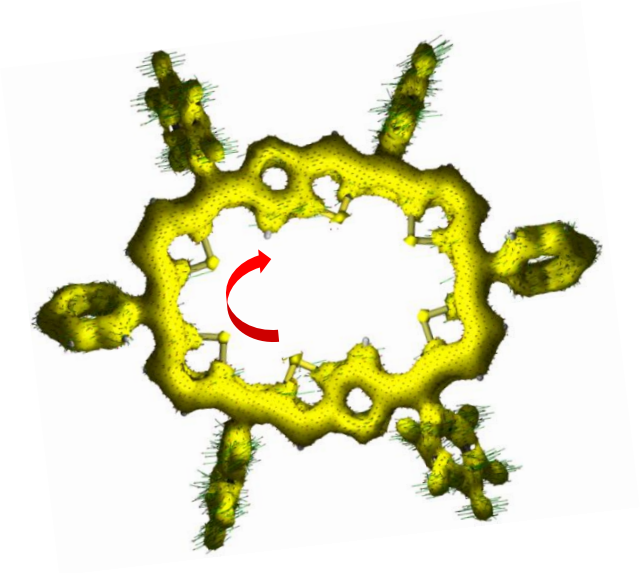

Figure III.14: AICD plot of **III.6** at an iso surface value 0.06 the external magnetic field is applied orthogonal to the macrocyclic plane.

Time-dependent TD-DFT computations were used on the optimized structures to simulate the steady-state absorption spectra. The absorption spectra of macrocycle **III.3**, were matched with the experimental results (figure – III.15). The HOMO and LUMO energy gap for both macrocycles **III.3**, (figure – III.16) and **III.6,** (figure – III.17) are 1.69 and 1.59 eV respectively.

Macrocycle	NICS(0) in ppm	AICD	Huckel aromaticity	HOMO-LUMO
III.3	-2.76	Clockwise	Aromatic	1.69
III.6	-14.07	Clockwise	Aromatic	1.59

Table II.1: Estimated NICS values for macrocycles **III.3** and **III.6**.

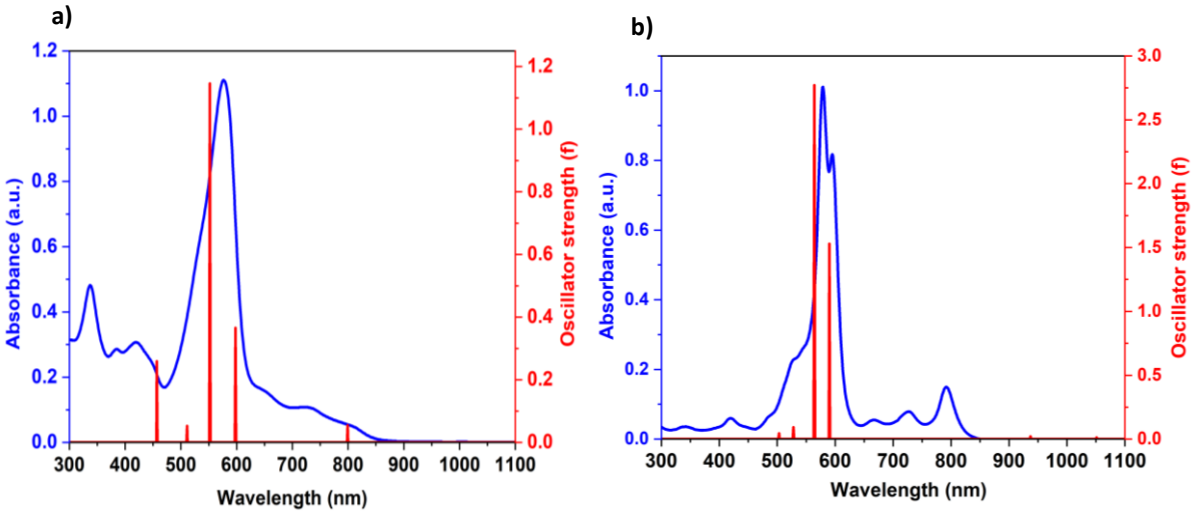

Figure III.15: The steady state absorption spectra (blue) of a) **III.3,** and b) **III.6**, recorded in DCM along with the theoretical vertical excitation energies (red) obtained from TD-DFT calculations carried out at the B3LYP/6-31G(d,p) level.

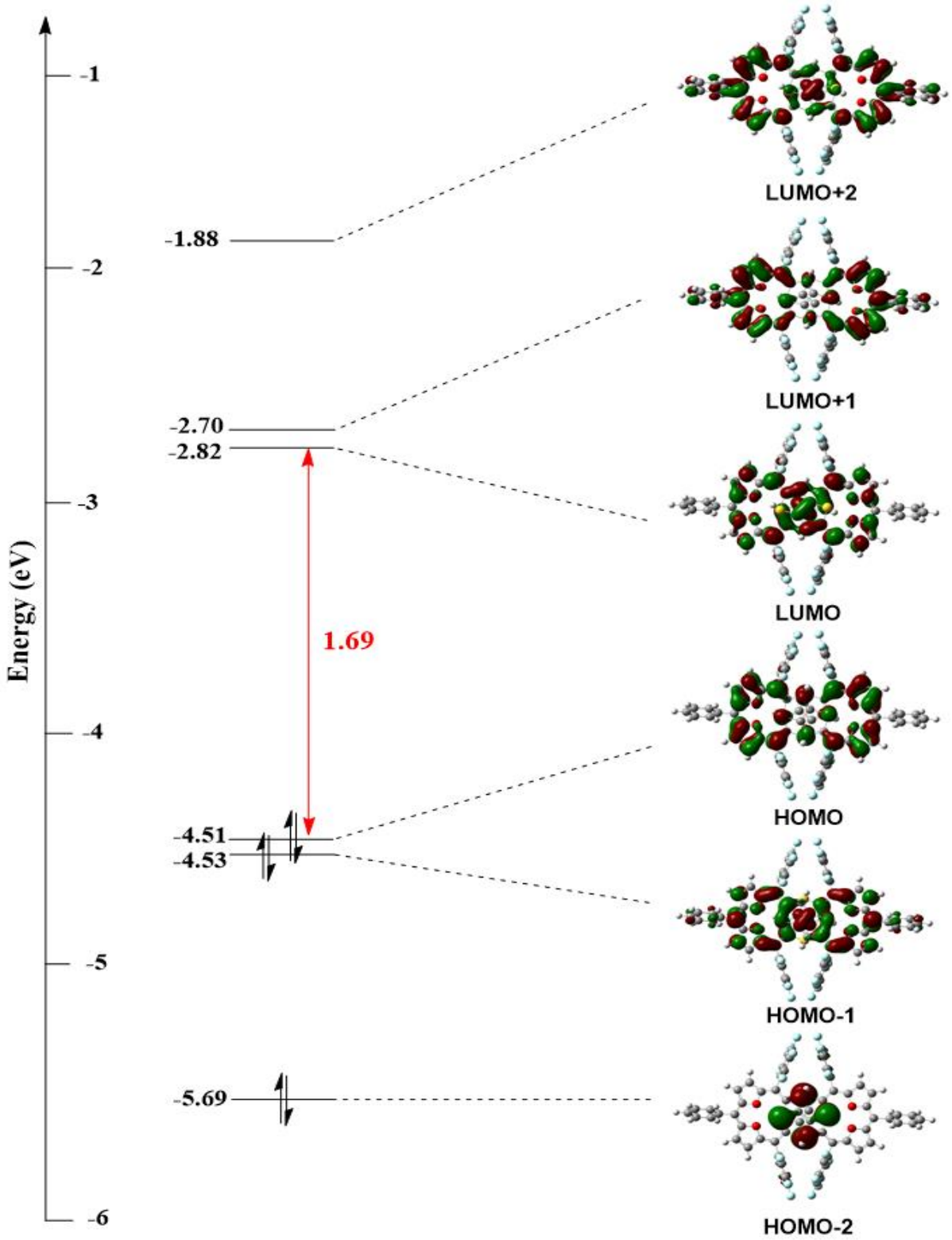

Figure III.16: Selected frontier MOs of **III.3,** calculated at the B3LYP/6-31G(d,p) level.

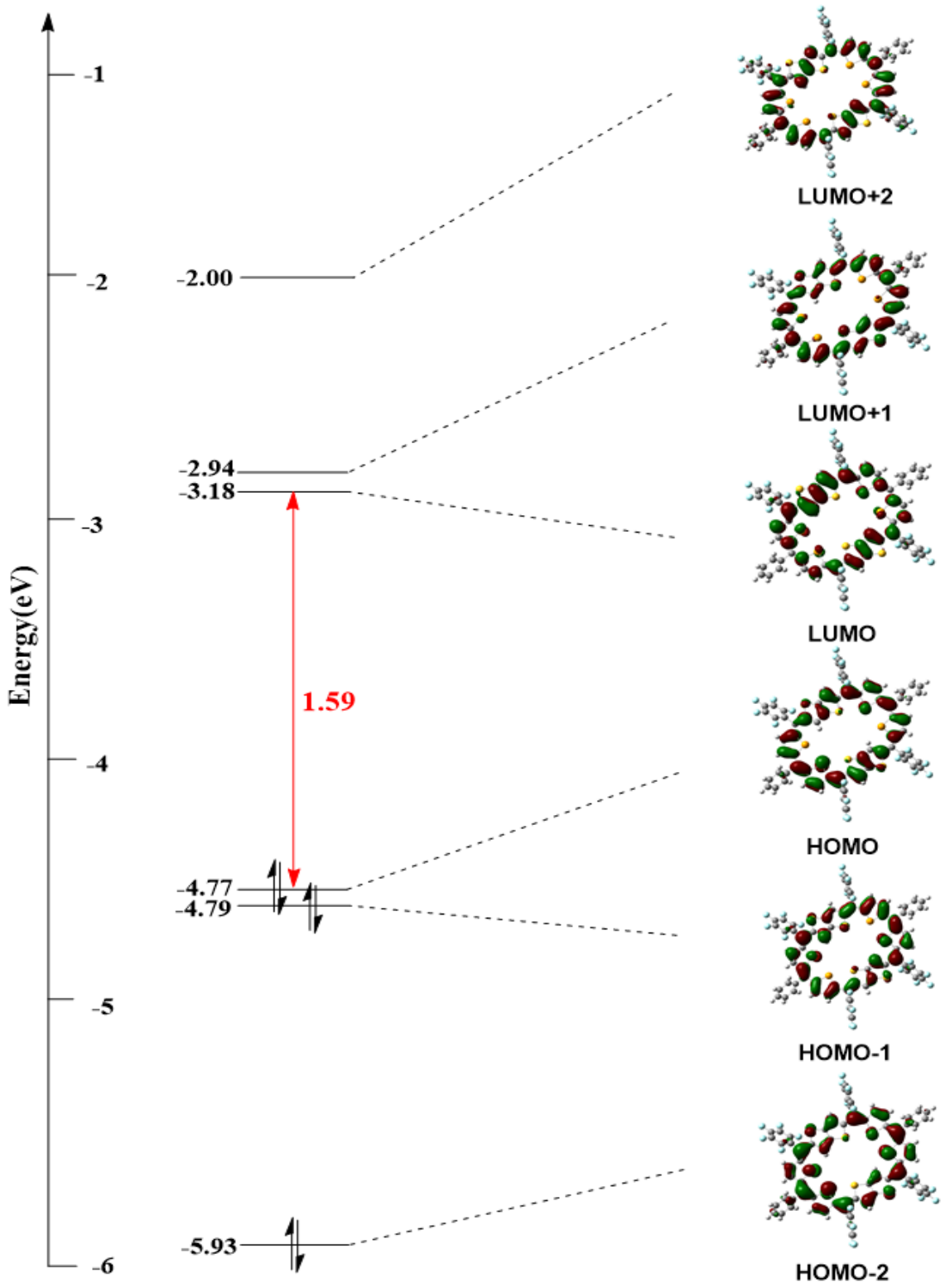

Figure III.17: Selected frontier MOs of **III.6** calculated at the B3LYP/6-31G(d,p) level.

III.7 Conclusion

The successful synthesis of Thieno-thiophene incorporated aromatic [34] hexaphyrin macrocycle was achieved by using simple precursor and employed McDonald type condensation reaction. Two distinct hexaphyrins, **III.3,** and **III.6**, were obtained by reacting an equimolar concentration of Thieno-thiophene diol and furan/selenophene based dipyrromethene. Both macrocycles were fully characterized, and also studied their redox chemistry.

The hexaphyrin accounts for 34π electrons accounts for (4n+2)π the Huckel's aromatic macrocycle, as in the case of **III.3**, observed the absence of the diatropic ring current effect. Single crystal X-ray diffraction analysis revealed that the molecular structure of **III.3**, it lost planarity and adopted a twisted conformation in solid state and solution state. The ^{1}H NMR spectrum of free base supported its conformational flexibility, indicating a non-aromatic character of the macrocycle. On the other hand, **III.6**, the selenophene based [34] hexahyrin, exhibited a strong diatropic ring current. The molecular structure of **III.6**, showed a nearly planar conformation, indicating the aromatic character of the macrocycle.

Both the [34] hexaphyrin macrocycle displayed a reversible redox reaction upon the addition of oxidizing agents like $NOBF_4$ or Meerwein's salt. This reaction involved a two-electron ring oxidation to form 32π dicationic species.

Thieno-thiophene insertion in the hexaphyrin contributes to the extension of π conjugation and also deviates from aromaticity. The furan based hexaphyrin lost the planarity to figure of eight conformation and the macrocycle is non-aromatic. However, in the case of selenophene hexaphyrin, bulkiness of the selenium maintains the macrocyclic planarity and its aromaticity confirmed by the ^{1}H NMR and single X-ray diffraction studies.

III.8 Experimental section

Synthetic Procedure and Characterisation

Thieno[3,2-b]thiophene dialdehyde

Thieno-thiophene (1 mmol) was dissolved in dry diethyl ether and placed in a flame dried two-necked of round bottom flask. n-BuLi (2.3 mmol) added dropwise at 0 ^{0}C, followed by stirring the reaction mixture for two hours at room temperature. Dry DMF (3 mmol) was then slowly added at 0 ^{0}C, and the reaction was stirred overnight. The reaction was quenched with 1M HCl, and the organic layer was extracted with ethyl acetate. The resulting product, highly insoluble in non-polar solvent, was filtered as a dark brown solid yielding 92%.

^{1}H NMR (400 MHz, Chloroform-*d*) δ 10.05 (s, 1H), 8.01 (s, 1H).

2, 5-Bis(pentafluorophenylhydroxymethyl) Thieno[3,2-b]thiophene:

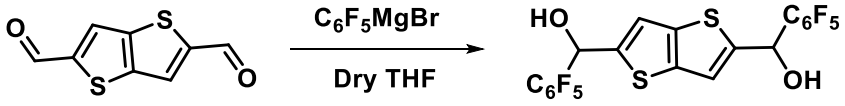

III. 2

Thieno-thiophene dialdehyde (1 mmol) was dissolved in anhydrous tetrahydrofuran (THF), and freshly prepared C_6F_5MgBr (2.5 mmol) was added at 0 ^{0}C. The reaction was stirred for three hours. Subsequently, the reaction mixture was quenched by the addition of saturated ammonium chloride. Then extracted the reaction mixture by ethyl acetate, and the resulting solution underwent recrystallization using a dichloromethane (DCM/n-Hexane) solvent combination. The final product was obtained in the form of a light yellowish solid, yielding 81%. recrystallize the reaction mixture by the DCM/ n-hexane combination. The product obtained as light yellowish solid in 81%.

^{1}H NMR (400 MHz, Chloroform-*d*) δ 7.82 (d, 2H), 6.14 (s, 2H), 3.12 ppm (brs, 2H).

2,2'-(phenylmethylene)difuran:

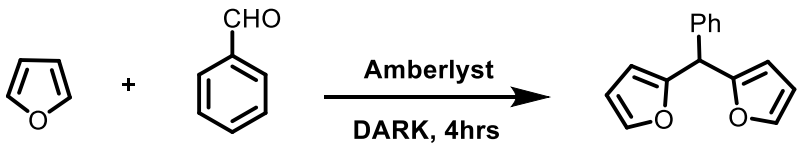

III.1

To a clean dried round bottom flask thiophene (5.0 mmol) was taken then the addition of benzaldehyde (1.0 mmol) followed by the addition of amberlyst 15 ion exchange resin (0.02 g/mmol) under dark and inert atmosphere. The resulting mixture was stirred at room temperature for 3hrs. the progress of reaction was observed by Thin Layer Chromatography then the reaction mixture was diluted with DCM, filtered and concentrated under vacuum. The residue was isolated on silica gel column chromatography. Isolated as yellow oil compound with 60% yield.

^{1}H NMR (400 MHz, $CDCl_3$): δ (ppm) 7.29-7.35 (4H, m, ArH), 7.21-7.27 (3H, m, ArH), 6.30-6.31 (2H, m, ArH), 6.01-6.02 (2H, m, ArH), 5.44 (1H, s, *meso*-CH);

2,2'-(phenylmethylene)diselenophene:

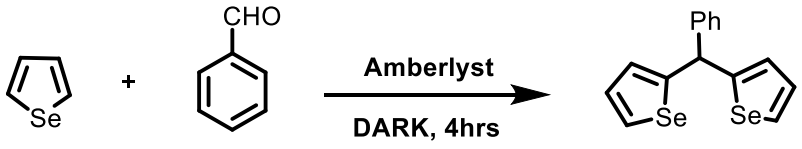

III.5

To a clean dried round bottom flask selenophene (5.0 mmol) was taken then the addition of benzaldehyde (1.0 mmol) followed by the addition of amberlyst 15 ion exchange resin (0.02 g/mmol) under dark and inert atmosphere. The resulting mixture was stirred at room temperature for overnight. The progress of reaction was observed by Thin Layer Chromatography then the reaction mixture was diluted with DCM, filtered and concentrated under vacuum. The residue was isolated on silica gel column chromatography in hexane and isolated as yellow oil compound with 65% yield.

^{1}H NMR (400 MHz, $CDCl_3$): δ = 5.90 (s, 1H), 7.04-7.04 (d, 2H, *J* = 3.2 Hz), 7.16-7.18 (m, 2H), 7.27-7.38 (m, 5H), 7.89 ppm (s, 2H).

Synthesis of [34] Hexaphyrin:

An equimolar concentration of Thieno-thiophene diol and dipyrromethene based on furan/selenophene was prepared by dissolving them in dry dichloromethane. The solution was then degassed with argon for ten minutes. Next, a catalytic amount of boron trifluoride diethyl etherate $BF_3.OEt_2$ under dark conditions and stirring for two hours. The addition of DDQ followed this, and the reaction was allowed to proceed for a further two hours. Subsequently, the reaction was quenched by adding a small amount of triethyl amine, and the resulting mixture was filtered through a column containing basic alumina. The pure product was separated by performing a basic alumina column chromatography using a mixture of dichloromethane (DCM) and n-hexane as the eluent.

III.3: Furan based dipyrromethene (224 mg, 1 mmol) **III.1** and Thieno-thiophene diol (585 mg, 1.1 mmol) **III.2** were reacted in presence of $BF_3.OEt_2$ (0.12 ml, 1 mmol), as described above to yield **III.3** in 15% yields.

III.3: ^{1}H NMR (400 MHz, Chloroform-*d*) δ 7.72 – 7.66 (m, 3H), 7.50 (d, *J* = 7.4 Hz, 3H), 6.78 (d, *J* = 5.0 Hz, 1H), 6.70 (s, 1H), 6.53 (d, *J* = 4.2 Hz, 1H), 6.21 (d, *J* = 4.9 Hz, 1H), 5.94 (s, 1H), 5.28 (s, 1H). **UV/Vis/NIR** (CH_2Cl_2): λ_{max} nm (ε) $Lmol^{-1}cm^{-1}$ = 342 (54205) and 575 (94357). **HR-MS** (ESI-TOF): m/z = 1434.0104 (found), 1434.0082 (Calcd. For $C_{70}H_{22}F_{20}S_4O_4$).

Selected Crystal data of III.3: $C_{70}H_{22}F_{20}S_4O_4$, (M_r = 1435.11), trigonal, space group *R -3c*, *a* = 30.481 (4), *b* = 30.481 (4), *c* = 51.690 (7) Å, $\alpha = 90^0$, $\beta = 90^0$, $\gamma = 120^0$; *V* = 41592 $Å^3$, *Z* = 18, *T* = 150 K, D_{calcd} = 1.031 gcm^{-3}, R_1 = 0.0526 (I > 2sigma (I)), R_w (all data) = 0.1808, GOF = 1.063;

III.6: selenophene based dipyrromethene (350 mg, 1 mmol) **III.5** and Thieno-thiophene diol (642 mg, 1.1 mmol) **III.2** were reacted in presence of $BF_3.OEt_2$ (0.12 ml, 1 mmol), as described above to yield **III.6** in 15% yields.

III.6: ^{1}H NMR (400 MHz, Chloroform-*d*): δ 9.99 (d, *J* = 5.3 Hz, 2H), 9.85 (d, *J* = 5.3 Hz, 2H), 8.47 (s, 2H), 8.04 (s, 3H), 4.01 (s, 2H). **UV/Vis/NIR** (CH_2Cl_2): λ_{max} nm (ε) $Lmol^{-1}cm^{-1}$ = 578 (123972), and 792 (55400). **HR-MS** (ESI-TOF): m/z = 1689.7057 (found), 1689.6946 (Calcd. For $C_{70}H_{22}F_{20}S_4Se_4$).

Selected Crystal data of III.6: $C_{70}H_{22}F_{20}S_4Se_4$, ($M_r$ = 1686.95), monoclinic, space group *P* $2_1/C$, *a* = 16.279 (3), *b* = 24.692 (4), *c* = 17.647 (3) Å, $\alpha = 90^0$, $\beta = 97.562^0$, $\gamma = 90^0$; *V* = 7031.72 $Å^3$, *Z* = 4, *T* = 150 K, D_{calcd} = 1.593 gcm^{-3}, R_1 = 0.1048 (I > 2sigma (I)), R_w (all data) = 0.2640, GOF = 1.008;

Chapter 4

Synthesis and Characterization of 24π core-modified Sapphyrin and its higher analogues

IV.1 Introduction

Sapphyrins are a class of expanded porphyrins, which are large, conjugated macrocyclic compounds composed of pyrrole or other heterocyclic units. The serendipitous discovery of sapphyrin occurred in 1960 during the synthesis of Vitamin B_{12} by R.B. Woodward and coworkers.[40] The name sapphyrin is derived from the deep blue colour of their complexes, resembling the gemstone sapphire. The distinctive feature of sapphyrin is their expanded structure, which includes either five pyrroles rings connected through four meso-carbon bridges and one direct pyrrole-pyrrole bond. This arrangement makes sapphyrin different from traditional porphyrins. The expanded ring system of sapphyrin gives rise to distinctive electronic properties, making them valuable in the field of chemistry.

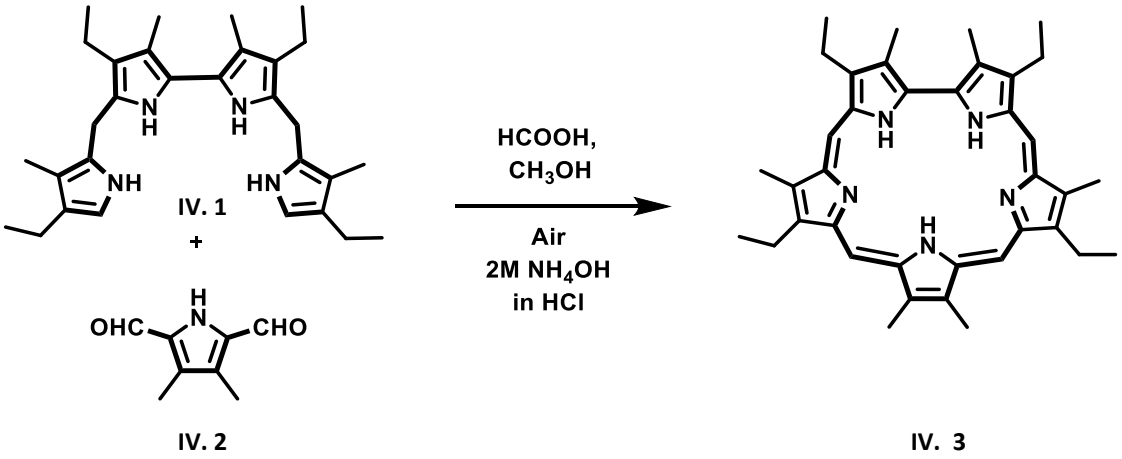

Scheme IV.1: Synthesis of β-alkyl Sapphyrin through [4+1] condensation.

In 1972, Johnson and coworkers were the first to report the synthesis of the dioxa analogue of sapphyrin **IV.5**.[75] The all azasapphyrin was first synthesised by R. B. Woodward and coworkers in 1983 by a [4+1] condensation between the linear tetrapyrrolic precursor **IV.1,** and 2,5-diformyl-3,4-dimethylpyrrole **IV.2**, under acidic conditions followed by air oxidation (Scheme – IV.1).[41]

Later, Sessler and coworkers[75] synthesised a β-alkyl sapphyrin by adopting the modified synthetic protocol [3+2] MacDonald condensation. The β-alkyl aza sapphyrin was formed using the acid-catalyzed condensation of diformylbipyrrole and tripyrromethane diacid, followed by aerial oxidation. The molecular structure of sapphyrin dication revealed a planar conformation wherein, the nitrogen atom of all pyrroles is facing towards the core of macrocycle.

To simplify the synthetic protocol, the same research group introduced the a [3+3+1] methodology. An acid catalysed condensation of bisformyl tripyrromethne with two

equivalents of β-substituted pyrrole followed by oxidation afforded the β-substituted azasapphyrin in 34% yield.[76] Various research groups have utilized diverse precursors and methodologies to synthesis β-alkyl sapphyrins.[77,78]

Latos-Grazynski and coworkers reported the first meso-aryl substituted sapphyrin. A one-pot $BF_3.OEt_2$ catalysed condensation of pyrrole and benzaldehyde, resulted in the formation of all-aza meso aryl sapphyrin **IV.4a**, in 1% yields.[79] The ^{1}H NMR spectrum revealed that one of the pyrrole units was inverted, leading to a significant difference in chemical shift between CH protons and NH proton. A Soret-like band in absorption spectrum is in support the aromatic character of the meso aryl sapphyrin. Upon the addition of acid, the inverted pyrrole ring undewent a 180^o flipping, adopting a structure where all nitrogen atoms of pyrrole ring are faced inside the core of macrocycle **IV.4b** (Scheme -IV.2). Subsequently, Chandrashekar and coworkers reported an improvised yield of all-aza meso-aryl sapphyrin by varying the nature of the acid catalyst and its concentration.[80]

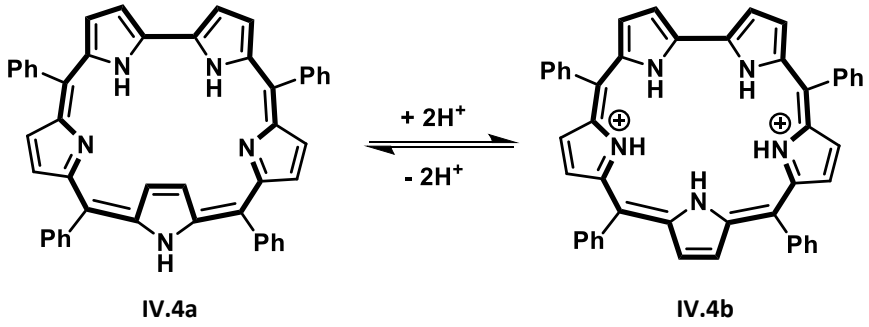

IV.4a IV.4b

Scheme IV.2: Ring inversion of all-aza sapphyrins in presence of Acid.

One or more pyrrolic units of the sapphyrin can be replaced by other chalcogens based rings such as furan, thiophene, selenophene, tellurophene and N-methyl pyrrole sapphyrin/heterosapphyrin. The core modification leads to a modified struture, cavity size, redox chemistry, electronic properties, and optical properties. The first core modified sappyrin was reported by Johnson and coworkers.[81] They achieved this modification through a [3+2] McDonald type condensation of tripyrromethane diacid with diformyl bifuran under acidic conditions, followed by oxidation to afforded the dioxasapphyrin **IV.5**, in 10% yields. Sessler and coworkers also reported a core modified monothiasapphyrin **IV.6a** and monoselenasapphyrin **IV.6b,** in ~25% yields.[82] The same group also reported a series of mono-, di-, and trioxasapphyrins synthesised by adopting a similar synthetic methodology. Additionally, Chandrashekar and coworkers reported the synthesis of multiple

derivatives of core modified sapphyrins in moderate yields **IV.7a-c** by using variety of precursors.[83]

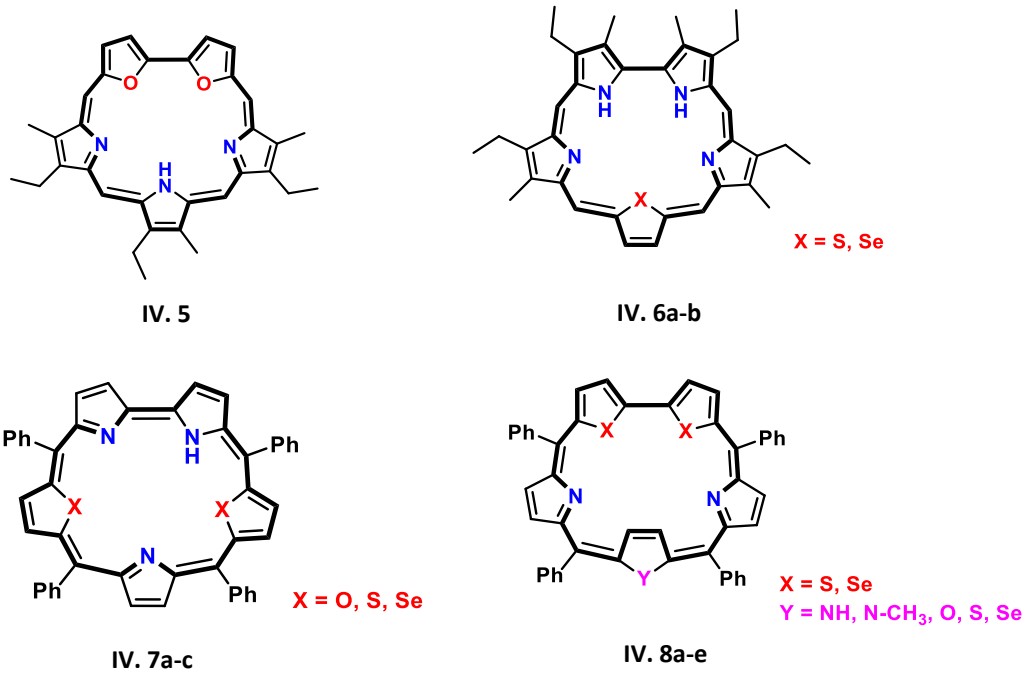

Figure IV.1: Mono/di/tri hetero substituted core modified 22π sapphyrin.

In case of meso free all-aza sapphyrin and core modified sapphyrins, all the hetero atoms were oriented towards the core of the macrocycle while in case of core modified aza meso-aryl substituted sapphyrins **IV. 8a-e,** one of the heterocyclic unit that was opposite to the bithiophene or biselenophene unit in core modified sapphyrin was in an inverted form[84] (figure – IV.1). Single crystal X-ray diffraction analysis revealed that the core size and the size of heteroatom decided the nature of structural diversity.

Aza based sapphyrins are challenging to oxidize to an antiaromatic state because these macrocycles are inherently stabilized in an aromatic state. Unlike other antiaromatic macrocycles, these sapphyrins resist oxidation owing to their stable aromatic nature. This may be attributed to the amine-imine interconversion that favours a stabilized 22π sapphyrin even after oxidation. However, upon complete core modification of sapphyrin and replacing all the pyrrole units with other heterocyclic units such as thiophene, furan, selenophene or tellurophene leads to formation of antiaromatic 24π sapphyrin. It is widely recognized that antiaromatic macrocycle undergo a two-electron ring oxidation, resulting in the formation aromatic dicationic species. This transformation provides valuable insights into the redox chemistry of sapphyrin. Therefore, an attempt has been made to synthesize completely core modified sapphyrin and their higher analogues.

IV.2 Synthesis of 24π Sapphyrin and its higher analogues (IV.11)

The synthesis of a core modified 24π sapphyrin, **IV.11**, was achieved by [3+2] type condensation. An equimolar concentration of biselenophene, **IV.10**, and tripyrromethane diol, **IV.9**, (scheme IV.3) was dissolved in 100 ml of dry dichloromethane. The solution was then degassed with Argon gas for 10 minutes. Next, a catalytic amount of boron trifluoride diethyl etherate ($BF_3.OEt_2$) was introduced in the absence of light using a syringe. The resulting mixture was stirred for 2 hours under inert conditions, after which 2.5 equivalents of DDQ were added as an oxidizing agent, and stirring continued for an additional two hours in an open atmosphere. Next, the reaction mixture was filtered through a short band of basic band of basic alumina. The reaction mixture was analysed using MALDI TOF/TOF mass spectrometry, confirming the anticipated mass for 24π sapphyrin, **IV.11**, along with unexpected higher analogues such as 48π decaphyrin, **IV.12,** and 72π pentadecaphyrin, **IV.13.** The progress of product formation was observed by MALDI TOF/TOF mass spectrometry (Figure - IV.2).

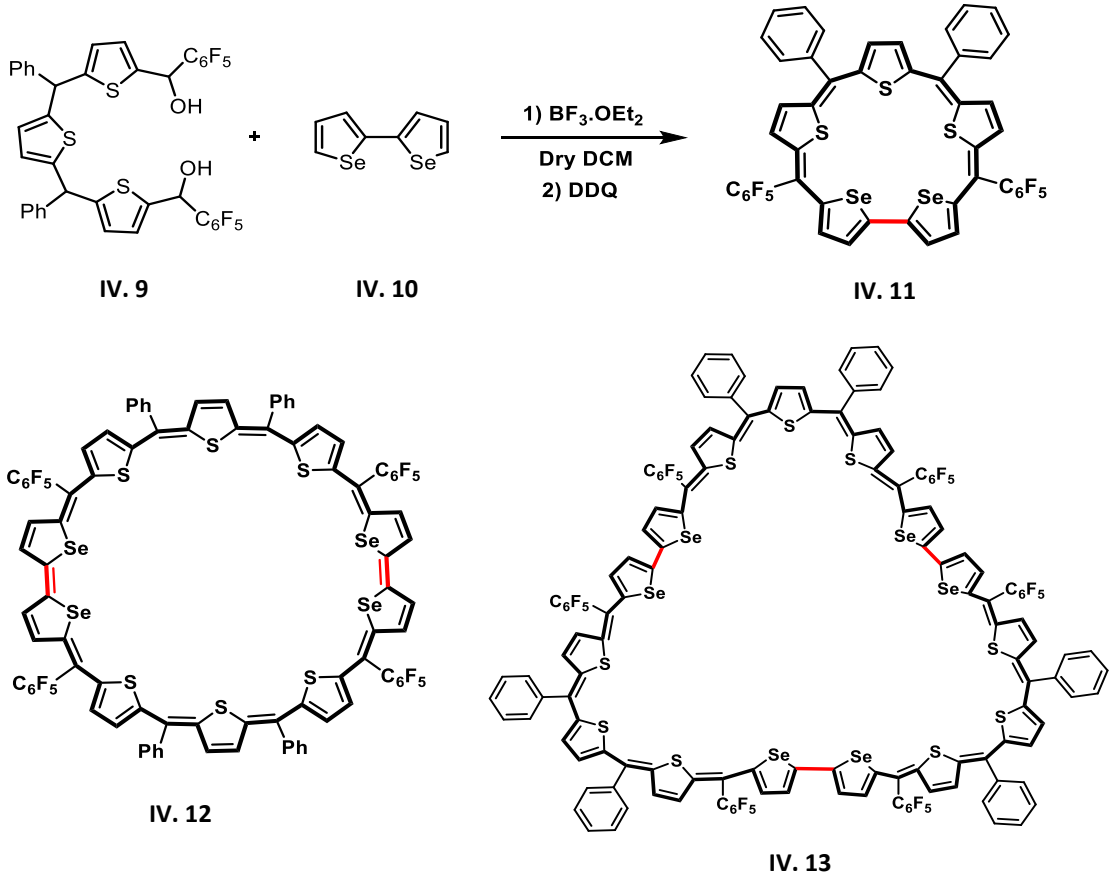

Scheme IV.3: Synthesis of core-modified 24π sapphyrin and higher analogues.

The reaction mixture was passed through a short pad of basic alumina pad to remove the impurities and further purified through column chromatography.

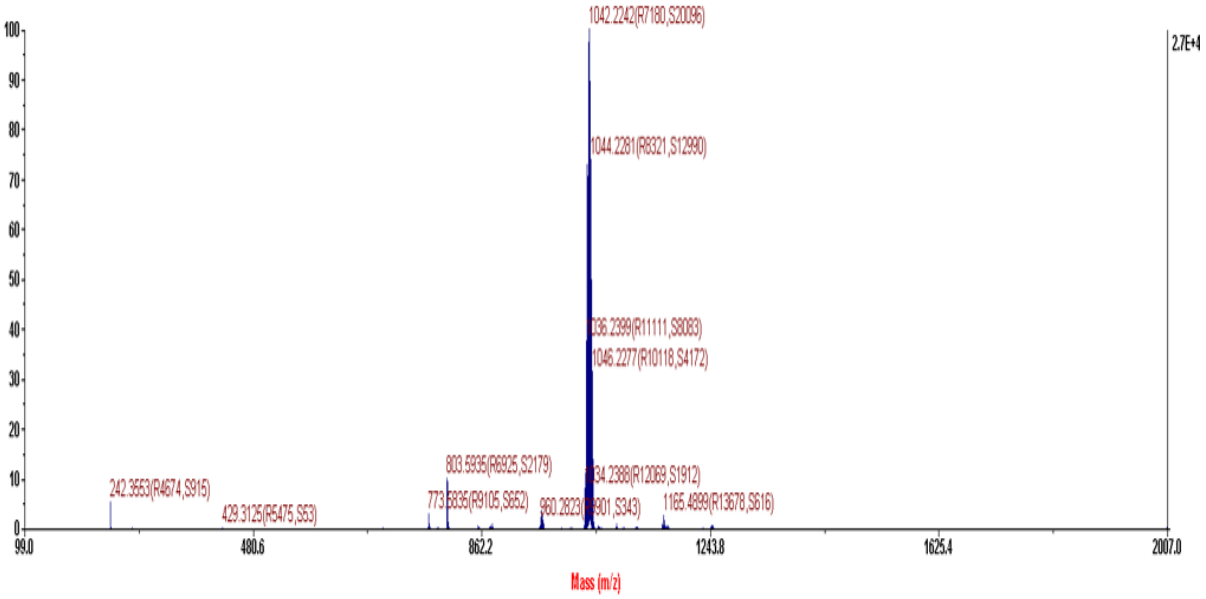

Figure IV.2: MALDI TOF/TOF mass spectrum of reaction mixture (scheme IV.4).

IV.3.1 Isolation and Characterisation of 24π Sapphyrin (IV.11)

The reaction mixture was concentrated under pressure followed by the purification/isolation of macrocycle by basic alumina column chromatography using CH_2Cl_2/Hexane as the eluents. Since the mass spectrum exhibited three different masses they were isolated sequentially through repeated basic alumina and also size exclusion chromatography. The first yellow-greenish band was separated and corresponded to the expected 24π sapphyrin **IV.11**, in 6% yields. An *m/z* value of 1041.8898 (1041.8898 Calcd. for $C_{48}H_{20}F_{10}S_3Se_2$) obtained from HR-ESI-MS mass spectrum confirmed the composition of this macrocycle **IV.11** (Figure - IV.3).

Varying the dilution of reaction mixture under identical reaction conditions provided substantial control over the yields of the product. For example, it was observed that a 1 mmol reaction in 100 ml of dry DCM as solvent the yielded the different macrocycles, **IV.11**, **IV.12,** and **IV.13**, in 2%, 25% and 3% yields respectively. Upon doubling the dilution of reaction mixture, the yield of 24π sapphyrin, **IV.11** increased by 6%.

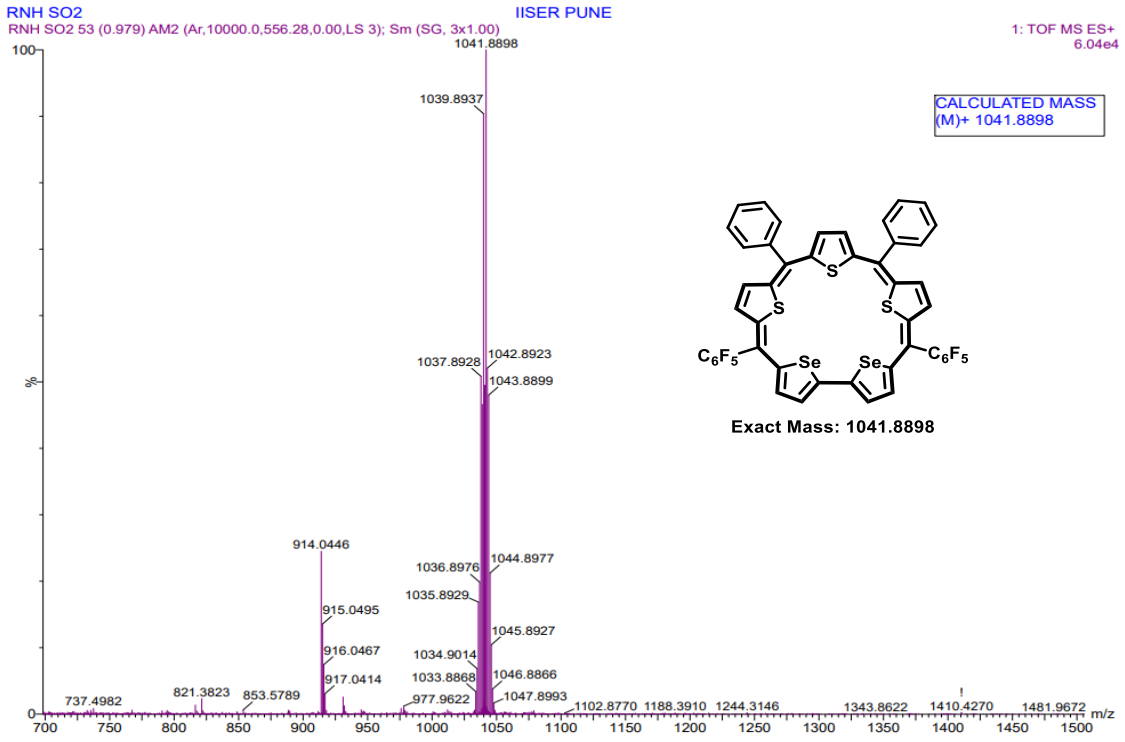

Figure IV.3: HR-ESI-TOF mass spectrum of **IV.11**

IV.3.2 ^{1}H NMR study of [24]Sapphyrin (IV.11)

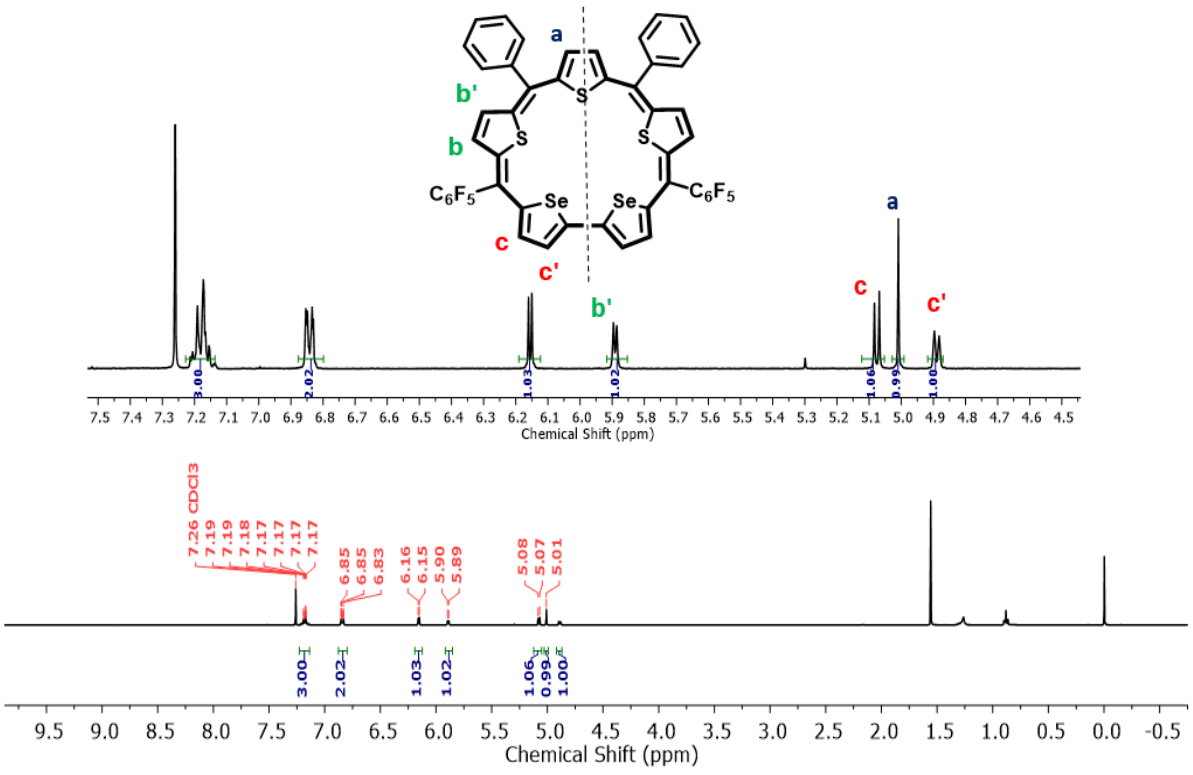

Figure IV.4: ^{1}H NMR spectrum of **IV.11** in Chloroform-d

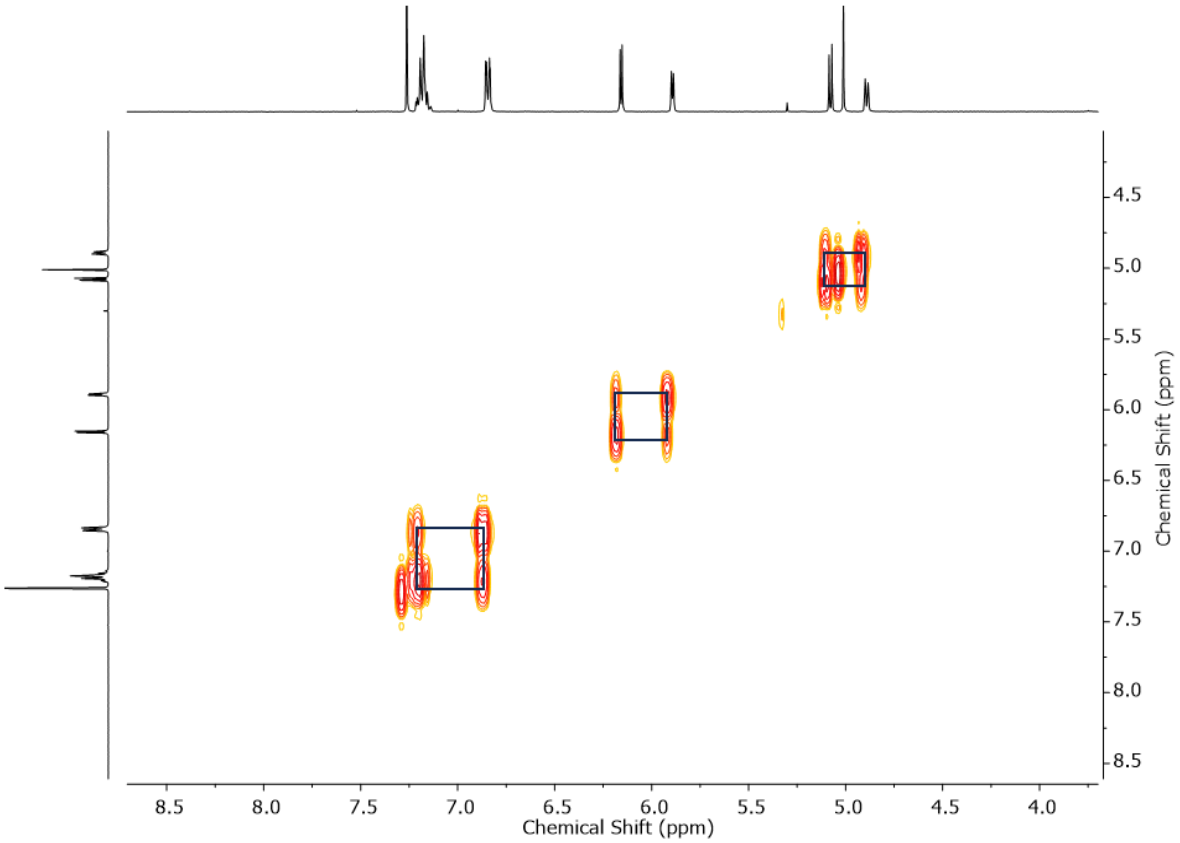

Figure IV.5: ^{1}H-^{1}H COSY spectrum of **IV.11** in Chloroform-d.

The macrocycle **IV.11**, accounts for 24π electrons, according to Huckel's theory, indicating its antiaromatic nature. In its ^{1}H NMR spectrum **IV.11**, displayed seven signals in the region between δ 4.9 to δ 7.2 ppm in $CDCl_3$ (figure - IV.4). This suggests a highly symmetrical structure in solution state showcasing the presence of C_2 axis of symmetry within the macrocycle. Four doublets were observed between of δ 4.9 to δ 6.16 ppm and a singlet at δ 5.0 ppm. These signals suggest that the β-protons of the all thiophene units are at the periphery while all the sulphur atoms of thiophenes are oriented towards the centre of the macrocycle. Hence it can be claimed that, there is no flipping of any thiophene rings in the macrocycle. As expected of an antiaromatic macrocycle, all the β-protons of the thiophenes were experiencing moderate paratropic ring current effect and hence, the signals were resonating in the upfield region. ^{1}H-^{1}H COSY spectrum, recorded at 298 K, revealed two sets correlations accounting for the four β-protons of thiophene rings. Additionally, phenyl protons were observed resonating between δ 6.8 to δ 7.3 ppm. Collectively, these findings confirm the planar nature of the macrocycle (figure - IV.5).

IV.3.3. Molecular structure of [24]Sapphyrin (IV.11)

Absolute conformation of molecular structure for **IV.11**, was elucidated from single-crystal x-ray diffraction analysis (figure - IV.6). Shiny dark blue coloured needle shaped crystals were isolated through recrystallization. Good quality of single crystals was grown by diffusion hexane vapours into a solution of **IV.11**, in DCM. Molecular structure revealed a planar geometry of the macrocycle **IV.11**, wherein all the sulphur atoms of all the thiophene and selenium atom of both the selenophene rings are facing the centre of the macrocycle. The biselenophene units were found slightly out of the plane, since one of the selenophene deviated away from the mean macrocyclic plane. Due to the large size of selenium atom, biselenophene was forced to out of plane which reduces the ring current effect in the macrocycle. The solid-state structure depicts the planar topology of the macrocycle **IV.11**, supported in its ^{1}H NMR.

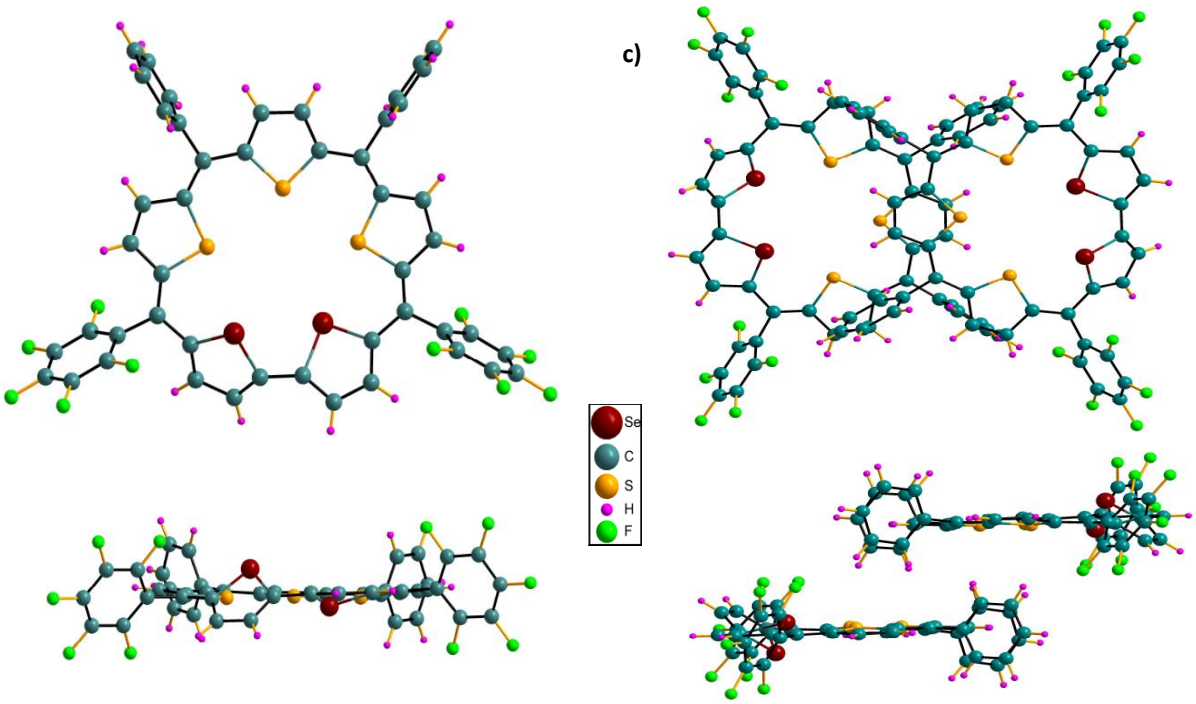

Figure IV.6: Molecular structure of **IV.11** determined from single crystal X-ray diffraction. a) (top view), b) (side view) and crystal packing (c and d).

IV.3.4 Electronic absorption and Cyclic Voltammogram studies

This macrocycle accounts for 24π electron in conjugation, and hence formally assigned as, antiaromatic 4nπ system. In its UV-Vis spectrum, this macrocycle displayed an intense and split absorption for Soret-like band at 440 nm (35300) and 413 nm (37600) in dichloromethane. The absence of any Q-like energy bands suggested the antiaromatic nature of macrocycle **IV.11**. Antiaromatic systems are prone to undergo two-electron ring oxidations to yield

aromatic 22π dicationic species**.** This macrocycle displayed characteristic UV-Vis absorption changes upon addition of oxidising agent such as trifluoroacetic acid (TFA), Meerwein's salt $[Et_3O]^+[SbCl_6]^-$ and $[NO^+BF_4^-]$.[66] The addition of Meerwein salt to **IV.11,** in dry dichloromethane transformed the greenish-yellow coloured solution of antiaromatic sapphyrin to intense pink colour. This remarkable shift in colour led to significant changes in absorption properties, displaying a pronounced red shift at 560 nm, along with two lower energy bands at 756 nm and 837 nm (figure - IV.7). These observations strongly supported the aromatic nature of the resulting 22π dicationic species **IV.14**, as outlined in (Scheme – IV.4). Furthermore, the addition of a suitable reducing agent such as Et_3N, Zn dust facilitated the reversion of this dicationic species back to its free base.

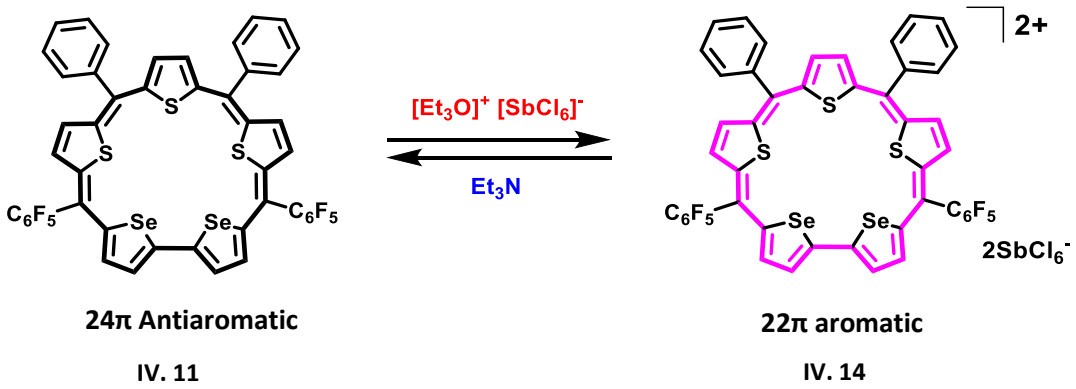

Scheme IV.4: Reversible two-electron oxidation of **IV.11** by Meerwein salt to its dication [**IV.14**]$^{2+}$.

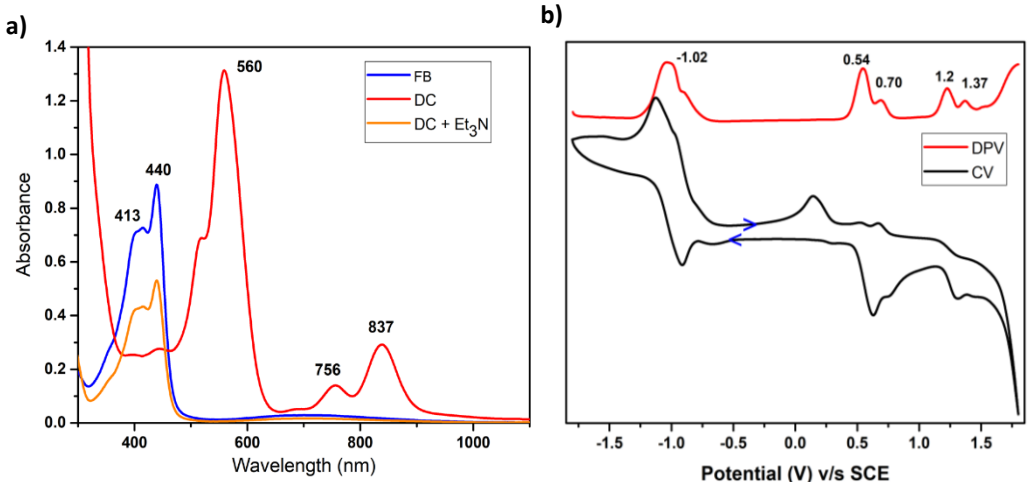

Figure IV.7: a) Electronic absorption spectrum of 10^{-5} M solution of **IV.11** (blue) (FB: Free Base) and its oxidised species [**IV.14**]$^{2+}$ (red) (DC: Dication) recorded in CH_2Cl_2. b) Cyclic voltammogram (CV, black) and differential pulse voltammogram (DPV, red) of **IV.11** in CH_2Cl_2 (with 0.1 M **$(Bu)_4NClO_4$** as the supporting electrolyte).

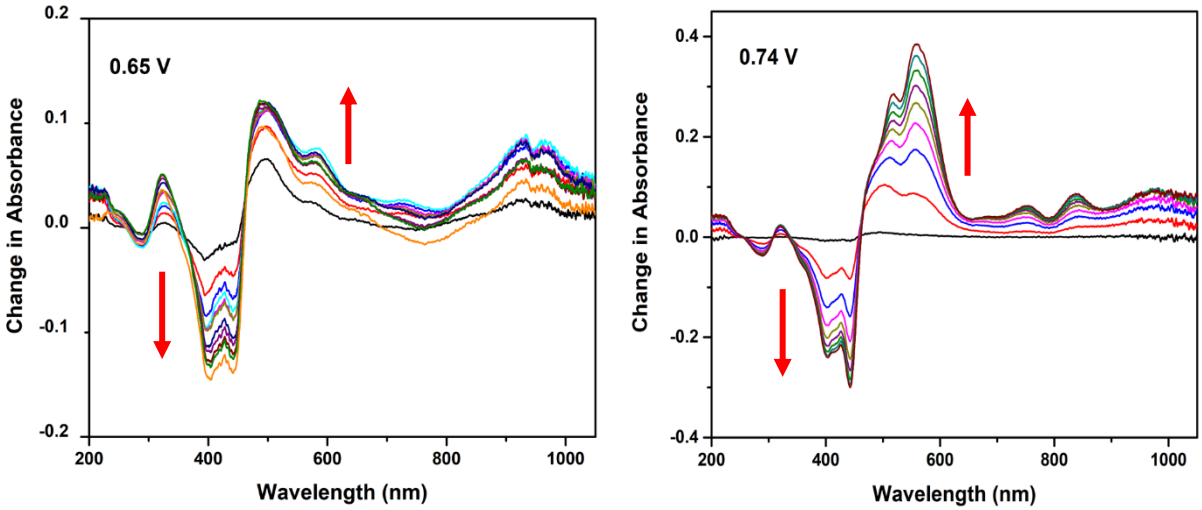

Figure IV.8: Spectro-electro chemistry studies of **IV.11**. Change in absorption spectra after applying a potential of + 0.65 V and + 0.74 V, respectively.

The cyclic voltammetry (CV) and differential pulse voltammetry (DPV) study displayed two reduction potentials at -1.02, - 0.98 V and four oxidation potentials at + 0.54, +0.70, +1.2, and +1.37 V respectively (figure – IV.8). To investigate the distinct oxidized species, spectro-electrochemical measurements were conducted identify the dicationic form. The change in absorption was observed during the electrochemical oxidation and reduction of **IV.11**, at two different potential, as indicated in the cyclic voltammogram. Lower oxidation potential at + 0.65 V showed one electron oxidation and at this potential showed maxima at 491 nm. Upon increasing the potential to + 0.74 V, a broadened band with a redshift at 560 nm was observed along with lower energy bands at 756 and 837 nm (figure – IV.8). This observation confirmed the formation of a dication, consistent with the earlier findings through chemical oxidation by Meerwein salt.

IV.4.1 Isolation and Characterisation of [48]decaphyrin (IV.12)

The next higher analogue of the series was 48π decaphyrin, which was isolated as a blue coloured band after 24π sapphyrin **IV.11**, in the basic alumina column. This macrocycle **IV.12**, formally accounts for 48π electrons in global conjugation and composition of the macrocycle was confirmed by HR-ESI-MS mass spectrum which displayed *m/z* value of 2083.7830 (2083.7796 Calcd. for $C_{96}H_{40}F_{20}S_6Se_4$) (figure– IV.9).

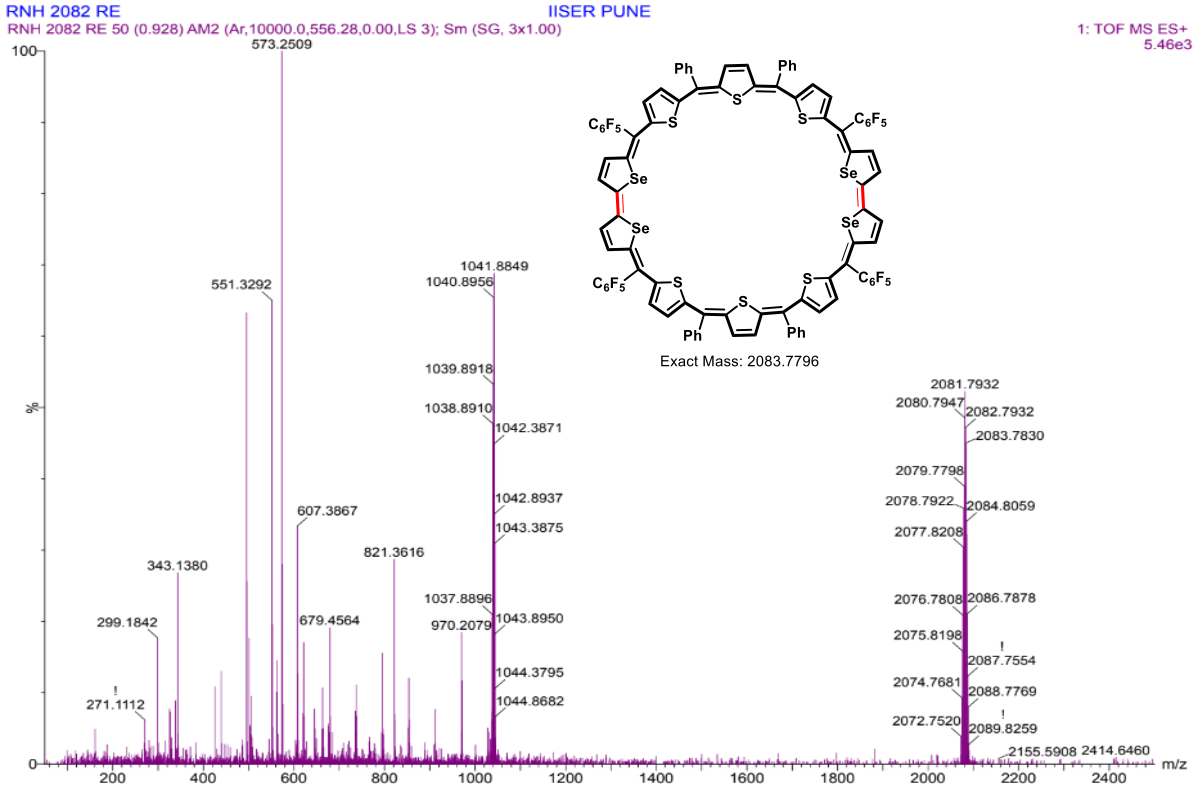

Figure IV.9: HR-ESI-TOF mass spectrum of **IV.12**.

IV.4.2 ^{1}H NMR study of [48]decaphyrin (IV.12)

Since this molecule accounts for 48π electrons, it is anticipated to exhibit the paratropic ring current effect due to its 4nπ system. Despite the anticipation of paratropic ring current effect due to its 48π electrons system, the observed signals resonated between δ 6.0 to 7.5 ppm in the spectrum (figure – IV.10) suggesting lack of paratropic ring current effects. This deviation from the expected antiaromaticity can be attributed to a non-planar nature of the macrocycle similar to other reported decaphyrins till date. **IV.12**, maintained a figure of eight geometry where the macrocycle possesses C_2 axis of symmetry and therefore showed few signals. The signal was resonating in the region between δ 6.1 and δ 7.0 ppm, which are corresponding to β-protons of the thiophene and selenophene moieties. All the five β-protons resonated in the aromatic region, suggesting absence of paratropic ring current effect. Consequently,

macrocycle can be classified as non-antiaromatic in the solution state. Moreover, the phenyl protons were resonating in the region between δ 7.3 to 7.5 ppm. Consistent with this expectation, the observed correlation of protons in the ^{1}H-^{1}H COSY spectrum (figure – IV.11) provided additional support for the possibility of the figure of eight structures.

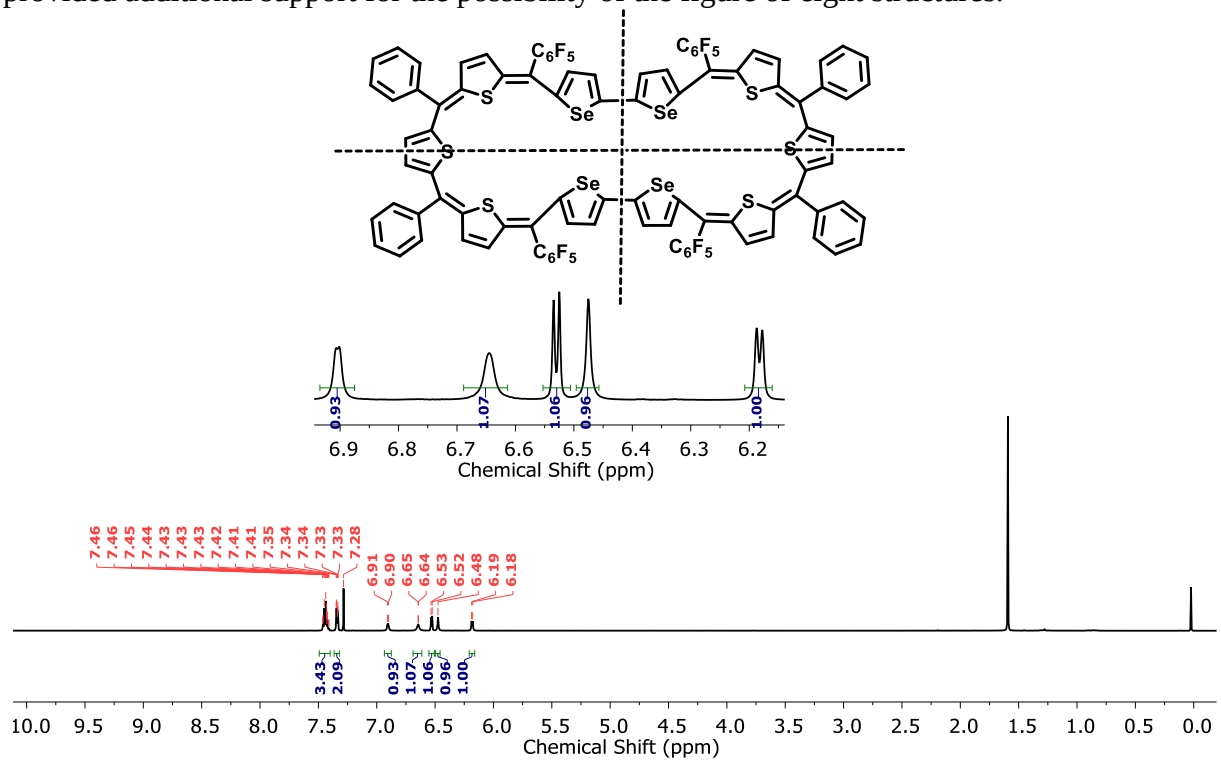

Figure IV.10: ^{1}H NMR spectrum of **IV.12** in Chloroform-d

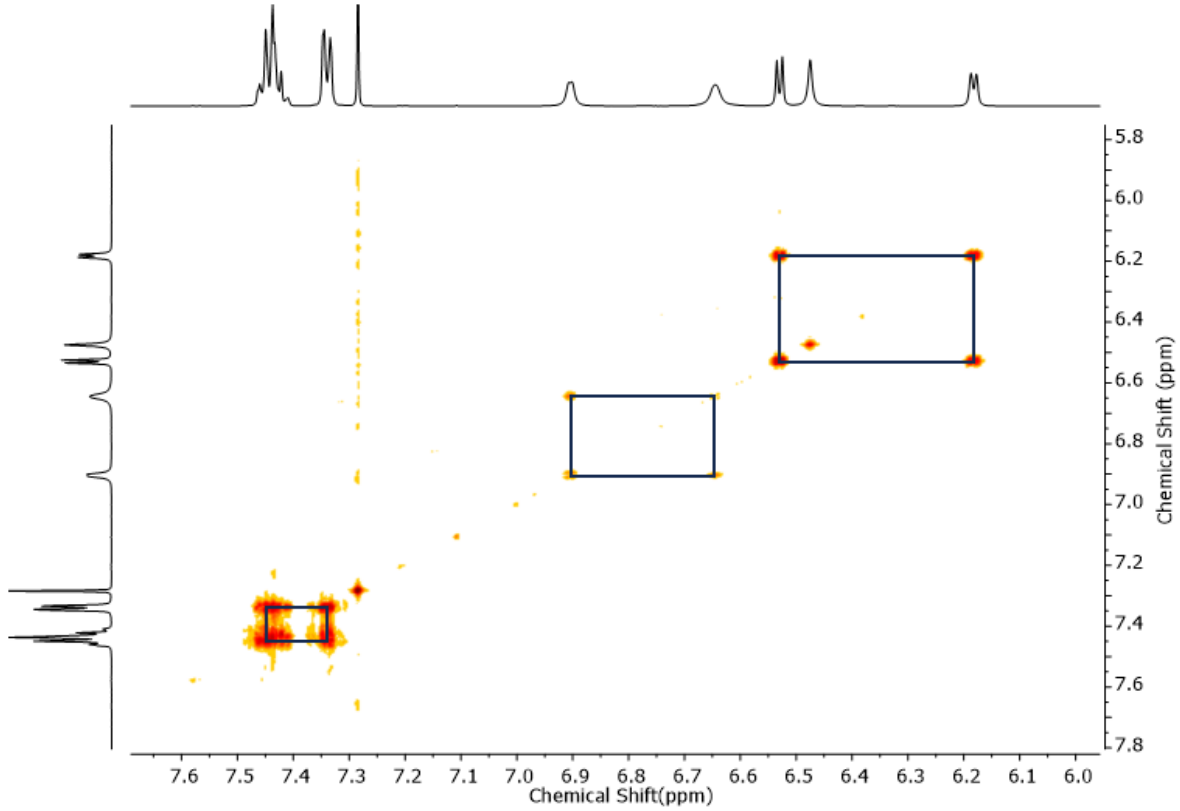

Figure IV.11: ^{1}H-^{1}H COSY spectrum of **IV.12** in Chloroform-d.

The ^{1}H-^{1}H COSY spectrum displayed three sets of correlations for this macrocycle in which two of them were observed in the upfield region at δ i) 6.91 and 6.64, ii) 6.53 and 6.18 ppm. These correlations could be attributed to β-protons of the heterocyclic units. The other correlations are assigned to the meso-phenyl protons at δ 7.46 and 7.33 ppm, suggests the symmetric macrocycle possessing the C_2 axis of symmetry.

IV.4.3 Molecular structure of [48]decaphyrin (IV.12)

Good quality single crystals were successfully grown by vapour diffusion method using $CHCl_3$/Heptane solvent combination. The molecular structure of **IV.12**, was elucidated from single crystal X-ray diffraction analysis (figure – IV.12). The analysis confirmed a twisted figure of eight conformation, divided into two symmetrical five membered rings resembling 24π sapphyrin. Both the biselenophene units were situated at the centre of the macrocycle, with the selenium pointing towards the centre of their respective macrocycle. In the solid state, the macrocycle **IV.12**, can be classified as non-antiaromatic, attributed to its 'figure of eight' geometry (two folded symmetry).

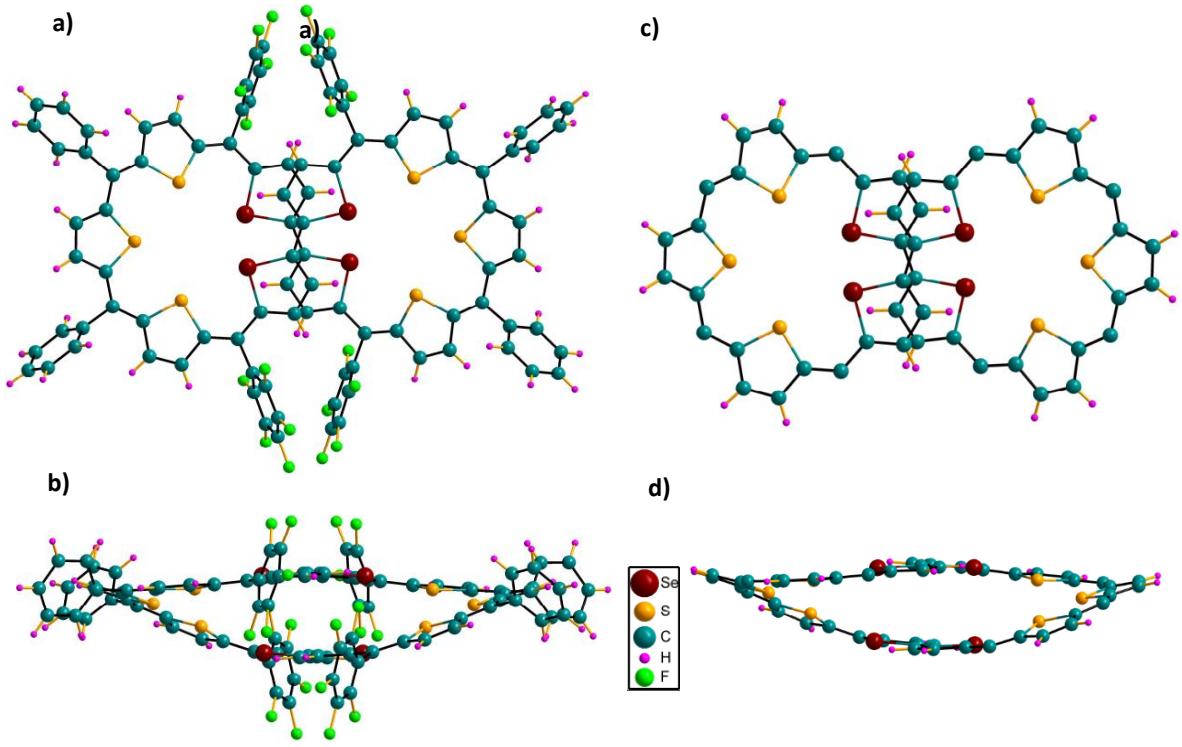

Figure IV.12: Molecular structure of [48]decaphyrin (**IV.12)** as determined from single crystal X-ray diffraction. a) (top view) and b) (side view). The meso-ppentafluorophenyl and phenyl rings are omitted of clarity in the (c) (top view) and (d) (side view).

IV.4.4 Electronic absorption and Cyclic Voltammogram studies

This macrocycle comprises 48π electrons along its conjugated pathway, and the impact of extended conjugation is reflected in the ^{1}H NMR and UV-Vis spectroscopy, showing significantly red-shifted absorptions compared to the 24π sapphyrin. It exhibited an intense absorption band at 605 nm (138300) along with a less intense band at 417 nm (109000) in dichloromethane (figure – IV.13a). Being a 4nπ macrocycle, **IV.12**, readily undergoes two-electron oxidation to yield an aromatic 46π dicationic species **IV.15**, upon the addition of suitable oxidizing agents such as TFA or $NOBF_4$ or Meerwein's salt (scheme – IV.5). It induced an instant change from blue colour to light brown, accompanied by a bathochromic shift in the absorption maxima from 605 to 850 nm and a less intense band at 485 nm, along with broad, lower energy band at 1116 nm. This oxidized species can be reverted back to its free base by the addition of reducing agents such as Et_3N and Zn dust.

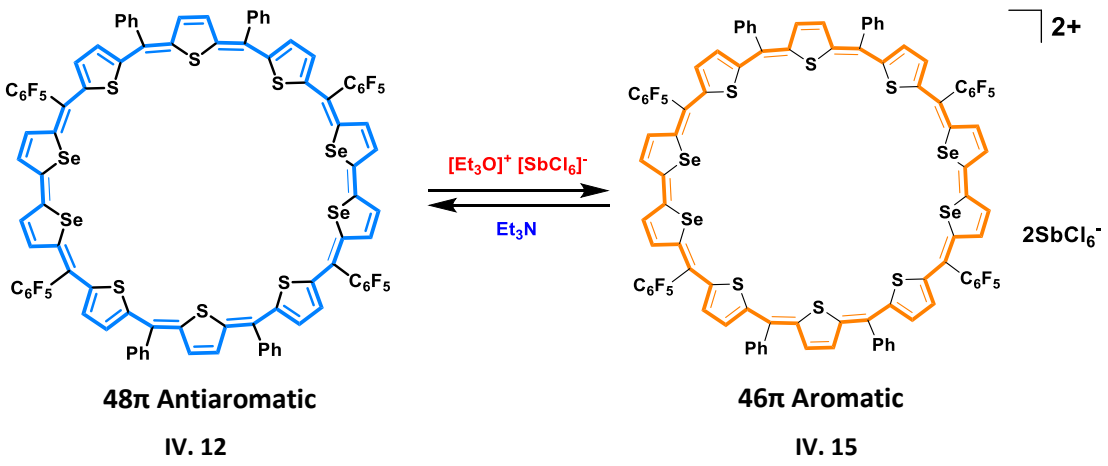

Scheme IV.5: Reversible two-electron oxidation of 48π (**IV.12**) to 46π dication (**IV.15**).

The interesting redox chemistry of **IV.12**, was studied through cyclic voltammetry (CV) and differential pulse voltammetry (DPV) in dichloromethane. The spectrum revealed two oxidations and two reduction potentials at + 0.42, + 1.21, - 0.92, and - 1.5 V, respectively (figure – IV.13b). During the Spectro-electrochemistry scan, among two oxidation potentials, at an applied potential of +1.26 V, i.e. the second oxidation potential, this macrocycle displayed a broad peak at 1104 nm confirming the formation of dicationic species [**IV.15**]$^{2+}$ (figure - IV.13c). The two-electron ring oxidation was further supported by an *m/z* value of 1041.8849 (Calcd. for 1041.8898) corresponding to *m/2* of the [**IV.15**]$^{2+}$ in the HR-MS spectra (figure – IV.9).

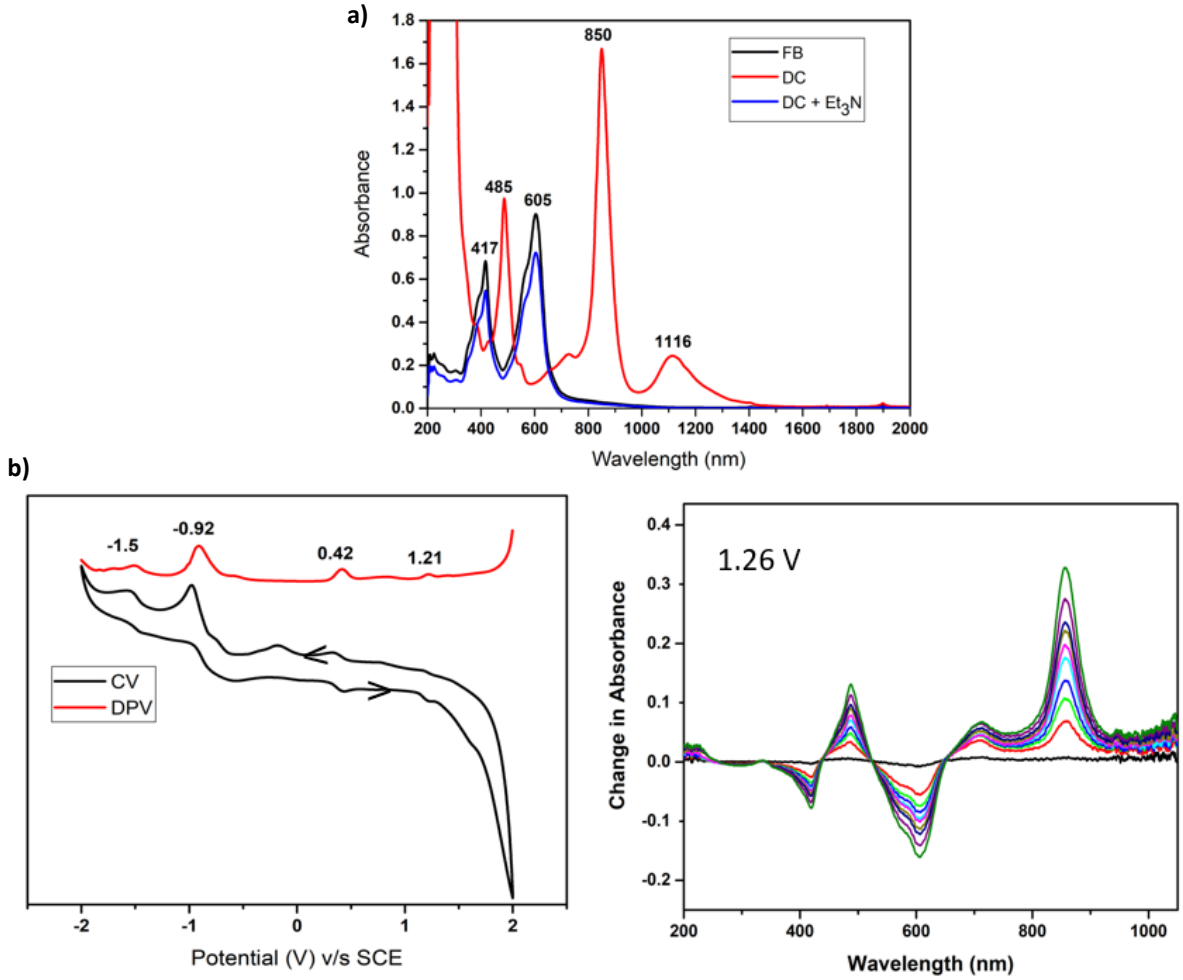

Figure IV.13: a) UV/vis/NIR absorption spectrum of a 10^{-5} M solution of **IV.12** (black) (FB: Free Base) and its oxidised species [**IV.15**]$^{2+}$ (red) (DC: Dication) recorded in CH_2Cl_2. b) Cyclic voltammogram (CV, black) and differential pulse voltammogram (DPV, red) of **IV.12** in CH_2Cl_2 (with 0.1 M $(Bu)_4NClO_4$ as the supporting electrolyte) (c) Change in absorption spectra of **IV.12** after applying a potential of + 1.26 V.

IV.5.1 Isolation and Characterisation of [72]pentadecaphyrin (IV.13)

One of the largest macrocycles observed in this series was an expanded porphyrinoid **IV.13**, composed of fifteen thiophene units observed. This macrocycle was isolated as a green coloured band through repeated basic alumina column chromatography and size exclusion chromatography, with only 3% yields. Formation of the macrocycle was confirmed by the MALDI TOF/TOF mass spectrometry analysis, which showed an *m/z* value of 3125.2063 (3125.6694 Calc. for $C_{144}H_{60}F_{30}S_9Se_6$) corresponding to the **IV.13** (figure - IV.14).

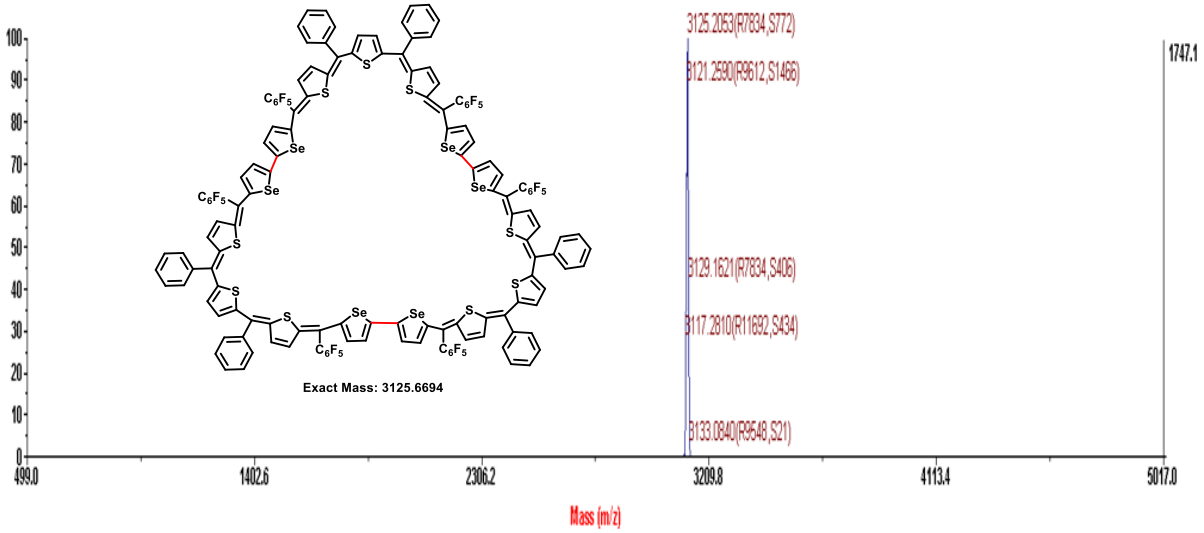

Figure IV.14: MALDI-TOF/TOF mass spectrum of **IV.13**

IV.5.2 ^{1}H NMR study of [72]pentadecaphyrin (IV.13)

This macrocycle formally accounts or 72π electrons and hence expected to be antiaromatic as per Huckel's 4nπ rule. However, in the ^{1}H NMR spectrum **IV.13**, displayed signals only in the region between δ 7.5 to 6.2 ppm at room temperature, clearly signifying the absence of paratropic ring current effects. Therefore, the macrocycle is expected to be non-antiaromatic in solution state. The number of signals observed was much less than expected; while the macrocycle was anticipated to exhibit sixty signals, only ten signals were observed at room temperature (figure - IV.15). This suggests that the macrocycle is threefold symmetric, with each component possessing C_2 symmetry. This implies that the **IV.13**, macrocycle was arranged in such a way that it forms symmetric three 'five-membered rings' and each undergoe C_2 symmetry operation. As a result, a reduced number of signals was observed in the NMR spectrum. The phenyl protons resonated in the region between δ 7.5 to δ 7.2 ppm. Three doublets at δ 6.63, 6.50, 6.25 ppm, and one singlet at δ 6.55 correspond to β-protons of the heterocyclic units.

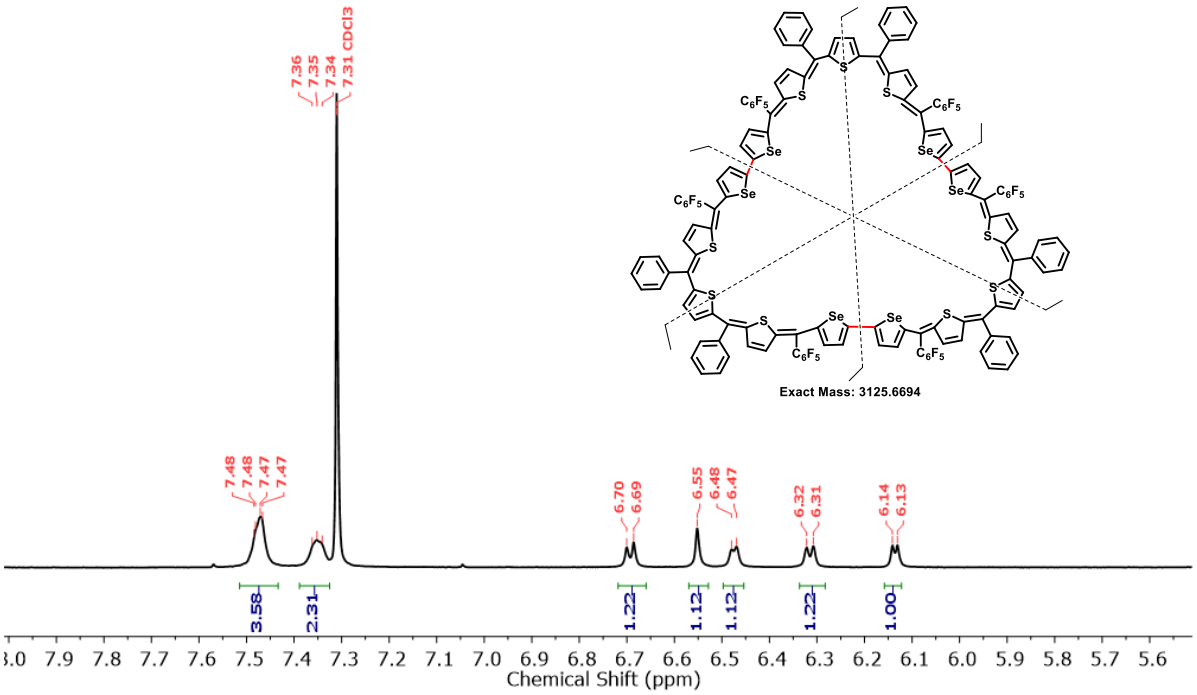

Figure IV.15: ^{1}H NMR spectrum of **IV.13** in Chloroform-d at 218K.

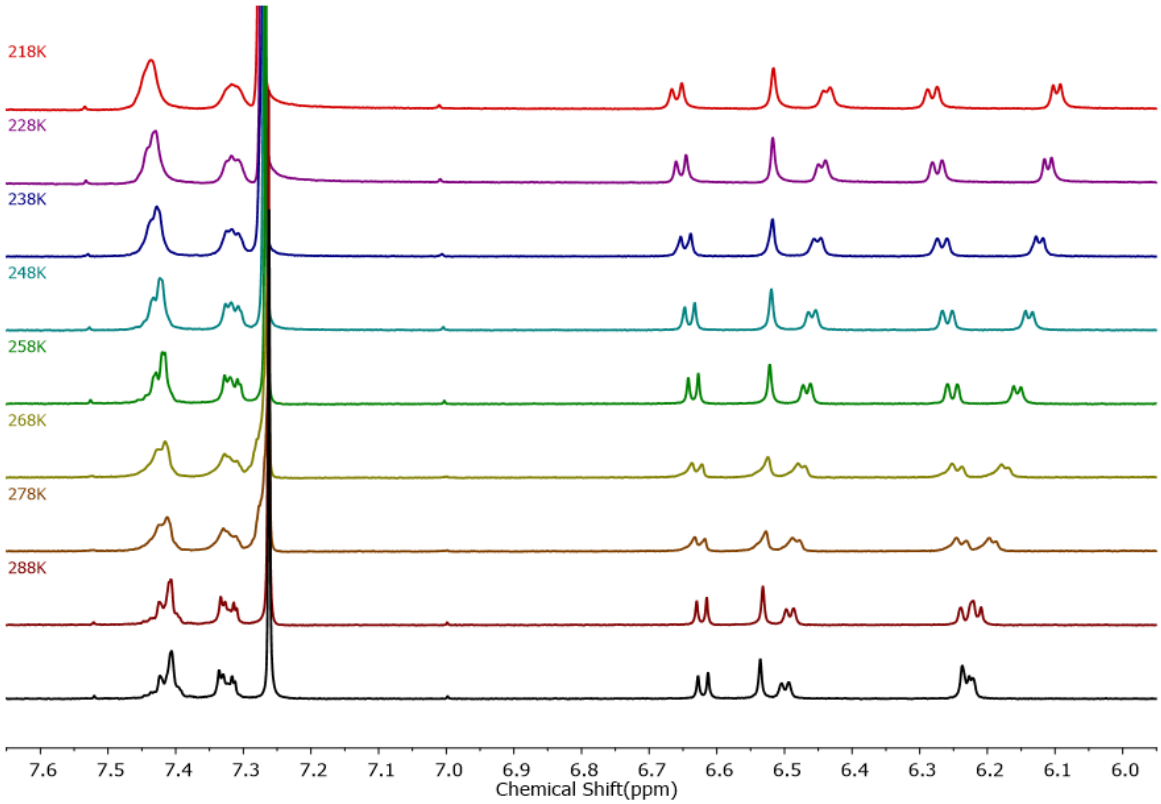

Figure IV.16: Variable temperature ^{1}H NMR spectra of **IV.13** in $CDCl_3$

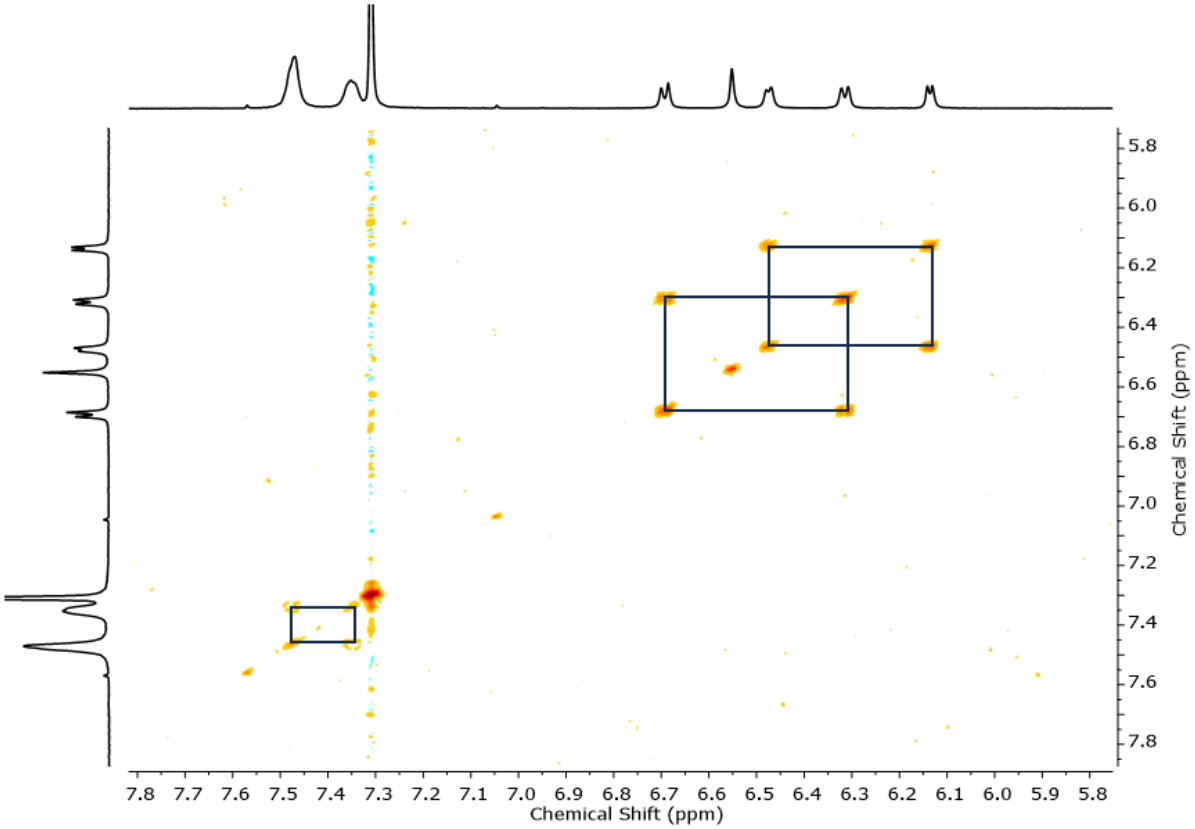

Figure IV.17: ^{1}H-^{1}H COSY spectrum of **IV.13** in Chloroform-d

To rule out the possibility of fluxional nature of the macrocycle **IV.13**, low temperature ^{1}H NMR spectra was recorded which, revealed no substantial changes in the chemical shift of all protons even up to 218 K (figure – IV.16). For **IV.11**, the protons resonated in the region between 4.9 and 6.2 ppm, whereas in the case of **IV.13**, these protons resonated in the range of 6.2 to 7.5 ppm. This unequivocally suggests that 72π pentadecaphyrin is less antiaromatic compared to **IV.11**, which can be attributed to the larger ring size leading to a loss of planarity in the macrocycle. Therefore, the protons of heterocyclic ring didn't experience ring current effect. The observed ^{1}H NMR spectrum further supported by ^{1}H-^{1}H COSY spectrum (figure - IV.17), displayed two couplings for the peripheral protons of the heterocyclic units.

IV.5.3 Molecular structure of [72]pentadecaphyrin (IV.13)

Based on ^{1}H NMR spectroscopy, the macrocycle **IV.13**, is expected to lose its planarity, causing it to adopt a three-fold symmetry. Consequently, reduced number of signals were observed in the spectrum. After numerous attempts and experimenting with various solvent combinations, we were able to grow the high-quality crystal in $CHCl_3$/Heptane. Single crystal X-ray diffraction analysis confirmed the formation of a tripod-shaped macrocycle **IV.13**, as

expected. The molecular structure of 72π pentadecaphyrin showed a non-planar topology (figure – IV.18) in support of ^{1}H NMR spectrum. Generally, a higher-membered macrocycle adopts twisted figure-of-eight geometry, but in this case, it's pretty different from the usual one, which is symmetrically divided into three 'pentaphyrin pocket.' Each pentaphyrin pocket is the combination of tripyrromethane and biselenophene wherein all the thiophenes are oriented towards the core of the macrocycle, and one of the selenophene units of biselenophene are faced towards the core of the macrocycle, while the other one is oriented toward the neighbouring pentaphyrin pocket. The phenyl rings were discovered to be in close proximity to an orthogonal orientation with respect to the average plane defined by the meso-carbons of the macrocycle. Tripyrromethane units are positioned at the three corners, and they are bridged by biselenophene units, which is located at the centre of the tripod, alternately leading to three sapphyrin-like pockets. Due to the large size of selenophene, the deviation one of the selenophene is faced upward while the second one is downward.

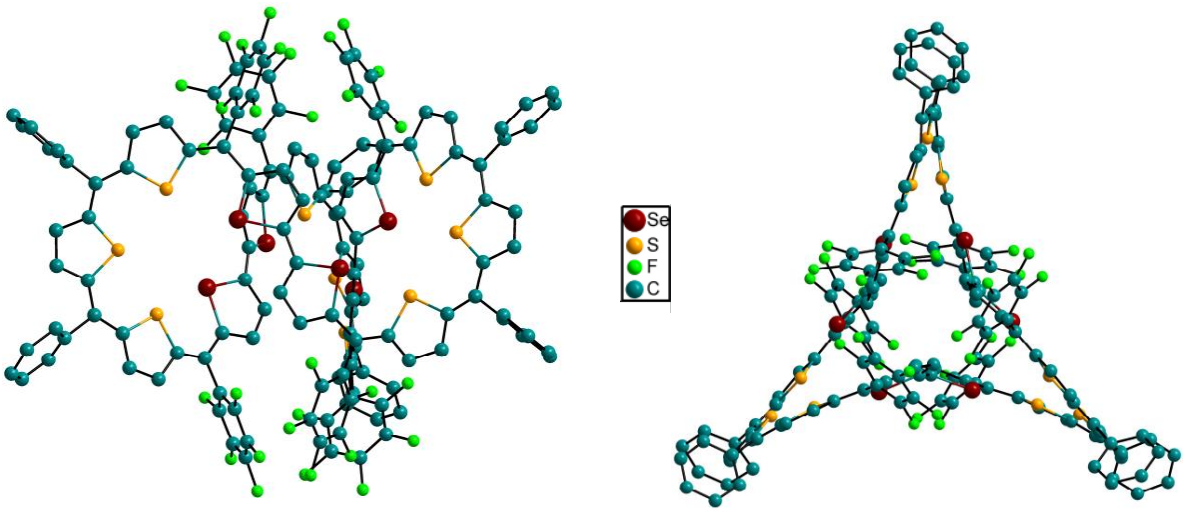

Figure IV.18: Molecular structure of [72]decaphyrin (**IV.13)** as determined from single crystal X-ray diffraction. a) (top view) and b) (side view).

IV.5.4 Electronic absorption studies

The 72π pentadecaphyrin macrocycle having 72π electrons in the global conjugation, would be expected to exhibit Huckel's antiaromaticity as a 4nπ electronic system. Due to its nonplanar geometry, it is identified as non-antiaromatic in the solution state. The electronic absorption for **IV.13**, showed the multiple bands in the range between 400 – 800 nm. It displayed λ_{max} at 446 nm (42700) along with that two less intense band at 550 nm (40000) and 706 nm (19600).

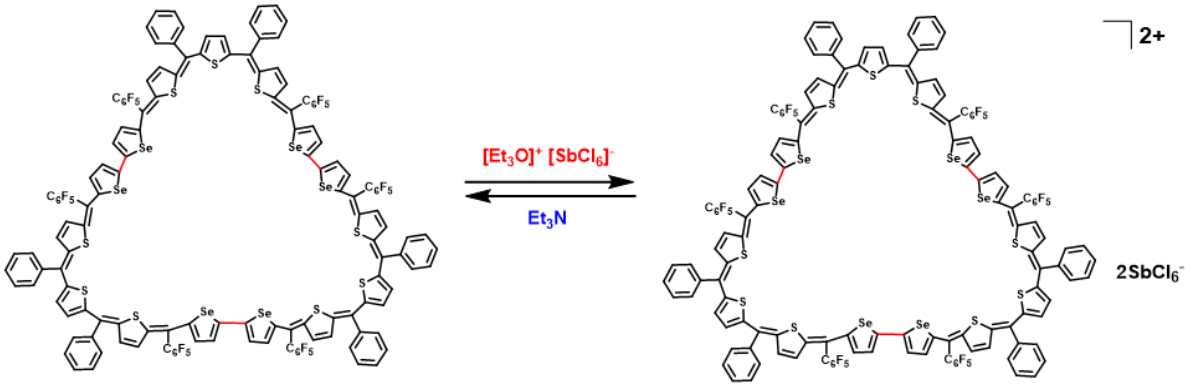

Scheme IV.6: oxidation of 72π (**IV.13**) to 70π dication (**IV.16**) upon addition of Meerwein salt.

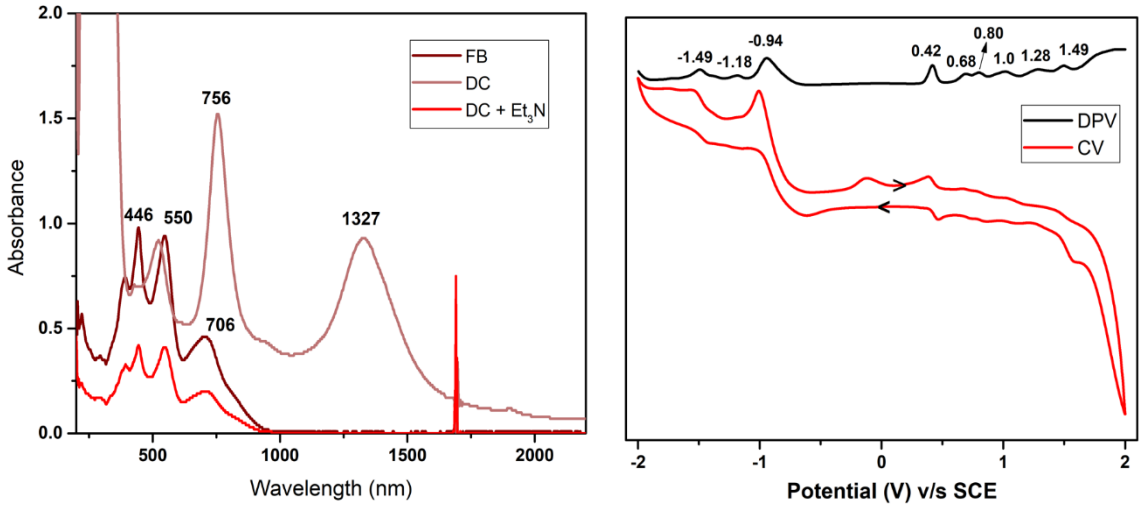

Figure IV.19: a) UV/vis/NIR absorption spectrum of 10^{-5} M solution of **IV.13** (brown) (FB: Free Base0 and its oxidised species [**IV.16**]$^{2+}$ (faint brown) (DC: Dication) recorded in CH_2Cl_2. b) Cyclic voltammogram (CV, red) and differential pulse voltammogram (DPV, black) of **IV.16** in CH_2Cl_2 (with 0.1 M $(Bu)_4NClO_4$ as the supporting electrolyte)

Being a 4nπ system it undergoes two electron ring oxidation to its dicationic species **[IV.16]$^{+2}$** upon the addition of Meerwein's salt as oxidising agent shifted the band towards red shift region with 756 nm and 1327 nm band[66] (scheme – IV.6). Subsequent addition of triethyl amine to the oxidized species reverted back to the free base (figure – IV.19a). For further understanding the redox active nature of macrocycle, cyclic voltammetry (CV) and differential pulse voltammetry (DPV) studies were performed whichd showed three reduction potentials at -0.94, -1.18, -1.49 V respectively, and multiple oxidation potentials at +0.42, +0.68, +1.0, +1.28, and +1.49 V respectively. (figure – IV.19b).

IV.6 Quantum mechanical calculations

Quantum chemical calculations further supported the antiaromatic characteristics of [24]sapphyrin as observed from ^{1}H NMR spectroscopy. An estimated NICS(0) value of δ +1.67 ppm for **IV.11**, reflected weak antiaromatic characteristics for the 24π macrocycle and AICD plot displayed anti-clockwise ring current suggests the paratropic ring current and for **IV.12**, +2.45 ppm clarifies the very weak antiaromatic character and was further supported by AICD plot also which displayed the anticlockwise ring current (figure - IV.20).

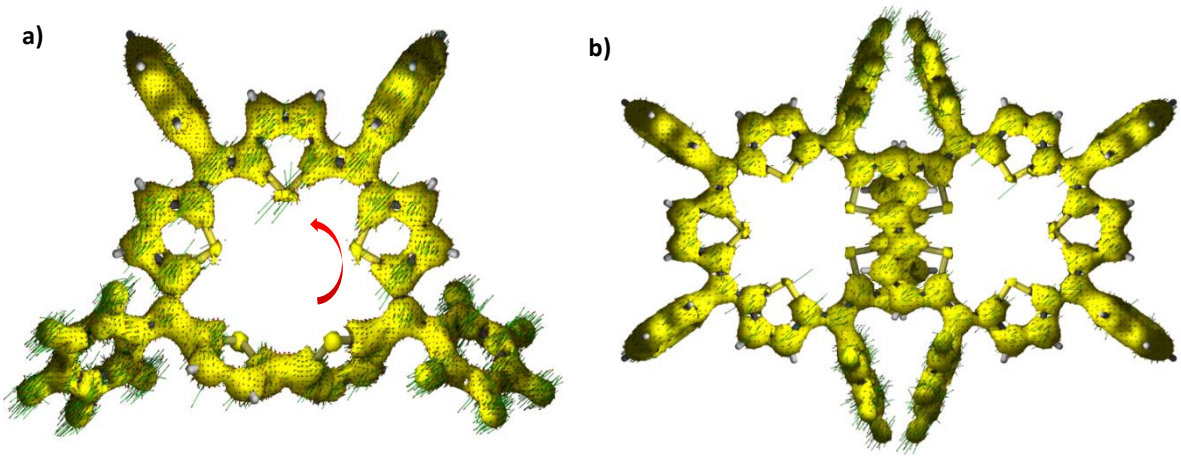

Figure IV.20: AICD plot of a) **IV.11 and** b) **IV.12** at an iso surface value 0.05 the external magnetic field is applied orthogonal to the macrocycle plane.

Macrocycle	NICS(0) ppm	AICD	Huckel aromaticity
IV.11	+1.67	anticlockwise	Antiaromatic
IV.12	+2.45	anticlockwise	Antiaromatic

Table II.1: Estimated NICS values for macrocycles **IV.11** and **IV.12**.

IV.7 Synthesis of [24] Sapphyrin and its higher analogues (IV.19)

The structural modification was carried out by replacing selenophene with furan. Subsequently, an effort was made to substitute biselenophene with bifuran units, resulting in the formation of the isoelectronic species **IV.11**. The aim was to investigate the impact of furan which is less aromatic compared to the selenophene, on the macrocycle. This exploration sought to understand how these changes would affect electronic properties, structural features, aromaticity of the macrocycle. The [3+2] condensation reaction involved an equimolar concentration of bifuran **IV.18**, and thiophene based tripyrromethane diol **IV.17**, in the presence of a catalytic amount of $BF_3.OEt_2$ under dark conditions in an inert atmosphere (Scheme - IV.7). The reaction progress was monitored using Thin Layer Chromatography (TLC). Subsequently MALDI TOF/TOF mass spectroscopy analysis of the reaction mixture confirmed the successful formation of the series of macrocycle (figure - IV.21).

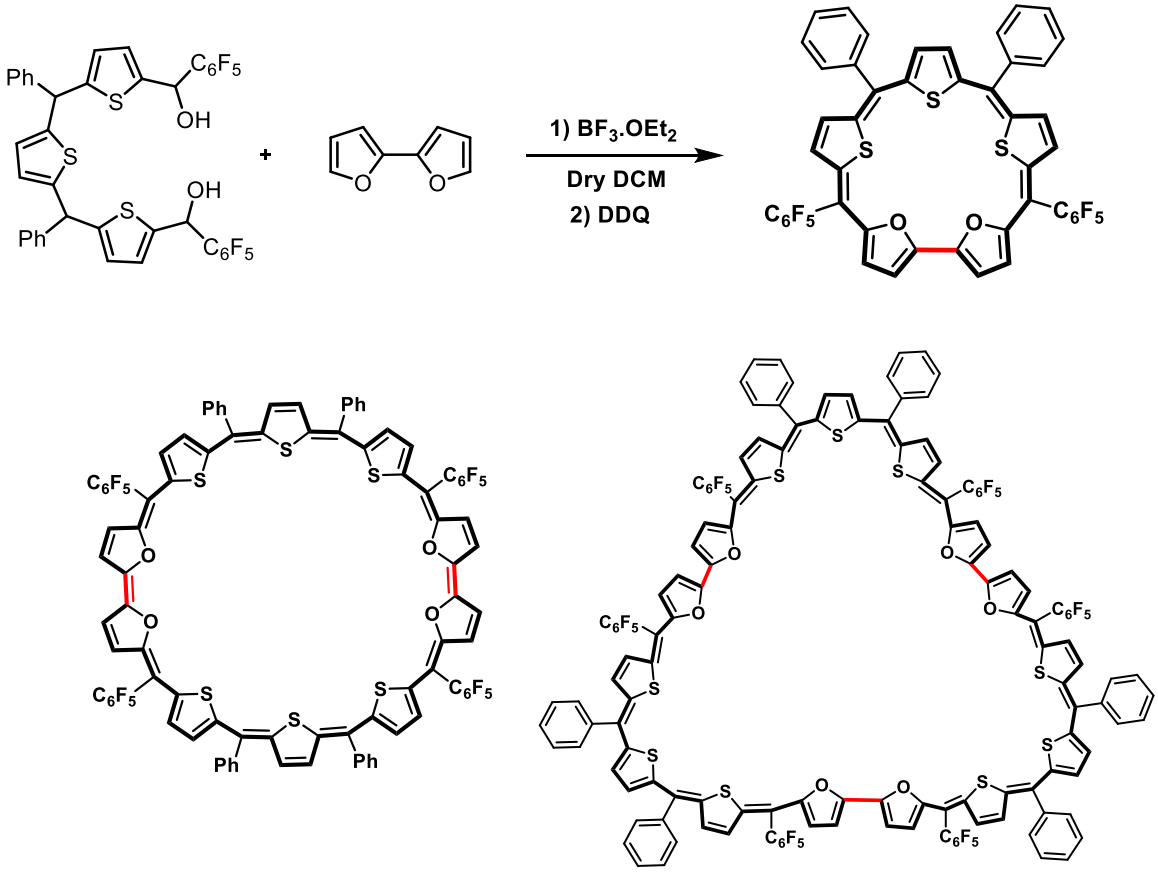

Scheme IV.7: Synthesis of core-modified 24π Sapphyrin, **IV.19**, and its higher analogues.

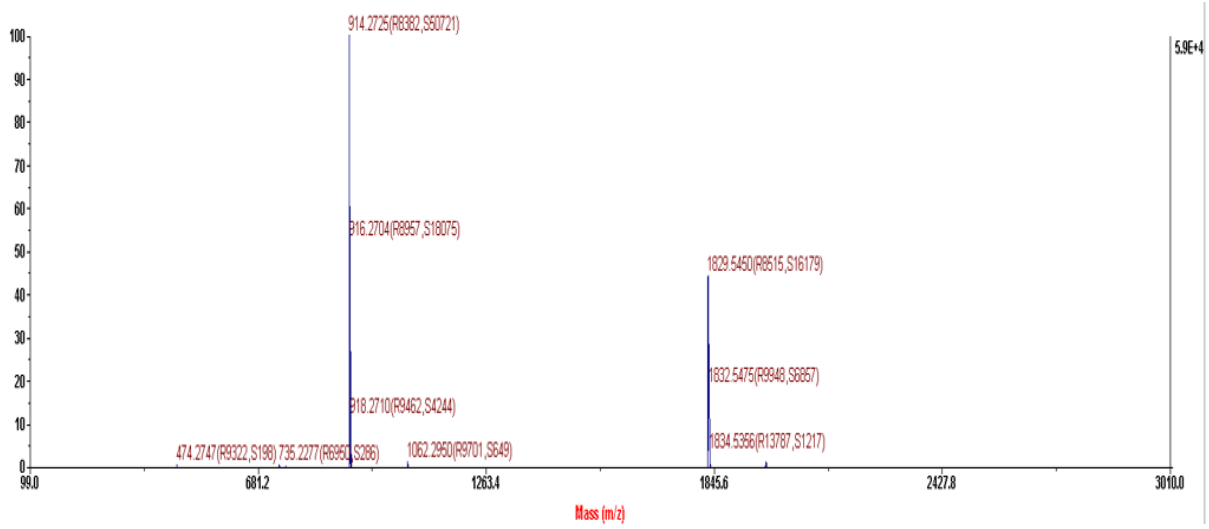

Figure IV.21: MALDI-TOF/TOF mass spectrum of reaction mixture (scheme IV.7).

IV.8.1 Isolation and Characterisation of [24] Sapphyrin (IV.19)

The expected macrocycle was isolated from the reaction mixture using successive basic alumina column chromatography and size exclusion chromatography. A greenish yellow coloured band was isolated and its HR-ESI-MS mass spectrum displayed an m/z value 914.0463, (914.0466 Calcd. for $C_{48}H_{20}F_{10}S_3O_2$) corresponding to the expected macrocycle **IV.19**, (figure – IV.22).

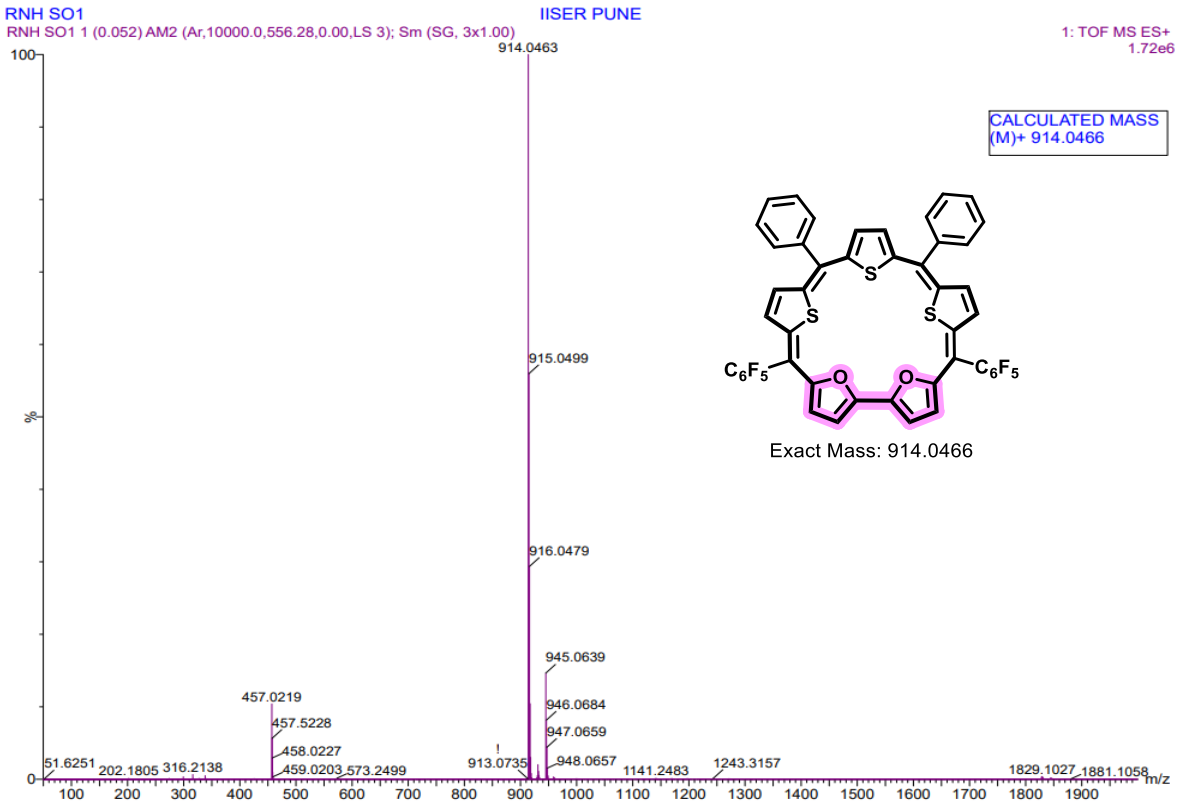

Figure IV.22: HR-MS-ESI mass spectrum of **IV.19**

IV.8.2 ^{1}H NMR study of [24]Sapphyrin (IV.19)

This macrocycle accounts for 24π electrons in the conjugation and satisfies Huckel's antiaromatic 4nπ electronic system. ^{1}H NMR spectrum of **IV.19,** was recorded in $CDCl_3$ at 298 K (figure – IV.23). The observation was quite similar to **IV.11,** but the number of signals were comparatively less, indicating merging of the signals. In its ^{1}H NMR spectrum, six signals were observed in the region between δ 7.5 to δ 3.6 ppm. Signals resonating in the region between δ 4.2 to δ 3.6 ppm correspond to β-protons of furan and thiophene units in the macrocycle, and the other signals corresponded to phenyl protons. Compared to **IV.11**, macrocycle **IV.19,** experienced a stronger paratropic ring effect, causing the signals to shift to the upfield region. Hence, this observation indicates that **IV.19**, is relatively more anti aromatic in nature than **IV.11**.

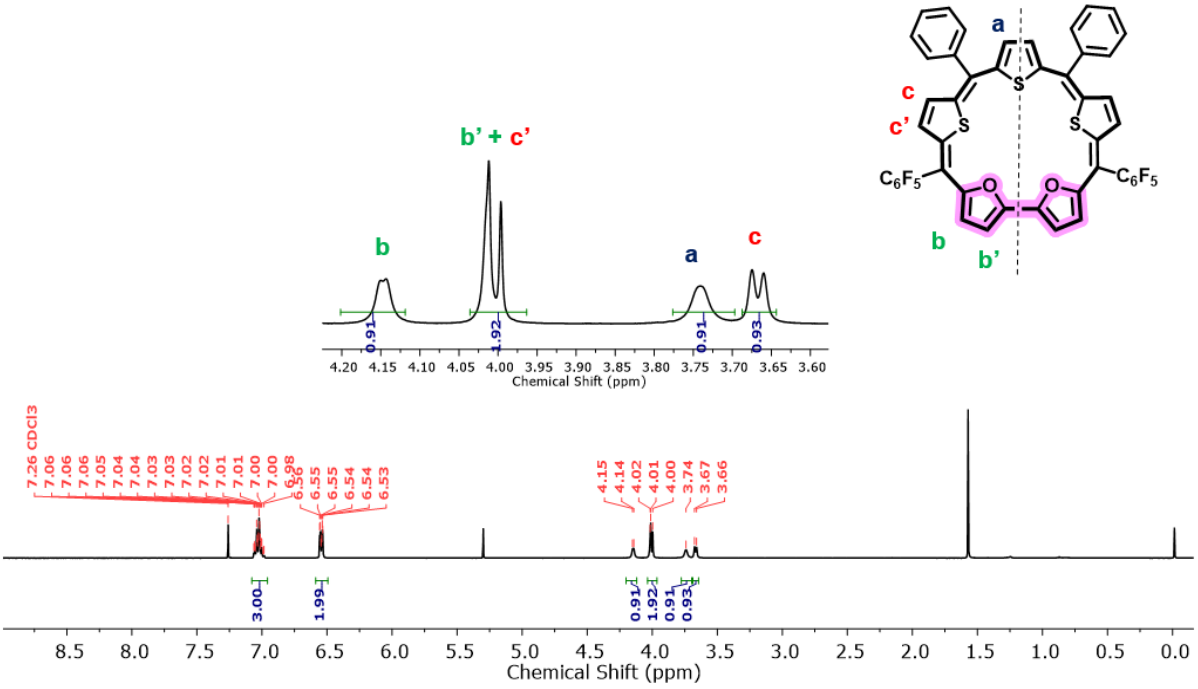

Figure IV.23: ^{1}H NMR spectrum of **IV.19** in Chloroform-d

The analysis was further supported by the ^{1}H-^{1}H COSY spectrum (figure - IV.24), which displayed two sets of correlations: one for phenyl protons and another for the coupling of adjacent β-protons of the heterocyclic rings. Based on these NMR data, it can be expected that the macrocycle adopts a planar conformation in the solution state.

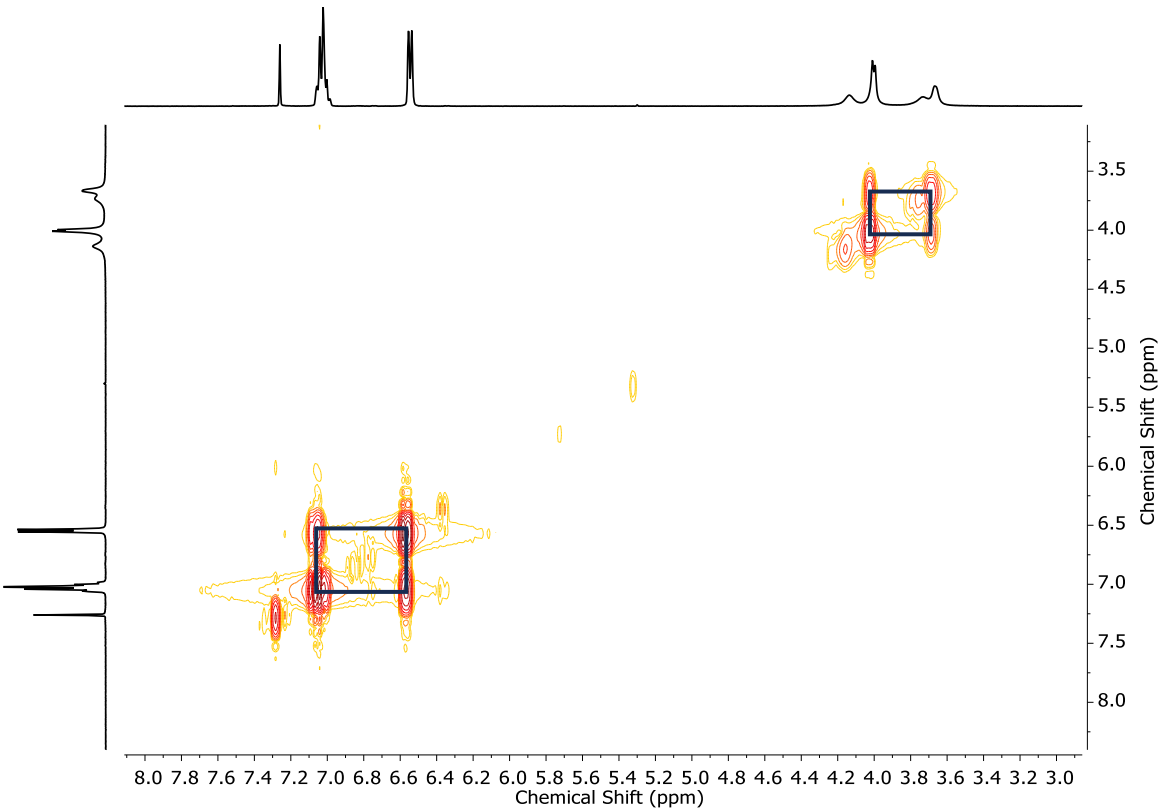

Figure IV.24: ^{1}H-^{1}H COSY spectrum of **IV.19** in Chloroform-d

IV.8.3 Molecular structure of [24]Sapphyrin (IV.19)

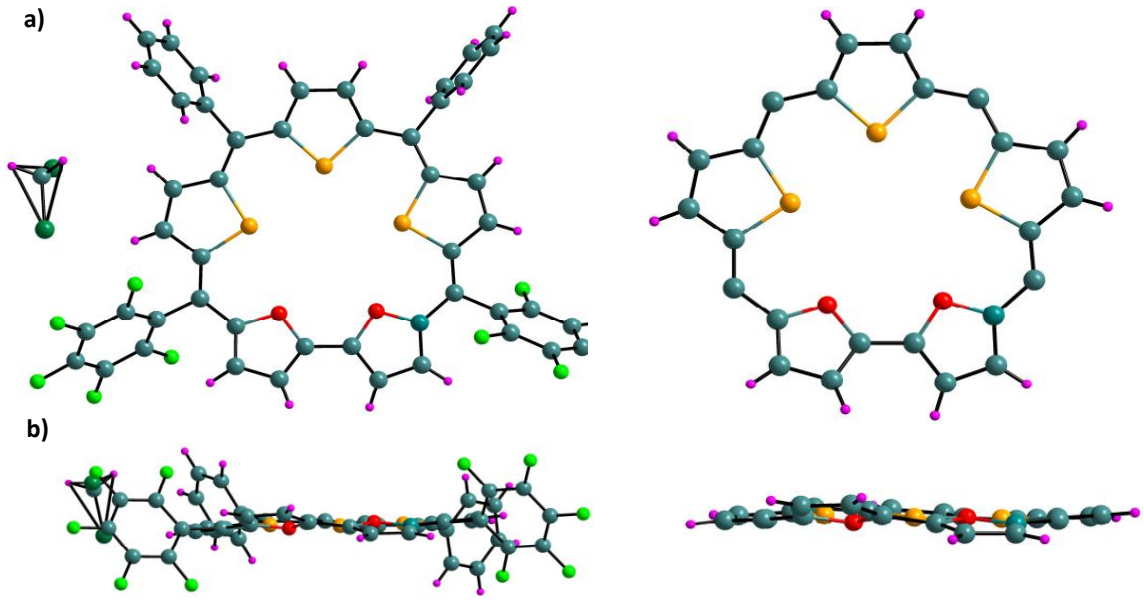

Figure IV.25: Molecular structure of [48]decaphyrin (**IV.19)** as determined from single crystal X-ray diffraction. (a) (top view) and (b) (side view).

As a characteristic colour of sapphyrin, even with bifuran condensed sapphyrin **IV.19,** same blue colour needle shape crystals were obtained. Good quality crystals were grown by passing vapours of hexane to a solution of macrocycle in DCM. Single crystal X-ray diffraction analysis revealed a planar structure with sulphur atom of thiophenes and oxygen atom of furan units pointing towards the centre of the macrocycle (figure - IV.25). Unlike sapphyrin **IV.11**, the oxygen atom of furan deviates only slightly from the macrocyclic plane probably due its smaller size compared to selenophene.

IV.8.4 Electronic absorption and cyclic voltammogram studies

Sapphyrin **IV.19**, accounts for 24π electrons in conjugation follows the Huckel's antiaromatic 4nπ system. In the absorption spectrum, this macrocycle displayed a Soret-like band at 419 nm (31900) which was split in to less intense shoulder band at 388 nm (30600) in dichloromethane (figure - IV.26a). Due to its antiaromatic character, it is highly probable to undergo reversible two-electron ring oxidations, forming the corresponding dicationic species **IV.22** (scheme - IV.8).

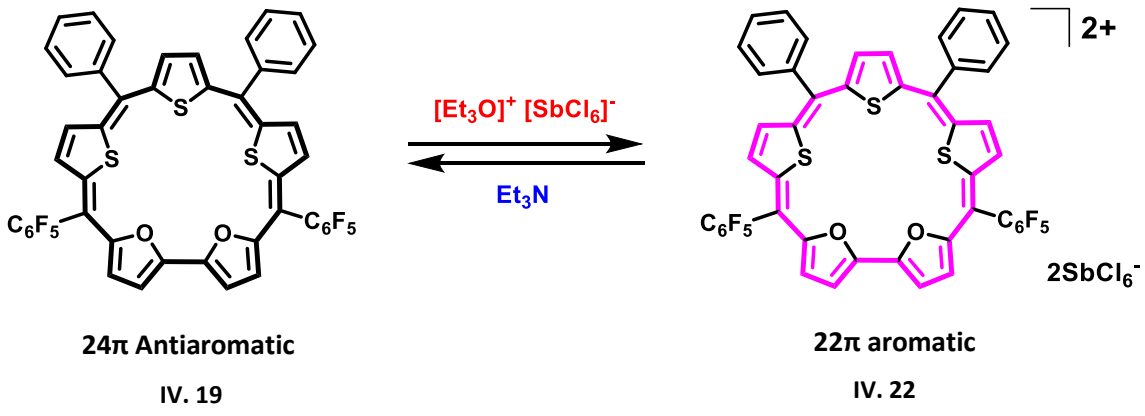

Scheme IV.8: oxidation of 48π (**IV.19**) to 46π dication (**IV.22**)$^{+2}$ upon addition of Meerwein salt.

Upon the oxidation with Meerwein salt, a significantly red shifted absorption maxima were observed at 500 nm, changing the colour from greenish-yellow to brown, accompanied by two other weak transitions in the region between 600-800 nm. A bathochromic shift of 100 nm, coupled with significant increase in the absorption coefficient of its intense absorption band, suggested the formation of the ring oxidised 22π dicationic species **IV.22**. This oxidised species reverts to free base upon the addition of a reductant such as Et_3N/, Zn dust.

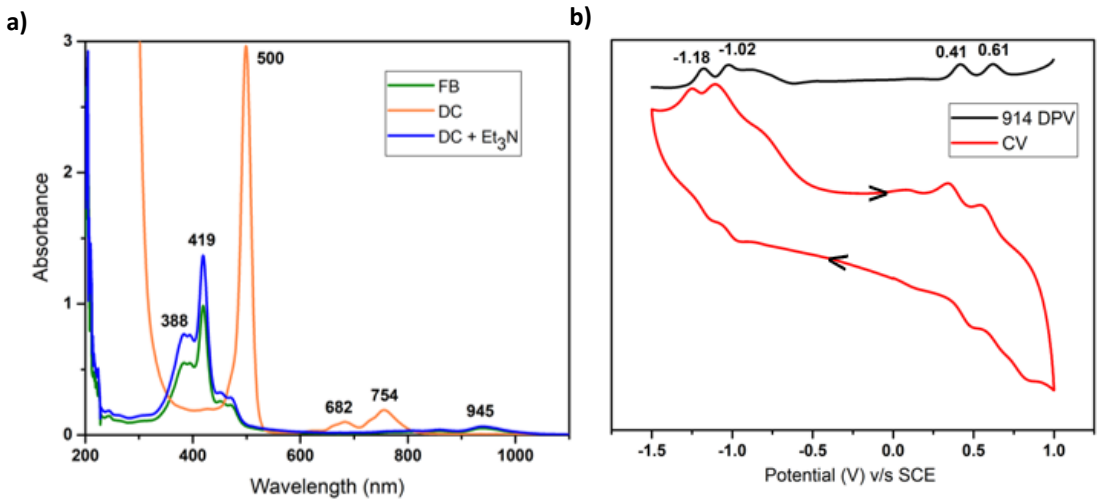

Figure IV.26: a) UV/vis/NIR absorption spectrum of 10^{-5} M solution of **IV.19** (Green) (FB: Free Base) and its oxidised species [**IV.22**]$^{2+}$ (orange) (DC: Dication) recorded in CH_2Cl_2. b) Cyclic voltammogram (CV, Red) and differential pulse voltammogram (DPV, black) of **IV.19** in CH_2Cl_2 (with 0.1 M $(Bu)_4NClO_4$ as the supporting electrolyte).

Its optoelectronic and chemical redox property were further studied through electrochemical analysis, such as cyclic voltammetry (CV) and differential pulse voltammetry (DPV). In the cyclic voltammogram two reversible oxidation waves were observed at +0.41 and +0.61 V and two reduction potential waves at -1.02 and -1.18 V respectively. All these potentials were further confirmed by differential pulse voltammetry (figure – IV.26b).

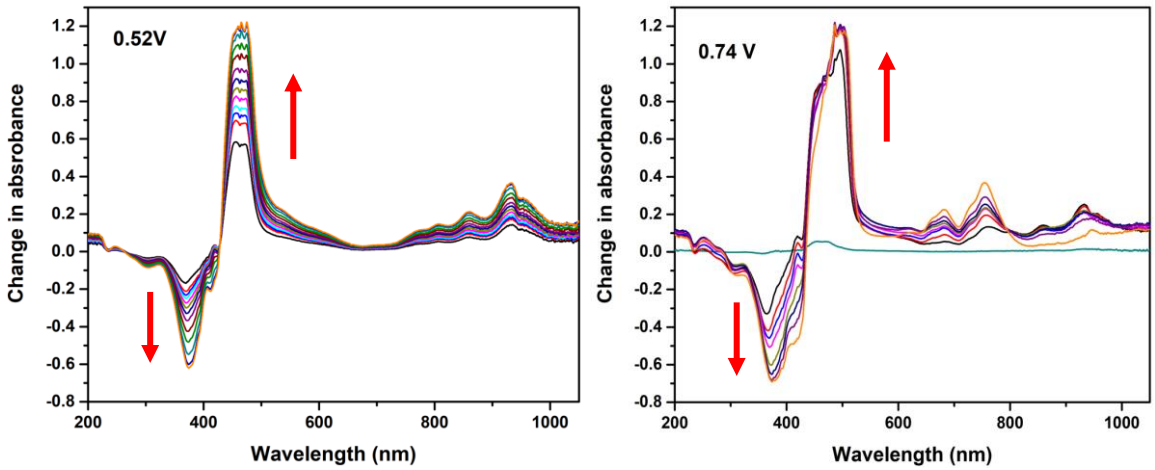

Figure IV.27: Spectro-electro chemistry studies of **IV.19**. Change in absorption spectra after applying a potential of +0.52 v (left) and +0.74 V (right), respectively.

To explain the observed change in color due to oxidation, spectro-electrochemical studies (figure - IV.27) were used to examine the resulting oxidized species. Upon applying the first oxidation potential + 0.52 V the free base peak decreased and new peak observed at 467 nm corresponding to the radical cation of **IV.19**. The absorption maxima of the parent neutral species progressively decreased upon applying the second higher potential + 0.74 V and a

showed the absorption band at 500 nm along with lower energy bands at 682 and 754 nm. The new peak was analogous to the one achieved through chemical oxidation of the macrocycle using Meerwein's salt. Therefore, it verifies the formation of a 22π dicationic species.

IV.8.5 Synthesis and characterisation of [22]sapphyrin dication (IV.22)

The HR-ESI-MS analysis of **IV.19**, revealed an *m/z* value of 914.0466, which precisely corresponds to *m/2* mass of **IV.22**, confirming the formation of dicationic species (figure - IV.22). Additionally, the absorption spectra exhibited a significant red shift with the introduction of an oxidising agent. Moreover, the cyclic voltammetry displayed two oxidation waves. To further substantiate these findings, chemical synthesis of the dicationic species was conducted by dissolving the free base in dry dichloromethane and addition of Meerwein salt at -20 ^{0}C (scheme - IV.9).[67] The ^{1}H NMR spectra of **IV.22**, were recorded at 298 K in DCM-d_2 solvent (figure - IV.28). As expected, the shift in the ring current from paratropic to diatropic unequivocally the confirmed the formation of dicationic species. In the neutral 24π sapphyrin, β-protons were found to resonate in the range δ 3.5 to 4.2 ppm whereas in case of the 22π dicationic species all the β-protons of the furan and thiophene moieties resonated in the downfield region between δ 11.0 to 12.5 ppm. The ^{1}H NMR spectra of **IV.19**, displayed significant change in the chemical shift, suggesting the formation of aromatic 22π sapphyrin dicationic species **IV.22**. Not only β-protons of heterocyclic moieties, but also the phenyl protons displayed a significant shift in the range of δ 8.2 - 9.0 ppm. In summary, the antiaromatic 24π sapphyrin readily undergoe reversible two electron oxidation, leading to the formation of its 22π dicationic species. This transformation has been thoroughly characterised using cyclic voltammetry (CV), UV-Vis spectroscopy and also ^{1}H NMR spectroscopy.

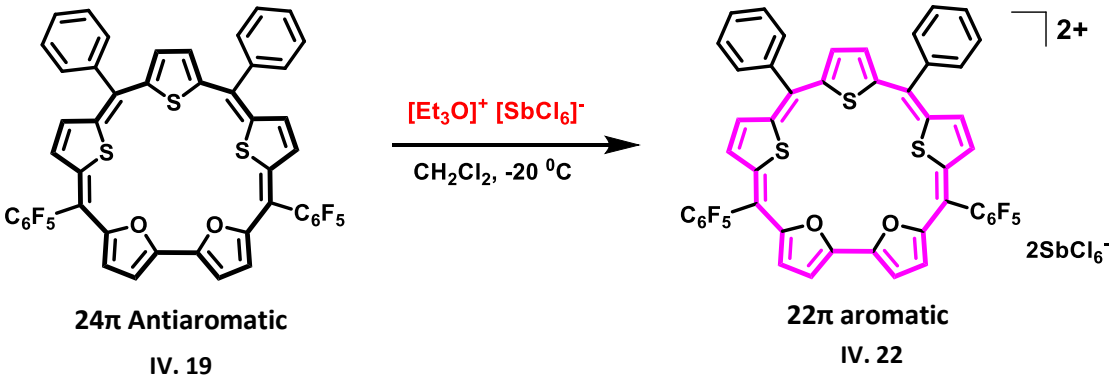

Scheme IV.9: synthesis of 22π dication, **[IV.22]**$^{2+}$ from addition of Meerwein salt.

Further support from ^{1}H-^{1}H COSY spectrum, displayed three sets of correlations. The phenyl protons correlation was observed in the range between δ 8 – 13 ppm. Two sets of correlations for the β-protons of the thiophene and furan while a singlet resonating at δ 11.08 ppm is assigned to the central thiophene along the C_2 axis of a planar macrocycle (figure - IV.29).

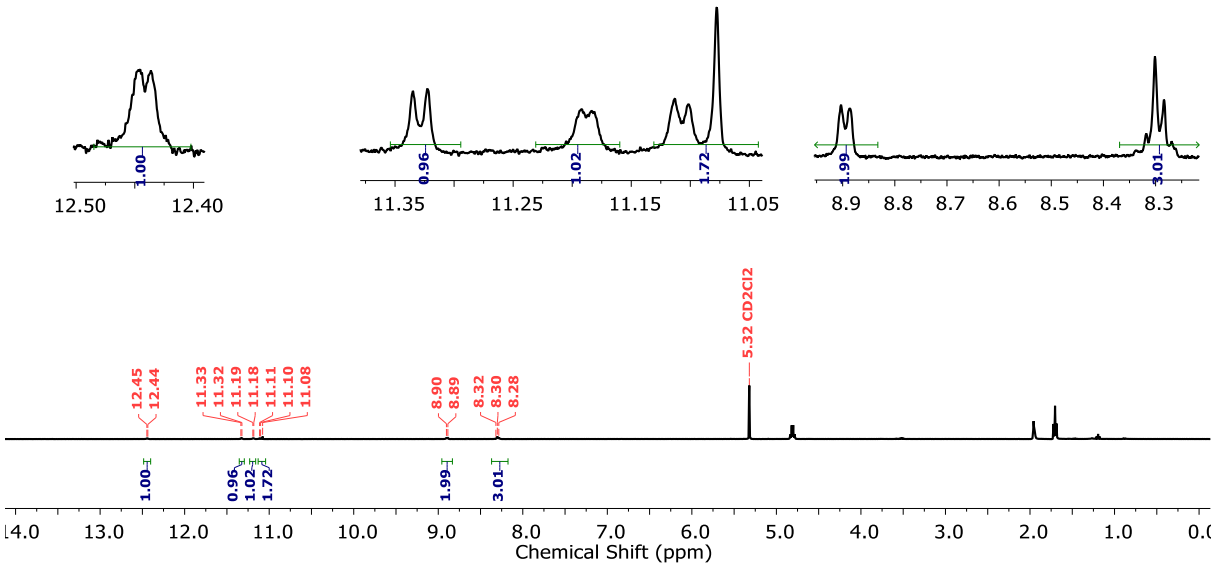

Figure IV.28: ^{1}H NMR spectrum of **[IV.22]**$^{2+}$ in Dichloromethane-d_2.

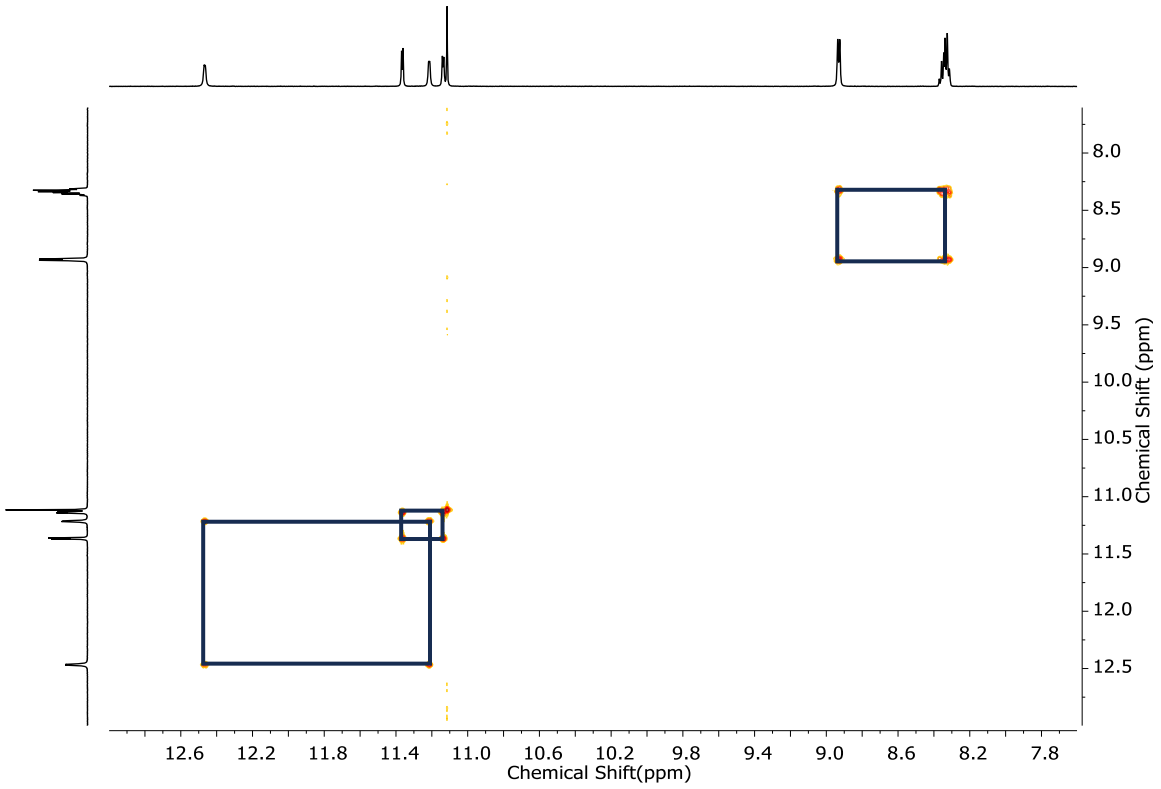

Figure IV.29: ^{1}H-^{1}H COSY spectrum of [**IV.22**]$^{2+}$ in Chloroform-d

IV.8.6 Molecular structure of [22]sapphyrin Dication (IV.22)

[24]sapphyrin is antiaromatic in both solid and solution state and undergoe a facile two-electron ring oxidation as confirmed by Spectro-electrochemical studies and also the HR-MS-ESI spectrum showed the *m/2* mass for dication species **IV.22**. Fortunately, high-quality of single crystals by vapor diffusion of hexane into a solution of **IV.22** in DCM.

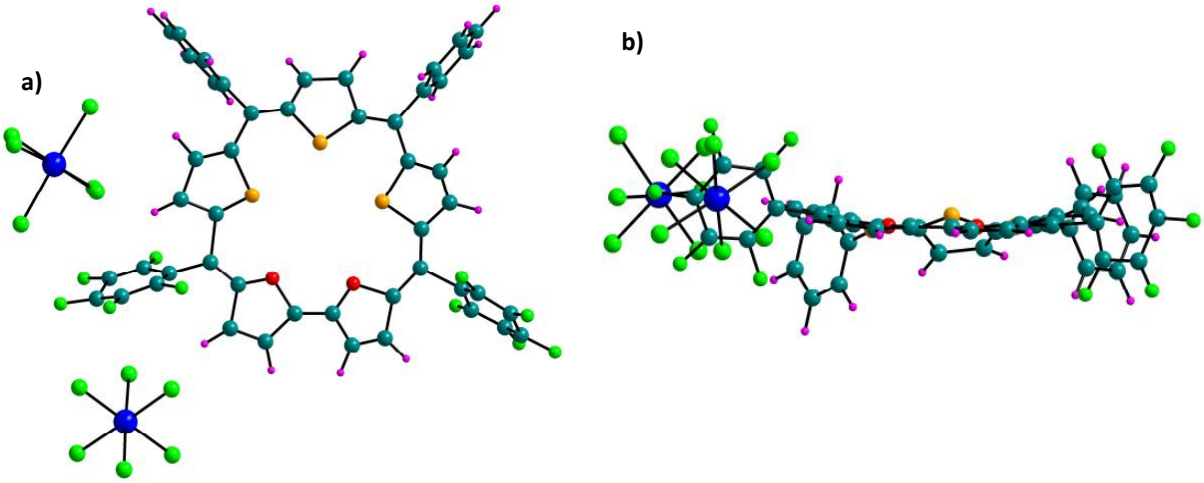

Figure IV.30: Molecular structure of [24]sapphyrin dication (**IV.22)** as determined from single crystal X-ray diffraction. a) (top view) and b) (side view)

The single crystal X-ray diffraction study revealed a planar structure where all the thiophenes and furan units were faced towards the core of the macrocycle. Two $[SbCl_6]^-$ counter anions were associated with macrocycle in support of the two-electron oxidized species (figure – IV.30). Remarkably, the estimated NICS (0) values at the centre of the pentaphyrin-like pockets of δ -12.56 ppm suggest the aromatic character of dicationic species.

IV.9.1 Isolation and Characterisation of [48]decaphyrin (IV.20)

After the 24π sapphyrin **IV.19**, a violet-coloured band was isolated from the basic alumina column chromatography. The primary confirmation was done by the MALDI TOF/TOF spectrum and the elucidation of its molecular composition and purity was accomplished through high resolution mass spectrometry (HR-MS), revealing a prominent *m/z* value of 1828.1134, (1828.0931 Calcd. for $C_{96}H_{40}F_{20}S_6O_4$) corresponding to 48π decaphyrin **IV.20** (figure - IV.31).

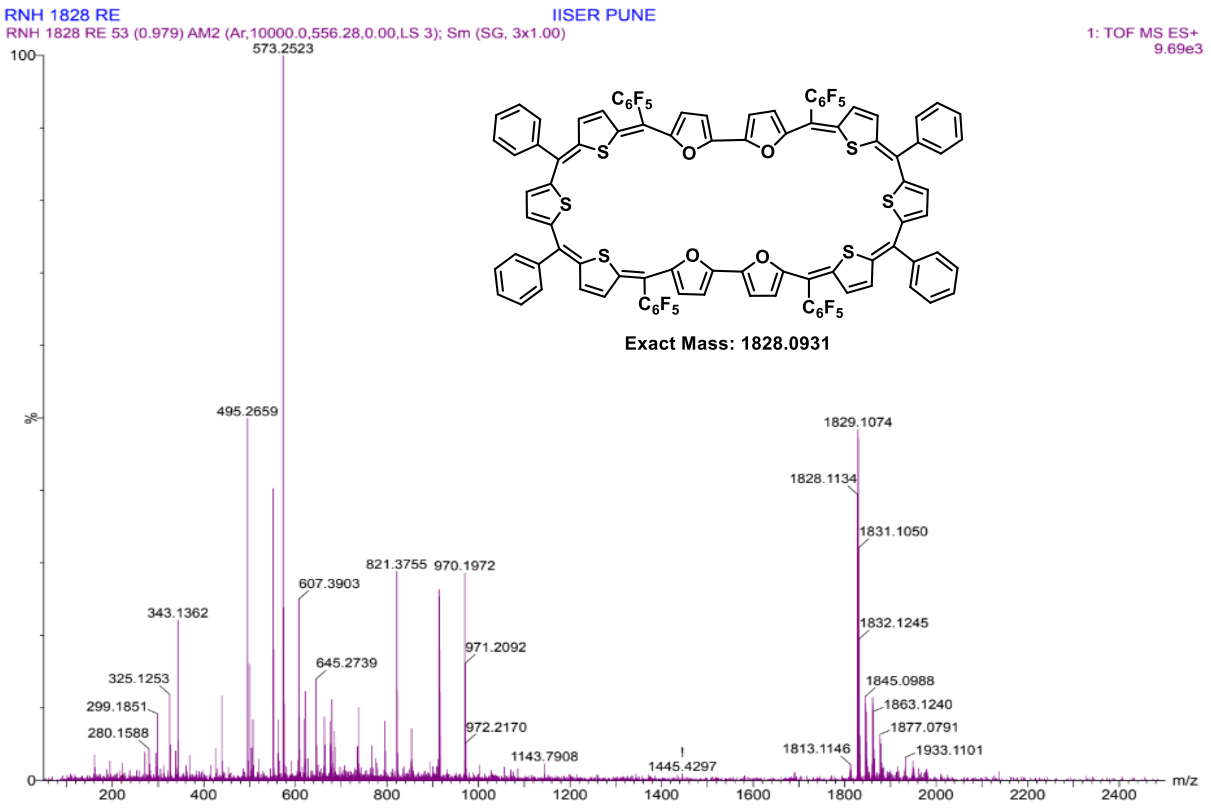

Figure IV.31: HR-ESI-TOF mass spectrum of **IV.20**.

IV.9.2 ^{1}H NMR spectra of [48]decaphyrin (IV.20)

The pink coloured decaphyrin accounts for 48π electrons and hence considered to be Huckel's antiaromatic system. In the ^{1}H NMR spectrum of **I.20**, at room temperature showed a broad singlet observed at δ 6.52 ppm (figure - IV.32), representing all the protons, whereas in **IV.12,** it displayed the well resolved spectra at room temperature showing four doublets corresponding to the β- protons of the heterocyclic ring. A broad singlet in **IV.20**, suggests the possible fluxional behaviour due to continuous flipping of thiophene and furan rings. An effort was made to reduce this fluxionality by recording the ^{1}H NMR spectrum at a low temperature. (figure - IV.32). As expected, two new doublets were observed at 248 K which corresponds to the β-protons of thiophene and furan ring. Based on the number of signals, it suggested the macrocycle with a C_2 axis and non-planar confirmation. All the signals resonated in the range between δ 7.5 to 6.2 ppm which clearly indicates the absence of paratropic ring current effect therefore it is considered as non-antiaromatic macrocycle (figure - IV.33). Further decrease in the temperature resulted in broad signals possibly due to the aggregation of macrocycle.

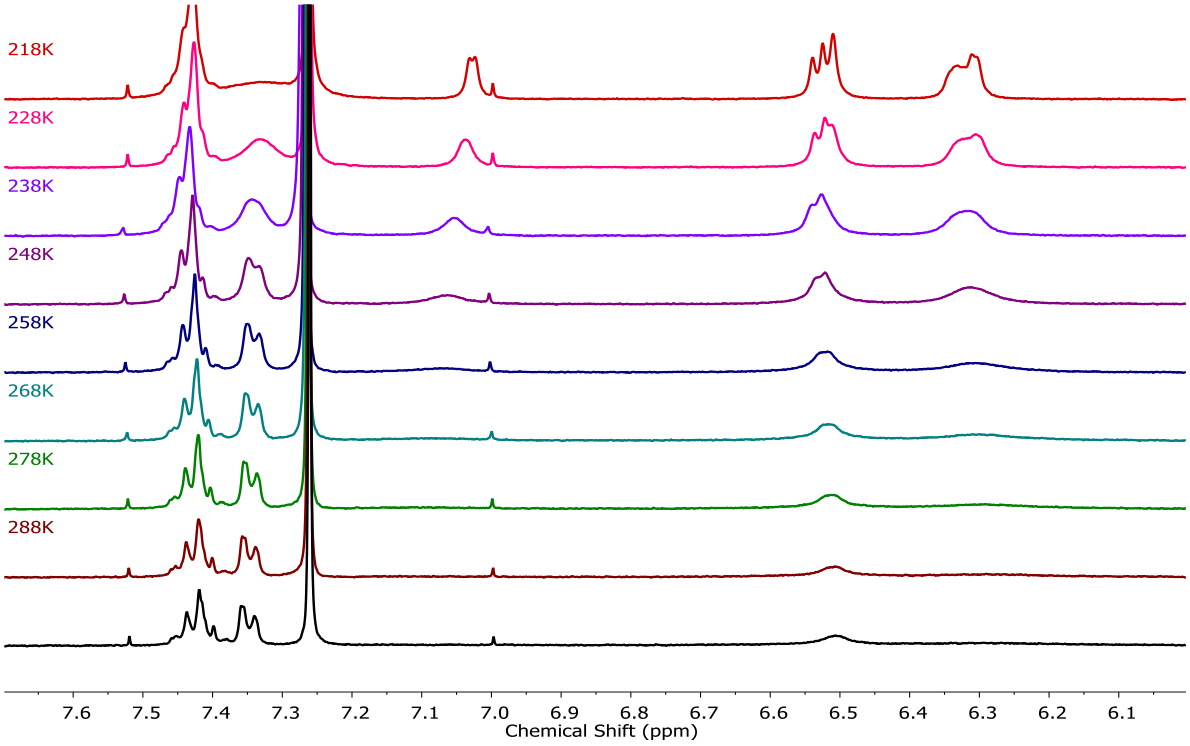

Figure IV.32: Variable temperature ^{1}H NMR spectra of **IV.20** in $CDCl_3$

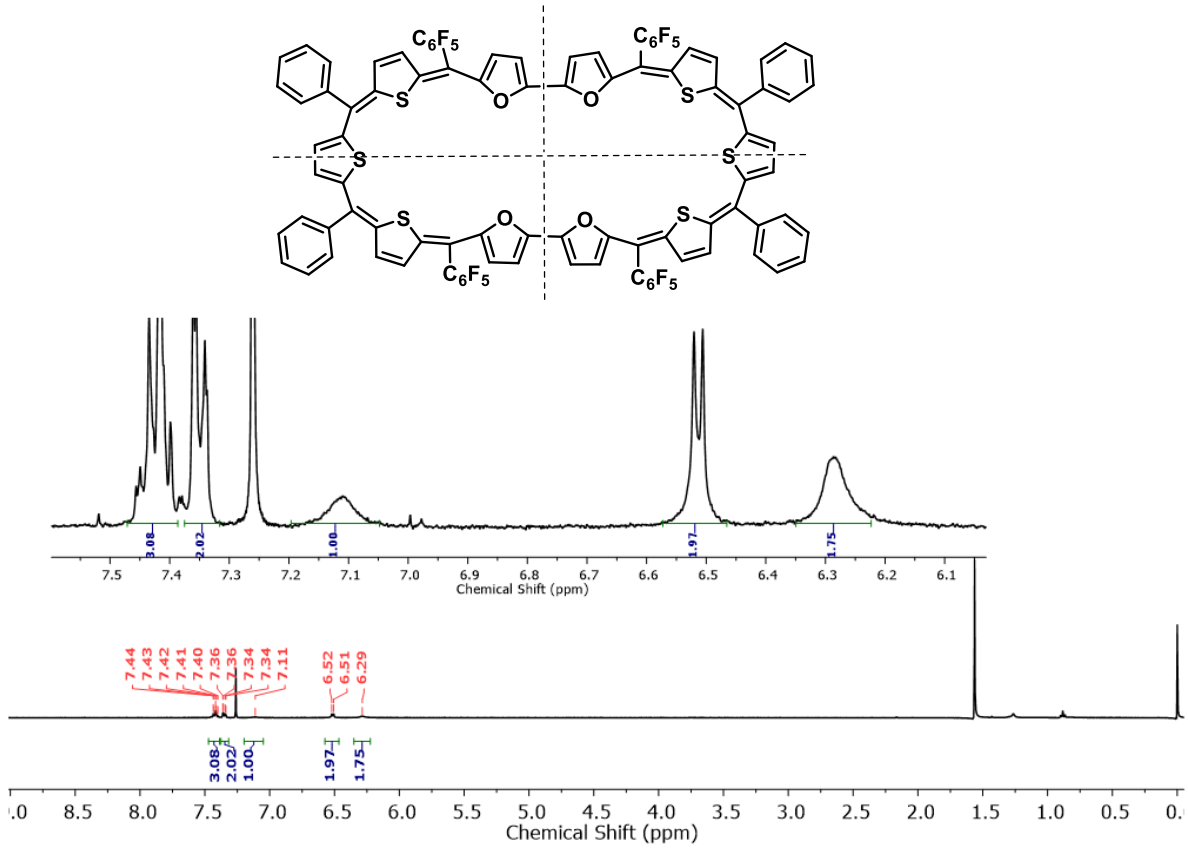

Figure IV.33: ^{1}H NMR spectrum of **IV.20** in $CDCl_3$

.

Additionally, the ^{1}H-^{1}H COSY spectrum helps to understand the correlation of the neighbouring protons (figure - IV.34). It displayed the two sets of correlations one of them which is resonated in the region of 6.6 – 6.1 ppm for the β-protons of thiophene and furan and another one for phenyl protons. This spectrum suggests the macrocycle possess the C_2 axis of symmetry.

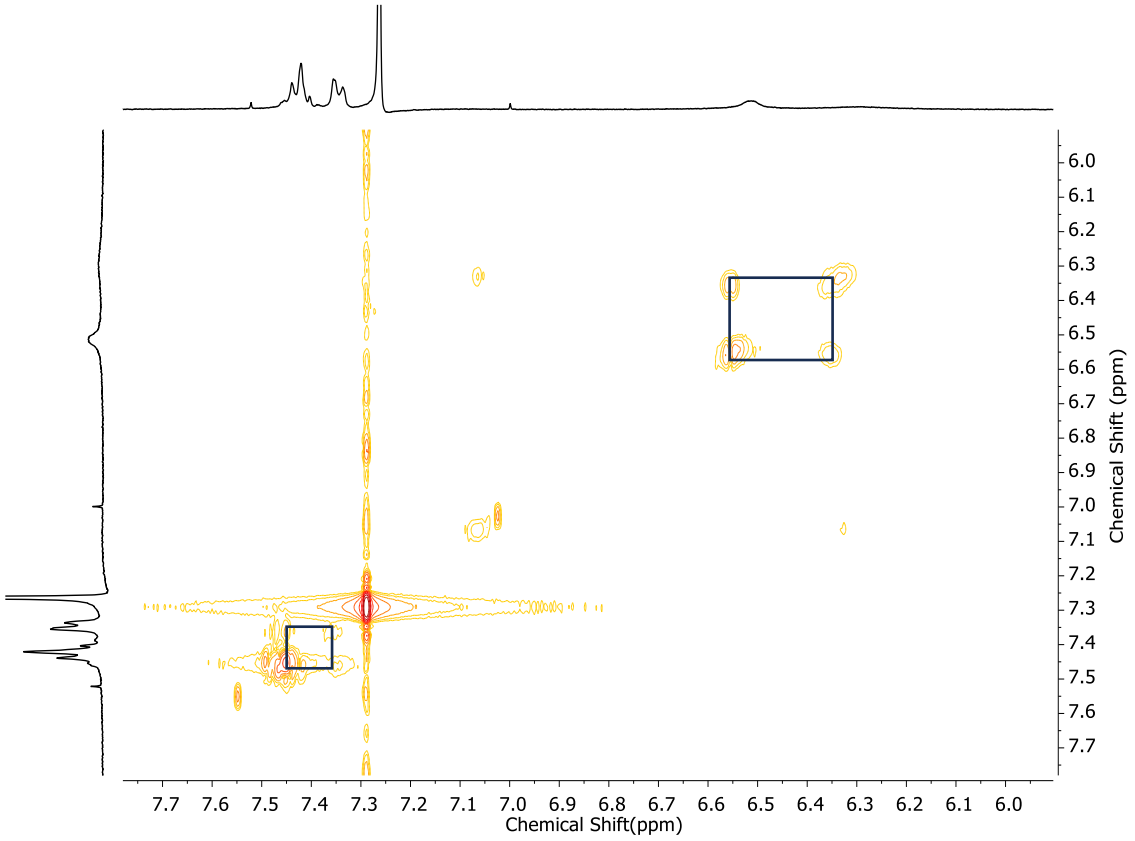

Figure IV.34: ^{1}H-^{1}H COSY spectrum of **IV.20** in Chloroform-d

IV.9.3 Molecular structure of [48]decaphyrin (IV.20)

The ^{1}H NMR spectrum revealed a lower number of signals than expected, necessitating a comprehensive analysis to elucidate the molecular structure of **IV.20**. To address this, good quality crystals of the isolated product was grown in $CHCl_3$/MeOH solvent system employing solvent diffusion method. Single crystal X-ray diffraction analysis revealed the molecular structure same as like observed in the selenophene derivative, with a figure of eight conformation (figure - IV.35). Decaphyrin macrocycle twisted into two five membered pockets like sapphyrin where both tripyrromethane was positioned in opposite direction and bifuran unit were located in the middle of the macrocycle. Each furan moiety of bifuran unit displayed an inverted orientation, facing the core of the macrocycle. In each sapphyrin pocket,

sulfur of all thiophenes and one of the furan of bifuran units were oriented towards the centre of their respective pockets. The structural findings obtained align with the patterns observed in the ^{1}H NMR spectrum and hence, it proved that the **IV.20**, can be identified as non-aromatic macrocycle due to its figure of eight conformation.

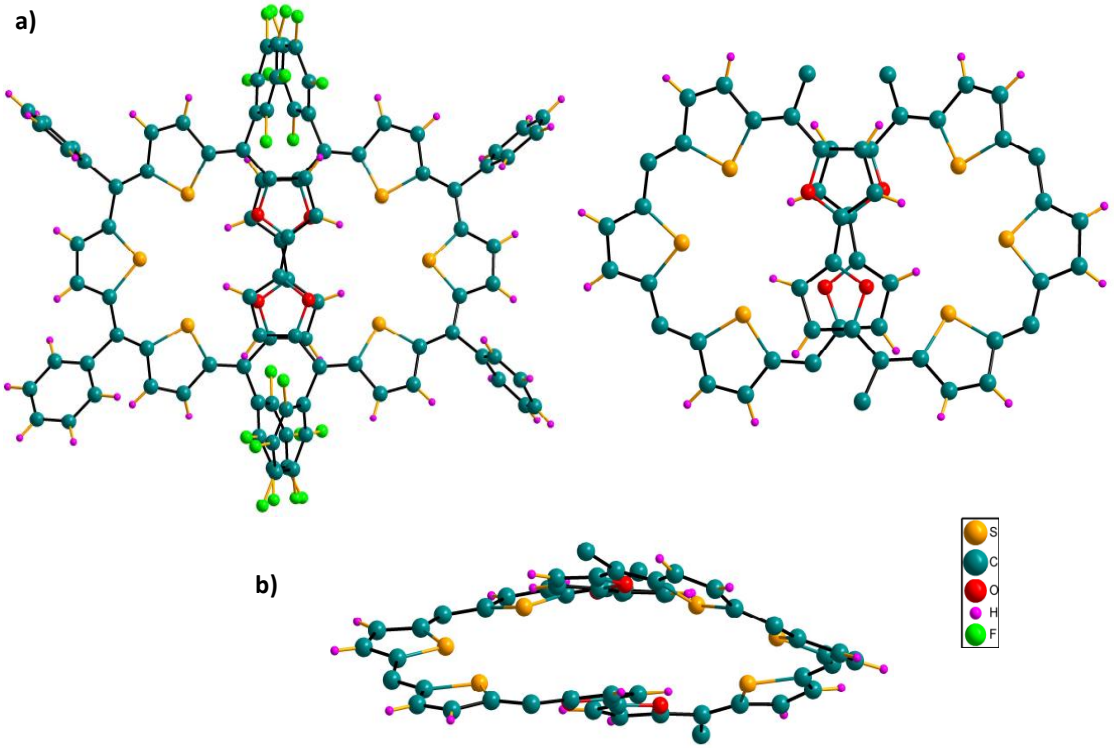

Figure IV.35: Molecular structure of [48]decaphyrin (**IV.20)** as determined from single crystal X-ray diffraction. a) (top view) and b) (side view).

IV.9.4 Electronic absorption and Cyclic Voltammogram studies

The structural diversity in the 48π decaphyrin was confirmed using ^{1}H NMR spectroscopy and single crystal x-ray diffraction analysis. Furthermore, the expansion of the delocalized π electrons network was confirmed by the significant red shift in absorption, akin to those observed in **IV.12.** Specifically, the 48π decaphyrin **IV.20**, exhibited distinctive absorption band at 573 nm (63500) along with low energy band at 388 nm (78800) (figure - IV.36a). This 4nπ antiaromatic macrocycle is widely recognised for its ability to undergo two electron ring oxidations, resulting in the formation of a stable (4n+2) π aromatic 46π dicationic species **IV.23**.

When treated with oxidizing agents such as TFA or $NOBF_4$ or Meerwein's salt, (scheme – IV.10) a subtle colour changes from pink to brownish colour, was accompanied by a strong red shifted absorption at 870 nm. Additionally, two broad bands at 1191 nm and 1382 nm, were also observed in the spectroscopic analysis.

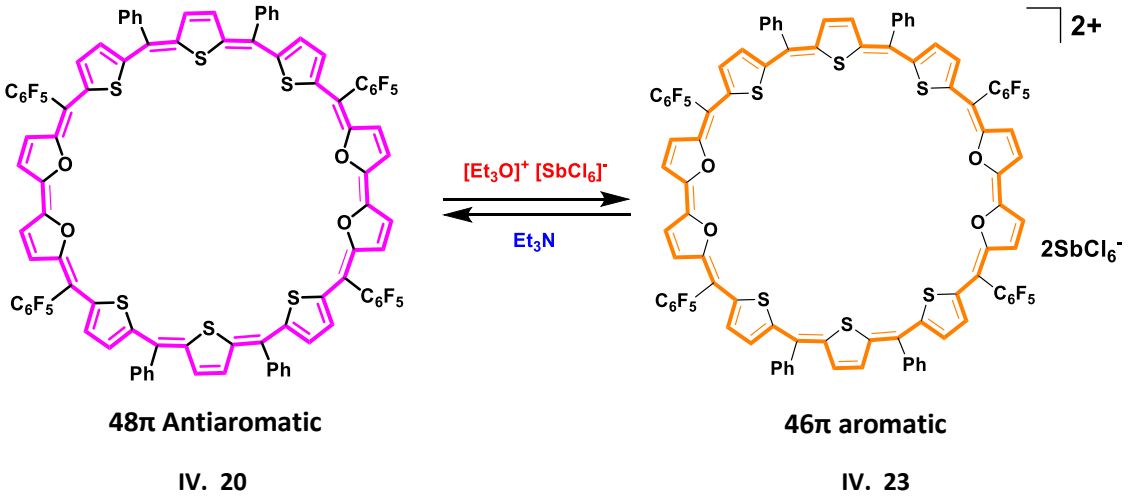

IV. 20 IV. 23

Scheme IV.10: oxidation of 48π (**IV.20**) to 46π dication (**IV.23**)$^{+2}$ upon addition of Meerwein salt.

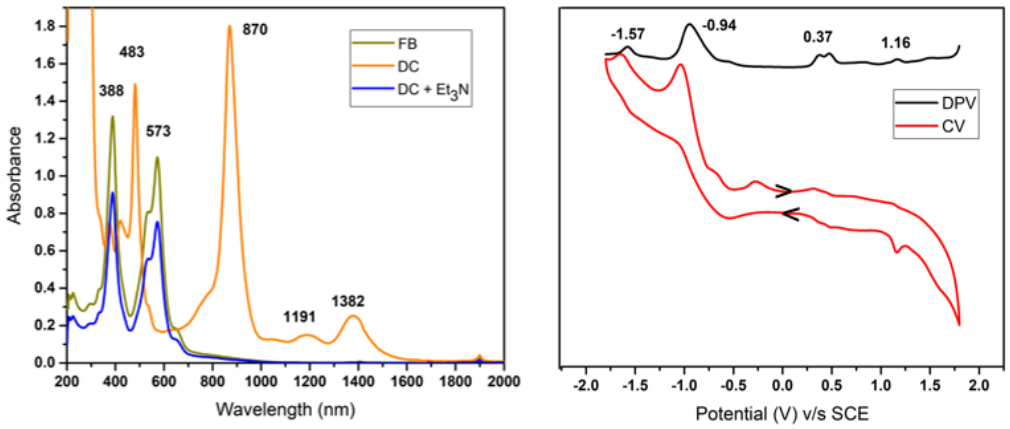

Figure IV.36: a) UV/vis/NIR absorption spectrum of 10^{-5} M solution of **IV.20** (48π) (olive green) (FB: Free Base) and its oxidised species [**IV.23**]$^{2+}$ (46π) (orange) (DC: Dication) recorded in CH_2Cl_2. b) Cyclic voltammogram (CV, red) and differential pulse voltammogram (DPV, black) of **IV.20** in CH_2Cl_2 (with 0.1 M $(Bu)_4NClO_4$ as the supporting electrolyte).

A bathochromic shift of more than 300 nm, accompanied by an increase in the absorption coefficient of its strong absorption band, signifies a remarkable change in the electronic character of the macrocycle. The addition of triethyl amine or Zn dust to the oxidized species revert back to neutral 48π decaphyrin state confirmed by absorption spectroscopy. Further study of redox chemistry of **IV.20**, was explored by cyclic voltammetry and differential pulse

voltammetry where it showed the two oxidation potentials at +0.37, +0.48 and +1.16 V and two reduction potentials at -0.94 and -1.57 V (figure - IV.36b).

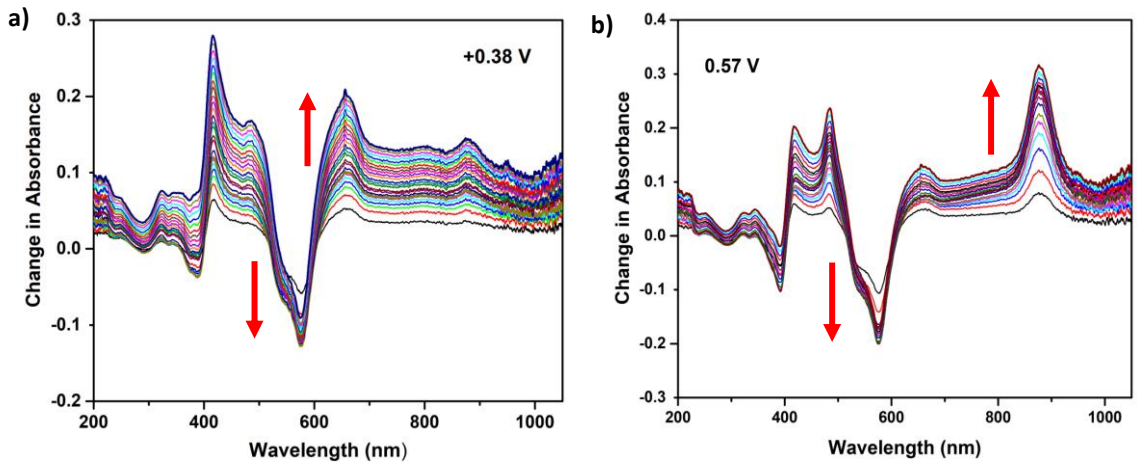

Figure IV.37: Spectro-electro chemistry studies of **IV.20**. Change in absorption spectra after applying a potential of +0.38 v (left) and +0.57 V (right), respectively.

Using these two different oxidation potential values, spectro-electrochemistry studies were performed for better understanding of redox processes. Upon applying the first oxidation potential at + 0.38 V, it showed a band with λ_{max} at 656 nm corresponding to one electron oxidation, which leads to radical cation intermediate with 47π electrons (figure – IV.37a). Later application of the second potential at + 0.57 V, radical cation was completely oxidized to 22π dication, corresponding to an absorption at 870 nm and slowly the absorption maxima of radical cation start decreasing, which confirms the macrocycle undergoe two electron ring oxidations forming 46π dication decaphyrin (figure - IV.37b).

IV.10.1 Isolation and Characterisation of [72]pentadecaphyrin (IV.21)

As like observed in the selenophene derivative series of macrocycle, here also navy-blue coloured band was isolated through repeated basic alumina and size exclusion chromatography. The MALDI TOF/TOF spectrum obtained from the isolated band unveiled a distinctive peak at an *m/z* value of 2742.8770, (2742.1397 Calc. for $C_{144}H_{60}F_{30}S_9O_6$) confirming the presence of the species as a 72π pentadecaphyrin (figure - IV.38). Due to poor yields a comprehensive study and characterization of **IV.21**, could not be achieved.

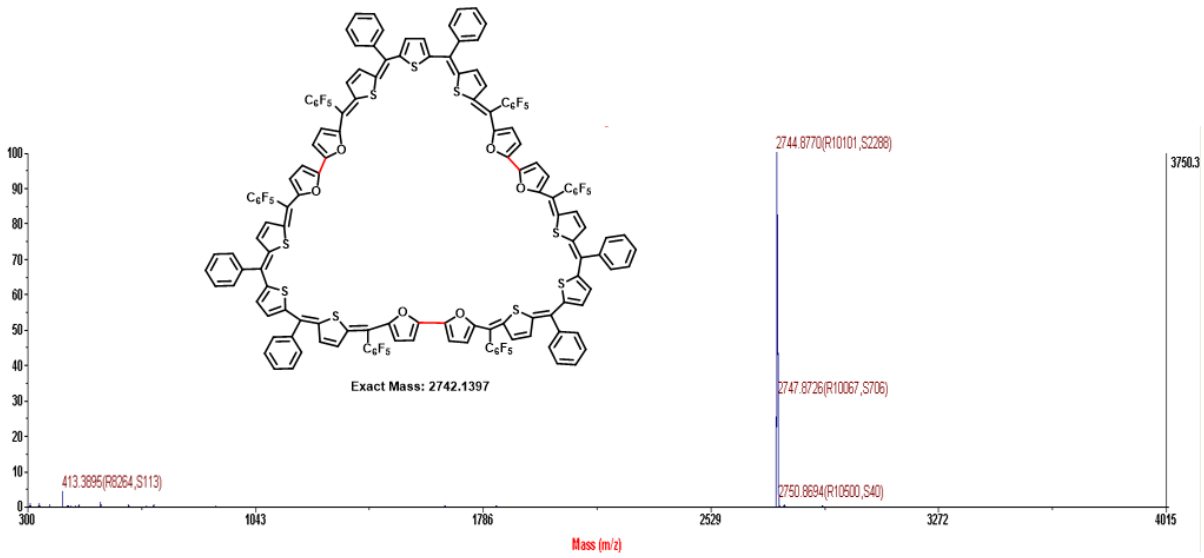

Figure IV.38: MALDI-TOF/TOF mass spectrum of **IV.21**.

IV.10.2 ^{1}H NMR spectra of [72]pentadecaphyrin (IV.21)

The [72] macrocycle accounts to Hückel's antiaromatic system and it is expected that the larger macrocycle due to increased number heterocyclic ring, loses the planarity as a result it shows non antiaromatic character. The ^{1}H NMR spectrum of **IV.21**, was recorded in THF-d_8 solvent and at room temperature showed the few signals than the anticipated (figure – IV.40).

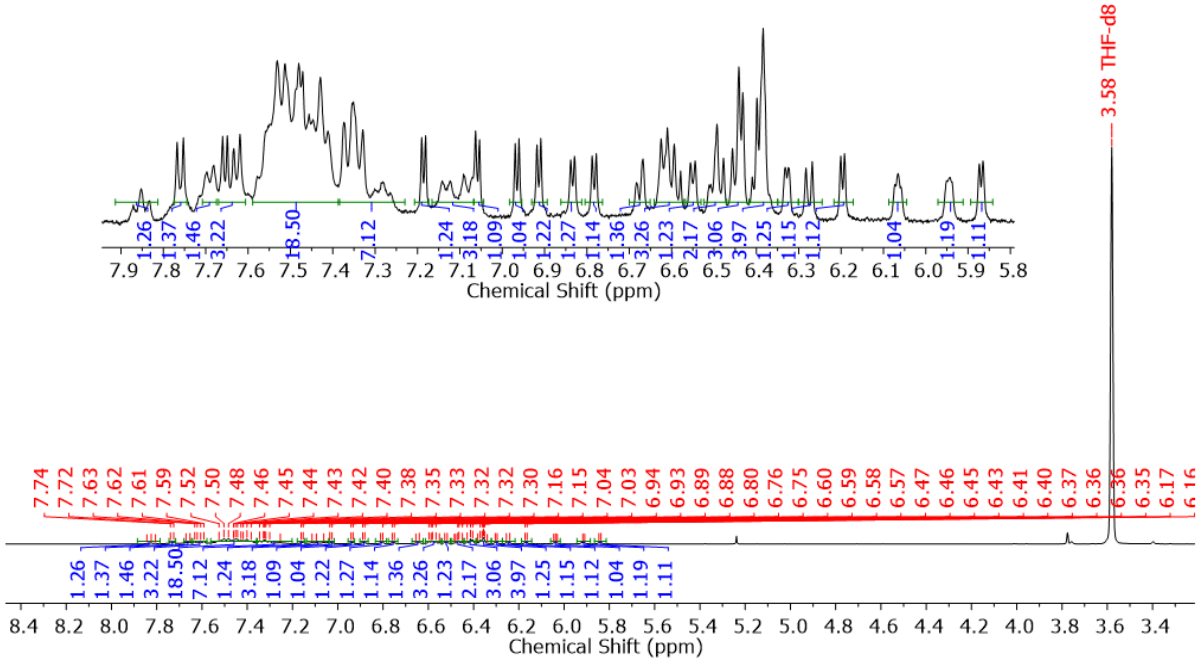

Figure IV.39: ^{1}H NMR spectrum of **IV.21** in THF-d_8 at 223 K.

Lowering the temperature up to 233 K showed the clean and well resolved ^{1}H NMR spectrum where number signal increased (figure - IV.39). All the signals were resonated in the region of 5.8 to 8.0 ppm reflects that absence of paratropic ring current. Hence it also shows the non-antiaromatic character.

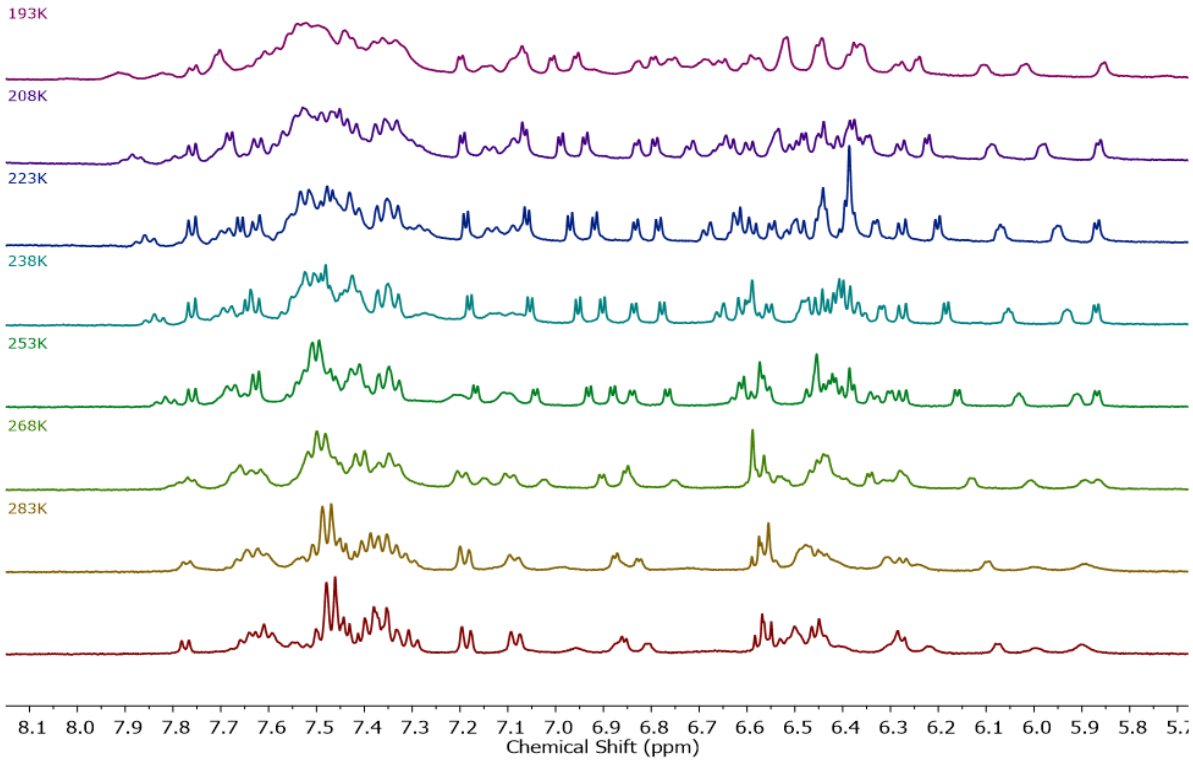

Figure IV.40: Variable temperature ^{1}H NMR spectra of **IV.21** in THF-d_8.

IV.10.3 Electronic absorption studies

One of the higher macrocycles in the series, 72π pentadecphyrin macrocycle classified as Huckel's antiaromatic 4nπ electronic system. Due to the extended conjugation, **IV.21**, absorbs in the visible region of electromagnetic spectrum and found to have multiple absorption at 665 (157400), 435 (77800), and 357 nm (182100). The extension of the delocalized π electrons network was also well confirmed by the large red shifted absorption in comparison to the parent 20π isophlorin derivatives. Addition of oxidizing agents such as Meerwein's salt or $NOBF_4$ oxidized the 72π macrocycle to its corresponding 70π dicationic species, [**IV.24**]$^{+2}$ (figure - IV.41) which induced a subtle colour change from faint blue to faint brownish colour. The spectra showed a strong red shift and its absorption maxima displayed a broad band at 1201 nm suggesting the formation of a dicationic species. The oxidized species could be reduced back to its free base by the addition of Et_3N or Zn dust as reducing agent.

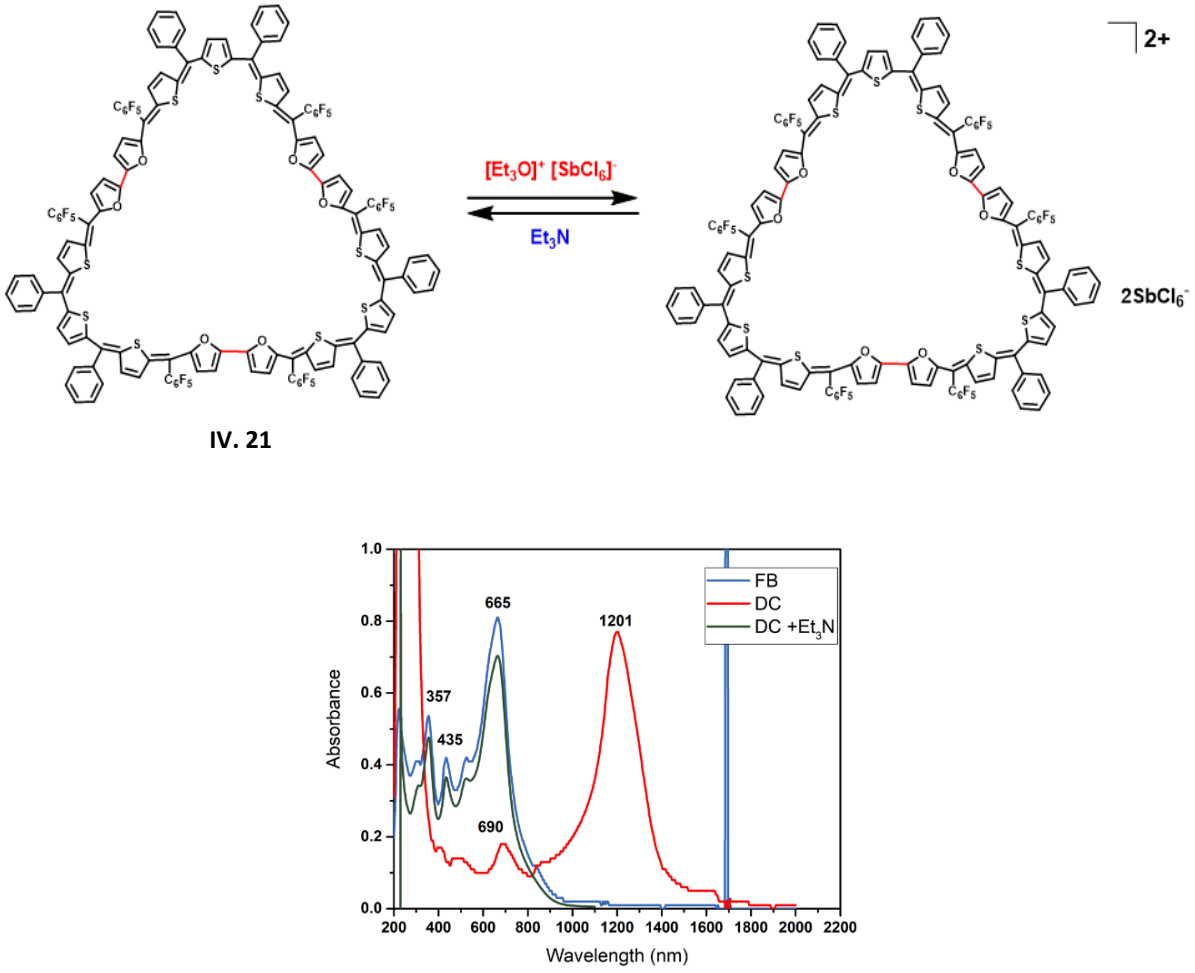

Figure IV.41: UV/vis/NIR absorption spectrum of 10^{-5} M solution of **IV.21** (72π) (blue) (FB: Free Base) and its oxidised species [**IV.24**]$^{2+}$ (70π) (red) (DC: Dication) recorded in CH_2Cl_2.

IV.11 Quantum mechanical calculations

An estimated NICS value of δ + 15.27 for the [24] sapphyrin **IV.19**, is attributed to its planar structure, indicating a strong antiaromatic character. On the other hand, in the case of **IV.11**, a partial positive NICS value is noted. These findings align with observations made in the ^{1}H NMR spectrum of the macrocycles. The correlation between the NICS value and the ^{1}H NMR spectrum provides valuable insights into the aromatic or antiaromatic nature of the molecules, further supporting the understanding of their electronic and structural properties. As in the case of dicationic species **IV.22**, the estimated NICS value is -12.56, supports its aromatic nature of the macrocycle. [48] decaphyrin **IV.20**, accounts for 48π electrons and satisfy the (4n)π electrons count. However, being a non-planar structure, it does not exhibit paratropic ring current effect and hence non-antiaromatic in nature. In support of this understanding, the

estimated NICS value is δ +2.21 ppm reflected weak antiaromatic nature of the macrocycle as observed from its ^{1}H NMR spectrum (table - IV.2). Accordingly, AICD plot displayed anticlockwise ring current (figure - IV.42), in support of 4nπ system.

Macrocycle	NICS(0) ppm	AICD	Huckel aromaticity
IV.19	+ 15.27	Anticlockwise	Antiaromatic
IV.22	-12.56	Clockwise	Aromatic
IV.20	+ 2.21	Anticlockwise	Antiaromatic

Table IV.2: Estimated NICS values for macrocycles **IV.19, IV.20** and **IV.22**.

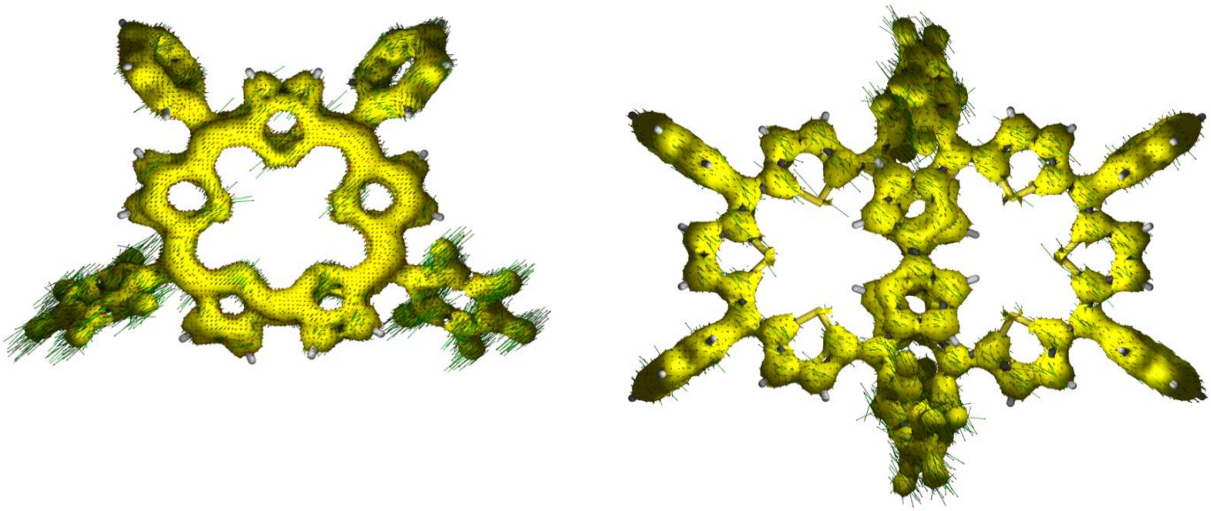

Figure IV.42: AICD plot of **IV.19 and IV.20** at an iso surface value 0.05 the external magnetic field is applied orthogonal to the macrocycle plane.

IV.12 Conclusions

Till date there are no reports on completely core modified 24π sapphyrins. This chapter describes the first attempts to synthesis not only sapphyrin but also its higher analogues and also characterized in solution and solid states. ^{1}H NMR spectrum and single crystal X-ray diffraction studies of 24π sapphyrin **IV.19,** displayed planar geometry and exhibit notable paratropic ring current effect. Further these 4nπ macrocycles readily undergo two-electron oxidations to yield the 22π dicationic species **IV.22**. The ^{1}H NMR spectra of oxidised species displayed diatropic ring current and confirms the aromatic nature of macrocycle. In contrast, the 24π sapphyrin **IV.11,** exhibited a moderate paratropic ring current effect in their ^{1}H NMR spectrum and their molecular structure revealed that biselenophene unit deviated from the mean of macrocyclic plane due to the large size of the selenium atom. To the best of knowledge, this represents the first instance of completely core modified meso-aryl substituted sapphyrin macrocycles without ring inverted heterocyclic unit.

Single crystal X-ray diffraction analysis of both 48π decaphyrin **IV.12, IV.20,** revealed macrocycles lost its planarity and adopted the figure of eight conformation in solution as well as in solid state. These conformational changes resulted in the absence of any strong ring current in the NMR spectra, indicating the non-antiaromatic nature of the macrocycles. Similar to 24π congeners, both the 48π macrocycles also undergo reversible two electron oxidation to yield their respective dicationic species as evidenced by mass spectrometry, electronic absorption and electrochemical measurements.

The higher congeners in this series, 72π pentadecaphyrin **IV.13** and **IV.21**, were isolated with low yields through column chromatography. To date, it is the first fifteen membered macrocycle series to be thoroughly characterized in solid state. The molecular structure of **IV.13**, revealed a three-folded structure, forming three sapphyrin like pockets. These results were of further support to the observed ^{1}H NMR spectrum which exhibited a reduced number of signals. Unlike the **IV.13**, furan based 72π pentadecaphyrin **IV.21**, showed all the proton signals and suggest the completely non planar structure.

Molecular structure of both 24π sapphyrin **IV.11, IV.19** showed the planar structure whereas in case of higher member they adopted non planar topology. The 48π decaphyrin exhibited fluxional behaviour in the solution, leading to figure of eight geometry in solid state and as reflected in its molecular structure. Similarly, the 72π pentadecaphyrin displayed fluxional

behaviour in solution state. All these experimental results were adequately supported by computational calculations through estimating the strength of the aromaticity.

IV.13 Experimental section

Synthetic Procedure and Characterisation

General synthetic procedure for 24π and its higher analogues and their dication:

An equimolar concentration of compound 1 equivalent biselenophene or bifuran and 1.2 equivalent thiophene tripyromethane was dissolved in dry 100 ml dichloromethane and stirred for five minutes under N_2 atmosphere and degassed with Nitrogen for 10 minutes. A catalytic amount of $BF_3.OEt_2$ was added under Dark condition using syringe resulting solution was added further 1 hour under an inert condition. Then, 2.5 equivalent of 2,3-Dichloro-5,6-dicyano-1,4- benzoquinone (DDQ) was added to the solution and stirred for additional 2 hours under open air condition. then the solution was passed through short pad of basic alumina. The resulting reaction mixture was concentrated under reduced pressure and purified through basic alumina column chromatography using 20-25% CH_2Cl_2/Hexane as eluent and size exclusion chromatography using THF.

The dication synthesised by the addition of oxidising agent Meerwein's salt in Dry CH_2Cl_2 solution at -20^{o}C. Dicationic salt of hexachloroantimonate was prepared as per earlier report.[66]

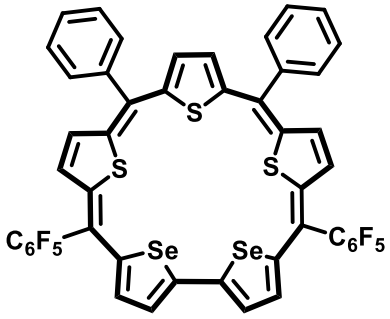

IV.11

IV.11: ^{1}H NMR (400 MHz, Chloroform-*d*) δ 7.23 – 7.14 (m, 3H), 6.88 – 6.80 (m, 2H), 6.16 (d, *J* = 4.1 Hz, 1H), 5.89 (d, *J* = 4.1 Hz, 1H), 5.08 (d, *J* = 6.0 Hz, 1H), 5.01 (s, 1H), 4.89 (dt, *J* = 6.0, 1.3 Hz, 1H). **UV/Vis/NIR** (CH_2Cl_2): λ_{max} nm (ε) $Lmol^{-1}cm^{-1}$ = 413 (37580), 440 (35289). **HR-MS** (ESI-TOF): m/z = 1041.8898 (found), 1041.8898 (Calcd. For $C_{48}H_{20}F_{10}S_3Se_2$).

Selected Crystal data of IV.12: $C_{48}H_{20}F_{10}S_3Se_2$, ($M_r$ = 1040.74), monoclinic, space group *P* $2_1/n$, *a* = 16.1050(15), *b* = 14.7521(13), *c* = 21.0353(19) Å, $\alpha = 90^0$, $\beta = 93.455^0$, $\gamma = 90^0$; *V* = 4988.54 $Å^3$, *Z* = 4, *T* = 150 K, D_{calcd} = 1.386 gcm^{-3}, R_1 = 0.0450 (I > 2sigma (I)), R_w (all data) = 0.1092, GOF = 1.069.

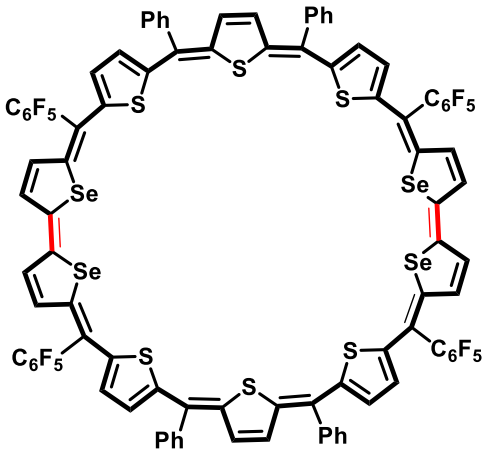

Exact Mass: 2083.7796

IV.12

IV.12: ^{1}H NMR (400 MHz, Chloroform-*d*) δ 7.42 (d, *J* = 7.0 Hz, 3H), 7.32 (dd, *J* = 7.4, 2.0 Hz, 2H), 6.88 (s, 1H), 6.62 (s, 1H), 6.50 (d, *J* = 5.8 Hz, 1H), 6.45 (s, 1H), 6.16 (s, 1H). **UV/Vis/NIR** (CH_2Cl_2): λ_{max} nm (ε) $Lmol^{-1}cm^{-1}$ = 417 (108990), 605 (138280). **HR-MS** (ESI-TOF): m/z = 2082.7932 (found), 2082.7837 (Calcd. For $C_{96}H_{40}F_{20}S_6Se_4$).

Selected Crystal data of IV.12: $C_{96}H_{40}F_{20}S_6Se_4$, ($M_r$ = 2081.48), monoclinic, space group *P* $2_1/C$, *a* = 17.739(4), *b* = 11.313(2), *c* = 28.350(6) Å, $\alpha = 90^0$ (3), $\beta = 99.35^0$(3), $\gamma = 90^0$ (3); *V* = 5613 $Å^3$, *Z* = 2, *T* = 150 K, D_{calcd} = 1.231 gcm^{-3}, R_1 = 0.0390 (I > 2sigma (I)), R_w (all data) = 0.0949, GOF = 1.035;

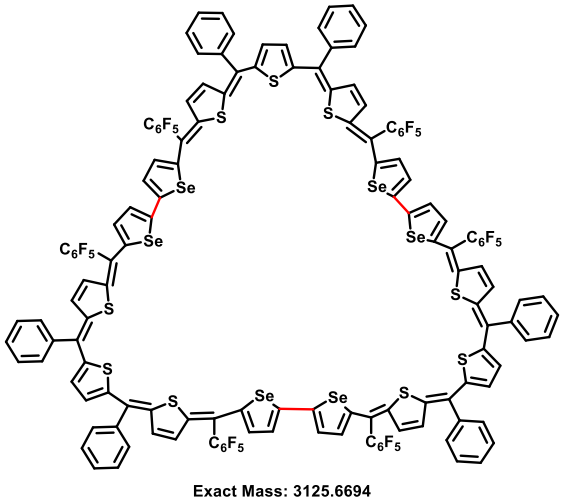

IV.13

IV.13: ^{1}H NMR (400 MHz, Chloroform-*d*) δ 7.47 – 7.37 (m, 3H), 7.32 (dd, *J* = 7.4, 2.2 Hz, 2H), 6.62 (d, *J* = 5.9 Hz, 1H), 6.54 (s, 1H), 6.50 (d, *J* = 4.4 Hz, 1H), 6.27 – 6.20 (m, 2H). **UV/Vis/NIR** (CH_2Cl_2): λ_{max} nm (ε) $Lmol^{-1}cm^{-1}$ = 446 (42722), 550 (40500), 706 (19612). **MALDI TOF/TOF**: m/z = 3125.2063 (found), 3125.6884 (Calcd. For $C_{144}H_{60}F_{30}S_9Se_6$).

Crystal data of IV.19: $C_{144}H_{60}F_{30}S_9Se_6$, ($M_r$ = 3121.63), triclinic, space group *P -1*, *a* = 14.456(13), *b* = 15.8125(14), *c* = 17.3301(16) Å, *α* = 77.085(13)^0, *β* = 81.783^0(3), *γ* = 65.372(3)^0; *V* = 2866.5 Å^3, *Z* = 1, *T* = 150 K, D_{calcd} = 1.37 gcm^{-3}, R_1 = 0.0824 (I > 2sigma (I)), R_w (all data) = 0.2205, GOF = 1.080;

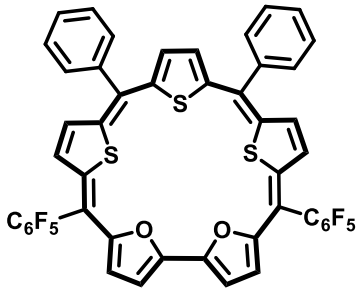

IV.19

IV.19: ^{1}H NMR (400 MHz, Chloroform-*d*) δ 7.08 – 6.96 (m, 3H), 6.59 – 6.49 (m, 2H), 4.15 (d, *J* = 3.8 Hz, 1H), 4.04 – 3.96 (m, 2H), 3.74 (s, 1H), 3.67 (d, *J* = 6.0 Hz, 1H). **UV/Vis/NIR** (CH_2Cl_2): λ_{max} nm (ε) $Lmol^{-1}cm^{-1}$ = 388 (30678), 419 (31989). **HR-MS** (ESI-TOF): m/z = 914.0463 (found), 914.0466 (Calcd. For $C_{48}H_{20}F_{10}O_2S_3$).

Crystal data of IV.19: $C_{48}H_{20}F_{10}O_2S_3$, (M_r = 999.74), triclinic, space group *P -1*, *a* = 12.1456(13), *b* = 13.5761(14), *c* = 15.2329(16) Å, α = 74.508(3)^0, β = 80.163^0(3), γ = 63.732(3)^0; *V* = 2166.5 Å^3, *Z* = 2, *T* = 150 K, D_{calcd} = 1.533 gcm^{-3}, R_1 = 0.0424 (I > 2sigma (I)), R_w (all data) = 0.1205, GOF = 1.010;

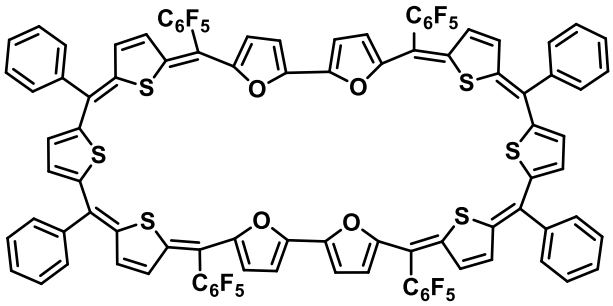

Exact Mass: 1828.0931

IV.20

IV.20: ^{1}H NMR (400 MHz, Chloroform-*d*) δ 7.47 – 7.39 (m, 3H), 7.35 (dd, *J* = 7.6, 1.9 Hz, 2H), 7.11 (s, 1H), 6.51 (d, *J* = 5.9 Hz, 2H), 6.29 (s, 2H). **UV/Vis/NIR** (CH_2Cl_2): λ_{max} nm (ε) Lmol^{-1}cm^{-1} = 388 (78800), 573 (63528). **HR-MS** (ESI-TOF): m/z = 1828.1134 (found), 1829.0965 (Calcd. For $C_{96}H_{40}F_{20}O_4S_6$).

Crystal data of IV.20: $C_{96}H_{40}F_{20}O_4S_6$, (M_r = 1829.64), triclinic, space group *P -1*, *a* = 11.980(5), *b* = 16.121(6), *c* = 25.042(10) Å, α = 88.561(16)^0, β = 87.195^0 (16), γ = 73.967^0 (16); *V* = 4642 Å^3, *Z* = 2, *T* = 150 K, D_{calcd} = 1.309 gcm^{-3}, R_1 = 0.0921 (I > 2sigma (I)), R_w (all data) = 0.2778, GOF = 1.018;

Synthesis of 2, 2'-Biselenophene:

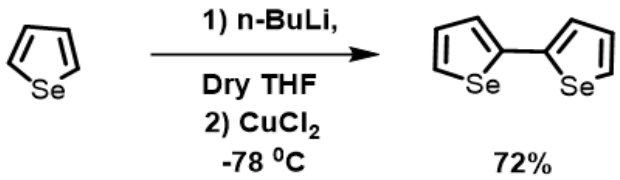

A selenophene (1 mmol) was dissolved in 100 ml of anhydrous THF in a flame dried two-neck round bottom flask. The temperature was lowered to – 78 ^{0}C, and n-BuLi in hexane (1.2 mmol) was added dropwise. The reaction mixture was stirred for 10 minutes at the same

temperature. Subsequently, anhydrous $CuCl_2$ (1.5 mmol) was added in one portion at -78 ^{0}C, and stirring continued for one hour. The reaction mixture was slowly warmed to room temperature, and stirring was sustained overnight. The reaction was quenched with water, followed by extraction with EtOAc. The compound was dried over Na_2SO_4, and the product was purified by silica gel column chromatography using hexane as the eluent. The resulting light yellow was isolated with a yield of 72%.

^{1}H NMR ($CDCl_3$, 400 MHz): δ (ppm) = 7.87 (dd, JH,H = 5.6, 1.1 Hz, 2H), 7.27 (dd, JH,H = 3.8, 1.1 Hz, 2H), 7.22 (dd, JH,H = 5.6, 3.8 Hz, 2H).

Synthesis of 2, 2'-Bisfuran:

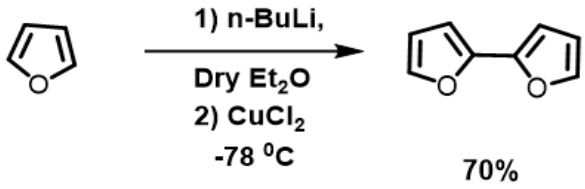

A Furan (1 mmol) was dissolved in 100 ml of anhydrous THF in a flame dried two-neck roun bottom flask. The temperature was lowered to – 78 ^{0}C, and n-BuLi in hexane (1.2 mmol) was added dropwise. The reaction mixture was stirred for 10 minutes at the same temperature. Subsequently, anhydrous $CuCl_2$ (1.5 mmol) was added in one portion at -78 ^{0}C, and stirring continued for one hour. The reaction mixture was slowly warmed to room temperature, and stirring was sustained overnight. The reaction was quenched with water, followed by extraction with EtOAc. The compound was dried over Na_2SO_4, and the product was purified by silica gel column chromatography using hexane as the eluent. The resulting light yellow was isolated with a yield of 70%.

^{1}H NMR ($CDCl_3$, 400 MHz): δ (ppm) = δ = 7.41 (dd, J = 1.8, 0.8 Hz, 2H), 6.55 (dd, J = 3.3, 0.8 Hz, 2H), 6.46 (dd, J = 3.4, 1.8 Hz, 2H)

5, 5'-Trithienyldimethane-2, 2'-bis (perfluorophenyl)dicarbinol:

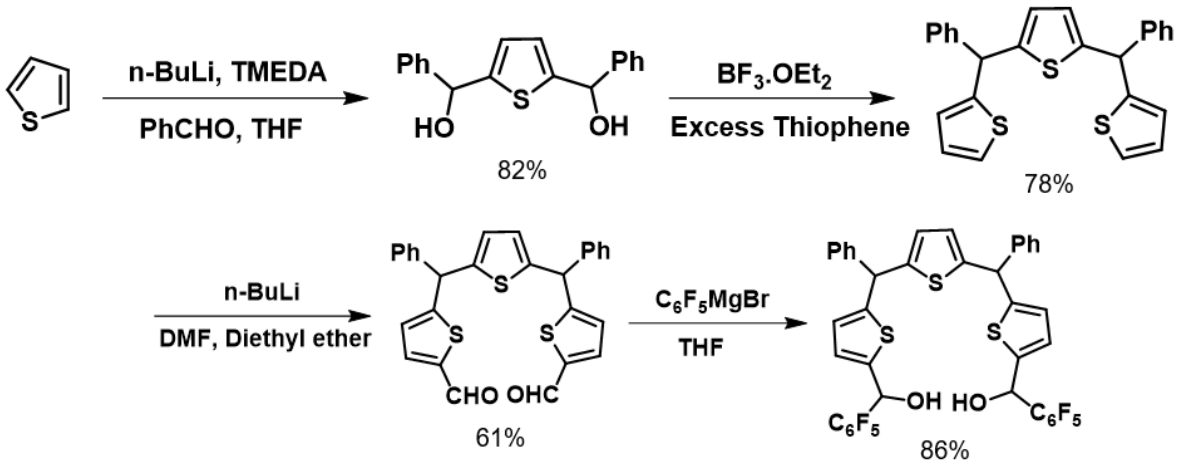

Preparation of 2, 5-Bis(phenylhydroxymethyl)thiophene:

In a nitrogen filled round bottom flask, a solution of thiophene (1 mmol) in dry n-hexane was treated with n-BuLi (2.5 mmol). followed by the addition of TMEDA (2.5 mmol) and the reaction mixture was refluxed for one hour. The temperature was then reduced to 0 ^{0}C, and benzaldehyde (3 mmol) in THF (25 ml) was slowly added with continuous stirring for an additional three hours. the reaction was quenched with saturated NH_4Cl, and the resulting mixture was extracted with EtOAc. The diol was purified through recrystallization using a DCM/n-hexane, resulting in a white powder with an 82% yield.

^{1}H NMR ($CDCl_3$, 400 MHz): δ = 7.44-7.45 (m, 4H), 7.34-7.40 (m, 4H), 7.31-7.33 (m, 2H), 6.72 (s, 2H), 5.97 (s, 2H), 2.46 ppm (brs, 2H).

5, 5'-Trithienyldimethane:

Excess thiophene diol was placed in a dried round bottom flask, and BF_3.OEt_2 was added in dark condition. The reaction mixture was stirred for around 30 minutes, and the progress of the reaction was verified by TLC. The organic compound was quenched, extracted with dichloromethane, and subjected to purification through silica column chromatography using n-hexane as the eluent. The product was isolated with a yield of 78%.

^{1}**H NMR** (400 MHz, $CDCl_3$): δ 7.21-7.36 (m, 10H), 7.18 (dd, 2H), 6.95 (d, 2H), 6.81 (m, 2H), 6.61(s, 2H), 5.77 (s, 2H).

5, 5'-Trithienyldimethane-2, 2'-dicarbaldehyde:

In a flame dried round bottom flask, trithienyldimethane (1.1 mmol) was dissolved in dry diethyl ether under a nitrogen atmosphere. n-BuLi (5 mmol) was added dropwise to the stirred solution. DMF (5 mmol) in diethyl ether was then added dropwise with stirring at room temperature, and the stirring was continued for an additional three hours. the resulting mixture was quenched with dilute HCl, extracted with EtOAc, dried and evaporated. The product was subjected to purification by silica column chromatography (20% EtOAc: Pet ether), yielding an orange residue at 61% yield.

^{1}**H NMR** (400 MHz, $CDCl_3$): δ 9.81 (2H, s), 7.28-7.33 (10H, m), 7.61 (2H, d), 6.94 (2H, d), 6.66 (2H, s), 5.77 (2H, s).

5, 5'-Trithienyldimethane-2, 2'-bis (perfluorophenyl)dicarbinol:

In a nitrogen atmosphere, trithienyl dialdehyde (1 mmol) was placed in dry THF, and a freshly prepared Grignard reagent (C_6F_5MgBr, 2.7 mmol) was added at 0 ^{o}C. stirring continued for an additional three hours, and the reaction was quenched by using saturated NH_4Cl. The reaction mixture was then extracted with EtOAc to obtain the organic layer, which was subsequently dried over Na_2SO_4. The product underwent purification via silica column chromatography, resulting in the isolation of brown residue with an 86% yield.[11]

^{1}H NMR (400 MHz, $CDCl_3$): δ 7.33 -7.26 (5H, m), 7.71 (1H, d), 6.65 (1H, s), 6.61 (1H, s), 6.29 (1H, d), 5.68 (1H, s) 2.81(1H, d).

Summary of the thesis

The thesis describes the synthesis, characterization and redox properties of the contracted and expanded isophlorinoids derived from different heterocycles such as thiophene, furan, selenophene. From the synthetic perspective, easy and effective routes were devised to obtain the [8] and [16] isophlorins in reasonable yields, from easily available precursors. The McMurry coupling reaction that favors the formation of contracted isophlorin and comprehensively characterized through spectroscopic techniques. The molecular structure of [16] isophlorin displayed the planar structure but in solution state it is suspected to display fluxional behaviour for ethylene protons as observed by the time averages signals. According to Huckel's 4nπ theory, they are supposed to show antiaromatic character. However, the absence of paratropic ring current effect in ^{1}H NMR spectrum confirms their non-antiaromatic in nature. In presence of oxidizing agents, they form dicationic species which was further confirmed by electrochemical analysis such as CV and UV-Vis analysis.

The incorporation of Thieno-thiophene in isophlorin which increase the π-electron conjugation while maintains its aromaticity as a result the reactivity alters. The solid state and solution state results proves different results for both [34] hexaphyrin. One of the hexaphyrins adopted a nearly planar geometry and its ^{1}H NMR study displayed a strong ring current effect whereas another one due to its non-planar structure, was characterized as a non-aromatic species. The strength of aromaticity was also proved with computational methods such as NICS and AICD.

The first examples of completely core-modified [24] sapphyrin was successfully synthesized and characterized thoroughly using various analytical and spectroscopic techniques. For sapphyrin, upon changing the size of atoms from oxygen atom of furan ring to selenium atom of selenophene, a significant variation in the ring current effect in solution state was observed due to the nearly planar geometry in solid state. The electrochemical measurements further confirmed the redox nature of the macrocycles. The properties of expanded isophlorins showed a significant change in the length of π-electron conjugation pathway. Extended π-circuits not only alters the structural characteristics but also varies the electronic properties with respect to 20π isophlorin. The higher analogues [48] were also isolated and characterized with ^{1}H NMR, electronic absorption, cyclic voltammetry, spectro-electrochemical studies. A twisted figure-of-eight conformation of these decaphyrin, arising from loss of planarity leads to absence of ring current effect and hence becomes non-antiaromatic character. The molecular structure of the [72] pentadecaphyrin revealed that the formation of three sapphyrin pockets called as three

folded macrocycles. The redox active nature of these macrocycles showed the multiple oxidation and reduction bands in cyclic voltammetry and further SEC measurements confirmed the facial reversible two electron ring oxidation through unstable radical cation intermediate. All these experimental measurements further supported by computational calculations through estimating the strength of aromaticity.

VI. References

(1) Sondheimer, F. The Annulenes. *Acc Chem Res* **1972**, *5* (3), 81–91. https://doi.org/10.1021/AR50051A001/ASSET/AR50051A001.FP.PNG_V03.

(2) Spitler, E. L.; Johnson, C. A.; Haley, M. M. Renaissance of Annulene Chemistry. *Chem Rev* **2006**, *106* (12), 5344–5386. https://doi.org/10.1021/CR050541C/ASSET/IMAGES/LARGE/CR050541CF00035.JPEG.

(3) Breslow, Ronald. "Antiaromaticity." *Accounts of chemical research* **1973**, *12*.

(4) "Recent advances in the chemistry of large-ring conjugated systems." Sondheimer, F. *Pure and Applied Chemistry* **1963**, *7*.

(5) McQuilkin, R. M.; Metcalf, B. W.; Sondheimer, F. [22]Annulene. *J. Chem. Soc. D* **1971**, No. 7, 338–339. https://doi.org/10.1039/C29710000338.

(6) Oth, J. F. M.; Gilles, J.-M. Mobilite Conformationnelle et Isomerie de Valence Rapide Reversible Dans Le [16] Annulene. *Tetrahedron Lett* **1968**, *9* (60), 6259–6264. https://doi.org/https://doi.org/10.1016/S0040-4039(00)75448-7.

(7) Calder, I. C.; Sondheimer, F. [24]Annulene: Dependence of Nuclear Magnetic Resonance Spectrum on Temperature. *Chem. Commun. (London)* **1966**, No. 24, 904–905. https://doi.org/10.1039/C19660000904.

(8) Vogel, E.; Roth, H. D. The Cyclodecapentaene System. *Angewandte Chemie International Edition in English* **1964**, *3* (3), 228–229. https://doi.org/10.1002/ANIE.196402282.

(9) Vogel, E. Novel Porphyrinoids. *Pure and Applied Chemistry* **1990**, *62* (3), 557–564. https://doi.org/10.1351/PAC199062030557/MACHINEREADABLECITATION/RIS.

(10) Vogel, E.; Pretzer, W.; Böll, W. A. 1.6-Imino-Cyclodecapentaen (1.6-Imino-[10]Annulen). *Tetrahedron Lett* **1965**, *6* (40), 3613–3617. https://doi.org/10.1016/S0040-4039(01)99549-8.

(11) Reddy, B. K.; Rawson, J.; Gadekar, S. C.; Kögerler, P.; Anand, V. G. A Naphthalene-Fused Dimer of an Anti-Aromatic Expanded Isophlorin. *Chemical Communications* **2017**, *53* (58), 8211–8214. https://doi.org/10.1039/C7CC04050D.

(12) Udaya, H. S.; Basavarajappa, A.; Gopalakrishna, T. Y.; Anand, V. G. Topoisomers and Aromaticity of a Redox Active 50π Core-Modified Isophlorinoid. *Chemical Communications* **2022**, *58* (100), 13931–13934. https://doi.org/10.1039/D2CC05637B.

(13) Vogel, E. The Porphyrins from the 'annulene Chemist's'' Perspective.' *Pure and Applied Chemistry* **1993**, *65* (1), 143–152. https://doi.org/10.1351/PAC199365010143/PDF.

(14) Liu, C.; Shen, D. M.; Chen, Q. Y. Synthesis and Reactions of 20 Pi-Electron Beta-Tetrakis(Trifluoromethyl)-Meso-Tetraphenylporphyrins. *J Am Chem Soc* **2007**, *129* (18), 5814–5815. https://doi.org/10.1021/JA070855C.

(15) Aviv-Harel, I.; Gross, Z. Coordination Chemistry of Corroles with Focus on Main Group Elements. *Coord Chem Rev* **2011**, *255* (7–8), 717–736. https://doi.org/10.1016/J.CCR.2010.09.013.

(16) Toganoh, M.; Furuta, H. Blooming of Confused Porphyrinoids—Fusion, Expansion, Contraction, and More Confusion. *Chemical Communications* **2012**, *48* (7), 937–954. https://doi.org/10.1039/C1CC14633E.

(17) Szyszko, B.; Latos-Grazyński, L. Core Chemistry and Skeletal Rearrangements of Porphyrinoids and Metalloporphyrinoids. *Chem Soc Rev* **2015**, *44* (11), 3588–3616. https://doi.org/10.1039/C4CS00398E.

(18) Roznyatovskiy, V. V.; Lee, C. H.; Sessler, J. L. π-Extended Isomeric and Expanded Porphyrins. *Chem Soc Rev* **2013**, *42* (5), 1921–1933. https://doi.org/10.1039/C2CS35418G.

(19) Chmielewski, P. J.; Latos-Grażyński, L.; Rachlewicz, K.; Glowiak, T. Tetra-p-Tolylporphyrin with an Inverted Pyrrole Ring: A Novel Isomer of Porphyrin. *Angewandte Chemie International Edition in English* **1994**, *33* (7), 779–781. https://doi.org/10.1002/ANIE.199407791.

(20) Furuta, H.; Asano, T.; Ogawa, T. "N-Confused Porphyrin": A New Isomer of Tetraphenylporphyrin. *J Am Chem Soc* **1994**, *116* (2), 767–768. https://doi.org/10.1021/JA00081A047/SUPPL_FILE/JA767.PDF.

(21) Yoon, D.-W.; Lee, C.-H. Synthesis and MNR Studies of Core-Modified, N-Confused Porphyrins Possessing Alkyl Groups at the Rim Nitrogen. *Bull Korean Chem Soc* **2000**, *21* (6), 618–622. https://doi.org/10.5012/BKCS.2000.21.6.618.

(22) Pacholska, E.; Latos-Grazynski, L.; Szterenberg, L.; Ciunik, Z. Pyrrole-Inverted Isomer of 5,10,15,20-Tetraaryl-21-Selenaporphyrin. *Journal of Organic Chemistry* **2000**, *65* (24), 8188–8196. https://doi.org/10.1021/JO000639L/SUPPL_FILE/JO000639L_S.PDF.

(23) Pushpan, S. K.; Srinivasan, A.; Anand, V. R. G.; Chandrashekar, T. K.; Subramanian, A.; Roy, R.; Sugiura, K.; Sakata, Y. Inverted Meso-Aryl Porphyrins with Heteroatoms; Characterization of Thia, Selena, and Oxa N-Confused Porphyrins. *Journal of Organic Chemistry* **2001**, *66* (1), 153–161. https://doi.org/10.1021/JO001209Y/SUPPL_FILE/JO001209Y_S.PDF.

(24) Sprutta, N.; Latos-Grazyński, L. 25,27-Dithiasapphyrin and Pyrrole-Inverted Isomer of 21,23-Dithiaporphyrin from Condensation of Pyrrole and 2,5-Bis(p-Tolylhydroxymethyl)Thiophene. *Org Lett* **2001**, *3* (12), 1933–1936. https://doi.org/10.1021/OL0159773/SUPPL_FILE/OL0159773_S1.PDF.

(25) Sprutta, N.; Latos-Grazyński, L. A Tetraphenylthiaporphyrin with an Inverted Thiophene Ring. *Tetrahedron Lett* **1999**, *40* (48), 8457–8460. https://doi.org/10.1016/S0040-4039(99)01773-6.

(26) Szterenberg, L.; Sprutta, N.; Latos-GrażYński, L. Thiaporphyrin with an Inverted Thiophene Ring - DFT Studies. *Journal of Inclusion Phenomena* **2001**, *41* (1–4), 209–213. https://doi.org/10.1023/A:1014428204834/METRICS.

(27) Pawlicki, M.; Latos-Grazyński, L. Pyrrole-Appended Derivatives of O-Confused Oxaporphyrins and Their Complexes with Nickel(II), Palladium(II), and Silver(III). *Chemistry – A European Journal* **2003**, *9* (19), 4650–4660. https://doi.org/10.1002/CHEM.200304899.

(28) Mishra, V.; Udaya, H. S.; Anand, V. G. Tetra S-Confused Porphyrinoids. *Org Biomol Chem* **2023**, *21* (38), 7691–7695. https://doi.org/10.1039/D3OB01270K.

(29) Lash, T. D.; Lammer, A. D.; Ferrence, G. M. Neo-Confused Porphyrins, a New Class of Porphyrin Isomers. *Angewandte Chemie* **2011**, *123* (41), 9892–9895. https://doi.org/10.1002/ANGE.201104826.

(30) Vogel, E.; Köcher, M.; Schmickler, H.; Lex, J. Porphycene—a Novel Porphin Isomer. *Angewandte Chemie International Edition in English* **1986**, *25* (3), 257–259. https://doi.org/10.1002/ANIE.198602571.

(31) Vogel, E.; Sicken, M.; Röhrig, P.; Schmickler, H.; Lex, J.; Ermer, O. Tetraoxaporphycene Dication. *Angewandte Chemie International Edition in English* **1988**, *27* (3), 411–414. https://doi.org/10.1002/ANIE.198804111.

(32) Ellinger, F.; Gieren, A.; Hübner, T.; Lex, J.; Lucchesini, F.; Merz, A.; Neidlein, R.; Salbeck, J. Ein Beitrag Zum Tetrathiaporphycen-Redoxsystem: Elektrochemische Reduktion Eines 20π-Cyclophans Zum Diatropen 22π-Dianion. *Monatshefte für Chemie Chemical Monthly* **1993**, *124* (8–9), 931–943. https://doi.org/10.1007/BF00816416/METRICS.

(33) Hu, Z.; Atwood, J. L.; Cava, M. P. A Simple Route to Sulfur Bridged Annulenes. *Journal of Organic Chemistry* **1994**, *59* (26), 8071–8075. https://doi.org/10.1021/JO00105A025/ASSET/JO00105A025.FP.PNG_V03.

(34) Reddy, B. K.; Basavarajappa, A.; Ambhore, M. D.; Anand, V. G. Isophlorinoids: The Antiaromatic Congeners of Porphyrinoids. *Chem Rev* **2017**, *117* (4), 3420–3443. https://doi.org/10.1021/ACS.CHEMREV.6B00544/ASSET/IMAGES/MEDIUM/CR-2016-00544K_0044.GIF.

(35) Panchal, S. P.; Gadekar, S. C.; Anand, V. G. Controlled Core-Modification of a Porphyrin into an Antiaromatic Isophlorin. *Angew Chem Int Ed Engl* **2016**, *55* (27), 7797–7800. https://doi.org/10.1002/ANIE.201511883.

(36) Reddy, J. S.; Anand, V. G. Planar Meso Pentafluorophenyl Core Modified Isophlorins. *J Am Chem Soc* **2008**, *130* (12), 3718–3719. https://doi.org/10.1021/JA710664Y.

(37) Kon-No, M.; MacK, J.; Kobayashi, N.; Suenaga, M.; Yoza, K.; Shinmyozu, T. Synthesis, Optical Properties, and Electronic Structures of Fully Core-Modified Porphyrin Dications and Isophlorins. *Chemistry* **2012**, *18* (42), 13361–13371. https://doi.org/10.1002/CHEM.201200776.

(38) J. L. Sessler, S. J. W. *Tetrahedron Organic Chemistry Series,*; 1997; Vol. 15.

(39) Sessler, J. L.; Seidel, D. Synthetic Expanded Porphyrin Chemistry. *Angewandte Chemie International Edition* **2003**, *42* (42), 5134–5175. https://doi.org/10.1002/ANIE.200200561.

(40) R. B. Woodward. First Mentioned by R. B. Woodward in Aromaticity: An International Symposium, Sheffield, U.K., ; 1966.

(41) Bauer, V. J.; Clive, D. L. J.; King, M. M.; Dolphin, D.; Harris, F. L.; Loder, J.; Wang, S. W. C.; Paine, J. B.; Woodward, R. B. Sapphyrins: Novel Aromatic Pentapyrrolic Macrocycles. *J Am Chem Soc* **1983**, *105* (21), 6429–6436. https://doi.org/10.1021/JA00359A012/ASSET/JA00359A012.FP.PNG_V03.

(42) J Broadhurst, B. M.; Grigg, R.; Johnson, A. W.; N Harris, R. L.; Kay, I. T.; Dolphin, D.; Leng, J.; van den Broek, P.; Johnson, A. P.; Smith, M.; Broadhurst, M. J.; Chem, J.; Badger, G. M.; Lewis, G. E.; Singh, U. P.; Arsenault, G. B.; Bullock, E.; MacDonald, F. S.; Amer, J. Sulphur Extrusion Reactions Applied to the Synthesis of Corroles and Related Systems. *J Chem Soc Perkin 1* **1972**, *19* (0), 1124–1135. https://doi.org/10.1039/P19720001124.

(43) Pareek, Y.; Ravikanth, M.; Chandrashekar, T. K. Smaragdyrins: Emeralds of Expanded Porphyrin Family. *Acc Chem Res* **2012**, *45* (10), 1801–1816. https://doi.org/10.1021/AR300136S/ASSET/IMAGES/LARGE/AR-2012-00136S_0010.JPEG.

(44) Hannah, S.; Seidel, D.; Sessler, J. L.; Lynch, V. New Chemistry of Amethyrin. *Inorganica Chim Acta* **2001**, *317* (1–2), 211–217. https://doi.org/10.1016/S0020-1693(01)00363-2.

(45) Sessler, J. L.; Weghorn, S. J.; Hiseada, Y.; Lynch, V. Hexaalkyl Terpyrrole: A New Building Block for the Preparation of Expanded Porphyrins. *Chemistry – A European Journal* **1995**, *1* (1), 56–67. https://doi.org/10.1002/CHEM.19950010110.

(46) Sessler, J. L.; Weghorn, S. J.; Morishima, T.; Rosingana, M.; Lynch, V.; Lee, V. Rosarin: A New, Easily Prepared Hexapyrrolic Expanded Porphyrin. *J Am Chem Soc* **1992**, *114* (21), 8306–8307. https://doi.org/10.1021/JA00047A061/SUPPL_FILE/JA00047A061_SI_001.PDF.

(47) Sessler, J. L.; Morishima, T.; Lynch, V. Rubyrin: A New Hexapyrrolic Expanded Porphyrin. *Angewandte Chemie International Edition in English* **1991**, *30* (8), 977–980. https://doi.org/10.1002/ANIE.199109771.

(48) Sessler, J. L.; Weghorn, S. J.; Lynch, V.; Johnson, M. R. Turcasarin, the Largest Expanded Porphyrin to Date. *Angewandte Chemie International Edition in English* **1994**, *33* (14), 1509–1512. https://doi.org/10.1002/ANIE.199415091.

(49) Lindsey, J. S.; Schreiman, I. C.; Hsu, H. C.; Kearney, P. C.; Marguerettaz, A. M. Rothemund and Adler-Longo Reactions Revisited: Synthesis of Tetraphenylporphyrins under Equilibrium Conditions. *Journal of Organic Chemistry* **1987**, *52* (5), 827–836. https://doi.org/10.1021/JO00381A022/ASSET/JO00381A022.FP.PNG_V03.

(50) Shin, J. Y.; Furuta, H.; Yoza, K.; Igarashi, S.; Osuka, A. Meso-Aryl-Substituted Expanded Porphyrins. *J Am Chem Soc* **2001**, *123* (29), 7190–7191. https://doi.org/10.1021/JA0106624.

(51) Udaya, H. S.; Mishra, V.; Gopalakrishna, T. Y.; Anand, V. G. Topological Diversity in Electrochemically Active Core-Modified Expanded Porphyrinoids. *Org Lett* **2023**, *25* (36), 6628–6632. https://doi.org/10.1021/ACS.ORGLETT.3C02328.

(52) Reddy, J. S.; Anand, V. G. Aromatic Expanded Isophlorins: Stable 30pi Annulene Analogues with Diverse Structural Features. *J Am Chem Soc* **2009**, *131* (42), 15433–15439. https://doi.org/10.1021/JA906290D.

(53) Reddy, J. S.; Mandal, S.; Anand, V. G. Cyclic Oligofurans: One-Pot Synthesis of 30π and 40π Expanded Porphyrinoids. *Org Lett* **2006**, *8* (24), 5541–5543. https://doi.org/10.1021/ol062359j.

(54) M. Stepien´ and L. Latos-Graz˙yn´ski. Tetraphenylbenziporphyrin-A Ligand for Organometallic. . *Chem. – Eur. J* **2001**, *7*, 5113–5117.

(55) Sreedhar Reddy, J.; Anand, V. G. π-Conjugated Macrocycles from Thiophenes and Benzenes. *Chemical Communications* **2008**, No. 11, 1326–1328. https://doi.org/10.1039/B715553K.

(56) Gopalakrishna, T. Y.; Reddy, J. S.; Anand, V. G. Antiaromatic Supramolecules: F···S, F···Se, and F···π Intermolecular Interactions in 32 π Expanded Isophlorins. *Angewandte Chemie International Edition* **2013**, *52* (6), 1763–1767. https://doi.org/10.1002/ANIE.201207987.

(57) Gopalakrishna, T. Y.; Anand, V. G. Reversible Redox Reaction Between Antiaromatic and Aromatic States of 32π-Expanded Isophlorins. *Angewandte Chemie International Edition* **2014**, *53* (26), 6678–6682. https://doi.org/10.1002/ANIE.201403372.

(58) Ishida, M.; Kim, S. J.; Preihs, C.; Ohkubo, K.; Lim, J. M.; Lee, B. S.; Park, J. S.; Lynch, V. M.; Roznyatovskiy, V. V.; Sarma, T.; Panda, P. K.; Lee, C. H.; Fukuzumi, S.; Kim, D.; Sessler, J. L. Protonation-Coupled Redox Reactions in Planar Antiaromatic Meso-Pentafluorophenyl-Substituted o-Phenylene-Bridged Annulated Rosarins. *Nat Chem* **2013**, *5* (1), 15–20. https://doi.org/10.1038/NCHEM.1501.

(59) Neves, M. G. P. M. S.; Martins, R. M.; Tomé, A. C.; Silvestre, A. J. D.; Silva, A. M. S.; Félix, V.; Drew, M. G. B.; Cavaleiro, J. A. S. Meso-Substituted Expanded Porphyrins: New and Stable Hexaphyrins. *Chemical Communications* **1999**, No. 4, 385–386. https://doi.org/10.1039/A808952C.

(60) Figure-Eight Tetrathiaoctaphyrin and Dihydrotetrathiaoctaphyrin Natasza Sprutta and Lechos¯aw Latos-Graz «yn ¬ Ski* [a]-in(1.1.1.1.1.1.1.1) (S 4 OPH 2). https://doi.org/10.1002/1521-3765(20011203)7:23.

(61) Ambhore, M. D.; Basavarajappa, A.; Anand, V. G. A Wide-Range of Redox States of Core-Modified Expanded Porphyrinoids. *Chemical Communications* **2019**, *55* (47), 6763–6766. https://doi.org/10.1039/C9CC02326G.

(62) Vogel, E.; Haas, W.; Knipp, B.; Lex, J.; Schmickler, H. Tetraoxaporphyrin Dication. *Angewandte Chemie International Edition in English* **1988**, *27* (3), 406–409. https://doi.org/https://doi.org/10.1002/anie.198804061.

(63) Vogel, E.; Pohl, M.; Herrmann, A.; Wiss, T.; König, C.; Lex, J.; Gross, M.; Gisselbrecht, J. P. Porphyrinoid Macrocycles Based on Thiophene—The Octaethyltetrathiaporphyrin Dication. *Angewandte Chemie International Edition in English* **1996**, *35* (13–14), 1520–1524. https://doi.org/https://doi.org/10.1002/anie.199615201.

(64) Kon-no, M.; Mack, J.; Kobayashi, N.; Suenaga, M.; Yoza, K.; Shinmyozu, T. Synthesis, Optical Properties, and Electronic Structures of Fully Core-Modified Porphyrin Dications and Isophlorins. *Chemistry – A European Journal* **2012**, *18* (42), 13361–13371. https://doi.org/https://doi.org/10.1002/chem.201200776.

(65) Panchal, S. P.; Anand, V. G. Oxidative Transformation of a Tetrathia S-Confused Isophlorin into Porphyrin Cation. *Org Lett* **2017**, *19* (18), 4854–4857. https://doi.org/10.1021/acs.orglett.7b02317.

(66) Rathore, R.; Kumar, A. S.; Lindeman, S. V; Kochi, J. K. Preparation and Structures of Crystalline Aromatic Cation-Radical Salts. Triethyloxonium Hexachloroantimonate as a Novel (One-Electron) Oxidant. *J Org Chem* **1998**, *63* (17), 5847–5856. https://doi.org/10.1021/jo980407a.

(67) Chen, Z.; Wannere, C. S.; Corminboeuf, C.; Puchta, R.; Schleyer, P. von R. Nucleus-Independent Chemical Shifts (NICS) as an Aromaticity Criterion. *Chem Rev* **2005**, *105* (10), 3842–3888. https://doi.org/10.1021/cr030088+.

(68) Schleyer, P. von R.; Maerker, C.; Dransfeld, A.; Jiao, H.; van Eikema Hommes, N. J. R. Nucleus-Independent Chemical Shifts: A Simple and Efficient Aromaticity Probe. *J Am Chem Soc* **1996**, *118* (26), 6317–6318. https://doi.org/10.1021/ja960582d.

(69) Geuenich, D.; Hess, K.; Köhler, F.; Herges, R. Anisotropy of the Induced Current Density (ACID), a General Method To Quantify and Visualize Electronic Delocalization. *Chem Rev* **2005**, *105* (10), 3758–3772. https://doi.org/10.1021/cr0300901.

(70) MacDowell, D. W. H.; Patrick, T. B. The Synthesis of 4,6-Dihydrothieno[3,4-b]Thiophene. *J Org Chem* **1966**, *31* (11), 3592–3595. https://doi.org/10.1021/jo01349a028.

(71) Rath, H.; Mallick, A.; Ghosh, T.; Kalita, A. Aromatic Fused Heterocyclic [22] Macrocycles with NIR Absorption. *Chem. Commun.* **2014**, *50* (65), 9094–9096. https://doi.org/10.1039/C4CC02749C.

(72) Mallick, A.; Oh, J.; Kim, D.; Rath, H. Aromatic Fused [30] Heteroannulenes with NIR Absorption and NIR Emission: Synthesis, Characterization, and Excited-State Dynamics. *Chemistry – A European Journal* **2016**, *22* (24), 8026–8031. https://doi.org/https://doi.org/10.1002/chem.201600917.

(73) Mallick, A.; Oh, J.; Majewski, M. A.; Stępień, M.; Kim, D.; Rath, H. Protonation Dependent Topological Dichotomy of Core Modified Hexaphyrins: Synthesis, Characterization, and Excited State Dynamics. *J Org Chem* **2017**, *82* (1), 556–566. https://doi.org/10.1021/acs.joc.6b02576.

(74) Soya, T.; Osuka, A. Internally Bridged Hückel Aromatic [46]Decaphyrins: (Doubly-Twisted-Annuleno)Doubly-Twisted-Annulene Variants. *Chemistry – A European Journal* **2019**, *25* (20), 5173–5176. https://doi.org/https://doi.org/10.1002/chem.201900819.

(75) Sessler, J. L.; Cyr, M. J.; Lynch, V.; McGhee, E.; Ibers, J. A. Synthetic and Structural Studies of Sapphyrin, a 22-.Pi.-Electron Pentapyrrolic “Expanded Porphyrin.” *J Am Chem Soc* **1990**, *112* (7), 2810–2813. https://doi.org/10.1021/ja00163a059.

(76) Shevchuk, S. V; Davis, J. M.; Sessler, J. L. Synthesis of Sapphyrins via a '3+1+1' Procedure. *Tetrahedron Lett* **2001**, *42* (13), 2447–2450. https://doi.org/https://doi.org/10.1016/S0040-4039(01)00198-8.

(77) Paolesse, R.; Licoccia, S.; Spagnoli, M.; Boschi, T.; Khoury, R. G.; Smith, K. M. A Novel Synthetic Route to Sapphyrins. *J Org Chem* **1997**, *62* (15), 5133–5137. https://doi.org/10.1021/jo9704117.

(78) Rana, A.; Sathish Kumar, B.; Panda, P. K. β-Decamethoxysapphyrin and Its N-Benzyl Analogue. *Org Lett* **2015**, *17* (12), 3030–3033. https://doi.org/10.1021/acs.orglett.5b01306.

(79) Chmielewski, P. J.; Latos-Grażyński, L.; Rachlewicz, K. 5,10,15,20-Tetraphenylsapphyrin-Identification of a Pentapyrrolic Expanded Porphyrin in the Rothemund Synthesis. *Chemistry – A European Journal* **1995**, *1* (1), 68–73. https://doi.org/https://doi.org/10.1002/chem.19950010111.

(80) Jeyaprakash Narayanan, S.; Sridevi, B.; Srinivasan, A.; Chandrashekar, T. K.; Roy, R. One Step Synthesis of Sapphyrin and N-Confused Porphyrin Using Dipyrromethane. *Tetrahedron Lett* **1998**, *39* (40), 7389–7392. https://doi.org/https://doi.org/10.1016/S0040-4039(98)01603-7.

(81) Broadhurst, M. J.; Grigg, R.; Johnson, A. W. The Synthesis of 22 π-Electron Macrocycles. Sapphyrins and Related Compounds. *J. Chem. Soc., Perkin Trans. 1* **1972**, No. 0, 2111–2116. https://doi.org/10.1039/P19720002111.

(82) Lisowski, J.; Sessler, J. L.; Lynch, V. Synthesis and X-Ray Structure of Selenasapphyrin. *Inorg Chem* **1995**, *34* (13), 3567–3572. https://doi.org/10.1021/ic00117a032.

(83) Narayanan, S. J.; Sridevi, B.; Chandrashekar, T. K.; Vij, A.; Roy, R. Novel Core-Modified Expanded Porphyrins with Meso-Aryl Substituents: Synthesis, Spectral and Structural Characterization. *J Am Chem Soc* **1999**, *121* (39), 9053–9068. https://doi.org/10.1021/ja991472k.

(84) Srinivasan, A.; K. Pushpan, S.; Ravi Kumar, M.; Mahajan, S.; K. Chandrashekar, T.; Roy, R.; Ramamurthy, P. Meso-Aryl Sapphyrins with Heteroatoms; Synthesis, Characterization, Spectral and Electrochemical Properties. *J. Chem. Soc., Perkin Trans. 2* **1999**, No. 5, 961–968. https://doi.org/10.1039/A900137I.